Elaboration de glycopolymères et glycocapsules mannosylés à propriétés anti-adhésives

Xibo Yan

N° d'ordre 2015-ISAL-0011 Année 2015

THESE

PRÉSENTÉE DEVANT

l'Institut National des Sciences Appliquees de Lyon

pour obtenir

le grade de docteur

ECOLE DOCTORALE: Matériaux de Lyon

soutenue publiquement le 13 Février 2015 par

Xibo YAN

Heptyl mannoside based polymers and nanocapsules: Towards potent anti-adhesive glycomaterials and nanocarriers

JURY

BERNARD Julien	Chargé de Recherche CNRS (INSA de Lyon)	Directeur de thèse
BOUCKAERT Julie	Chargée de Recherche CNRS (Université de Lille 1)	Examinateur
FLEURY Etienne	Professor (INSA de Lyon)	Directeur de thèse
GANACHAUD François	Directeur de Recherche CNRS (INSA de Lyon)	Examinateur
MALKOCH Michael	Professor (KTH Royal Institute of Technology)	Rapporteur
NICOLAS Julien	Chargé de Recherche CNRS (Université Paris-Sud)	Rapporteur

Résumé

Ce travail de thèse est consacré à la préparation de glycopolymères porteurs de groupements pendants mannoside d'heptyle et à l'évaluation de la capacité de ces ligands multivalents à inhiber la fixation bactérienne sur les cellules humaines.

Nous avons synthétisé, par polymérisation radicalaire contrôlée, une série de glycopolymères linéaires ou en étoile présentant des masses molaires, des densités en mannoside et des microstructures modulables dans le but d'évaluer l'influence de ces paramètres sur les processus d'interactions avec diverses souches de bactéries *E coli* (AIEC LF82 et UTI 89). Nous avons tout d'abord mis en évidence par diffusion dynamique et statique de la lumière, la formation d'agrégats entre ces glycopolymères et FimH, la lectine à l'origine de la fixation de souches de bactéries *E coli*, traduisant des interactions fortes entre les motifs mannosides et les sites de reconnaissance au mannose de la lectine. Nous avons ensuite évalué l'aptitude de ces ligands multivalents à bloquer l'adhésion bactérienne d'AIEC LF82 (impliquée dans la maladie de Crohn) sur des cellules épithéliales intestinales T84. Il a été démontré en conditions *in vitro* que l'ajout de 10 nM ou 100 nM d'unités mannoside (respectivement en pré- ou post-incubation) réduit de moitié l'adhésion des bactéries sur les cellules épithéliales. L'effet anti-adhésif de ces glycopolymères a été confirmé par des tests *ex vivo* réalisés sur des intestins isolés de souris transgéniques CEABAC10.

Enfin, nous avons exploité la technique de nanoprécipitation pour l'élaboration de nanocapsules de glycopolymères à cœur huileux. Le procédé développé permet la synthèse de nanocapsules de dimensions contrôlées, porteuses de groupements fonctionnels (fluorophores, ligands) ou de particules métalliques et l'encapsulation de molécules actives à cœur en une seule étape.

Abstract

This PhD work focuses on the preparation of glycopolymers bearing pendent heptyl mannose groups and the evaluation of the capability of such multivalent ligands to inhibit bacterial adhesion to human cells.

Aiming at understanding the impact of various structural parameters on glycopolymer/ *E coli* interactions (AIEC LF82 et UTI 89 strains of *E. coli*), a series of linear and star-shaped glycopolymers with tunable molecular weight, mannoside density and microstructure (block copolymers, gradient copolymers, random copolymers) has been constructed. The association of the glycopolymers with FimH adhesin, a lectin which possesses a mannose-specific receptor site and is responsible for recognition and binding to host cells, was first confirmed by static and dynamic light scattering experiments. The propensity of the glycopolymers to prevent attachment of *E. coli* (AIEC LF82 involved in Crohn's disease) to intestinal epithelial cells (T84 cells) was further investigated through adhesion assays. It was shown that under in vitro conditions, the addition of 10 nM or 100 nM of glycopolymer on a mannose unit basis (in pre-incubation and post-incubation respectively) decreases by half the bacterial adhesion to intestinal epithelial cells. The anti-adhesive effect of these multivalent ligands was further confirmed in *ex vivo* conditions for colonic loops of transgenic CEABAC10 mice (Crohn's disease model mouse).

Finally we took advantage of the nanoprecipitation process to generate glyconanocapsules with oily core. The employed strategy allowed for preparing well-defined nanocapsules bearing groups of interest (tags, ligands) or metal particles within the shell and loaded with active molecules in the core in one step.

Acknowledgement

First of all I would like to thank my supervisors, Pr. Etienne Fleury and Dr. Julien Bernard, for giving me an opportunity to be a member of IMP@INSA, and for providing guidance and direction over the years, they always encouraged me and gave me excellent suggestions which enable me to finish my thesis successfully.

My extraordinary thank goes to Dr. François Ganachaud, my colleague of IMP@INSA, who always gave much excellent advice on “nanoprecipitation” to solve the problems encountered during my work.

During my project, I am honored to have been working with Dr. Sébastien Gouin at LUNAM Université for synthesis of monomers, Dr. Julie Bouckaert at Université des Sciences et Technologies de Lille for bio-evaluation of glycopolymers and Dr. Christophe Travelet at Centre de Recherches sur les Macromolécules Végétales for investigation of glycopolymer/FimH aggregates using dynamic light scattering. I would like to express my appreciation for their professional guidance and support.

During my project, I was able to communicate and cooperate with scientists from different scientific areas. In such an environment, it was very productive. Therefore, I would like to thank all our collaborators involved in the thesis, Dr. Arlette Darfeuille-Michaud, Dr. Nicolas Barnich and Adeline Sivignon at Clermont Université, Dr. Rostyslav Bilyy at National Academy of Sciences of Ukraine, Dr. Béatrice Burdin and Dr. Sabine Favre-Bonté at Université Claude Bernard Lyon 1, Dr. David Deniaud at LUNAM Université and Dr. Redouane Borsali at Centre de Recherches sur les Macromolécules Végétales,

Moreover, I would like to show my thanks to Isabella Polo, Mallaouia Bengoua, Pierre Alcouffe, Marion Colella, Agnès Crepet, Dr. Fernande Boisson, Cécile Chamignon, Annick Waton, Patrick Goetinck, Dr. Senbin Chen, Dr. Jing Chen, Dr. Huagui Zhang, Dr. Wenyong Zhang, Biao Zhang, Jing Yang, Dr. Marco Delgado, Dr. Ali Ghadban, Olivier Gribelin, Ludovic Sallet who were always nice and helpful for my lab work, and thank all the colleagues in the lab.

I would like to thank Dr. François Ganachaud, Dr. Michael Malkoch, Dr. Julien Nicolas and Dr. Julie Bouckaert for reading through my thesis and serving on my Ph.D. examination board.

Great thanks to Chinese Scholarship Council for my Ph. D grant.

Last but not least, I would like to express my special thanks to my best friend, Shuai Wang, she was always there whenever I needed help.

Finally, I would like to dedicate my work to my parents, Hong Tian and Hesheng Yan.

Abbreviations

ACPA	4,4'-Azobis(4-cyanopentanoic acid)
AFM	atomic force microscopy
AIBN	2,2-azobisisobutyronitrile
ATRP	atom transfer radical polymerization
$CDCl_3$	deuterated chloroform
CH_2Cl_2	dichloromethane
CPADB	4-cyano-4-(phenylcarbonothioylthio) pentanoic acid
CRP	controlled radical polymerization
CTA	chain transfer agents
D_2O	deuterium oxide
DCC	N,N'-dicyclohexylcarbodiimide
***d*-DMSO**	deuterated dimethyl sulfoxide
DLS	dynamic light scattering
DNA	deoxyribonucleic acid
DMAP	4-dimethylaminopyridine
DMF	dimethylformamide
DMSO	dimethyl sulfoxide
E. Coli	*Escherichia coli*
ELISA	enzyme-linked immunosorbent assay
ESI-MS	electrospray ionization mass spectrometry
GFP	green fluorescent protein
GPC	gel permeation chromatography
HEPES	4-(2-hydroxyethyl)-1-piperazineethanesulfonic acid
HM	heptyl mannoside
IPDI	isophorone diisocyanate
M	monomer
MW	molecular weight
NaOH	sodium hydroxide

NHS	hydroxysuccinimide
NOESY	Nuclear Overhauser Effect Spectroscopy
NMR	nuclear magnetic resonance
PCL	polycaprolactone
PEG	polyethylene glycol
PLA	poly(lactic acid)
PS	polystyrene
RAFT	reversible addition fragmentation chain transfer polymerization
RNA	ribonucleic acid
ROMP	ring-opening methathesis polymerization
SEC	size exclusion chromatography
TEM	transmission electron microscopy
THF	tetrahydrofuran

Table of Contents

General introduction

General introduction

In the history of humanity, bacteria have been responsible for a wide number of diseases and are considered as the cause of numerous deaths. Over the last century, water purification, vaccination and the systematic use of antibiotics have considerably reduced the risk of these illnesses. Nowadays, the traditional antibiotic treatments become less and less efficient since bacteria have acquired resistance. This problem is so important and global that the World Health Organization (WHO) declared in 2014 that "this serious threat is no longer a prediction for the future, it is happening right now in every region of the world and has the potential to affect anyone, of any age, in any country. Antibiotic resistance–when bacteria change so antibiotics no longer work in people who need them to treat infections–is now a major threat to public health."[1] Because of this emergency, several lines of research are currently explored. One of them consists in blocking the adhesion between the bacterial pathogens and the host cells or the tissues which leads to the infection and then to the disease. Adhesion is governed by multivalent interactions between bacterial surface lectins and carbohydrates groups on the cells surface. For instance *Escherichia coli* (*E. coli*) bacteria, which are associated with numerous infections, express adhesive hair-like organelles with mannose-specific receptor to promote adhesion and infection of tissues. Monosaccharides such as mannose derivatives have been widely described as antagonists that competitively interact with bacterial lectins to inhibit or disrupt the bacterial adhesion towards host cells.[2] Their use has gradually emerged as valuable alternative to antibiotics. To enhance their efficiency, carbohydrate moieties can also be tethered along a polymer backbone resulting in functional glycopolymer.[3] In such a way, the activity of a glycopolymer will depend on its architecture, the degree of polymerization, the density of carbohydrate groups… Therefore, the generation of glycopolymer with well-defined architecture is of crucial importance in order to precisely determine the relationship between the structure of the glycopolymer and its anti-adhesive properties.

Controlled radical polymerizations (CRP) are ideal methods to control the

polymerization process and design polymers having narrow distribution and complex architectures such as block copolymers, comb like, stars, star blocks, dumbbell, dendrigrafts and so on… The living character of CRP also limits the ability of growing chains to terminate and leads to an accurate control of chain end composition. Reversible Addition-Fragmentation chain Transfer (RAFT) is one of the most effective CRP methods and is very attractive since it allows the polymerization of a wide range of monomers including glycomonomers. In addition, the lability of the thiocarbonylthio end group paves the way to post-functionalizations.[4]

For all these reasons we have chosen to design well-defined multivalent glycopolymers via RAFT polymerization of n-heptyl α-D-mannose-based monomers and to deeply investigate their efficiency as lectin FimH antagonists for anti-inflammatory treatment of adherent-invasive *E.Coli* (AIEC) infection.

To further explore the potential of such glycomaterials, we have subsequently explored the propensity of our tailor-made glycopolymers to form glyconanocapsules via the Ouzo process. Indeed, as core-shell structures can protect actives against degradation and elimination, nanocapsules can be advantageously applied as nano-carriers for various molecules or (bio)macromolecules (fluorescent probes, drugs, DNA, RNA…).[5] With carbohydrates moieties present at the surface of glyconanocapsules one can favor specific interactions with targeted cells or tissues and enhance the cellular uptake.

The present manuscript is organized in five chapters. First (***chapter 1***) a literature review describes the different routes to get carbohydrate-functionalized nanocapsules from polysaccharides and glycopolymers. Note that we have chosen to investigate the latter subject because interactions between glycopolymers and lectins have been profusely reviewed over the last decade.[3,6]

The synthesis and characterization of n-heptyl α-D-mannose-based glycopolymers are described in ***chapter 2***. Based on RAFT polymerization of mannosylated monomers the preparation of linear/star-shaped glycopolymers and of a

glyco-copolymer library (block, gradient, statistical, post-modified) is reported.

In the ***chapter 3***, the application of glycopolymers against bacterial adhesion is explored, the evaluation of anti-adhesive properties being evaluated from molecular level to *in vitro* and *ex vivo*.

As underlined in ***chapter 1***, the Ouzo technique is a simple route to generate nanocapsules through nanoprecipitation. This feature will be investigated in ***chapter 4*** with the glycopolymers described in ***chapter 2***.

Finally all the experimental parts are provided in ***chapter 5***, including characterization methods, synthetic procedures, bio-assays and preparation of nanocapsules.

1. http://www.who.int/mediacentre/news/releases/2014/amr-report/en/ (2014/12/07)

2. Deniaud, D.; Julienne, K.; Gouin, S. G. *Organic & Biomolecular Chemistry*, **2011**, *9*, 966-979.

3. Ting, S. S. R.; Chen G.; Stenzel, M. H. *Polymer Chemistry*, **2010**, *1*, 1392-1412.

4. Lowe, A. B. *Polym. Chem.* **2010**, *1*, 17-36.

5. van Dongen, S. F. M.; de Hoog, H.-P. M.; Peters, R. J. R. W.; Nallani, M.; Nolte, R. J. M.; van Hest, J. C. M. *Chem. Rev.*, **2009**, *109*, 6212–6274.

6. Becer, B. *Macromol. Rapid Commun.* **2012**, *33*, 742-752.

Chapter 1

Preparation of Carbohydrate-based nanocapsules

Chapter 1 Preparation of Carbohydrate-based nanocapsules

1.1 Introduction

Over the past decades, polymer capsules have attracted significant attention owing to their capability to mask a smell, or a taste, to protect an active molecule from degradation or elimination and to release it in a controlled manner. For all these reasons, polymer capsules which can be constituted of biopolymers or of synthetic polymers are commonly used in numerous applications in adhesives, paintings, food and flavor industry, pharmaceutical industry, cosmetics and so on.

Synthetic capsules can be likened to vesicular systems in which an encapsulated product is confined in a cavity consisting of an inner liquid core surrounded by a polymer membrane[1]. Synthetic capsules display a core-shell structure[2] (**Scheme 1.1**). Both core and shell can be loaded with (macro)molecules to deliver and the shell can also be functionalized with probes or ligands[3]. The polymer(s) composing the capsules can be chosen so that the capsules exhibit a stimuli-responsive character (pH, temperature, light, redox…) in order to facilitate or trigger the release of the sequestrated active molecules.[4-5] The shell of the capsules can be made of synthetic or natural polymers. The inner part of the capsules can contain encapsulated colloids, solids, liquids or gas. According to the techniques of preparation, the reservoir of capsules can be either lipophilic or hydrophilic and depending on the particle size, the prepared capsules can be classified into microcapsules or nanocapsules.

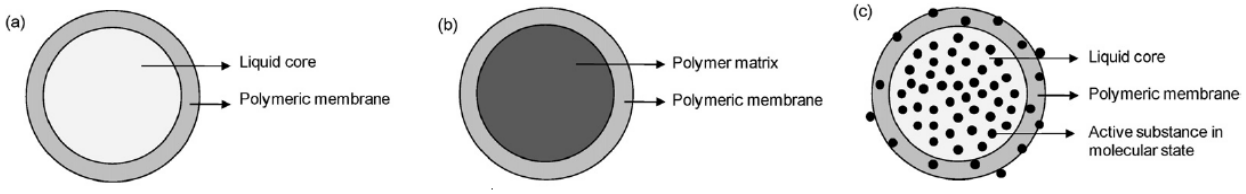

Scheme 1.1: Different Capsular Structures[2]: (a) Liquid Core, (b) Polymer Matrix and (c) Active substance in molecular dispersion.

Microcapsules

Capsules with diameters ranging from one to one thousand micrometers are called microcapsules. Microcapsules possess a high surface area and a large inner volume

which facilitates the loading of molecules of interest (dyes, catalysts, drugs, ink...). Microcapsules are thus utilized as microcarriers[6], microsensors[7] or microreactors[8]. Two major advantages of synthetic microcapsules over nanocapsules are that 1) microcapsules are relatively fragile and can thus be easily broken by friction, a very desirable feature for cosmetic, flavor, food or textile applications and 2) that a large number of simple and cheap routes of microcapsules have been established for decades. The most common methodologies affording microcapsules are listed below.[9-10]

(1) Coacervation. Coacervation is a phase separation process due to partial desolvation of (fully solvated) macromolecules upon addition of salt, oppositely charged polymer, non-solvent, pH or temperature change. The solution separates into two liquid phases, a polymer-rich and polymer-lean phase. The use of coacervation to build polymer microcapsules was first developed in the fifties for carbonless copy paper applications. The general procedure consists in dispersing (for instance) oils or drugs intended to form the core of the capsules into a solution containing the polymer. Coacervation results in the deposition of the polymer at the surface of dispersed particles and in the formation of a membrane which is finally hardened through chemical or thermal treatments.

(2) Spray-drying. Spray drying is a mechanical technique developed in the thirties for microencapsulation. It is notably a popular route for encapsulation of molecules of hydrophobic nature, such as oils and flavors. These molecules that further constitute the core of the capsules are first dispersed in an aqueous concentrated solution of shell precursor (generally polysaccharides or proteins). The resulting oil-in-water emulsion is then atomized into a spray of droplets in a hot chamber. The evaporation of the solvent leads to the formation of microcapsules.

(3) Pan coating. Pan coating is widely applied in the pharmaceutical industry for manufacturing coated particles or tablets. Generally, solid particles are mixed with a coating material. As temperature increases, the coating material is melted to enclose the core particles. Afterwards, microcapsules are solidified by cooling. Alternatively,

the coating material can be gradually added to core particles which are tumbling in a vessel.

(4) Centrifugal extrusion. The core and coating materials, which are immiscible with one another, are co-extruded through a spinning two-fluid nozzle. Owing to Rayleigh instability, after clearing the nozzle the jet splits into tiny round droplets of core material engulfed with the coating material. The shell can be directly hardened in flight or after the formation of the capsules through treatment in a hardening bath. This technique is ideally suitable for preparation of microcapsules with a diameter ranging from 250 to 2000 micrometer.

(5) Air-suspension coating. In this process, the core material is first dispersed (as particles) by an upward-moving (and usually heated) air stream and coated while suspended. This method is widely applied in pharmaceutical, food and cosmetic industry.

(6) Solvent evaporation. To apply this method, a coating polymer solution which is immiscible with liquid manufacturing vehicle (LMV) is first prepared. The core materials are either dissolved or dispersed in the polymer solution. Then the resulting solution is added into LMV with agitation. The polymer is deposited on the core materials to form microcapsules after solvent evaporation. This technique is widely used in pharmaceutical industry.

(7) Polymerization techniques. The generation of microcapsules by direct polymerization has represented a main development in the field of polymer colloids. Microcapsules can be built through emulsion, suspension, dispersion polymerizations (using the osmotic swelling technique or hydrocarbon encapsulation) or interfacial polymerizations.

Whereas microcapsules are widely used for industrial purposes, the scope of nanocapsules is presently limited by the absence of cheap and straightforward routes to these classes of objects.

Nanocapsules

The size of nanocapsules typically ranges from 10 nm to 500 nm. Owing to their peculiar dimensions, nanocapsules have raised great interest over the last two decades in biomedical applications, especially in the field of nanomedicine.[11-14] Nanocapsules allow for improving the efficacy of drugs or biomolecules (proteins, nucleic acids) while reducing side effects and toxicity issues. Nanocarriers are indeed capable to protect sequestrated active molecules, to control their release and, in the meantime, to overcome biological barriers, to target specific sites (for release) and to enable bio-imaging through incorporation of appropriate tags (**Scheme 1.2**).[15-17]

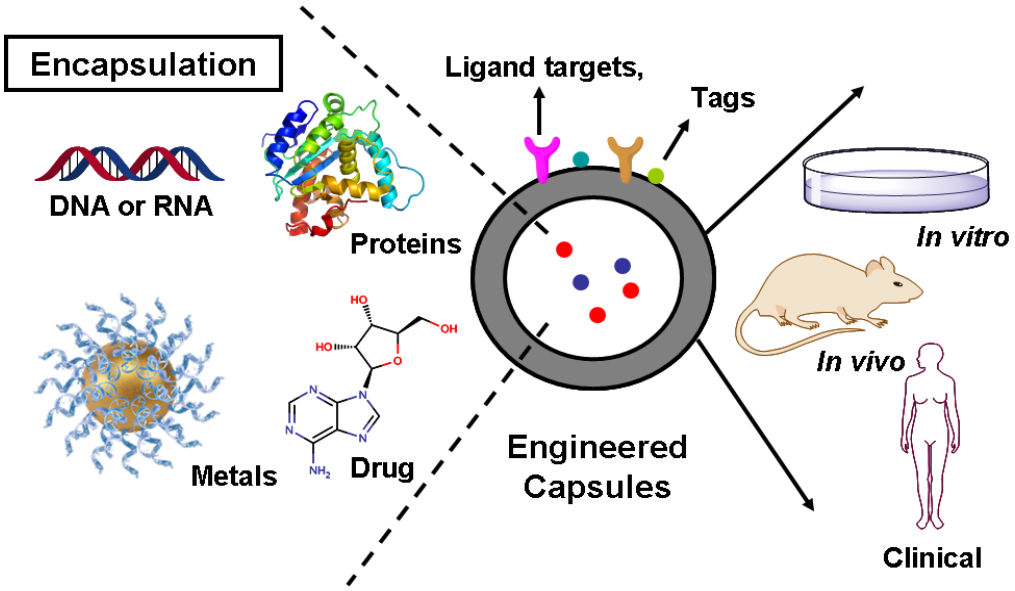

Scheme 1.2: Engineered capsules for drug delivery applications.

The size distribution of nanocarriers is a highly important parameter for drug delivery applications, especially for intravenous applications: 1) to avoid recognition by macrophages of the reticuloendothelial system (RES) and thus rapid clearance from the bloodstream, the size of the nanocarriers should be as small as possible to limit the adsorption of plasma proteins (opsonins); 2) to take advantage of the Enhanced Permeation and Retention effect (EPR) in cancer therapy or treatments of various inflammatory diseases, the size of the nanocarriers should be under 200 nm and preferentially below 100 nm.

In quest for smart and sophisticated nano-objects, considerable attention has been lately paid to the generation of nanocapsules decorated with a myriad of functions ensuring selective targeting, bio-imaging and so on. In this context, the fabrication of nanocapsules bearing carbohydrate moieties is very attractive. Together with DNA and proteins, sugar moieties are indeed key molecules in living organisms. Sugars play a significant role in cellular communication, biological recognition events,[18] immune function[19] and signal transduction.[20] To enhance bioactivity (and eventually biocompatibility), glycopolymers, polysaccharides and molecular carbohydrate derivatives are then commonly used to prepare functional glyconanocapsules.

1.2 Routes to carbohydrate-functionalized nanocapsules

As nanocapsules are attractive materials for drug delivery applications, numerous methodologies have been developed over the last two decades. In this chapter, we will describe the most common routes to this category of nanocarriers. More precisely, this chapter will be dedicated to the physical and chemical routes (**Scheme 1.3**) to glycopolymer and polysaccharide based nanocapsules.[21-26] Construction of glyconanocapsules exclusively based on molecular carbohydrate derivatives (liposomes, cyclodextrine…) will not be reported.

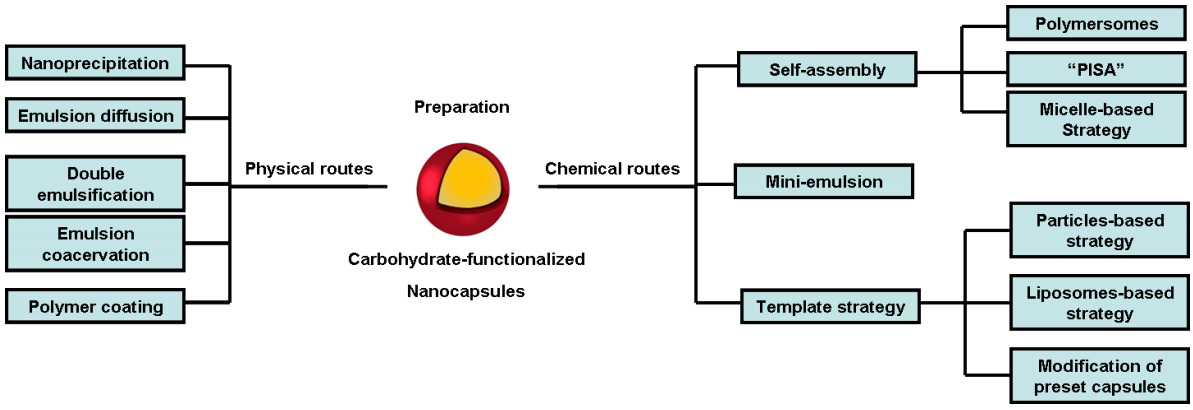

Scheme 1.3: Routes to carbohydrate-functionalized nanocapsules.

1.2.1 Emulsification routes to carbohydrate-functionalized nanocapsules

Emulsification routes are classical methods to prepare nanocapsules. The principle of the most common methods, that is to say, the emulsion diffusion technique, the

double emulsification technique, the emulsion coacervation technique, the polymer coating technique and the mini-emulsion technique will be described and their application in the field of glyconanocapsules will be discussed below.

1.2.1.1 Emulsion diffusion technique

In the emulsion diffusion process, the polymer-dissolved oil/water system needs to be emulsified via vigorous agitation. Nanocapsules are then generated by subsequent addition of aqueous solution into the emulsion which causes the diffusion of the solvent into the external phase. The formation of nanocapsules is induced by polymer precipitation and interfacial deposition during the diffusion of solvent. The size distribution of nanocapsules prepared through this method is generally ranging from 150 nm to 200 nm. This method has been extensively applied to prepare PCL or PLA-based polymeric nanocapsules. Up to now, no carbohydrate-based nanocapsules have been reported based on this technique.

1.2.1.2 Double emulsification technique

Double emulsification, also called “emulsion of emulsion”, is a process which consists in the preparation of either water-oil-water emulsion or oil-water-oil emulsion. To realize the double emulsion process, both hydrophobic and hydrophilic surfactants are needed and should be used in this two-step emulsification process. The formation of nanocapsules induced by double emulsification is also associated with nanoprecipitation and emulsion-diffusion methods.

Holban and co-workers prepared double cross-linked chitosan nanocapsules by double emulsification (**Table 1.1, entry 1**).[27] In a preliminary phase, an o/w/o emulsion was prepared by two-step emulsification. A toluene solution of Span80 was first co-emulsified with an aqueous solution of chitosan-gelatin (1/1, w/w) containing Tween80 (low-molecular weight chitosan, 75-85% DA). The resulting emulsion was then added to a second Span80 toluene solution (final o/w/o conditions, 1/3/17, volume ratio). After a first cross-linking step (induced by addition of sodium sulphate), the solution was emulsified by mechanical agitation. Chitosan containing

nanocapsules were finally obtained after cross-linking with glutaraldehyde. The size of nanocapsules (ranging from 100 nm to 700 nm) was controlled by the molar ratio between amino groups of chitosan and gelatin and sodium sulfate. Increasing the content of sodium sulfate made the nanocapsules shrink owing to ionic cross-linking. The resulting nanocapsules were capable to load anti-tumor drug L-phenylalanine derivatives with efficiency up to 79%. In comparison with free drug treatment, the encapsulation improved the anti-tumor activity against implanted Guerin's carcinoma *in vivo*.

In 2013, Wu and coworkers reported on alginate/chitosan coated nanocapsules which could be used as insulin delivery system (**Table 1.1, entry 2**).[28] A w/o/w double emulsion was prepared by a two-step process; a w/o emulsion was first generated by emulsification of an insulin aqueous solution/Labrafac, Span 80 with phospholipid oily phase. This emulsion was then poured into an alginate aqueous solution and a second emulsification was carried out (by stirring) to generate a w/o/w emulsion. After sequentially adding calcium chloride and chitosan (low-molecular weight, 75-85% DA), alginate-coated nanocapsules were finally obtained with a diameter of around 490 nm. The release of insulin was proven to be controlled by the acidity of the solution. For instance in simulated gastric conditions (pH 1-3), only 20 % of insulin could be released out of the alginate/chitosan shell at pH 2.5 after 30 min (37°C), while more than 85% and no leakage at all were observed at pH 1.0 and 3.0, respectively. As revealed by *in vivo* studies, these nanocapsules were also shown to effectively prolong the hypoglycemic effect after oral administration.

1.2.1.3 Emulsion coacervation technique

In the emulsion coacervation process, emulsion is generated through o/w emulsification by mechanical stirring or ultrasound. The polymer then precipitates from the continuous solution to form a coacervate layer on the emulsion template. This polymer layer then generates the walls of the nanocapsules after cross-linking reactions. The crucial point of this technique is the formation of the coacervate layer which is triggered by the addition of salt, oppositely charged polymer or non-solvent,

or by pH or temperature change. Up to now, sodium alginate and gelatin have been commonly used for the generation of nanocapsules by the emulsion coacervation technique.

In 2008, Lertsutthiwong's group reported on the preparation of turmeric oil loaded alginate nanocapsules by emulsion coacervation technique (**Table 1.1, entry 3**).[29-30] Practically, a solution of turmeric oil in acetone or ethanol was added into an alginate (800~120 kg/mol) aqueous solution. After o/w emulsification by sonication, cross-linked nanocapsules were directly generated by addition of calcium chloride and solvent removal. The size of capsules obtained from the ethanol/water system (diameter around 260 nm) was smaller than capsules obtained from the acetone/water system (diameter around 370 nm). An increase of oil concentration or oil/alginate mass ratio caused an increase of nanocapsules' size. Alternatively, the alginate coacervate layer was cross-linked by sequential addition of calcium chloride and chitosan (41 or 72 kg/mol). However, involvement of chitosan led to the formation of larger nanocapsules (above 500 nm).

Grebinsan *et al.* developed glutamine derivatives loaded alginate-based nanocapsules (**Table 1.1, entry 4**).[31] Starting from L-glutamine, formyl and acetyl groups grafted N-(p-aminobenzoyl)-L-glutamines were synthesized in five steps. The glutamine derivatives (constituting the core material) were dissolved in a mixture of ethanol, benzyl alcohol and DMSO, which was then poured into an alginate aqueous solution. After emulsification by sonication, glutamine derivatives loaded alginate-based nanocapsules (size about 400 nm) were obtained after chitosan-induced cross-linking reaction and solvent evaporation. According to *in vitro* anti-tumor studies, no enhancement of activity could be observed with these nanocarriers in comparison with free drugs.

Jana and coworkers recently prepared testosterone-loaded nanocapsules using the emulsion-coacervation technique (**Table 1.1, entry 5**).[32] Testosterone (a steroidal male hormone) dissolved in hexane was added into an alginate aqueous solution. Nanocapsules with diameter of 34 nm were directly obtained after emulsification (first

stirring and then sonication) and calcium-induced cross-linking. These nanocapsules were capable to load 30% of testosterone during the preparation and enhanced its bioavailability in Female Sprague Dawley rats.

1.2.1.4 Polymer coating technique

The polymer coating technique consists in depositing a layer of polymer on preformed nanoparticles surface. This route thus relies on a preliminary emulsification step leading to the formation of nanodroplets and a subsequent polymer deposition step at the oil/water interface. In contrast with the emulsion-coacervation technique, the adsorption of the polymer chains is generally triggered by solvent evaporation.

In 1997, Alonso's group took advantage of this approach to generate polysaccharide-based nanocapsules. Poly-ε-caprolactone (PCL, *Mw* = 40 kg/mol), Miglyol 840 and lecithin were dissolved in acetone (**Table 1.1, entry 6**). After pouring the organic solution into aqueous solution of chitosan (molecular weight > 100 kg/mol), chitosan-coated PCL nanocapsules (size ranging from 300 to 500 nm) were generated by an interfacial deposition technique after evaporation of acetone (One-stage procedure). These positively charged nanocapsules were capable to encapsulate indomethacin (an anti-inflammatory drug) and enhance the corneal penetration. It was demonstrated that 85% of the drug diffuses out of the nanocapsules within 2h.[33-35] More recently (2006), the same group reported on the preparation of Miglyol-812 filled chitosan nanocapsules (**Table 1.1, entry 7**).[36-37] A miglyol nano-emulsion was first prepared by solvent shifting and further incubated in an aqueous solution of chitosan (MW < 10 kg/mol) for one hour to afford nanocapsules (diameter around 200 nm). The chitosan nanocapsules displayed a preferential association with HT29-M6 cells. Salmon Calcitonin, a polypeptide hormone, was encapsulated with an efficiency of 60% and released over a period of 6h. In 2013, the same authors post-modified the nanocapsules with hepatitis B surface antigen (HB) through electrostatic attraction (CS/HB = 1/0.025, w/w) resulting in a high antigen association efficiency (70%).[38] Imiquimod (a TLR7 receptor agonist) was also incorporated into the oily core of the nanocapsules to elicit a specific

T1-mediated immune response. Chitosan was also modified with MeO-PEG-COOH (5088 g/mol) and biotin-PEG-COOH (4060 g/mol) by EDC catalyzed coupling amidation. An analogous procedure was then used to afford PEG functionalized and biotin-PEG functionalized chitosan based nanocapsules (diameters around 250 and 200 nm, respectively). The presence of PEG (DS = 0.003) enhanced the stability, the biocompatibility and the cellular uptake capability of nanocapsules. The biotin-PEG functionalized nanocapsules were further functionalized with monoclonal antibody anti-TMEFF-2 through a convenient two-stepwise avidin-biotin interaction (**Figure 1.1**). The loading and delivery of docetaxel (DCX) was subsequently investigated. In comparison to free drug, increased efficacy (tumor weight reduced from 1.8 g to 0.8-1.0 g) of encapsulated DCX was shown from *in vitro* cell studies due to the efficient internalization of nanocapsules, but no enhancement of efficacy was observed from *in vivo* studies on lung cancer xenograft model.[39-40] Using a similar methodology, the same group also reported on squalene-loaded PG-nanocapsules (PG, polyglucosamine, highly deacetylated chitosan, 276 kg/mol) (**Table 1.1, entry 8**).[41] Specifically, squalene (core material) was dissolved with lecithin in 2-propanol. The solution was then poured into an aqueous PG solution under stirring, resulting in PG nanocapsules (diameter around 240 nm) after evaporation of 2-propanol. The biodistribution of nanocapsules was preferably limited to the lymphatic circulation, to inject indium-111 labeled nanocapsules into rabbits. The γ-scintigraphy imaging analysis revealed a slow clearance of the nanocapsules from the injection site and their progressive accumulation (3.8% of the injected dose) in the popliteal lymph node over 48h.

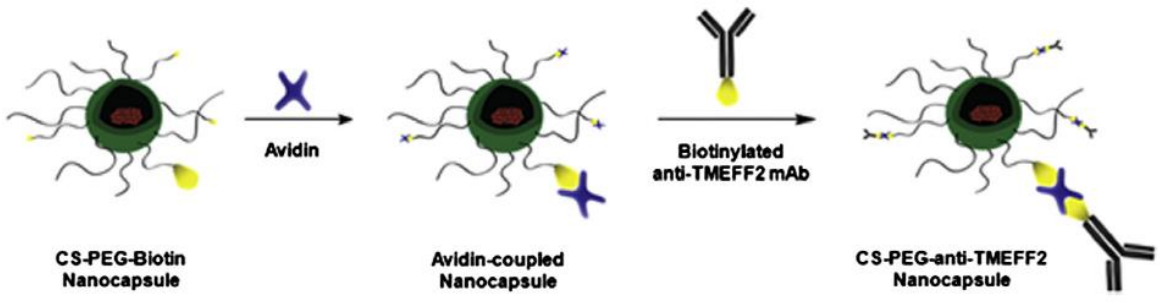

Figure 1.1. Functionalization of CS-PEG-Biotin nanocapsules with anti-TMEFF.[40]

A similar route was also used by Ortega-Vinuesa and coworkers to investigate the influence of molecular weight (MW) and of the acetylation degree (DA) of chitosan on capsules stability (**Table 1.1, entry 9**).[42] An acetone/ethanol solution of miglyol 812 and lecithin was added into aqueous solution of low MW (11 kg/mol, DA ranging from 1.4 to 51%) or high MW (~112 kg/mol, DA ranging from 1.6 to 56%) chitosan to give birth to chitosan-based nanocapsules (diameters ranging from 150 to 185 nm) after solvent evaporation. Interestingly, nanocapsules made of chitosan with intermediate MW and high DA (85%) displayed higher cell uptake capability and stability than epikuron or pluronic® F68 based liposomes.[43-44] Low molecular weight chitosan was capable to deposit at the interface of soybean oil nanoemulsion (generated by solvent evaporation) to afford nanocapsules with a size of 145 nm (**Table 1.1, entry 10**).[45] In view of developing materials for chemotherapy of leishmaniasis, amphotericin B (AmB, prototype leishmanicidal drug) was then loaded with a good steric stability *in vitro*. As revealed by *in vitro* and *in vivo* studies, the encapsulated drug exhibited an enhanced antileishmanial property compared with free drug.

Tzanov and coworkers prepared cationic polysaccharide nanocapsules coated with chitosan and cellulose (**Table 1.1, entry 11**).[46] Thiolated chitosan (TC) was prepared by a coupling reaction between 2-iminothiolane and chitosan (~15kg/mol). Ethylenediamine functionalized cellulose (AC) was synthesized by substitution of tosylated cellulose with ethylenediamine. Oil-loaded nanocapsules were finally obtained through a sonication-induced emulsification of an aqueous solution of polysaccharide (TC or AC) with sunflower oil. The diameters of nanocapsules prepared from TC or AC were 268 and 247 nm, respectively. These cationic polysaccharide nanocapsules were shown to disrupt bacterial membranes and were no cytotoxic to human cells.

Chitosan (150 kg/mol) was also functionalized with mannose by reductive amination (DS = 0.06).[47] A tripolyphosphate (TPP) nanoemulsion with rifampicin (anti-tubercular drug) as core material was generated by stirring of the initial DMSO/water solution and subsequently poured into an aqueous solution of mannose-conjugated chitosan

to afford nanocapsules with a size of 215 nm. The encapsulation efficiency was about 39%, and more than 90% of loaded drug was released after 5h. Cellular uptake was 2.3 times higher in the presence of anchored mannose units (**Table 1.1, entry 12**).

Besides chitosan, Alonso and coworkers prepared miglyol 812-filled hyaluronic acid (HA, 29 or 160 kg/mol) nanocapsules through a one-stage procedure or through polymer coating on preset nanoemulsion (two stage procedure) (**Table 1.1, entry 13**).[48] The size of the HA nanocapsules prepared by the two stage procedure (~250 nm) was bigger than that from the one stage procedure (~180 nm). The HA nanocapsules were capable to load DCX in miglyol and enhance efficacy of DCX *in vitro*. Noteworthy, the HA nanocapsules were stable at 37°C for 90 days.

Preetz *et al.* reported the preparation of miglyol-filled polysaccharide-based nanocapsules by combining emulsification and layer-by-layer strategy (LbL) (**Table 1.1, entry 14**).[49-50] Typically, miglyol 812 was first added into an aqueous solution containing octenyl succinic anhydride modified starch (OSA starch, 400 kg/mol, DS = 0.006). Miglyol-loaded nanocapsules with an OSA starch layer were then generated after emulsification through high pressure homogenization. Chitosan (1400 kg/mol) and lambda-carrageenan (hydrocolloid composing of galactose sulfate esters, DS = 1.05) were then sequentially deposited at the surface of the capsules, generating three-layered nanocapsules with a size of around 130 nm (miglyol/OSA starch/chitosan/carrageenan = 47.35/47.5/1/2.25, mass ratio, PDI = 0.23). Due to the biocompatibility of all the materials, these nanocapsules were generated for applications in food or pharmaceutical industry.

Nanocapsules made of bovine serum albumin-Dextran (BSA-Dextran) conjugate and soybean oil (as core material) were used to load sensitizer/annihilator (s/a) couples for maintaining the mobility of chromophores and avoiding the quenching, displaying an intense photoluminescence emission (**Table 1.1, entry 15**).[51] The nanocapsules (UCNC) encapsulated different s/a couples [PtTPBP/BDP-G (UCNC-G), PtTPBP/BDP-Y (UCNC-Y) or PdOEP/DPA (UCNC-B) to afford green, yellow or blue luminescent emissive nanocapsules (**Figure 1.2**). UCNC-G and UCNC-Y exhibited

up conversion luminescence (UCL) emission (λ_{ex} = 635 nm) with quantum efficiencies of 1.7% and 4.8%, respectively. The resulting nanocapsules may be applied to *in vivo* UCL bio-imaging of mice without skin removal.

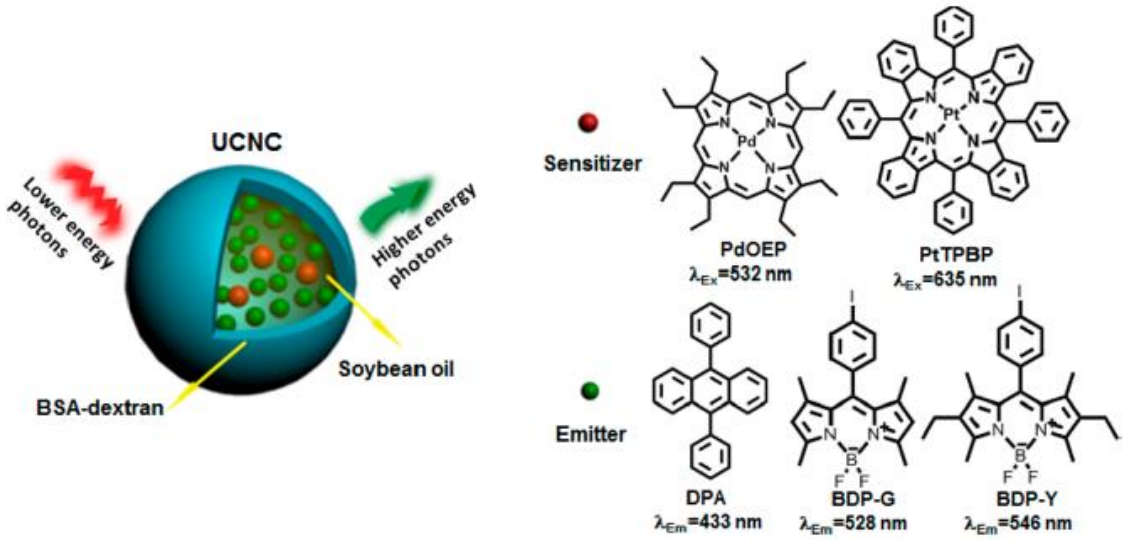

Figure 1.2. Schematic Illustration of TTA-UCL Process of the Upconversion Nanocapsules (UCNC), and Chemical Structures of Sensitizers (PdOEP and PtTPBP) and Annihilators (DPA, BDP-G, and BDP-Y).

Kansal and coworkers reported alginate-containing nanocapsules by combining polymer coating and LbL strategy (**Table 1.1, entry 16**).[52-53] Nano-emulsions were prepared by stirring-induced emulsification using soybean oil in o/w system. The resulting droplets were coated with protamine sulfate. Sodium alginate and protamine sulfate were then sequentially deposited on the capsules to finally generate multilayered nanocapsules (size of around 340 nm). Doxorubicin (DOX) was encapsulated with efficacy above 80%. The anti-leishmanial efficacy of (encapsulated) DOX was proven to be enhanced *in vitro*.

Beloqui *et al.* recently prepared dextran-protamine coated nanocapsules for enhancing the permeability of saquinavir mesylate (SQV, an antiretroviral drug) in cells (**Table 1.1, entry 17**).[54] SQV-loaded lipid nanocapsules (diameter around 150 nm) were prepared using Precirol ATO® 5 and miglyol 812 by high-pressure

homogenization technique and further added into a premixed dextran (3260 g/mol)-protamine solution. Dextran-protamine nanocapsules (D_h of 240 nm) were finally obtained after stirring for 30 min. These SQV loaded nanocapsules significantly enhanced the permeability of SQV (up to 9 times) across Caco-2 cells membranes in comparison to uncoated lipid nanocapsules.

Table 1.1: Emulsification routes to carbohydrate-functionalized nanocapsules.

Entry	Routes	Polymer	Solution	Emulsification Method	Cross-linker	Dimension (nm)	Ref.
1	Double emulsification	Chitosan, Gelatin	Toluene/water/Toluene	Mechanical agitation	Sodium sulphate, glutaraldehyde	100~700	27
2	Double emulsification	Alginate	Water/Phospholopid oil/Water	Stirring	Calcium chloride, chitosan	488	28
3	Emulsion coacervation	Alginate	Acetone or ethanol/Water	Sonication	Calcium chloride	263 (ethanol), 373 (acetone)	29-30
4	Emulsion coacervation	Alginate	Ethanol, benzyl alcohol or DMSO/Water	Sonication	Chitosan	400	31
5	Emulsion coacervation	Alginate	Hexane/Water	Stirring, sonication	Calcium chloride	34	32
6	Polymer coating	Oligochitosan, PECL	Acetone/Water	Stirring		300~500	33-35
7	Polymer coating	Oligochitosan	Acetone/Water	Solvent displacement		200	36-37
8	Polymer coating	Polyglucosamine	2-propanol/Water	Stirring		242	41
9	Polymer coating	Chitosan	Acetone-ethanol/Water	Solvent displacement		148~185	42
10	Polymer coating	Chitosan	Ethanol/Water	Solvent evaporation		145	45

11	Polymer coating	Thiolated Chitosan (TC) or Ethylenediamine- cellulose (AC)	Sunflower oil/Water	Sonication	268 (TC), 247 (AC)	46
12	Polymer coating	Mannose-conjugated Chitosan	DMSO/Water	Agitation	215	47
13	Polymer coating	Hyaluronic acid	Ethanol-acetone/Water	Solvent displacement	180~250	48
14	Polymer coating	OSA starch, Chitosan, lambda-carrageenan	Miglyol/Water	High pressure homogenization	134	49-50
15	Polymer coating	BSA-Dextran	Soybean oil-Toluene/water	High pressure homogenization	93~116	51
16	Polymer coating	Alginate, Protamine	Chlorofom/Water	Agitation	342	52-53
17	Polymer coating	Dextran, Protamine	Water	High pressure homogenization	244	54

1.2.1.5 Mini-emulsion technique

Miniemulsions are kinetically stable oil-in-water dispersions generated by high shear devices such as ultrasonicators. Nanoparticles or nanocapsules can be generated using miniemulsion conditions. In a typical mini-emulsion procedure, water, oil, hydrophobic agents and stabilizers are co-emulsified resulting in the formation of nanodroplets with size ranging from 50 to 500 nm (**Scheme 1.4**).[55] This technique has been successfully applied to radical, ionic, or metal-catalyzed polymerizations, enzymatic or chemical polycondensation and polyaddition reactions. Polymerization normally occurs in the dispersed phase or at the interface of droplets resulting in the formation of a polymeric membrane. Thanks to its potential application in pharmaceutical and cosmetic fields, numerous examples of nanocapsules prepared under miniemulsion conditions have been reported over the last twenty years.

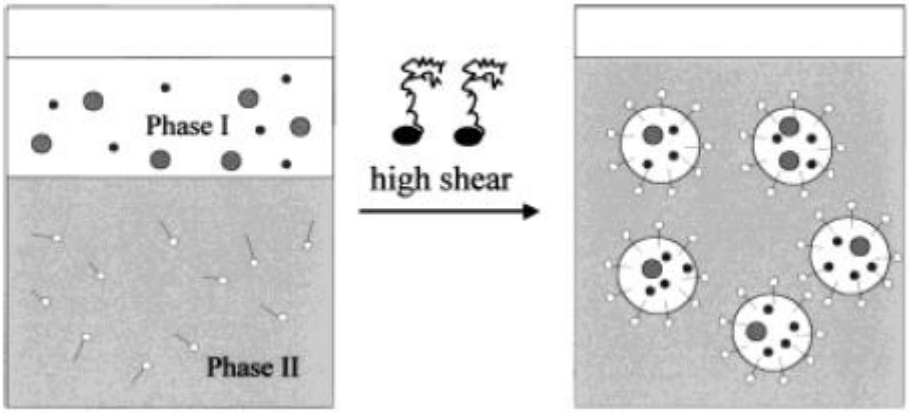

Scheme 1.4. The principle of mini-emulsion.[55]

Chitosan, a biocompatible polysaccharide has been proposed by Landfester and co-workers as candidate for constructing glyconanocapsule membranes via interfacial polymerization under miniemulsion conditions.

In 2002, her group reported the preparation of chitosan-containing nanocapsules using the miniemulsion technique (**Table 1.2, entry 1**).[56] In this seminal work, a solution of toluene containing a diepoxide as cross-linker (Epikote E828), Jeffamine D2000 as cosurfactant and various diamines (1,12-diaminododecane,

4,4'-diaminodicyclohexylmethane, 4,4'-diaminobibenzyl) were dispersed in an acidic aqueous solution of chitosan. Ultrasonication of the emulsion at 0°C afforded a stable mini-emulsion. Cross-linking via epoxy-amine reations was initiated by increasing the temperature of the medium up to 68°C, leading to the formation of polymeric nanocapsules with diameter ranging from 130 to 280 nm.

Zhu and co-workers described a route to chitosan-based nanocapsules loaded with felodipine, a hydrophobic anti-hypertensive drug (**Table 1.2, entry 2**).[57] Capsules were built using an interfacial free radical polymerization approach involving *N*-maleoylchitosan (NMCS) (Chitosan, 500 kg/mol, DS = 0.23) as macromonomer. A surfactant Triton X-100 and a felodipine/chloroform mixture were dispersed in an aqueous phase containing NMCS. Polymerization of the vinyl groups at the (chloroform/water) interface initiated by $K_2S_2O8/NaHSO_3$ gave birth to nanocapsules with a diameter of 100 nm. Kinetics of drug release was in correlation with feed concentration and the DS of NMCS. The drug encapsulation efficiency was independent of feed concentration (~80%). In a similar manner, Chen *et al.* cross-linked *N*-maleoyl-modified chitosan (MCS) (Chitosan, 5 kg/mol, DS = 0.48) with 1,4-butanediol bis(3-mercapto-propionate) via UV-induced thiol-ene reaction at the oil/water interface (**Figure 1.3**).[58] The generated chitosan nanocapsules (size of 60~390 nm) were used to encapsulate anti-cancer drug (DOX). Thanks to the presence of pH-sensitive cross-linkers, the release of DOX was easily mediated by adjustment of pH of the solution (**Table 1.2, entry 3**).

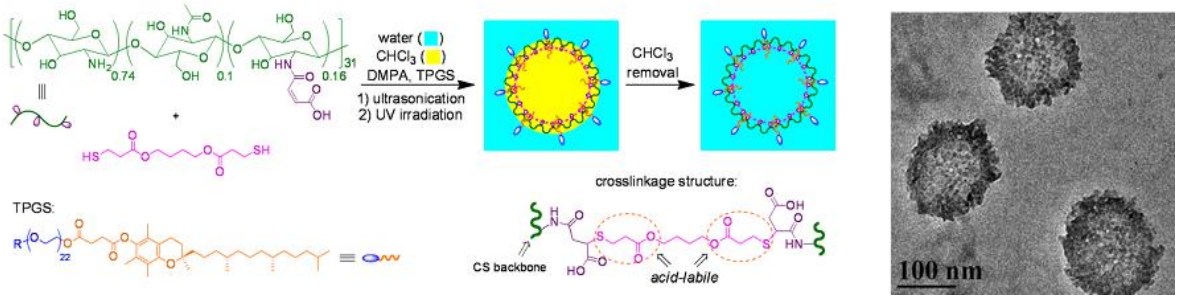

Figure 1.3. Preparation and TEM picture of modified chitosan nanocapsules.[58]

In 2010, Zhang *et al.* designed Pluronic F127-chitosan based nanocapsules (**Table**

1.2, entry 4).[59] The shell of the capsules was fabricated by interfacial reaction of chitosan (2.5 kg/mol) with carboxylic acid end-functionalized Pluronic F127 PEO_{100}-PPO_{65}-PEO_{100} (12.6 kg/mol) under mini-emulsion conditions. Owing to the thermo-responsible character of Pluronic F127, the size of nanocapsules evolved from 37 nm at 37°C to 240 nm at 4°C, thus modifying the permeability of capsules' shell. Therefore, encapsulation and release of small molecules drugs (ethidium bromide, Mw = 394.3 g/mol) were easily controlled by shifting the temperature. The biocompatible pluronic F127-chitosan nanocapsules were identified by the authors as potential candidates for drug delivery applications in cancer treatments (**Figure 1.4**).

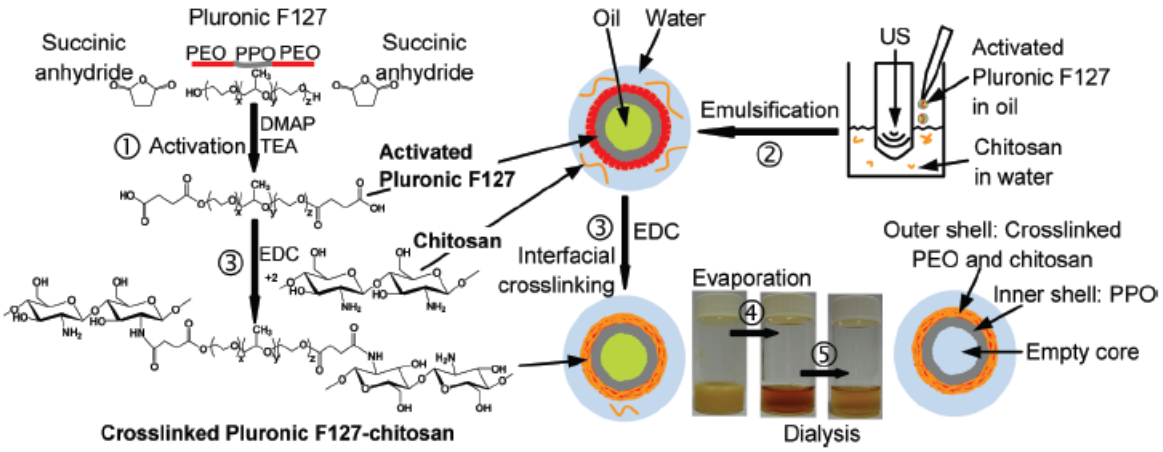

Figure 1.4. Schematic representation of the preparation of Pluronic F127-chitosan nanocapsules by interfacial polymerization in emulsion conditions.[59]

Besides chitosan, other polysaccharides have also been used to build nanocapsules. For instance, in 2006, dextran-based cross-linked nanocapsules were reported by Jiang *et al.*[60]. Nanocapsules were formed either from methacrylated N,N-diethylaminoethyl dextran (DexMA) (500 kg/mol) aqueous solution or from DexMA (in water) and methacrylated polylactide (PLAM) (M_n = 2.1 kg/mol) in chloroform. After emulsification by mechanical agitation and subsequent addition of initiator, interfacial polymerization started at the interface of the nanodroplets to generate capsules (**Figure 1.5, Table 1.2, entry 5**). In contrast to dextran-based nanocapsules (D_h = 200 nm, thickness = 30 nm), the nanocapsules composed of DexMA and PLAM possessed a much thicker membrane walls (D_h = 233 nm,

thickness = 60 nm), which significantly slowed down the release of core-loaded ibuprofen (an anti-inflammatory drug).

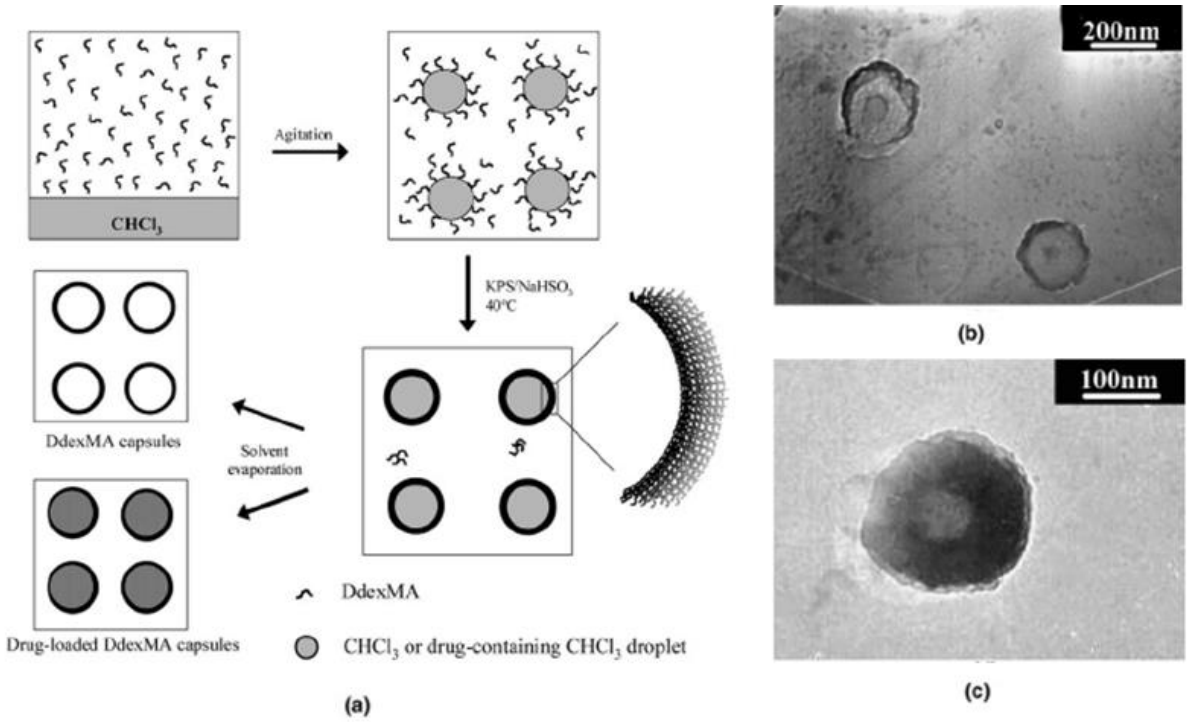

Figure 1.5. (a) Schematic diagram of the preparation of dextran based nanocapsules through interfacial polymerization under miniemulsion conditions. (b) TEM picture of DexMA based glyconanocapsules. (c) TEM picture of DexMA-PLMA based glyconanocapsules.[60]

In 2007, Landfester reported the preparation of hydrophilic compound-loaded nanocapsules by applying an inverse miniemulsion process.[61-63] After emulsification of dextran (70 kg/mol) or starch in water/cyclohexane solution, tolylene-2,4-diisocyanate (TDI, cross-linker) was added to initiate the interfacial polyaddition at 60°C to afford water-filled nanocapsules with a diameter of around 320 nm (dextran) or 520 nm (starch). The thickness of the shell was tuned by adjusting the concentration of reactants (ranging from 10 nm to 20 nm, dextran) (**Table 1.2, entry 6**). Dextran-containing capsules were used to encapsulate hydrophilic contrast agent Magnevist®, while starch-based nanocapsules were loaded with silver nanoparticles (diameter of 14 nm) or DNA (efficiency of 85%) during the emulsification step. The size of the starch-containing capsules (from 300 to 900 nm) could be mediated by introducing different concentration of surfactant poly[(ethylene-*co*-butylene)-

b-(ethylene oxide)] (P(E/B-*b*-EO), 7300 g/mol)[64] and of silver particles[65]. Recently, the same group described another route to dextran nanocapsules with aqueous core through inverse miniemulsion process.[66-67] After emulsification, acrylated dextran (40 kg/mol, DS between 0.13 and 0.55) was cross-linked by interfacial olefin metathesis with phenyl-di(undec-10-en-1-yl)-phosphate. The generated nanocapsules (diameter ~ 280 nm) were shown to be biocompatible (**Table 1.2 entry 7**).

Using a similar process, the Landfester's group also generated hydroxyethyl starch (HES)-based nanocapsules (**Table 1.2, entry 8**).[68] After emulsification in a water/cyclohexane system, HES (200 kg/mol) was cross-linked with TDI at the water/cyclohexane interface to generate water-loaded nanocapsules with a diameter of 275 nm (**Figure 1.6**). After covalent coupling with folic acid (FA), the functional nanocapsules were specifically uptaken by HeLa cells. The HES containing nanocapsules were also decorated with mannose moieties.[69] The targeting effect of these mannosylated HES nanocapsules was proven by *in vitro* experiments.

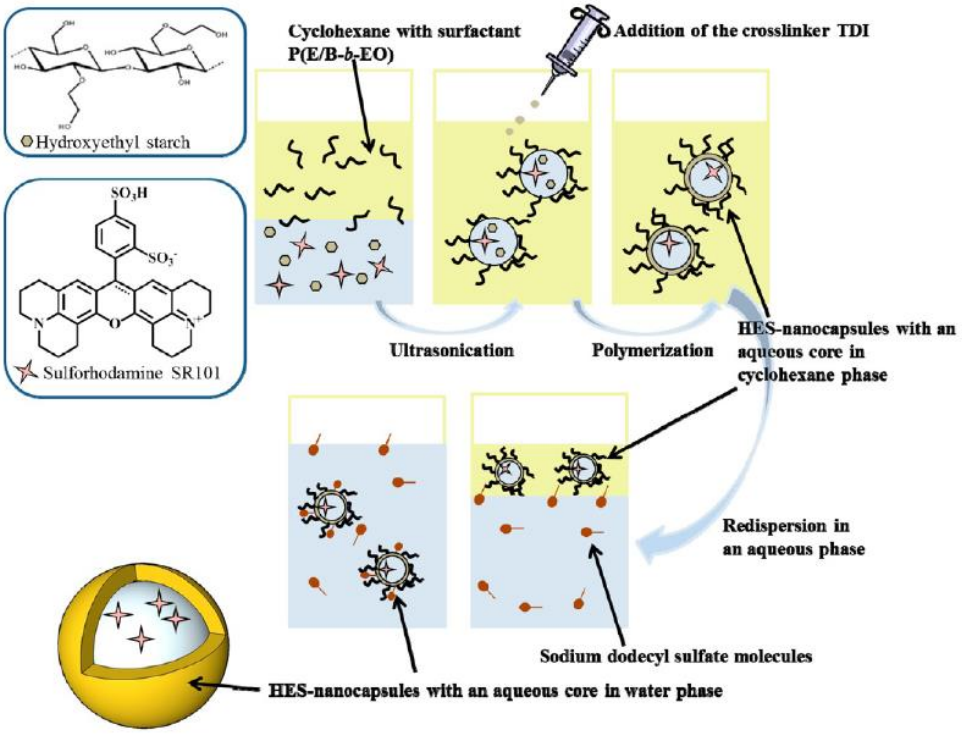

Figure 1.6. Preparation of HES nanocapsules using inverse miniemulsion process.[68]

The same group also described the preparation of enzyme-responsive hyaluronic

acid-based nanocapsules using the same approach (**Table 1.2, entry 9**).[70] After emulsification, hyaluronic acid (140 kg/mol) was cross-linked by TDI to form water-loading nanocapsules with a diameter of 350 nm. The nanocapsules were then used to load polyhexanide, an anti-bacterial agent. The release of polyhexanide was triggered by addition of enzyme hyaluronidase.

Glyconanocapsules were also generated from an A_2+B_2 interfacial step growth polymerization under oil/water miniemulsion conditions (**Table 1.2, entry 10**).[71] After emulsification by sonication, interfacial CuAAC polymerization of 6,6'-diazido-6.6'-dideoxysucrose (in the aqueous phase) and bi(propargyloxy)butane (in the miglyol phase) resulted in the formation of stable glyconanocapsules with a D_h value of 200 nm (**Figure 1.7**).

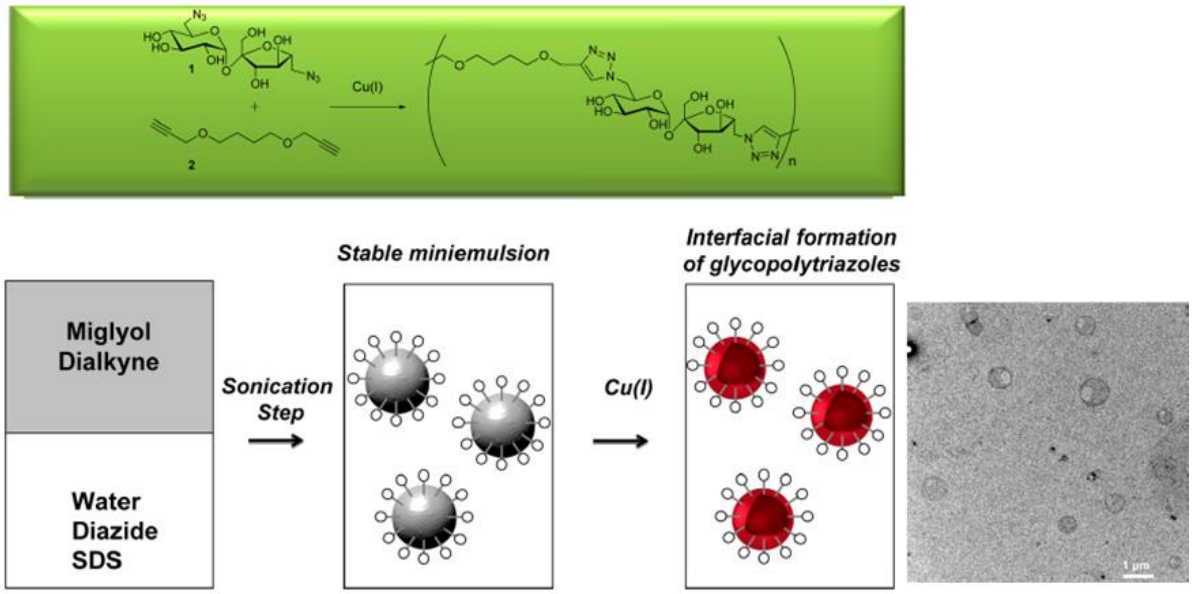

Figure 1.7. Preparation of glyconanocapsules by interfacial CuAAC step growth polymerization[71].

Table 1.2: Formation of carbohydrate-functionalized nanocapsules using mini-emulsion conditions.

Entry	Interfacial Reactions	Polymer	Monomer	Solution	Emulsion method	Cross-linker	Dimension (nm)	Ref.
1	Cross-linking	Diamine, Chitosan		Toluene/Water	Ultrasonication	diepoxide	130~280	56
2	Cross-linking	N-maleoylchitosan		Chloroform/Water	Mechanical agitation		100	57
3	Cross-linking	N-maleoylchitosan		Chloroform/Water	Ultrasonication	1,4-butanediol bis(3-mercapto-propionate)	57~388	58
4	Cross-linking	Chitosan		1,4-dioxane/Water	Ultrasonication	Pluronic F127 PEO_{100}-PPO_{65}-PEO_{100}	37~240	59
5	Cross-linking	N,N-diethylaminoethyl dextran, polylactide macromonomer		Chloroform/Water	Mechanical agitation		233	60
6	Cross-linking	Dextran or Starch		Water/Clyclohexane	Sonication	Tolylene diisocyanate	324 (dextran), 524 (starch)	61-63
7	Cross-linking	Acrylated dextran		Water/Clyclohexane	Sonication	Phenyl-di(undec-10-en-1-yl) phosphate	280	66-67
8	Cross-linking	Hydroxyethyl starch		Water/Clyclohexane	Sonication	Tolylene diisocyanate	275	68
9	Cross-linking	Hyaluronic acid		Water/Clyclohexane	Sonication	Tolylene diisocyanate	350	70
10	Polymerization		6,6'-diazido-6,6'-dideoxysucrose, bio(propargyloxy) butane	Miglyol/water	Sonication		200	71

1.2.2 Formation of hollow nano-objects from amphiphilic copolymer self-assembly

1.2.2.1 Polymersomes

The word *polymersome* was first coined by Discher in 1999 and refers to polymers capable to mimic the self-assembly of liposomes.[72] Polymersomes or polymeric vesicles are nano- or micro-sized polymeric capsules with a bilayered membrane comprising of amphiphilic block copolymers.[73] The amphiphilic membrane structure of polymersomes is very similar to liposomes, but liposomes are built from the assembly of phospholipids with molecular weight typically less than 1 kg/mol, while polymersomes are prepared by self-assembly of amphiphilic block copolymers with molecular weight up to several hundreds thousands g/mol. This provides superior physical and chemical stability to polymersomes over liposomes.

Owing to energetic repulsion effects between the (chemically different) macromolecular segments, amphiphilic block copolymers self-assemble in solution. The length of the blocks, the degree of repulsion and the nature of the solvent drive the self-assembly of the block copolymers into a myriad of morphologies such as spherical micelles, rods and vesicles (polymersomes). In general, the formation of polymersomes is observed when the fraction of the hydrophilic segment is less than 25%. Solvent displacement, rehydration and injection techniques have been applied for generating polymersomes with size ranging from 50 to 800 nm.

In the next section we provide an overview on the routes to carbohydrate-fuctionalized polymersomes relying on the self-assembly of amphiphilic carbohydrate-based block copolymers.

Amphiphilic block copolymers with a glycopolymer segment

In 1999, the group of Fu-Mian Li reported the first example of glyco-polymersomes through self-assembly of amphiphilic block copolymers (**Table 1.3, entry 1**).[74-75] Block copolymers with a glycopolymer segment, polystyrene-*b*-poly[(2-*β*-D-glucopyranosyloxy)ethyl acrylate] (PS-*b*-PGEA) and different block lengths were

designed by sequential ATRP polymerizations (PS_{101}-*b*-$PGEA_7$, PS_{88}-*b*-$PGEA_4$, PS_{77}-*b*-$PGEA_6$ and PS_{55}-*b*-$PGEA_9$). The block copolymers were then dissolved in organic solvents such as dioxane. Self-assembly of the block polymers was then induced by addition of DMF resulting in several morphologies (from vesicles to fibers) (**Figure 1.8**).

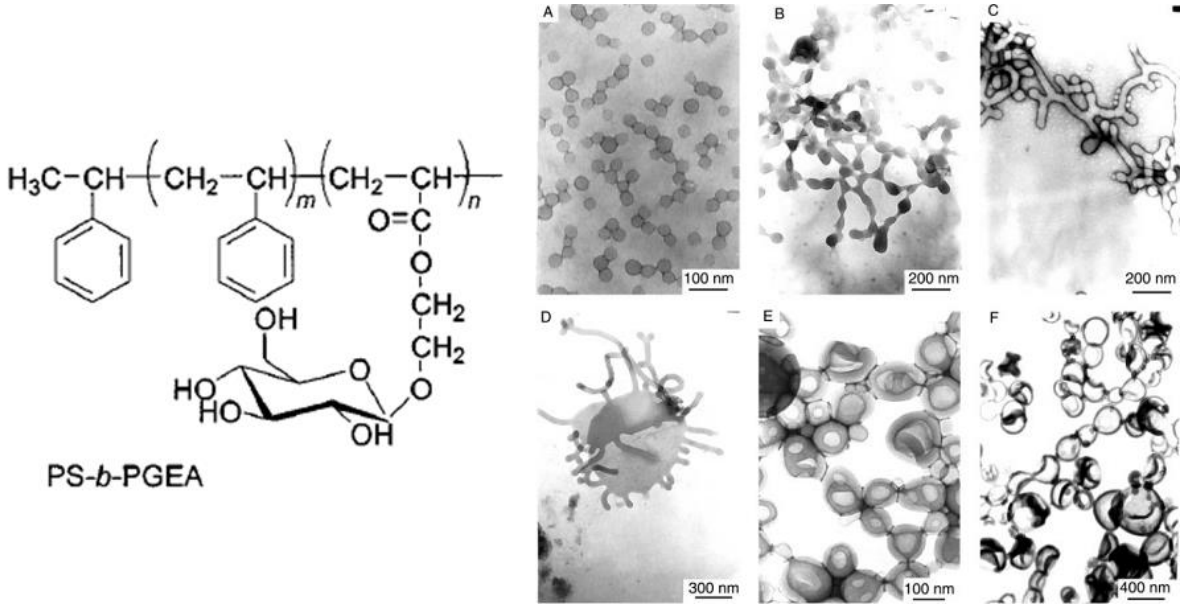

Figure 1.8. Morphologies obtained from PS_{55}-*b*-$PEGA_9$ in dioxane/DMF mixtures.[74-75] Content of dioxane (wt%): (A) 0, (B) 10, (C) 30, (D) 50, (E) 80, (F) 100.

In 2004, the group of Chaikof reported the preparation of triblock copolymers, poly(L-alanine)-*b*-poly(2-acryloyloxyethyllactoside)-*b*-poly(L-alanine) (**AGA**) with different segment ratios (From $A_{10}G_{10}A_{10}$ to $A_{22}G_{52}A_{22}$) by sequential ATRP and ring-opening polymerizations (**Table 1.3, entry 2**).[76-77] These block copolymers spontaneously self-assembled in aqueous solution. The resulting morphologies varied from spheres to worm-like aggregates and were controlled by the polymer concentration and the pH of the solution. A vesicular morphology was generated from $A_{22}G_{52}A_{22}$ at 10 mg/L in acidic aqueous solution (pH 2).

In 2006, the group of Schlaad post-modified 1,2-polybutadiene-*block*-polystyrene (PB_{85}-*b*-PS_{351}) by thiol-ene “click” reaction with thiol-functionalized glucose moieties. The prepared amphiphilic glycopolymer chains (17% wt glucose) spontaneously

self-assembled into glycopolymersomes (R_h = 250 nm) in THF or H_2O (**Table 1.3 entry 3**).[78-79] Three years later, the same group reported on the post-modification of 1,2-polybutadiene-*block*-poly(ethylene oxide) (PB_{68}-*b*-PEO_{34}) with thiol-functionalized glucose (6-9% wt per chain).[80] The obtained copolymers self-assembled in aqueous solution to form vesicles (R_h = 280 nm) (**Table 1.3, entry 4**). 2D-NOESY-NMR and surface-enhanced Raman proved that the formed membrane displays an asymmetric structure with sugar moieties on the outer surface and PEO inside.

In 2007, Murphy *et al.* produced glycopolymersomes using a multi-step strategy (**Table 1.3, entry 5)**.[81] Poly(macromonomer)s (PMMs) bearing various carbohydrate residues (galactose, glucose, ribose and xylose) were prepared by repeating ring opening metathesis polymerization (ROMP). Depending on terminal functionalization by norbornene, the PMMs were capable of conducting further polymerization. After coupling with polyethylene glycol (PEG), amphiphilic block copolymers (PMMs-*b*-PEG) with different segments ratios were prepared (**Figure 1.9**). Nano-objects exhibiting different morphologies were generated after self-assembly of these block copolymers in aqueous solution. Polymersomes with a hydrodynamic diameter of 230 nm were prepared from $PMMs_{20}$-*b*-PEG_{110}. One year later, Xiao *et al.* synthesized an aldehyde-functionalized glycomonomer, 1,2,3,4-di-isopropylidene-6-*O*-(2'-formyl-4'-vinylphenyl)-D-galactopyranose (IVDG), which was polymerized by RAFT polymerization (M_n = 13 kg/mol, $Đ$ = 1.09). After deprotection of the sugar moieties, glycopolymersomes with R_h ranging from 80 to 205 nm were generated through solubilization in water. The resulting vesicles were further used to immobilize BSA proteins thanks to the presence of aldehyde groups on the shell (**Table 1.3, entry 6)**.[82]

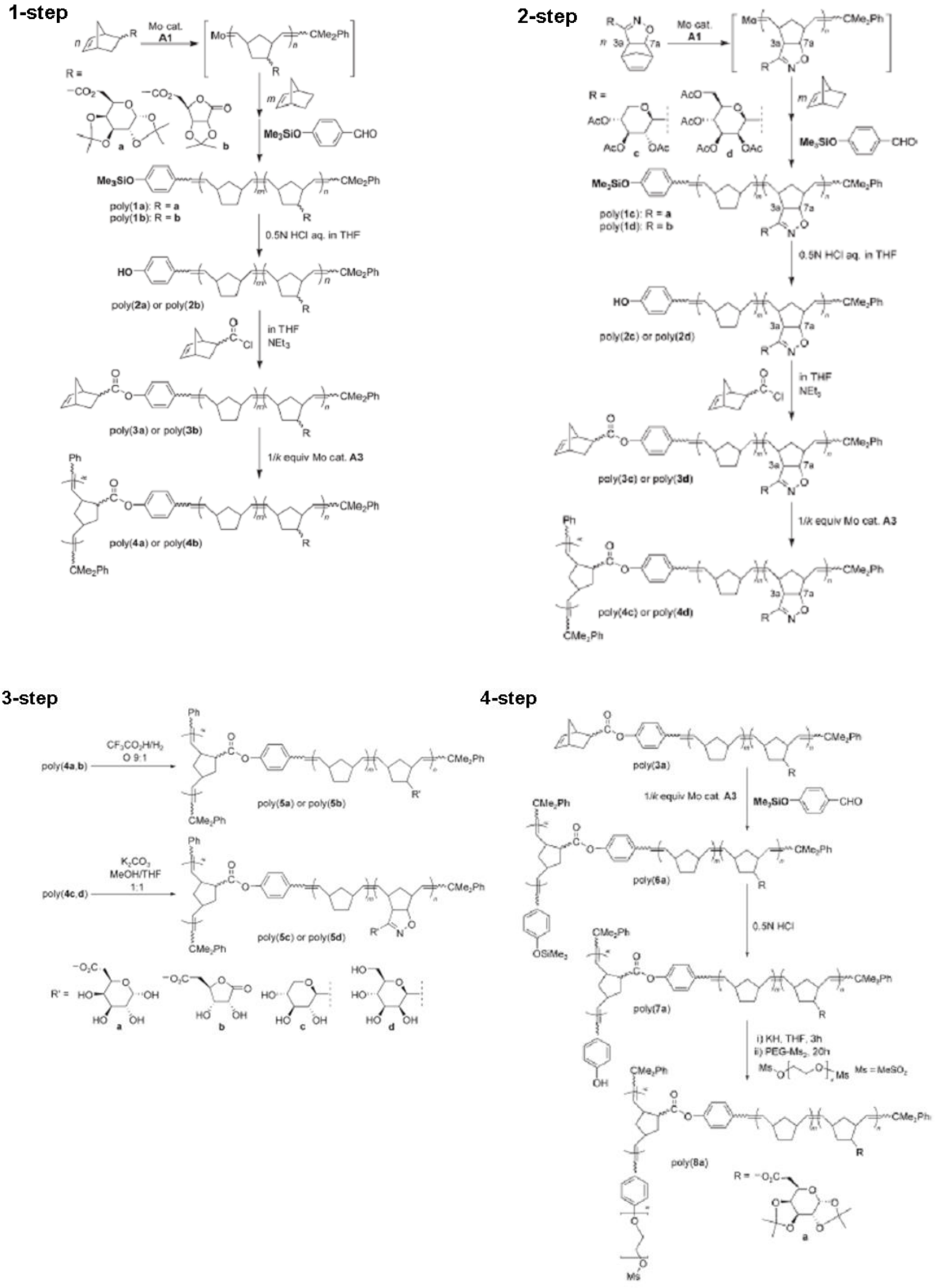

Figure 1.9. Synthetic route to PMMs-*b*-PEG.[81]

In 2008, Dong's group prepared 4-arm star-shaped poly(ε-caprolactone)-*b*-glycopolymer block copolymers (SPCL-*b*-PGAMA and SPCL-*b*-PLAMA) by combining ring opening polymerization (ROP) of ε-caprolactone using pentaerythritol as initiator and subsequent chain-extension ATRP polymerization of gluconamidoethylmethacrylate (GAMA) or lactobionamidoethylmethacrylate (LAMA).[83-84] By varying the length of the glycopolymer segments, the produced 4-arm glyco-copolymers (SPCL-*b*-PGAMA and SPCL-*b*-PLAMA) spontaneously self-assembled in aqueous solution to form vesicles, micelles or worm-like nano-objects (**Table 1.3, entry 7 and 8**). Vesicles were only generated by self-assembly of $SPCL_{50}$-*b*-$PGAMA_5$ (hydrodynamic diameter of 250 nm) or $SPCL_{75}$-*b*-$PLAMA_{11}$ (432 nm) in water. In order to enhance the overall biocompatibility of the objects, α-cyclodextrin molecules (α-CD) were included on PCL chains (1,6-Hexanediol initiated ROP) before chain-extension through ATRP polymerization of GAMA.[85] Polymersomes with a diameter of 81 nm were obtained via self-assembly of the α-CD functionalized $PGAMA_4$-PPR_{20}-$PGAMA_4$ (PPR for Pcl-based PolypseudoRotaxane) in the aqueous phase (**Table 1.3, entry 9**). Utilizing G0 PAMAM dendrimer as an initiator of ROP, Dong and coworkers synthesized a novel 4-arm star-shaped polypeptide-*b*-glycopolymer (SPBLG-*b*-PGAMA) composed of poly(γ-benzyl L-glutamate) core blocks and of poly(D-gluconamidoethyl methacrylate) shell blocks.[86] The resulting pH-sensitive vesicles ($SPBLG_{36}$-*b*-$PGAMA_{39}$, D_h = 274 nm) exhibited both good DOX-loading and long term release properties, making them promising candidates for drug release applications (**Table 1.3, entry 10**).

Stenzel's group reported block copolymers having pendent glucosamine and uridine moieties.[87] The monomers, 5'-*O*-methacryloyl uridine (MAU) and 2-methacrylamido glucopyranose (MAG), were first prepared by chemo-enzymatic reaction and sequentially polymerized through RAFT polymerization. Self-assembly of the block copolymers by solvent displacement process (DMA solution dialyzed against water) generated nano-objects with morphologies evolving from micelles to worm-like

micelles with increasing length of PMAU segments (**Table 1.3, entry 11**). Polymersomes having a hydrodynamic diameter around 35 nm were obtained by self-assembly of $PMAG_{59}$-*b*-$PMAU_{36}$. The polymersomes were shown to display an outer shell constituted of PMAG and a core built from PMAU segments. Owing to the establishment of H-bonding interactions between adenosine and PMAU, these materials were thought to be potential therapeutic carriers for ASONs (antisense oligonucleotides). More recently, the same group prepared random copolymers from *N*-isopropylacrylamide (NIPAAM)/ *N*-homocysteine thiolactone acrylamide (TiaAm) by RAFT copolymerization. After polymerization, the pendent thiolactone groups were then opened with various amines (*n*-propylamine, *n*-hexylamine and *n*-dodecylamine) to release thiol moieties which were finally reacted *in situ* with 2-bromoethyl-2′,3′,4′,6′-tetra-*O*-acetyl-α-D–mannopyranoside (**Figure 1.10**). Employing a solvent displacement strategy, these double modified copolymers gave birth to micelles (ring opening with *n*-propylamine), large compound micelles (ring opening with *n*-dodecylamine) or vesicles at 100-600 nm (ring opening with *n*-hexylamine) which could specifically bind ConA lectin (**Table 1.3, entry 12**).[88]

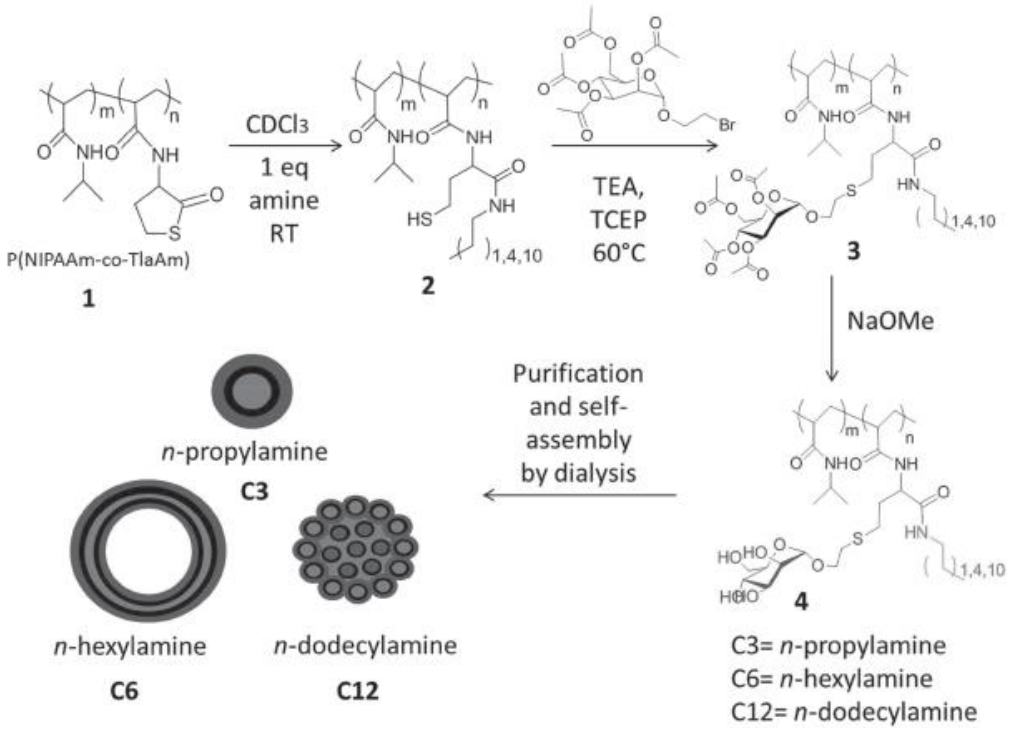

Figure 1.10. Access to various glyconano-objects through double post-polymerization

modification of block copolymers.[88]

In 2011, Aissou *et al.* reported on the preparation of fluorescent vesicles consisting of galactose-based amphiphilic copolymers with a π-conjugated sequence.[89] The block copolymer, poly(3-hexylthiophene)-*block*-poly(3-*O*-methacryloyl-D-galactopyranose), ($P3HT_{25}$-*b*-$PMAGP_{97}$) was prepared by coupling propargyl *ω*—functionalized PGMAP chains (M_n = 24.4 kg/mol, *Đ* = 1.06) with azide-functionalized poly(3-hexylthiophene) (M_n = 4.2 kg/mol, *Đ* = 1.06) through CuAAC. During the solvent shifting process (1% w/w polymer THF solution with water), the block copolymer self-assembled into signal-emitting fluorescent vesicles (R_h = 89 nm, λ_{ex} = 365 nm, $\lambda_{em,\ max}$ = 470 nm) without addition of any dye (**Figure 1.11, Table 1.3, entry 13**).

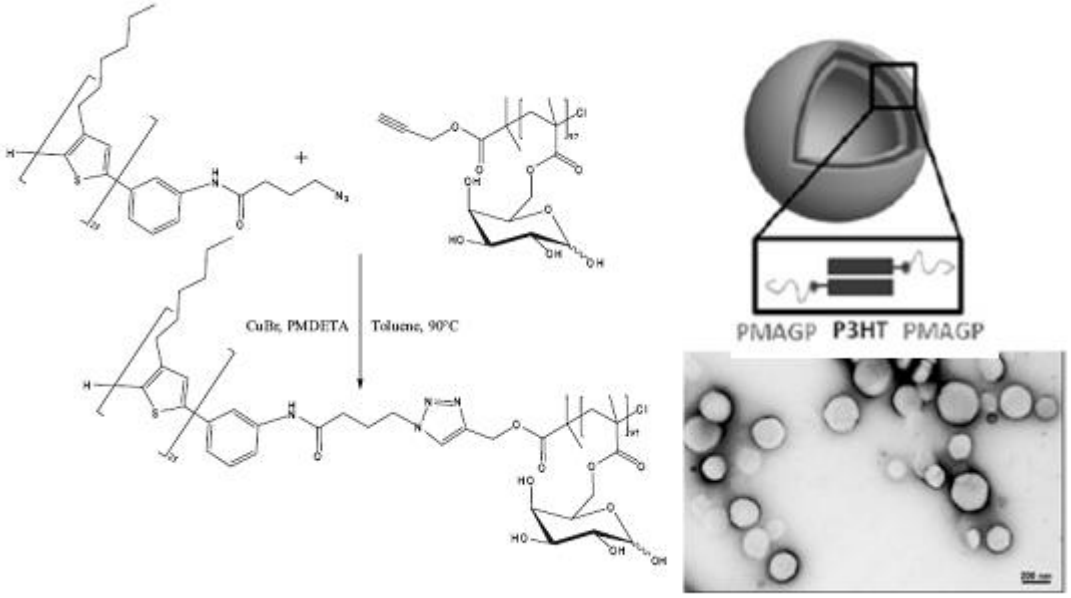

Figure 1.11. Fluorescent vesicles formed from self-assembly of $P3HT_{25}$-*b*-$PMAGP_{97}$.[89]

Du *et al.* studied the synthesis and self-assembly of glycosamide-grafted glycopolysiloxanes (**Table 1.3, entry 14**).[90] The authors first prepared aminopropyl functional polysiloxanes (APFPS) by ring opening polymerization of octamethylcyclotetrasiloxane (D4) in the presence of 3-aminopropyldiethoxymethylsilane (APDEMS) and tetramethylammonium hydroxide (TMAH, catalyst). The resulting polymers were further reacted with glyconolactone to give glycopolysiloxanes. Investigation on the self-assembly behavior of the

glycopolysiloxanes in aqueous solution highlighted the formation of large vesicles (300-600 nm).

Lecommandoux and coworkers synthesized polypeptide block copolymers (PBLG-*b*-PGG) through sequential ring-opening polymerization of benzyl-L-glutamate and propargylglycine (PG) *N*-carboxyanhydrides with different segments ratios ($PBLG_{20}$-*b*-PGG_n, n = 5~32).[91] The glycosylated block copolymers were further obtained by post-polymerization modifications with azide-functionalized galactosides through CuAAC ligation (**Figure 1.12**). The block copolymers self-assembled through solvent shifting process into morphologies ranging from worm-like micelles (addition of water in DMSO) to polymersomes (addition of DMSO in water) depending on polymer composition and on the solvent shifting process. Stable vesicles (R_h = 32 nm) were obtained from $PBLG_{20}$-*b*-PGG_{25} by adding water into DMF solution of copolymer. The vesicles were shown to specifically bind Con A lectin (**Table 1.3, entry 15**).

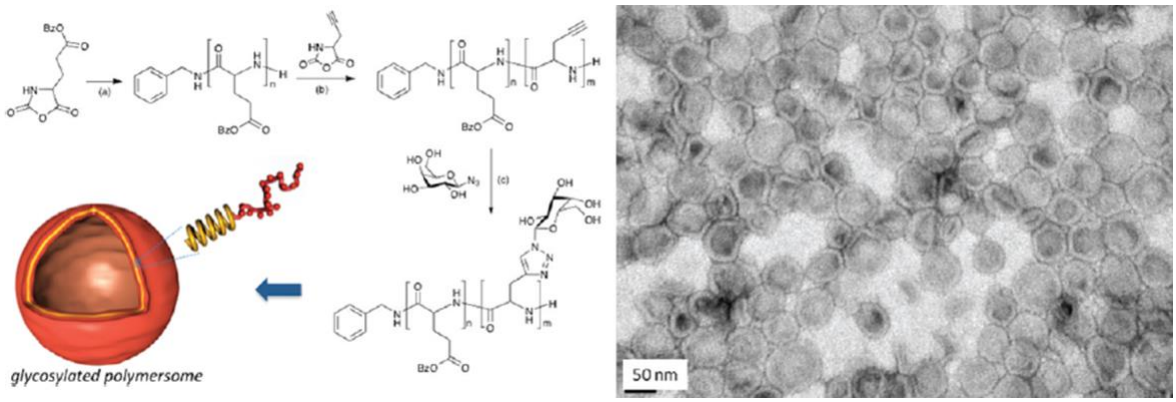

Figure 1.12. Synthesis of PBLG-*b*-PGG block copolymers (Left) and high magnification TEM image of galactosylated polymersomes made of $PBLG_{20}$-*b*-PGG_{25} (Right).[91]

Pasparakis and Alexander constructed block copolymers from 2-glucosyloxyethyl methacrylate (PGEMA) and diethyleneglycol methacrylate (PDEGMA) using sequential ATRP (P1, M_n = 11.2 g/mol, $Đ$ = 1.34, LCST = 28°C) or RAFT (P2, M_n = 15.2 g/mol, $Đ$ = 1.11, LCST = 28°C) polymerizations.[92] The self-assembly of the block copolymers in water led to the generation of temperature-responsive glycovesicles (20°C, 250 nm for P1 and 500 nm for P2). At 37°C (above the LCST of PDEGMA), the size of the vesicles decreased to 182 nm (P1) and 300 nm (P2), owing to the collapse

of the PDEGMA segments (**Table 1.3, entry 16**). The vesicles were capable to interact with Con A lectin and *E. Coli* bacteria. Interestingly, vesicles from P1 were proven to be considerably more efficient than vesicles from P2.

Huang *et al.* prepared poly(L-lysine)-*graft*-hexanoyl lactobionolactone by introducing lactose moieties on hexanoyl-grafted poly(L-lysine) through ring opening reaction of lactobinolactone (a model targeted ligand to HepG2 liver cells).[93] The resulting copolymers self-organized in water (the methanol solution of polymer was dialyzed against water) to form pH-sensitive vesicles (R_h = 110 nm at pH 7.4). The resulting morphologies were subsequently cross-linked by genipin (**Table 1.3, entry 17**). Decrease of pH to 4.68, resulted in an increase in size to 130 nm. The vesicles were finally used to load anti-cancer drug Dox (efficiency up to 70%) and release it (40.1% in 6h at pH 4.68) by adjusting the pH value.

Photosensitive glyconanocapsules were designed by Das and coworkers.[94] Poly(spiropyran methacrylate)-*b*-poly(3-*O*-4-vinylbezoyl-D-glucopyranose) (PSP_8-*b*-PBG_{32}) block copolymers were synthesized in two steps by ATRP polymerization (**Table 1.3, entry 18**). The prepared copolymers self-assembled to generate glyconanocapsules with a diameter of 366 nm by solvent shifting (addition of water into DMF). Due to the UV-sensitivity of the PSP segments, UV irradiation (1h, λ = 360 nm) led to photoisomerization resulting in conversion of hydrophobic PSP into hydrophilic groups and further disruption of the polymer aggregates into 48 nm nano-objects. Increasing the wavelength to 560 nm for another hour gave back the closed ring SP form resulting in regeneration of capsules with D_h of 160 nm. The capsules were subsequently used to encapsulate and release coumarin 7 (a hydrophobic fluorescent dye) by adjustment of the UV wavelength.

The group of Jiang developed thermo-sensitive polymer vesicles mimicking glycocalyx for studying carbohydrate-protein interactions.[95] The authors first prepared two hydrophilic glycopolymers (PGal, $\overline{M_w}$ = 14 kg/mol, *Đ* = 1.18 and PGlc, $\overline{M_w}$ = 14 kg/mol, *Đ* = 1.20) containing galactoside (Gal) and glucoside (Glc) pendent units

and a thermo-sensitive PNIPAAM ($\overline{M_w}$ = 7 kg/mol, *Đ* = 1.10) having a phenylboronic acid (BA) at one chain end using RAFT polymerization (**Table 1.3, entry 19**). Owing to the formation of dynamic covalent bonds between BA and the pendent sugars moieties in basic conditions (pH = 9), the authors prepared "graft copolymer like" structures. Thanks to the thermo-sensitive character of the PNIPAAM block (~32°C), the PNIPAAM-BA/glycopolymers (2/1) mixtures were shown to self-assemble at 33°C to give birth to uniform vesicles (R_h = 62 nm and 68 nm, PDI = 0.09 and 0.10 for V-PGal and V-PGlc, respectively). DLS experiments highlighted that sugar-coated vesicles were capable to specifically interact with appropriate lectin (PNA and ECA for PGal and none for PGlc). The same group also reported the preparation of glyco-vesicles with a sugar core and a PS shell (**Table 1.3 entry 20**).[96] A block copolymer polystyrene-*b*-poly(tetra-acyl-α-1-mannosyl styrene) (PS_{75}-*b*-$PManAc_{25}$) was generated by RAFT polymerization in THF. The deacetylation of the PManAc block in THF triggered a self-assembly process, leading to the formation of vesicles with glyco-inside structure (R_h = 42 nm, R_g/R_h = 0.96). The vesicles were decorated with gold nanoparticles in the core by directly adding $HAuCl_4$ (0.2 mM) to the vesicles solution of PS_{75}-*b*-$PMan_{25}$ in THF. Importantly, no addition of reducing agent was required. Solvent shifting (addition of water to THF) led to the destruction of vesicles and formation of micelles (R_h = 11 nm) with a glycopolymer shell and a PS core (**Figure 1.13**).

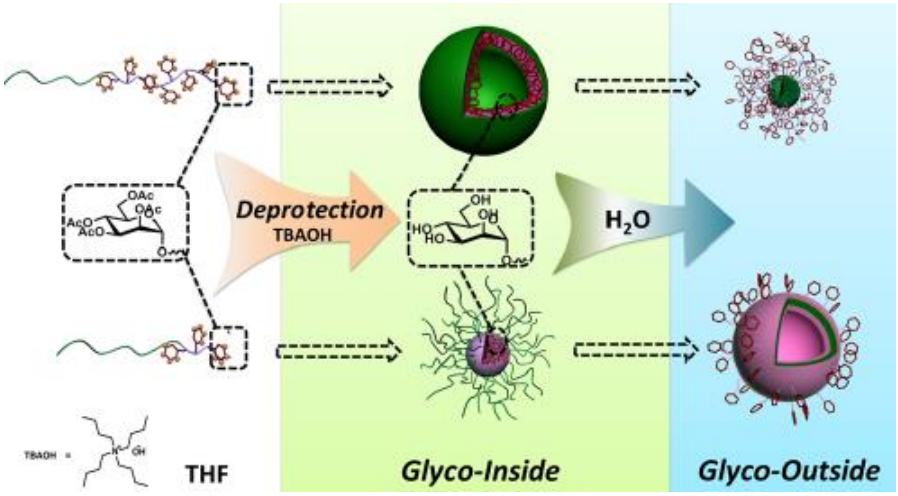

Figure 1.13. Glyco-inside and glycol-outside morphologies reported by Jiang and co-workers.[96]

Polysaccharide-based polymersomes

In view of generating nanocapsules for biomedical applications, polysaccharides which are natural polymers are ideal candidates due to their large availability, biocompatibility and biodegradability.

Dextran

The group of Gnanou designed dextran-based vesicles by self-assembly of amphiphilic dextran-*block*-PS (**Table 1.3 entry 21**).[97-98] The anomeric extremity of a commercial dextran (M_n = 6600 g/mol) was firstly converted into an ATRP initiating site by reductive amination. The resulting macroinitiator was then engaged into the controlled polymerization of styrene to afford Dextran$_{40}$-*b*-PS$_n$ (n = 5, 270, 775) block copolymers. Depending on the length of the PS block, micelles (Dextran$_{40}$-*b*-PS$_5$, R_h = 28 nm) and vesicles (Dextran$_{40}$-*b*-PS$_{270}$, R_h = 64 nm or Dextran$_{40}$-*b*-PS$_{775}$, R_h = 77 nm) were obtained upon displacement of the organic solvent (THF or DMSO-THF) by water. Finally, the size and the shape of the assembled nano-objects were frozen by cross-linking the dextran shell through reaction of hydroxyl groups with divinyl sulfone.

In 2009, Schatz *et al.* designed polysaccharide and polypeptide based nano-objects (**Table 1.3 entry 22**).[99] An alkyne-functionalized dextran (M_n = 6600 g/mol, $Đ$ = 1.35) was first synthesized by reductive amination with propargylamine, while an azide-functionalized PBLG (DP = 59) was obtained by ring opening polymerization of γ-benzyl L-glutamate N-carboxylic anhydride (BLGNCA). The coupling reaction between the two polymers applying CuAAC in DMF generated amphiphilic block copolymers Dextran-*b*-PBLG, which gave rise to thick-membrane vesicles (R_h = 45 nm, PDI = 0.2, thickness = 20 nm) through solvent shifting (addition of DMSO into water).

Borsali and coworkers reported the preparation of thermo-responsive vesicles based on maltoheptaose (**Table 1.3 entry 23**).[100] Alkyne-functionalized maltoheptaose (Mal) was first synthesized by reductive amination with propargylamine. Thermo-responsive PNIPAM having an azide chain-end (N_3-PNIPAM$_n$, n = 28~220) was then generated

through ATRP polymerization using an azide-functionalized initiator. Amphiphilic block copolymers Mal_7-*b*-$PNIPAM_n$ (n = 28~220) were finally obtained through CuAAC. Cloudy point temperature (T_{cp}) of the copolymers ranged from 36 to 51°C due to the thermo-responsive character of the PNIPAM blocks. Above T_{cp}, the copolymers Mal_7-*b*-$PNIPAM_{220}$ were capable to self-assemble in water to generate vesicles with a diameter of 300 nm at 90°C.

In 2012, Long *et al.* described the preparation of hollow nanocapsules (**Table 1.3 entry 24**) consisting of polylactic acid and cholesterol-modified dextran (Chol-Dex).[101] Poly(D,L-lactic acid) (PLA) (from 210 to 48000 g/mol) was first prepared by ring opening polymerization of LA in chloroform. Chol-Dex (DS = 0.025) was generated by esterification of Dextran (40 kg/mol) with cholesterol 3-hemisuccinyl chloride. After mixing the two polymers in DMSO, nanoparticles and hollow nanocapsules were obtained through solvent displacement (DMSO dialyzed against water). Hollow nanocapsules were generated using high MW PLA (above 360 g/mol) and high composition of Chol-Dex (Chol-Dex: PLA from 1:1 to 3:1), unfortunately no detail on the size of capsules was given.

A modified dextran T70 was introduced by Chiang *et al.* to generate nanometer and micrometer-scale polymersomes (**Table 1.3 entry 25**).[102] After partial esterification of dextran (70 kg/mol) with octadecanol-carbamate imidazole, octadecanol modified dextrans (OMD) with different composition ratios (DS = 0.03, 0.05, 0.09 and 0.12) were generated. OMD17 (DS = 0.05) self-assembled into vesicles (R_h = 96 nm, R_g/R_h = 1.56, 10% v/v initial water in DMF-water) through solvent displacement (addition of water into polymers/DMF/water solution). The size of the OMD17 polymersomes was tuned (R_h from 31 to 96 nm) by increasing the initial water/DMF ratio (initial water content, from 10% to 40%, v/v).

Jayakannan and coworkers developed original vesicular carriers from dextran derivatives (**Table 1.3 entry 26**).[103] Dextran (6 kg/mol) was initially partially functionalized with hydrophobic units, i.e. 3-pentadecyl phenol (PDP), cardanol (CAR), or stearic acid (SA) (**Figure 1.14**). As evidenced by light scattering and TEM/AFM

analysis, the resulting amphiphilic polymers self-assembled in aqueous solution to generate vesicles (solvent displacement, addition of water into DMSO). The size of the vesicles was shown to increase together with PDP substitution (DLS, from 120 to 300 nm for DS~0.05 and DS~0.17, respectively). The authors further demonstrated that both hydrophilic Rhodamine B (Rh-B) and hydrophobic camptothecin (CPT) can be efficiently encapsulated in the vesicles leading to a slight swelling of the vesicles (from 110 nm to 120 nm, TEM image). Addition of esterase (under physiological conditions) within the solution resulted in the cleavage of the ester linkages between the dextran backbone and the hydrophobic tails causing a fast release of CPT or Rh-B. Finally, CPT loaded vesicles were proven to be effective in killing fibroblasts.

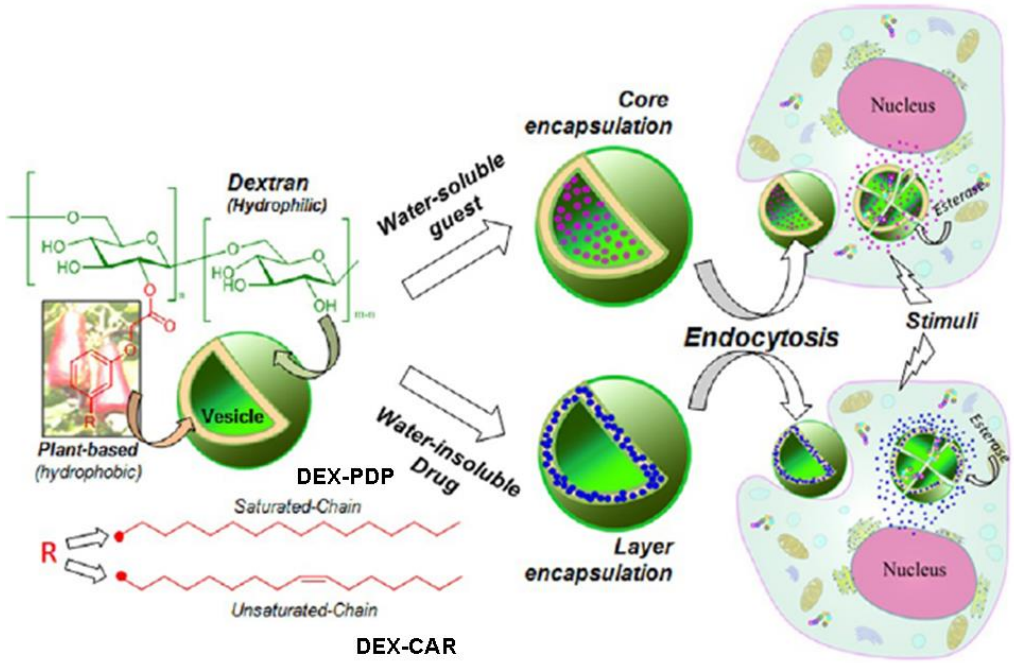

Figure 1.14. Dextran-based nanovesicles developed by Jayakannan and coworkers.[103]

Chitosan

Liu and coworkers designed an amphiphilic chitosan to prepare hollow nanocapsules in water (**Table 1.3 entry 27**).[104] Carboxymethyl-hexanoyl chitosans (CHC) with different DS (0.5 for carboxymethyl groups and 0~0.48 for hexanoyl groups) were primarily synthesized by substitution of chitosan (215 kg/mol). CHC generated hollow nanocapsules in aqueous solution. The self-assembly behavior of CHC was driven by

the DS of hexanoyl pendent groups. Large nanocapsules with a diameter of 200 nm were formed using CHC with high hexanoyl content (DS = 0.26~0.48), whereas very small capsules (D_h, ~20nm) were obtained from CHC with low hexanoyl content (DS lower than 0.26). The nanocapsules were capable to sequestrate DOX with an efficiency of 46.8%.

Yin and coworkers prepared photo-cross-linked chitosan hollow nanocapsules (**Figure 1.15**, **Table 1.3, entry 28**).[105-106] Chitosan (560 kg/mol) was modified by chloroacetic acid and azidobenzaldehyde through a two-step reaction. Self-assembly of modified chitosan chains in water afforded nanocapsules with a diameter of 150 nm at neutral pH. Due to the photo-sensitive character of the azidobenzyl groups, cross-linked nanocapsules (with hydrodynamic diameter around 120 nm) were finally obtained after UV exposition (15 min, λ = 253 nm). The nanocapsules were finally loaded with a pesticide (methomyl) during the assembly process (efficiency up to 90%) and showed an enhanced efficacy against armyworm larvae compared to the free drug.

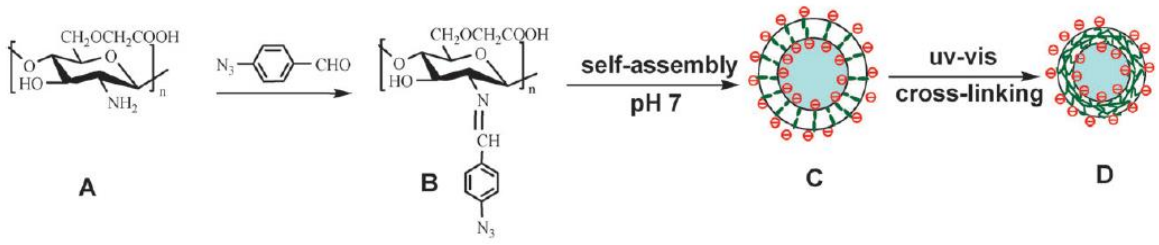

Figure 1.15. Route to photo-crosslinked chitosan hollow nanocapsules.[105-106]

In 2014, Zhou *et al.* prepared antibacterial chitosan-based nanocapsules (**Table 1.3, entry 29**).[107] In a first step, an antibacterial polypeptide poly(Lys_{11}-*stat*-Phe_{10}) was synthesized through random ring-opening polymerization of protected NCA-lysine and NCA-phenylalanine. The isocyanate-chain end functionalized polypeptide was then grafted to carboxylic acid-functionalized chitosan backbone (M_n = 17 kg/mol) to generate amphiphilic antibacterial chitosan. Half of the remaining carboxyl groups of chitosan were further esterified with methanol to afford amphiphilic copolymers (**Figure 1.16**). The resulting graft copolymers self-assembled in a water/THF (4/1, v/v)

solution to create biocompatible nanocapsules (D_h = 230 nm) with antibacterial properties. The nanocapsules were capable to load Dilantin (an antiepileptic drug, efficiency ~51.7%) or Dox (efficiency ~ 21.4%). The release of the drugs was triggered by the presence of proteases (trypsin), at a concentration of 6 mg/mL.

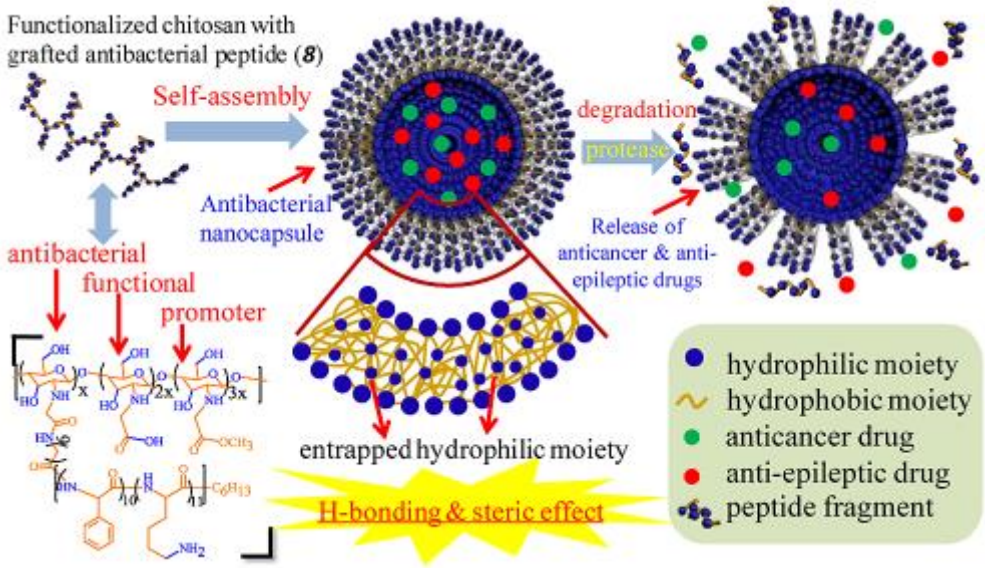

Figure 1.16. Preparation of antibacterial chitosan-based nanocapsules.[107]

Fan *et al.* prepared 200 nanometer-sized vesicles through self-assembly of amphiphilic chitosan and cationic surfactant (**Table 1.3, entry 30**).[108] Chitosan (200 kg/mol) was modified with alkylaldehyde (butyraldehyde or octaldehyde) in methanol to generate amphiphilic chitosan (DS, 0.26~0.27). The modified chitosan (5 mg/mL) was then mixed with a cationic surfactant cetyltrimethylammonium bromide (CTAB, 3×10^{-4} M) in water. This mixture spontaneously self-assembled into vesicles with a hydrodynamic diameter of 200 nm. As evidenced by DLS and TEM, the formation of vesicles was favoured when longer alkyl chains were incorporated on the chitosan backbone.

In addition to the straightforward assembly of modified chitosans in solution, some research groups investigated the co-self-assembly of lipids and amphiphilic chitosan into hybrid nanocapsules.

Li and coworkers described chitosan/lipid cationic liposomes for gene delivery

applications (**Table 1.3, entry 31**).[109] Tetradecyl-quaternized (carboxymethyl) chitosan (TQCMC) was prepared through reaction between glycidyltetradecyldimethylammonium chloride and carboxymethyl chitosan (MW ≤ 10 kg/mol). TQCMC and cholesterol (weight ratio of 1/0.81, chloroform) self-organized through thin-layer evaporation or reverse-phase evaporation and were subsequently redispersed in water to afford chitosan-containing liposomes with a hydrodynamic diameter of 184 nm. These low toxic chitosan/lipid liposomes showed higher gene delivery ability to cancer tissues *in vivo* than cationic liposomes such as Lipofectamine 2000.

Chang and coworkers also prepared chitosan/cholesterol based nano-objects (**Table 1.3, entry 32**).[110] Octadecyl-quaternized lysine modified chitosan (OQLCS, $M_{n\ (chitosan)}$ = 50 kg/mol) was functionalized with methoxyl PEG (mPEG, 2 kg/mol) or folic acid (FA) through a carbodiimide-induced coupling reaction to obtain mPEG-OQLCS and FA-OQLCS, respectively. OQLCS, mPEG-OQLCS and FA-OQLCS were then mixed with cholesterol (weight ratio, 1/1/1/1) in chloroform. These mixtures gave rise to FA-functionalized chitosan nanocapsules (size of 163 nm) by solvent evaporation. The release behavior of these nano-objects was mediated by tuning the ratio between cholesterol and OQLCS, and a higher permeability was observed for high weight ratio of cholesterol (OQLCS/cholesterol = 0.5/1). Due to the presence of FA moieties, these nanocapsules exhibited specific uptake capability for MCF-7 cells.

Mishra and coworkers also prepared chitosan/lipid nanocapsules using amphiphilic chitosan and cholesterol (**Table 1.3, entry 33**).[111] Glycol chitosan (90 kg/mol, DA~82.7%) was first modified with stearic acid (SA) to generate amphiphilic chitosan (DS = 0.08). The resulting polymer was then mixed with cholesterol at a ratio of 4/1 (chitosan/cholesterol) by stirring and further vortexing. Through solvent shifting (addition of ethanol/DMA into an aqueous solution), the mixture was shown to self-assemble into vesicles (D_h ~ 240 nm). Amphotericin B (AmB) was subsequently encapsulated into these vesicles during the self-assembly process with an efficiency of 26%. The vesicles exhibited high plasma stability and released 66% of AmB within

24h under sink condition. The loaded AmB showed an enhanced efficacy against leishmania *in vivo* compared to the free drug.

Other Polysaccharides

Besheer *et al.* prepared hydroxyethyl starch (HES)-containing micelles and vesicles through self-assembly process (**Table 1.3, entry 34**).[112] Amphiphilic HES was generated by esterification of HES (70, 200, 450 kg/mol) with lauric, palmitic and stearic acids (average DS, 0.29, 0.44 and 0.17). Fatty acid modified HES was then dissolved into a water/THF (3/1, v/v) solution. Mixture of micelles (D_h ~ 20-30 nm) and vesicles (D_h ~ 250~350 nm) mixtures were obtained after THF evaporation.

In 2009, hyaluronan-based polymersomes[113-115] were reported by Upadhyay *et al.* (**Table 1.3, entry 35**). The hyaluronan ($\overline{Mw}$ = 5140 g/mol, *Đ* = 1.41) was primarily functionalized with alkyne groups by reductive animation on the anomeric position with propargylamine. The amphiphilic copolymer $PBLG_{23}$-*b*-hyaluronan was then generated by CuAAC between ω-alkyne-functionalized hyaluronan and α-azide-PBLG ($\overline{Mw}$ = 5000 g/mol, *Đ* = 1.1). As evidenced by DLS, SANS, TEM and AFM, the copolymers self-assembled into bilayer vesicles (R_h = 220 nm, PDI = 0.08) through solvent shifting (addition of warm water to DMSO at 55°C). The obtained polymersomes were then used to load (efficiency close to 50%) and release doxorubicin (about 55% of released DOX after 2 days). In addition, it was shown that the hyaluronan-containing carriers display high colloidal stability and specifically bind CD44 glycoprotein receptors.

Wu *et al.* reported the synthesis of amphiphilic β-1,3-glucan ester using a two-step process.[116] The polysaccharide (200 kg/mol) was first reacted with formic acid to generate a pyridine-soluble glucan and further esterified with acetic or hexanoic anhydrates to yield β-1,3-glucan acetate (DS = 0.92~2.46, BGA) and hexanoate (DS = 1.87, BGH). Upon solvent displacement (acetone solution dialyzed against water), the resulting polymer chains self-organized into nanocapsules or solid nanoparticles (with diameters ranging from 132 to 487 nm). Vesicles (D_h = 490 nm) were only observed

from the self-assembly of BGH (**Table 1.3, entry 36**).

1.2.2.2 Polymerization-Induced Self-assembly (PISA)

In comparison with the traditional multi-step strategy which consists in the preparation of block copolymers, their purification and their final self-assembly, PISA has emerged as a powerful approach to prepare solutions of well-defined nano-objects with high solid contents in one step. The PISA process which can be applied to emulsion or dispersion polymerizations has been developed by Pan**,** Armes and Charleux. It relies on the use of a macromolecular precursor (soluble in the polymerization medium) which affords the controlled growth of a second block triggering the formation of nano-objects through *in situ* self-organization. By adjusting the composition of the block copolymers, it is possible to tune the morphology of the resulting nano-objects, i.e. spherical and cylindrical micelles or vesicles (**Scheme 1.5**).

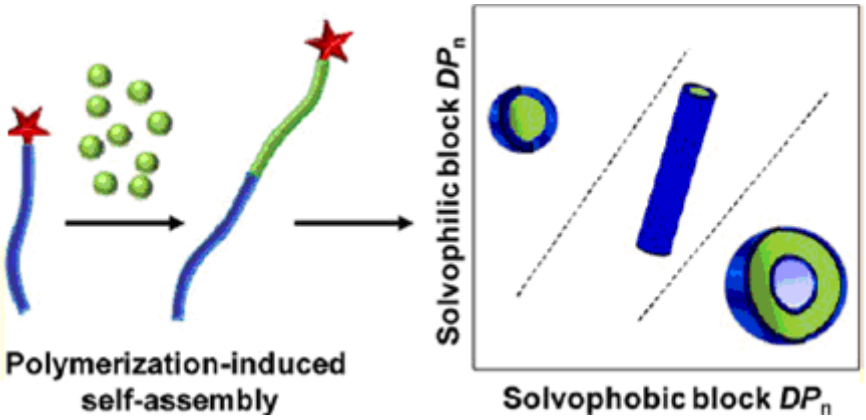

Scheme 1.5. Principle of the polymerization-induced self-assembly (PISA) method.[117]

In a recent work,[118] Armes and co-workers reported an application of “PISA” for the preparation of galactose-based nanocapsules. A galactose-based monomer (GalSMA) and Glycerol methacrylate (GMA) were homopolymerized via RAFT polymerization to obtain two water-soluble Macro-RAFT agents ($PGalSMA_{34}$, $\overline{Mw}$ = 16.3 g/mol, *Đ* = 1.13; $PGMA_{51}$, $\overline{Mw}$ = 16.2 g/mol, *Đ* = 1.15). These two macro-RAFT agents were mixed at a molar ratio of 9:1 ($PGMA_{51}$: $PGalSMA_{34}$) to mediate the polymerization of HPMA in deionized water ([M]/[CTAs] = 201, 70°C) and generate amphiphilic block copolymers. The resulting block copolymers were proven to self-assemble into

spherical, cylindrical micellar or vesicular ($PHPMA_{270}$, solid content of 15% and 20%) morphologies depending on the solid content of polymer in the solution and the DP_n of PHPMA. The generated nano-objects were shown to interact with galectin and allowed for effective delivery of rhodamine B in Human Dermal Fibroblasts cells (**Figure 1.17**, **Table 1.3, entry 37**).

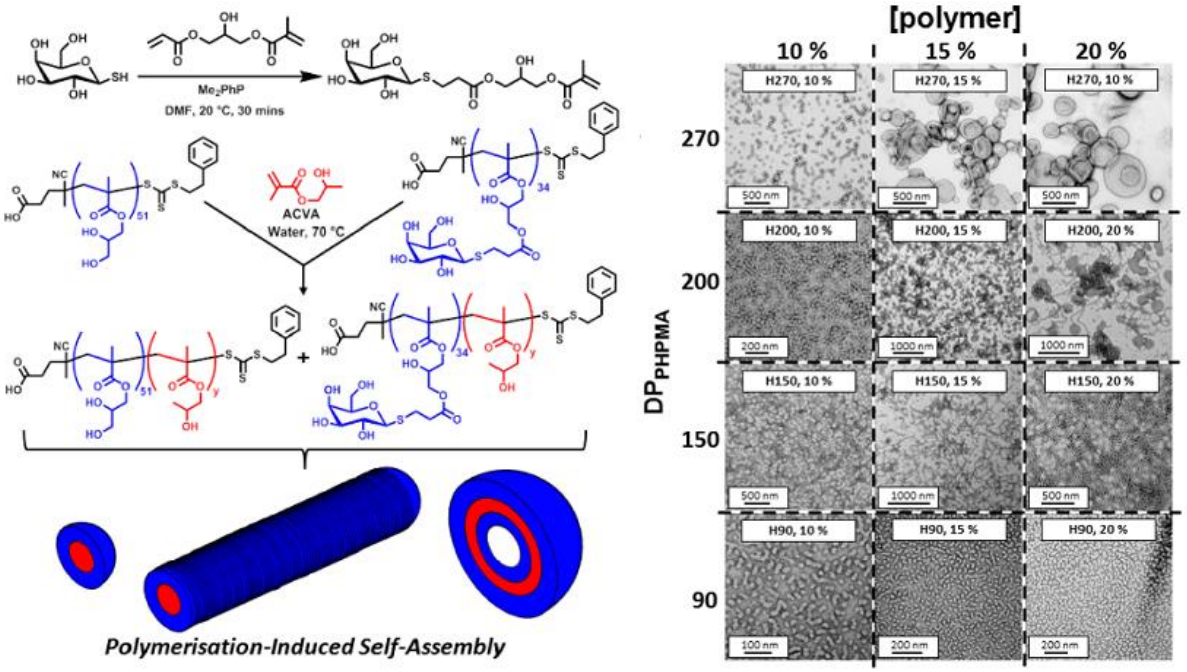

Figure 1.17. (Left) Preparation of nano-objects (spheres, worms or vesicles) by polymerization induced self-assembly; (Right) TEM images of the obtained nanoobjects.[118]

Table 1.3. Preparation of carbohydrate-functionalized nanocapsules by self-assembly.

Entry	Classification	Polymer	Protocol of Self-Assembly	Solvent	Size (nm)	Ref.
1	Polymersomes	Polystyrene-*b*-poly[(2-*β*-D-glucopyranosyloxy)ethyl acrylate]	Solvent shifting	Dioxane/DMF		74-75
2	Polymersomes	Poly(L-alanine)-*b*-poly(2-acryloyloxyethyllactoside)-*b*-poly(L-alanine)	CMC	H_2O		76-77
3	Polymersomes	2,3,4,6-tetra-*O*-acetyl-*β*-D-1-thioglucopyranose modified 1,2-polybutadiene-*block*-polystyrene	CMC	THF	250 (R_h)	78-79
4	Polymersomes	2,3,4,6-tetra-*O*-acetyl-1-thio-*β*-D-glucopyranose modified 1,2-polybutadieneblock-poly(ethylene oxide)	CMC	H_2O	280 (R_h)	80
5	Polymersomes	Poly(macromonomer)s-*b*-polyethylene glycol bearing galactose, glucose, ribose and xylose	Solvent shifting	THF/H_2O	231	81
6	Polymersomes	Poly[1,2,3,4-di-isopropylidene-6-*O*-(2'-formyl-4'-vinylphenyl)-D-galactopyranose]	Solvent shifting	DMSO/H_2O	80~205 (R_h)	82
7	Polymersomes	Poly(ε-caprolactone)-*b*-poly(lactobionamidoethylmethacrylate)	Solvent shifting	DMF/H_2O	432	83
8	Polymersomes	poly(ε-caprolactone)-*b*-poly(gluconamidoethylmethacrylate)	Solvent shifting	DMF/H_2O	250	84
9	Polymersomes	Poly(D-gluconamidoethyl methacrylate)-PPR-poly(D-gluconamidoethyl methacrylate)	Solvent shifting	DMF/H_2O	81	85
10	Polymersomes	Poly(γ-benzyl L-glutamate)–*b*-poly(D-gluconamidoethyl methacrylate)	Solvent shifting	DMF/H_2O	274	86
11	Polymersomes	Poly(5'-*O*-methacryloyl uridine)-*b*-poly(2-methacrylamido glucopyranose)	Solvent shifting	DMA/H_2O	35	87
12	Polymersomes	PNIPAAM-*co*-glycopolymer bearing mannoside and n-hexylamine	Solvent shifting	MeOH/H_2O	100-600	88
13	Polymersomes	Poly(3-hexylthiophene)-*b*-poly(3-*O*-methacryloyl-D-galactopyranose)	Solvent shifting	THF/H_2O	89 (R_h)	89
14	Polymersomes	Glucosamide-grafted amphiphilic glycopolysiloxanes	CMC	H_2O	300~600	90
15	Polymersomes	PBLG-*b*-PGG glycopeptides block copolymer	Solvent shifting	DMF/H_2O	32 (R_h)	91
16	Polymersomes	Poly(2-glucosyloxyethyl methacrylate)-*b*-poly(diethyleneglycol methacrylate)	T	H_2O	251, 500 (20°C)	92
17	Polymersomes	Poly(L-lysine)-*graft*-hexanoyl-lactobionolactone	Solvent shifting	MeOH/H_2O	110 (R_h, pH 7.4)	93
18	Polymersomes	Poly(spiropyran methacrylate)-*b*-poly(3-*O*-4-vinylbezoyl-D -glucopyranose)	Solvent shifting	DMF/H_2O	366	94

19	Polymersomes	Poly(1-*N*-β-galactosyl acrylamide) (PGal), Poly (1-*N*-β-glucosyl acrylamide)(PGlc)	T	H_2O	62 (R_h, V-PGal), 68 (R_h, V-PGlc)	95
20	Polymersomes	Polystyrene-*b*-poly(tetra-acyl-α-1-mannosyl styrene)	De- acetylaion	THF	42 (R_h)	96
21	Polymersomes	Dextran-*b*-PS	Solvent shifting	THF or DMSO-THF/ H_2O	64, 77 (R_h)	97-98
22	Polymersomes	Dextran-*b*-PBLG	Solvent shifting	DMSO/ H_2O	45 (R_h)	99
23	Polymersomes	Maltoheptaose-*b*-PNIPAM	T	H_2O	300	100
24	Polymersomes	Cholesterol modified dextran, PLA	Solvent shifting	DMSO/ H_2O		101
25	Polymersomes	Octadecanol-dextran	Solvent shifting	DMF- H_2O / H_2O	96 (R_h)	102
26	Polymersomes	3-pentadecyl phenol modified Dextran	Solvent shifting	DMSO/ H_2O	120-300	103
27	Polymersomes	Carboxymethyl-hexanoyl chitosan	Sonication	H_2O	20, 200	104
28	Polymersomes	Azidobenzaldehyde modified photocrosslinkable carboxymethyl chitosan	Sonication	H_2O	153	105-106
29	Polymersomes	Poly(Lys_{11}-stat-Phe_{10})-*g*-$Cs]_x$-*stat*-Cs_{2x}-*stat*-ECs_{3x}	Dissolution	THF/ H_2O	230	107
30	Polymersomes	Alkylaldehyde modified chitosan	CMC	H_2O	200	108
31	Polymersomes	Tetradecyl-quaternized chitosan	Evaporation	Chloroform	184	109
32	Polymersomes	Octadecyl-quaternized lysine modified chitosan	Evaporation	Chloroform	163	110
33	Polymersomes	Stearic acid modified glycol chitosan	Solvent shifting	EtOH-DMA / H_2O	243	111
34	Polymersomes	Fatty acid modified hydroxyethyl starch	Evaporation	THF/ H_2O	250-350	112
35	Polymersomes	PBLG-*b*-hyaluronan	Solvent shifting	DMSO/ H_2O	220 (R_h)	113-115
36	Polymersomes	β-1,3-glucan acetate and hexanoate	Solvent shifting	Acetone/ H_2O	487	116
37	PISA	Poly(GalSMA)-*b*-poly(HPMA), poly(GMA)-*b*-poly(HPMA)	PISA	H_2O		118
38	Micelles strategy	Pyrene-PCL-*b*-PVBG	Solvent shifting	DMF/ H_2O	50-120	119
39	Micelles strategy	PLA-*b*-poly(6-*O*-aryloyl-α-D-galactopyranose)	Solvent displacement	Formic acid /H_2O	250 (micelle)	120

CMC: Critical Micelle Concentration. T: Temperature.

1.2.2.3 Micelle core removal strategy

Apart from polymersomes, micelles obtained via self-assembly of amphiphilic block copolymers can also be used to generate hollow structures through selective removal of the core. Elimination of the core can then be achieved by enzymatic degradation, ozonolysis, hydrolysis or aminolysis.

Even though her group has not described the fabrication of glyconanocapsules, the preparation of hollow nanospheres via core degradation method was first introduced by Wooley and co-workers.[121-123] The first adaptation of Wooley's method for the formation of glyconanocapsules came from Lu *et al.* in 2005 (**Table 1.3 entry 38**).[119] Amphiphilic block copolymers (Py-PCL_{32}-*b*-$PVBG_{10}$, $Đ$ = 1.28) were prepared by ring-opening polymerization of ε-CL initiated by hydroxymethyl pyrene and subsequent ATRP polymerization of a galactose-based monomer, 6-*O*-(4-vinylbenzyl)-1,2:3,4-di-*O*-isopropylidene-D-galactose (VBIG). The self-assembly of these block copolymers resulted in the formation of micelles with a PCL core and a glycopolymer shell (size between 20 and 90 nm) by solvent shifting (addition of water into DMF). After cross-linking of the glycopolymer shell with glutaraldehyde, removal of the polyester core through basic hydrolysis afforded hollow glyconanocapsules with size ranging from 50 to 120 nm (**Figure 1.18**).

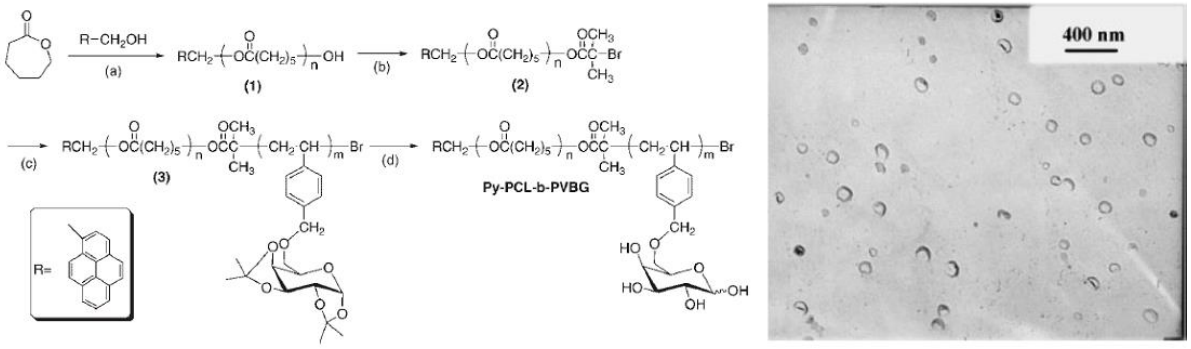

Figure 1.18. Synthesis of amphiphilic block glyco-copolymer (Left) and TEM image of hollow glyconanocapsules after hydrolysis (Right).[119]

In 2009, Ting *et al.* synthesized hollow galactose-based nanocapsules by combining RAFT polymerization and aminolysis (**Table 1.3 entry 39**).[120] A block copolymer

made of poly(lactide) (PLA) and poly (6-*O*-aryloyl-α-D-galactopyranose) (PLA_{170}-*b*-$PAGP_{216}$) was prepared through RAFT polymerization from a poly(lactide) macro RAFT agent previously obtained through ring-opening polymerization of 3,6-dimethyl-1,4-dioxane-2,5-dione initiated by a hydroxyl functionalized RAFT agent. The block copolymer then self-assembled into micelles (D_h about 250 nm in water) by solvent displacement (formic acid solution dialyzed against water). The structure of micelles was freezed via RAFT polymerization of hexanediol diacrylate (conversion of 86%), and hollow glyconanocapsules were finally obtained after aminolysis by hexylamine (**Figure 1.19**).

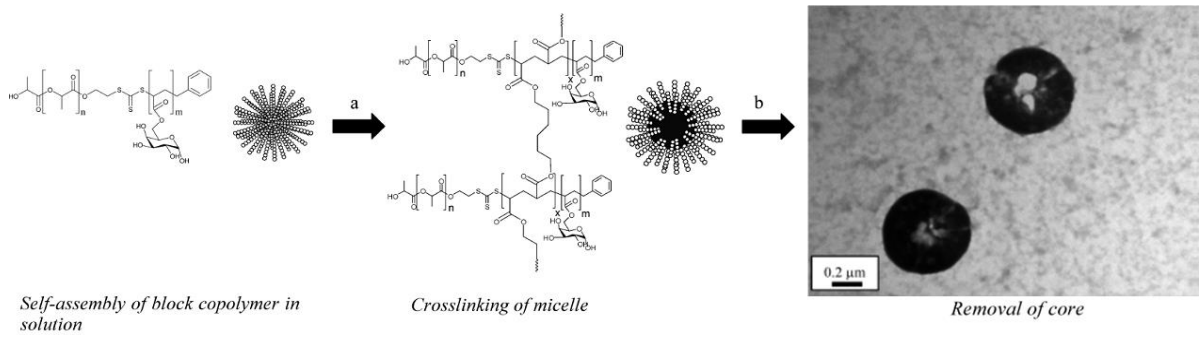

Figure 1.19. Fabrication of hollow sugar balls relying on the core removal approach.[120] (a) Hexanediol diacrylate/water/AIBN/60°C; (b) hexylamine.

1.2.3 Template strategy

The template strategy relies on preformed nano-sized templates (colloid, polymer, silica, polymer particles…) on which polymer chains are covalently grafted or adsorbed. Glyconanocapsules can be conveniently generated through grafting reactions and/or adsorption of glycopolymers or polysaccharides on the surface of the templates. The most common technique to build the walls of capsules is based on Layer-by-layer (L-b-L) deposition. L-b-L deposition is a methodology first introduced by G. Decher[124] based on electrostatic attraction between polycations and polyanions. The main advantage of this strategy is that thickness and morphology of particles can be precisely controlled through carefully selection of the materials. Nano- or microcapsules are typically obtained in two steps (**Scheme 1.6**): 1) sequential deposition of polymer chains at the surface of the template; 2) removal of the core.

The multi-layered capsules prepared by L-b-L combine the different properties of the assembled polymers in one system, highly reinforcing its potential for applications.

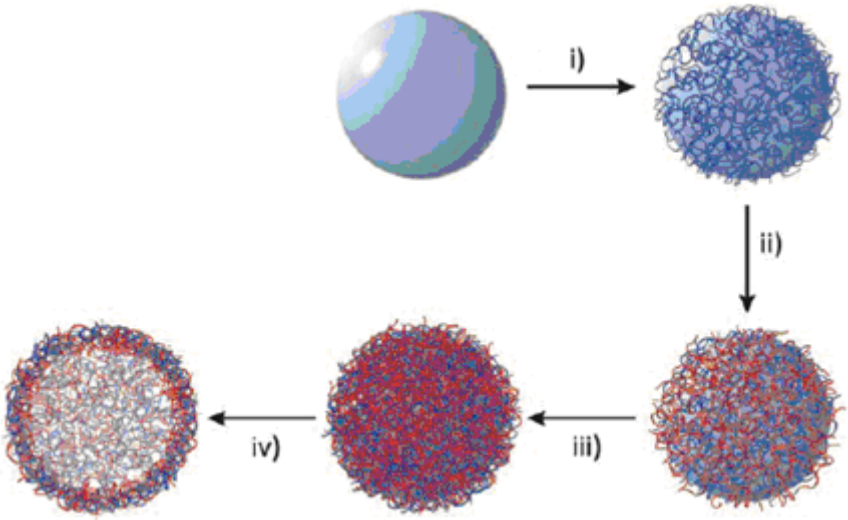

Scheme 1.6. L-b-L assembly on colloidal templates: i) deposition of a positively charged polyelectrolyte and washing; ii) deposition of a negatively charged polyelectrolyte and washing; iii) repeat i & ii to generate multi-layered core-shell particles; iv) core removal.[125]

1.2.3.1 Particles-based strategy

L-b-L assembly from particles as template is a common route to generate glyconanocapsules. Practically, oppositely charged polysaccharides/glycopolymers are deposited on the charged surface of degradable particles through electrostatic interactions to form mono or multilayers of carbohydrate polymer chains. Whereas multilayered polymer membranes are generally stable, cross-linking of the resulting shell is generally necessary for monolayer structures to maintain the assembly. In the final step, carbohydrate coated capsules are obtained after selective degradation of the particle core.

(1) Monolayer capsules

Liu *et al.* designed ibuprofen-loaded chitosan nanocapsules using a template strategy (**Table 1.4, entry 1, Figure 1.20**). The templates, carboxylic acid-functionalized P(S-*co*-MAA) particles (size about 200 nm), were prepared by surfactant-free emulsion copolymerization of styrene and MAA (initial wt ratio of styrene/MAA, 10/1).

Chitosan (M_n = 500 kg/mol) was then adsorbed on the PS particles through electrostatic interactions. After cross-linking of the shell with glutaraldehyde (GA), the core was dissolved in THF affording hollow nanocapsules (hydrodynamic diameter ranging from 190 to 250 nm). Ibuprofen was incorporated during the preparation of the P(S-*co*-MAA) particles (ibuprofen was initially dissolved into chloroform) and 85% of the loaded drug was released after 80h at pH 7.4 and 37°C.[126-127]

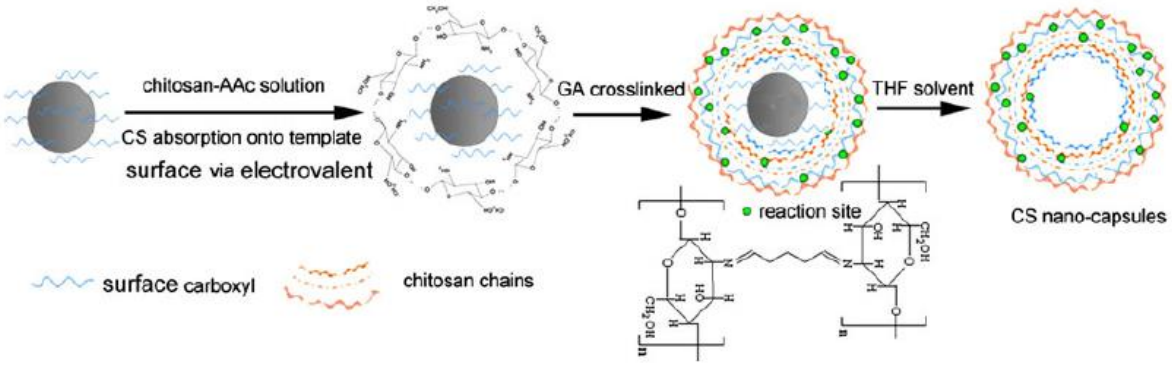

Figure 1.20. Route to chitosan coated nanocapsules.[126]

Solid core/mesoporous shell (SC/MS) silica nanoparticles (268, 382 and 574 nm) were coated by low molecular weight chitosan.[128-129] After cross-linking of the chitosan infiltrated into the shell and further degradation of the silica via HF treatment, chitosan nanocapsules with different size (220, 270 and 440 nm), wall thickness (31, 46 and 55 nm) and porosity were obtained. These biocompatible nanocapsules were loaded with curcumin, a natural lipophilic anti-cancer drug. The large and medium sized nanocapsules displayed respectively 145 and 13 times more loading capacity than the smallest ones (0.16 fg per capsule of 220 nm), but at the same time, the latter were shown to be the most efficient nanocarriers for chemotherapeutic purposes exhibiting six times higher efficiency in comparison to equivalent amount of free drug (**Table 1.4, entry 2**).

An original route was reported by Taniguchi *et al.* who developed glyconanocapsules and glycomicrocapsules by combining polymerization and core removal strategies (**Table 1.4, entry 3**).[130] Nano-sized particles (diameter of 440 nm) prepared by miniemulsion polymerization of styrene (St) and 2-chloropropionyloxyethyl

methacrylate (CPEM) were selected as templates. Surface initiated AGET-ATRP (activator generated by electron transfer for atom transfer radical polymerization) polymerization of N-[2-(4-vinylbenzenesulfoneamido)ethyl] lactobioneamide (VBSAELA) was further performed on the surface of core particles to generate lactose-functionalized glycoparticles. Hollow nanocapsules (diameter of 640 nm) were finally obtained after dissolution of PS template in THF solution. After core removal, the size of nanocapsules was shrunk by 15%. Glycomicrocapsules were prepared applying similar strategy using micro-sized PS as templates (**Figure 1.21**).

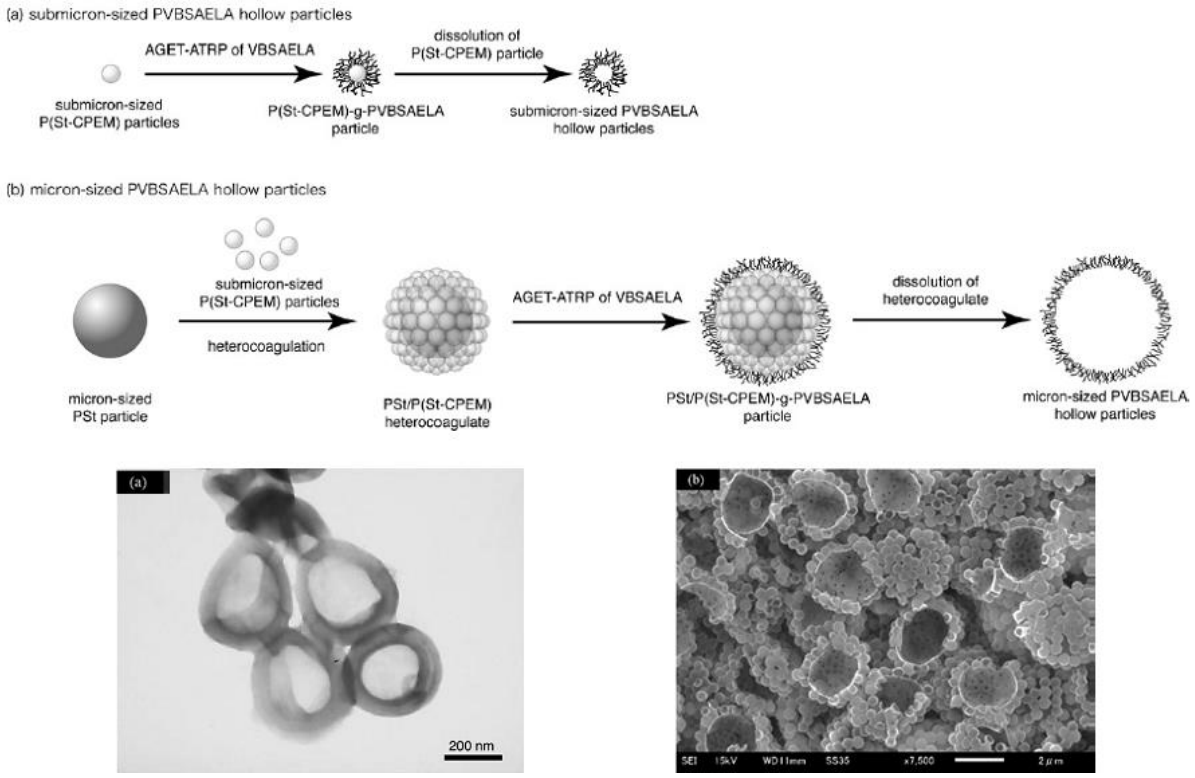

Figure 1.21. Glyconanocapsules fabrication through template strategy (Top) and TEM image (bottom) of preparation of glyconanocapsules and glycomicrocapsules.[130]

Kren *et al.* reported on the hyaluronan-coated nanocapsules for delivering genes to liver sinusoidal endothelial cells and hepatocytes (**Table 1.4, entry 4**).[131] The hyaluronan chains were coated on the positively charged DNA-PEI complexes through dispersion atomization process to generate hyaluronan-coated nanocapsules with a size of about 20 nm. These nanocapsules were proven to stably transfer *sleeping beauty* transposon into liver sinusoidal endothelial cells of mice, displaying a

very interesting therapeutic application.

(2) Multi-layered nanocapsules by L-b-L strategy

In 2004, Akashi and co-workers prepared multilayered hollow nanocapsules through L-b-L strategy from silica nanoparticles (**Table 1.4, entry 5**).[132] Chitosan as first layer (650 kg/mol) and dextran sulfate (500 kg/mol) were sequentially deposited on the surface of the nanoparticles (size of 330 nm) to form four layers. Polysaccharide multi-layered nanocapsules were finally generated with a diameter of about 300 nm after core removal. The same group also reported pH-responsive hollow nanocapsules using the same template (**Table 1.4, entry 6, Figure 1.22**).[133] The multilayered walls of the capsules were constructed from sequential deposition of chitosan (600 kg/mol) and poly(γ-glutamic acid) (γ-PGA, 1000 kg/mol), and cross-linking reactions between chitosan and γ-PGA chains (activated by carbodiimide reagent). After core removal, the size of the nanocapsules was stable (roughly 250 nm) between pH 4.0 to 10.0, and significantly increased (about 500 nm) at pH 1.0 due to electrostatic repulsion between the ammonium groups of chitosan. Modification of the pH also allowed for tuning the release behavior of the nanocapsules.

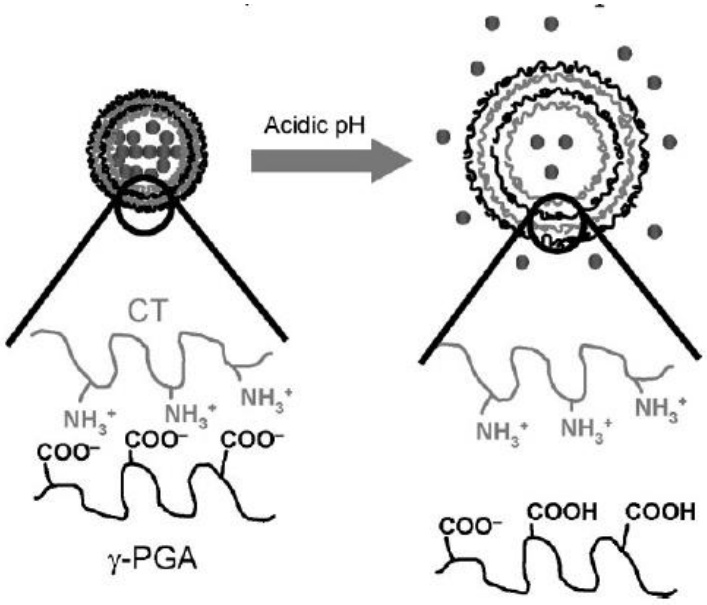

Figure 1.22. pH-triggered release behavior of CT-γ-PGA hollow nanocapsules.[133]

Poly(allylamine hydrochloride) (PAH, 70 kg/mol) and dextran sulfate (DS, 500 kg/mol) were sequentially deposited on silica particle templates (size of 500 nm) by Raichur and co-workers to form multilayered nanoparticles. These steps were followed by the deposition of silver nanoparticles (formation from reduction of silver nitrate during the deposition) (**Table 1.4, Entry 7**).[134] After core removal via HF/ NH_4F treatment, the authors demonstrated that it was possible to encapsulate FITC-dextran in the silver nanoparticles modified nanocapsules (D_h about 500 nm, thickness of 30 nm) through a permeation process. FITC-dextran was released through sonication owing to partial destruction of the polymer shell.

Silica nanoparticles (D_h = 220 nm) were also coated by chitosan and negative charged heparin through L-b-L deposition (**Table 1.4, Entry 8**).[135] Hollow nanocapsules of 200 nm were then generated after elimination of the silica core (0.2 M HF + 0.8 M NH_4F). DOX was loaded in the core of the resulting glyconanocapsules with an efficiency of 89%. Interestingly, the loading and the release of DOX were controlled by adjusting the pH of the solution (64% for pH 4.8 and 77% for pH 7.4).

Li and co-workers reported insulin-loaded chitosan nanocapsules using a L-b-L process from silica nanoparticles (size of 260 nm) (**Table 1.4, Entry 9**).[136] Chitosan (50 kg/mol) was first modified with L-cysteine to obtain thiol-functionalized chitosan. Poly(L-aspartic acid) (20.4 kg/mol) was reacted with L-cysteine to generate thiol-functionalized poly(L-aspartic acid). During the deposition process, the concomitant formation of disulfide bonds from coupling of thiol groups ensured the cross-linking of the polymer shell (size of 365 nm and thickness of 40 nm). Hollow nanocapsules were finally obtained after degradation of the silica core. The resulting biocompatible nanocapsules were capable to sequestrate insulin with a loading efficiency of around 13%. The release behavior of the nanocarriers was influenced by glutathione (GSH) which cleaves the disulfide bonds.

Chakravortty and co-workers reported chitosan-dextran nanocapsules as potential drug delivery system against pathogen Salmonella (**Table 1.4, Entry 10**).[137] Silica particles were coated by chitosan (150 kg/mol) and dextran sulphate (500 kg/mol) to

generate four layered nanoparticles. After silica dissolution, the biocompatible nanocapsules (diameter of 180 ± 20 nm) were capable to encapsulate ciprofloxacin and ceftriaxone (drugs for Salmonella infection) with 78% of efficiency. The release of drugs was influenced by the pH of solution (70% after 48h at pH 7.4; 51% after 48h at pH 4.8). These drug-loaded nanocapsules showed effective clearance ability of Salmonella infection *in vitro* and *in vivo*.

Li and co-workers deposited dextran sulfate (500 kg/mol) and chitosan (50 kg/mol) on SiO_2-NH_3^+ nanoparticles (size of 166 nm).[138] Hollow nanocapsules were obtained after removal of core particles by HF/ NH_4F treatment (D_h of 217 nm before core removal, **Table 1.4, entry 11**). The template was further modified with tosyl-β-cyclodextrin to afford β-cyclodextrin conjugated silica nanoparticles (D_h of 100 nm, PDI = 0.319), and chitosan was functionalized with cysteine through amidation to afford cysteine-conjugated chitosan (CH-SH, targeting modification of 5, 10, 20 and 40%).[139] Dextran sulfate and CH-SH were then sequentially deposited on β-cyclodextrin conjugated silica template by L-b-L deposition (**Table 1.4, entry 12**). Thanks to the presence of thiols along chitosane backbones, the shell was gradiently cross-linked through the formation of disulfide bonds. The gradiently disulfide cross-linked nanocapsules (before core removal, diameter of 151 nm) were obtained after the degradation of the silica core by HF/NH_4F treatment. These biocompatible nanocapsules were capable to encapsulate BSA (66.7 kg/mol) with an efficiency up to 80% by electrostatic attraction of the negatively charged BSA on the silica particles during the deposition. The release behavior was triggered by addition of glutathione (**Figure 1.23**).

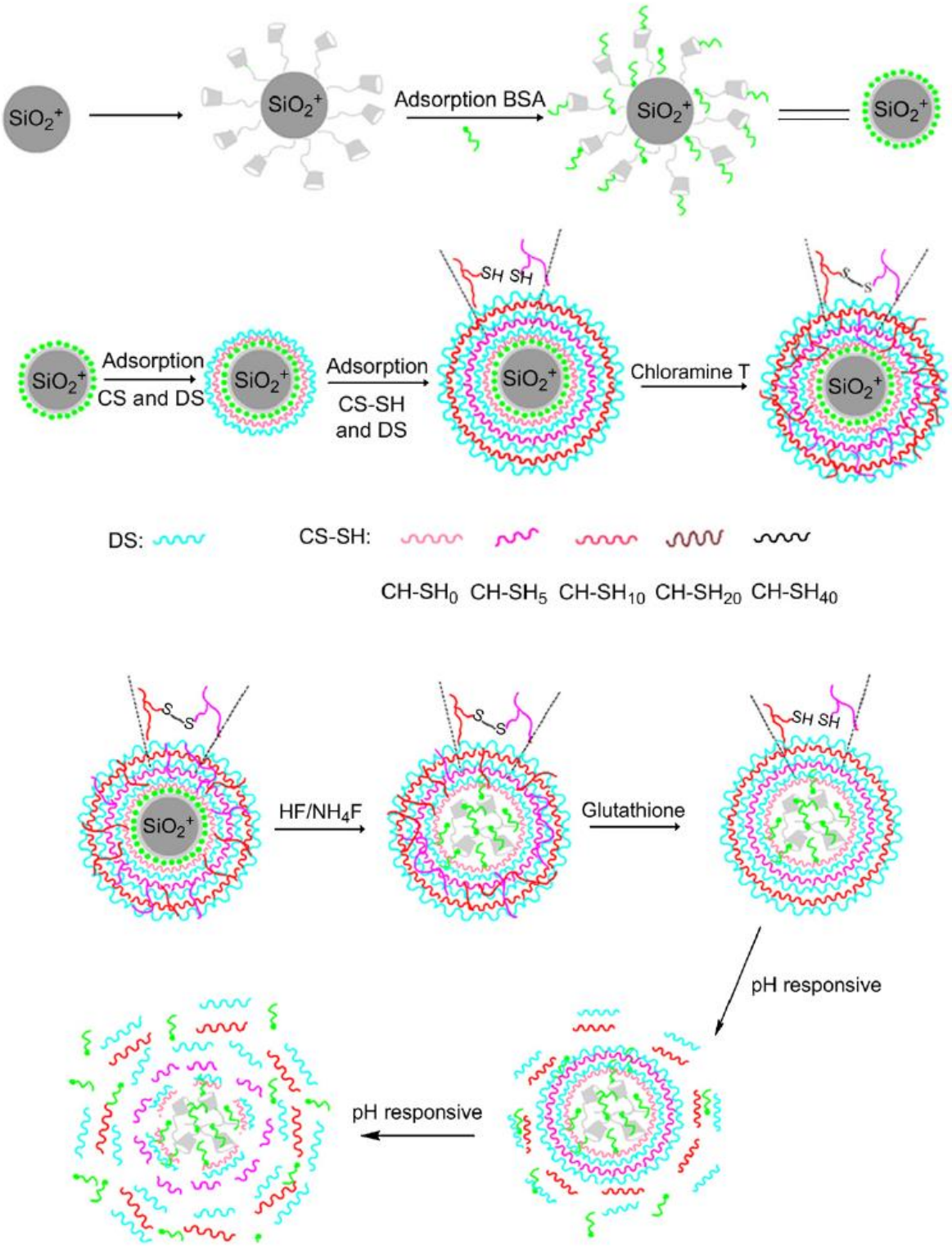

Figure 1.23. Schematic representation of pH-responsive dextran sulfate (DS)/chitosan (CS) nanocapsules through L-b-L strategy.[139]

Liu *et al.* prepared ionic and pH-responsive polysaccharide-based nanocapsules (**Table 1.4, Entry 13**)[140] from sequential deposition of chitosan (80 kg/mol) and

Iota-carrageenan (200 kg/mol) onto SiO_2-NH_3^+ nanoparticle templates (size of 100 nm) and subsequent shell cross-linking with glutaraldehyde. Hollow nanocapsules (size of 348 nm) were finally obtained after silica core removal. As evidenced by DLS, the size of these nanocapsules augmented with an increase of NaCl concentration and of pH value.

Recently, Guo *et al.* fabricated glucose-responsive [CS-NAC/p(GAMA-*r*-AAPBA)] nanocapsules through L-b-L process (**Table 1.4, Entry 14**).[141] A chitosan-*N*-acetyl-L-cysteine (CS-NAC) conjugate was first synthesized through introduction of *N*-acetyl-L-cysteine onto chitosan backbone by amidation. Poly(D-gluconamidoethyl methacrylate-*r*-3-acrylamidophenylboronic acid) [p(GAMA-*r*-AAPBA)] copolymers with different compositions (GMA/AAPBA=1/1, 2/1, 4/1, molar ratio) were generated by radical copolymerization. The polymers were then sequentially deposited on the SiO_2-NH_2 particles to form multi-layered nanoparticles (diameter ranging from 253 to 272 nm, PDI from 0.25 to 0.27). After oxydation of the thiols in the presence of chloramine T and silica core removal, disulfide cross-linked hollow nanocapsules (D_h about 250 nm) were obtained (**Figure 1.24**). These nanocapsules were shown to swell in the presence of glucose (D_h = 420 nm) and were capable to load (efficiency from 62 to 78%) and release insulin (24h, 74 to 84%). The release behavior of the nanocapsules can be controlled by changing the pH (from pH 1.4 to 7.4) and the concentration of glucose.

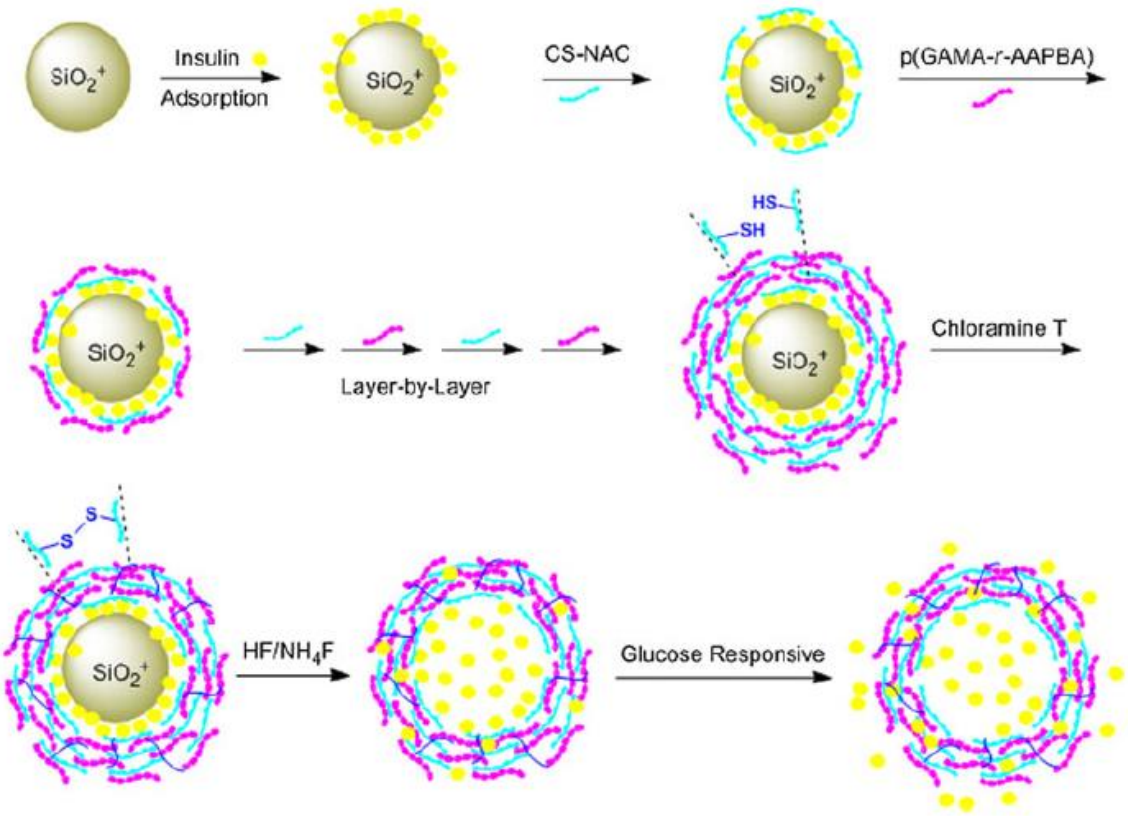

Figure 1.24. Schematic diagram of preparation of glucose-responsive glyconanocapsules by LBL strategy.[141]

Different from the above traditional template strategy using silica particles, Pishko and coworker directly deposited chitosan (MW value not mentioned) and dextran sulfate (MW > 500 kg/mol) on paclitaxel particles (antineoplastic drugs) (**Table 1.4, Entry 15**).[142] Paclitaxel nanoparticles with a diameter of 110 nm (SEM) were generated by a solvent emulsification evaporation method. These bilayered nanocapsules (D_h of 128 nm) were further surface-modified by poly(ethylene glycol) (3.4 kg/mol) and fluorescence-labeled wheat germ agglutinin by using carbodiimide chemistry. Due to the presence of lectin agglutinin, the nano-objects were proven to specifically bind Caco-2 cells (*in vitro* study).

Bui *et al.* reported an original solvent-shifting method to deposit hyaluronan-*b*-poly(g-benzyl-L-glutamate) on condensed siRNA-PEI complexes (**Figure 1.25**).[143] Specifically, positively charged complexes (N/P = 3~10, D_h = 150~185 nm) were initially generated by mixing siRNA (23 base pairs, 14.6 kg/mol)

and branched PEI (25 kg/mol) in buffer solution (pH 7.6). The complexes were then coated with negatively charged hyaluronan moieties through electrostatic interactions after addition of HYA-*b*-PGLG (M_n = 5 kg/mol for each block), resulting in monolayered capsules with pili-like PBLG blocks. Negatively charged nanocapsules (size of 90nm) were finally generated through solvent shifting process. Addition of water (aqueous solution at pH = 7.4) promoted the self-assembly of free block copolymer chains into a bilayer membrane at the surface of the complex. This block copolymer-coated gene carrier showed very high gene-silencing activity (**Table 1.4, entry 16**).

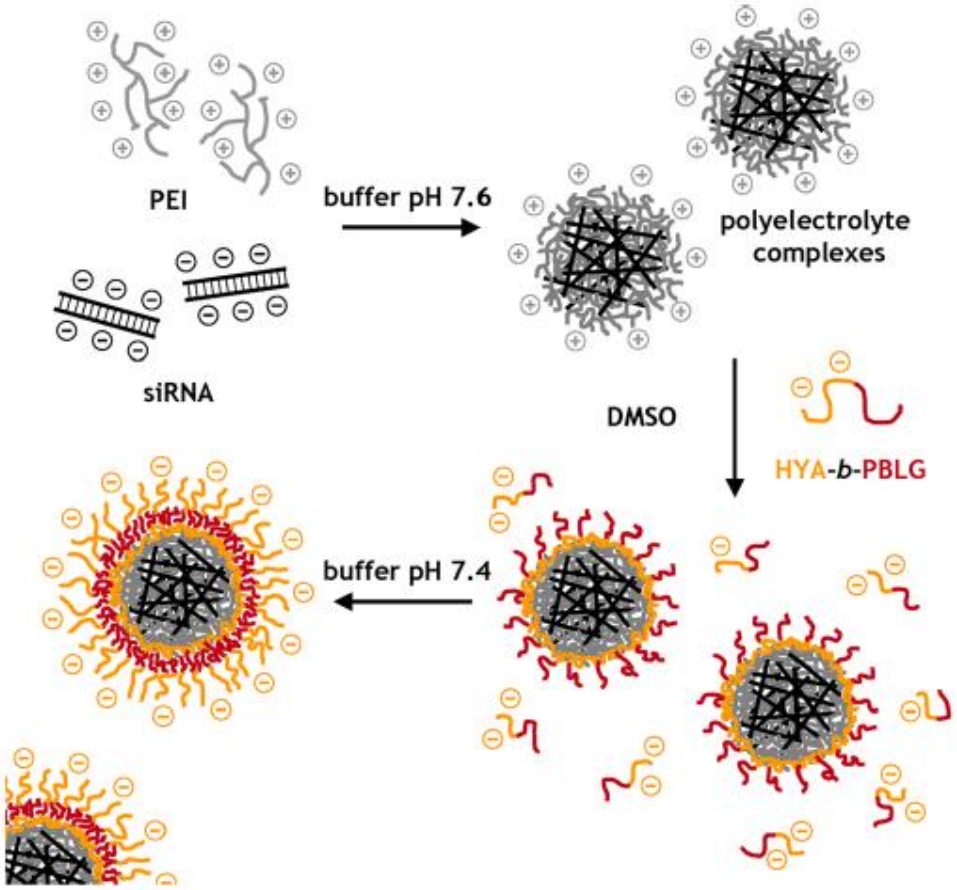

Figure 1.25. Design of Virus-like Polymer Particles by deposition of glycoprotein-mimic amphiphilic Block Copolymer chains around RNA-Based Polyelectrolyte Complexes.[143]

Table 1.4: Template strategy to prepare carbohydrate-functionalized nanocapsules.

Entries	Template	Template Dimension (nm)	Polymer	Deposition Manner	Cross-linker	Layers	Core Removal	Capsules Dimension (nm)	Ref.
1	P(S-*co*-MAA) particles	200	Chitosan	Electrostatic interaction	Glutaraledehyde	Monolayer	THF	190~250	126-127
2	SC/MC Silica particles	268, 382, 574	Chitosan	Electrostatic interaction	Glutaric dialdehyde	Monolayer	HF	220, 270, 440	128-129
3	P(St-CPEM) particles	440	P(VBSAELA)	Surface polymerization		Monolayer	THF	640	130
4	DNA-PEI complexes		Hyaluronan	Electrostatic interaction		Monolayer		20	131
5	Silica particles	330	Chitosan, Dextran sulfate	Electrostatic interaction		Multilayer	HF	300	132
6	Silica particles	330	Chitosan, γ-PGA	Electrostatic interaction		Multilayer	HF	250	133
7	Silica particles	500	PAH, Dextran sulfate	Electrostatic interaction		Multilayer	HF/NH_4F	500	134
8	Silica particles	220	Chitosan, Heparin	Electrostatic interaction		Multilayer	HF/NH_4F	200	135
9	Silica particles	260	Cysteine-Chitosan, Cysteine-PASA	Electrostatic interaction		Multilayer	HF	365 (before core removal)	136
10	Silica particles		Chitosan, Dextran sulphate	Electrostatic interaction		Multilayer	HF	180	137

11	SiO_2-NH_3^+ particles	166	Chitosan, Dextran sulfate	Electrostatic interaction		Multilayer	HF/NH_4F	217 (before core removal)	[138]
12	β-cyclodextran-SiO_2-NH_3^+ particles	100	Cystine-Chitosan, Dextran sulfate	Electrostatic interaction		Multilayer	HF/NH_4F	151 (before core removal)	[139]
13	SiO_2-NH_3^+ particles	100	Chitosan, lota-carrageenan	Electrostatic interaction	Glutaraledehyde	Multilayer	HF	348	[140]
14	SiO_2-NH_2 particles	152	Chitosan-NAC, P(GAMA-γ-AAPBA)	Electrostatic interaction		Multilayer	HF/NH_4F	254	[141]
15	Paclitaxel particles	110	Chitosan, Dextran sulfate	Electrostatic interaction		Multilayer		128	[142]
16	PEI-siRNA complexes	150~185	Hyaluronan-*b*-PBLG	Electrostatic interaction		Monolayer		90	[143]
17	Liposomes		Chitosan	Electrostatic interaction		Monolayer		96	[144]
18	Liposomes		Folate-Chitosan	Electrostatic interaction		Monolayer		182	[145]
19	Liposomes		Pectin	Electrostatic interaction		Monolayer		229~418	[146]
20	Polymersomes	180~414	Chitosan	Electrostatic interaction		Monolayer		183~712	[147]
21	Liposomes		Alginate, Chitosan	Electrostatic interaction		Multilayer		414	[148]
22	Cationic Vesicles	220	Alginate, Chitosan	Electrostatic interaction		Multilayer	Triton X-100	500	[149]
23	Liposomes	80	Alginate, Chitosan	Electrostatic interaction		Multilayer		300	[150-151]

24	Liposomes	100	Chitosan, Dextran sulphate, DNA	Electrostatic interaction	Multilayer		152-153
25	Liposomes	108	PAA, Chitosan	Electrostatic interaction	Multilayer	215	154
26	Lipid nanocapsules	59	Hydroxylamine-Dextran	Post-insertion		73	155
27	Lipid nanocapsules	49	Lipochitosan, Chitosan, Dextran sulphate	Post-insertion, Electrostatic interaction	Multilayer	200	156
28	Lipid nanocapsules	49	Lipochitosan, Lipodextran	Post-insertion			157
29	Liposomes	163	N-palmitoyl chitosan	Post-insertion		130	158
30	Liposomes		Hyaluronan acid	Grafting		100	159-160
31	Liposomes		Carboxymethyl chitosan	Grafting		200~300	161
32	Liposomes	201	Chitosan-thioglycolic	Grafting		354, 590	162

1.2.3.2 Liposomes-based strategy

Deposition of polysaccharides can also be efficiently performed on nano-sized liposomes. The preparation of carbohydrate-functionalized capsules from deposition of polysaccharide chains on liposomes was first reported by Sunamoto *et al.* in 1980.[163-164] It is now a very mature research area and lots of papers describing the coating of nano-sized liposomes have been published for drug delivery applications.[165-177] Herein, some of the most recent works will be described. In a general procedure, nano-sized liposomes are prepared in the first step. Then, charged polysaccharides are sequentially deposited at the surface of liposomes through electrostatic interaction to produce monolayer or multilayer carbohydrate-functionalized capsules. No core removal step is required for this approach.

(1) Monolayer capsules

Park and coworkers reported Vitamin C loaded chitosan (4 kg/mol)-coated nanoliposomes.[144] Liposomes were first prepared through self-assembly using phosphatidylcholine and cholesterol and further coated with chitosan. The resulting nanocapsules (D_h = 96 nm) were capable to load vitamin C with a maximal efficiency up to 96.5%, while the payload was about 46.8% (**Table 1.4, Entry 17**).

In order to increase bioavailability of the nanocarriers, Yang *et al.* introduced folate groups onto chitosan-coated liposomes. Folate groups were incorporated on chitosan chains (10kg/mol, DS is not given) using carbodiimide chemistry (**Table 1.4, Entry 18**).[145] Liposome templates were then prepared from phosphatidylcholine (PC) using the injection method. After deposition of chitosan chains, the nanocapsules (D_h = 182 nm) were used to encapsulate fluorescein (efficiency ~ 94%). The release of fluorescein was slowed down by the incorporation of the chitosan layer (56% vs 65.5% for the uncoated liposomes after 24h). Due to the presence of folate groups, the nanocapsules were easily uptaken by MCF-7 cells.

Besides chitosan, pectin with different molecular weight (76, 110 and 96 kg/mol, LM,

HM and AM pectin) was also introduced by Klemetsrud and coworkers to investigate the interaction between pectin-coated liposomes and mucin (**Table 1.4, Entry 19**).[146] Liposomes were firstly prepared using dipalmitoyl phosphatidylcholine (DPPC) and dipalmitoyl trimethylammoniumpropane (DPTAP) through the lipid film hydration method. Due to the mucoadhesive properties of pectin, these coated liposomes (0.02% of coated pectin, diameter of 229, 302 and 418 nm for LM, AM and HM pectin based capsules, respectively) were shown to interact with mucin to form aggregates (diameter of 312, 446 and 582 nm for aggregates of LM, AM and HM-based capsules/mucin, respectively).

Borsali and Soldi decorated PS-*b*-PAA based polymersomes with chitosan (37CS and 5CS, molecular weight of 37 kg/mol and 5 kg/mol) for generating finasteride-loaded nanocarriers (finasteride is a drug for benign prostatic hyperplasia and male pattern baldness).[147] PS_{139}-*b*-PAA_{17} and PS_{404}-*b*-PAA_{63} were first employed to construct polymersomes (C3 and C7, diameter of 414 and 180 nm, respectively) through a co-solvent self-assembly process. The chitosan-coated polymersomes (C3/37CS, C3/5CS, C7/37CS and C7/5CS, hydrodynamic diameter of 712, 404, 363 and 183 nm, respectively) were capable to encapsulate finasteride and enhance the permeation of the drug in *ex vivo* studies. Due to the presence of positively charged chitosan, the coated polymersomes exhibited strong interaction with skin components compared to uncoated ones (**Table 1.4, Entry 20**).

(2) Multilayer capsules through Layer-by-layer strategy

In 2010, Ge and coworkers prepared alginate-chitosan containing liposomes (**Table 1.4, Entry 21**). Unilamellar liposomes were first generated from DPPC, N-dioctadecyldimethylammonium bromide (DDAB) and cholesterol applying evaporation and post-extrusion techniques (the solution was finally filtrated by 100 or 200 nm polycarbonate filters). Nanocapsules (four layers, D_h = 414 nm) were then obtained by successive deposition of alginate and chitosan (10 kg/mol) on the cationic liposomes through L-b-L process. The nanocapsules were stable in SDS aqueous solution and hydrophilic solution (1/10 water/ethanol, v/v).[148]

Using a similar L-b-L process, Cuomo and coworkers constructed alginate/chitosan based nanocapsules from cationic liposomes (diameter of 220 nm) of DDAB (**Table 1.4, Entry 22**, **Figure 1.26**).[149] After removal of DDAB (triggered by the introduction of nonionic surfactant Triton X-100), nanocapsules with a diameter of about 500 nm were obtained. The same group also described the synthesis of dextran-loaded multi-layered nanocapsules from liposome templates.[150-151] In a preliminary step unilamellar liposomes (D_h of 80 nm) were prepared using DPPC and DDAB (molar ratio at 6.5:3.5) by reverse-phase evaporation. The polyelectrolyte shell was then formed by L-b-L sequential deposition of chitosan and alginate resulting in multi-layered nanocapsules with a diameter of 300 nm (thickness of 20 nm). These nanocapsules were capable to load FITC-Dextran (efficiency ~ 50%) with different MW (20, 40 and 70 kg/mol). The release of FITC-Dextran was triggered by the dissolution of the (liposome) inner part of the nanocapsules. The release behavior was further controlled by adjustment of pH and by the MW of FITC-Dextran (**Table 1.4, Entry 23**).

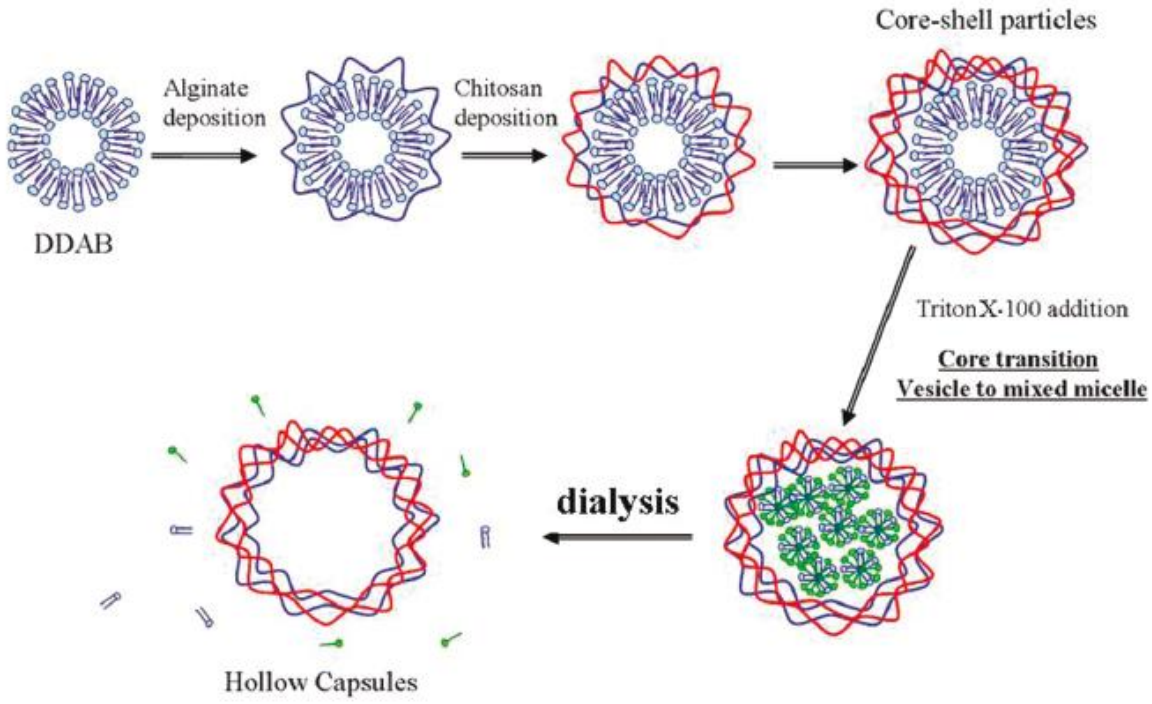

Figure 1.26. Alginate-Chitosan nanocapsules through L-b-L strategy. [149]

Fujimoto and coworkers employed negatively-charged dilauroyl phosphatidic acid

(DLPA)/dimyristoyl phosphatidylcholine (DMPC) (1/1, molar ratio) based unilamellar liposomes (D_h = 100 nm) as templates for the preparation of polysaccharide based nanocapsules (**Table 1.4, Entry 24, Figure 1.27**).[152-153] The shell of capsules was prepared by sequential disposition of chitosan (CHI) and dextran sulphate or DNA. In contrast to the liposome precursors, the resulting capsules were proven to be stable against Triton X-100. The capsules were then loaded with 1-hydroxy pyrene-3,6,8-trisulfonic acid (HPTS), alendronate, calcium phosphate (CaP) and glucose (encapsulation was performed before L-b-L deposition). At room temperature, release was mostly suppressed after polymer deposition. Owing to denaturation, release was observed for DNA-containing nanocapsules upon heating to 60°C.

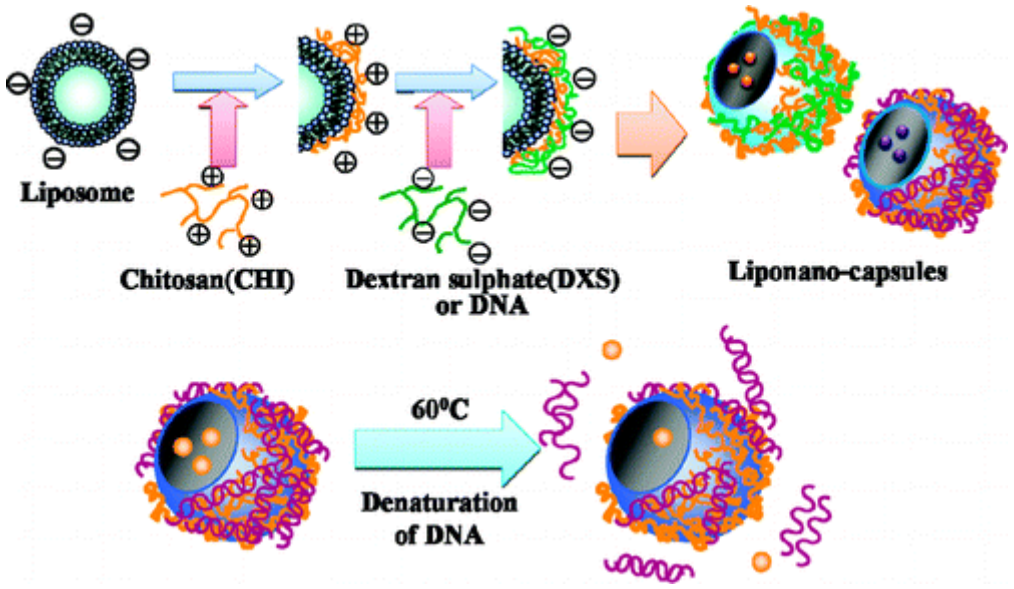

Figure 1.27. Preparation and decomposition of multi-layered glyconanocapsules through DNA denaturation.[152]

Peng and coworkers prepared paclitaxel-loaded chitosan-coated nanocapsules (**Table 1.4, Entry 25**).[154] Liposomes (size of 108 nm) were prepared using soya lecithin, cholesterol and stearyl amine through the thin film hydration technique. Polyacrylic acid (PAA) and chitosan (50 kg/mol) were then used to build double layered capsules (D_h = 215 nm). Paclitaxel was encapsulated during the preparation of the liposomes with an efficiency of 71%. Due to the presence of two polyelectrolyte layers, the release of paclitaxel was sustained with a lag time of 3h compared to

uncoated liposomes.

1.2.3.3 Modification of preset capsules.

In addition to the template strategy described above, carbohydrate functionalized nanocapsules can also be prepared through post-modification of preformed nanocapsules. In general, the sugar moieties are introduced on the preset capsules through chemical coupling reaction or physical post-insertion of polysaccharide chains. In contrast to other strategies, the shell of preset capsules is then only partially decorated with carbohydrates (**Scheme 1.7**).

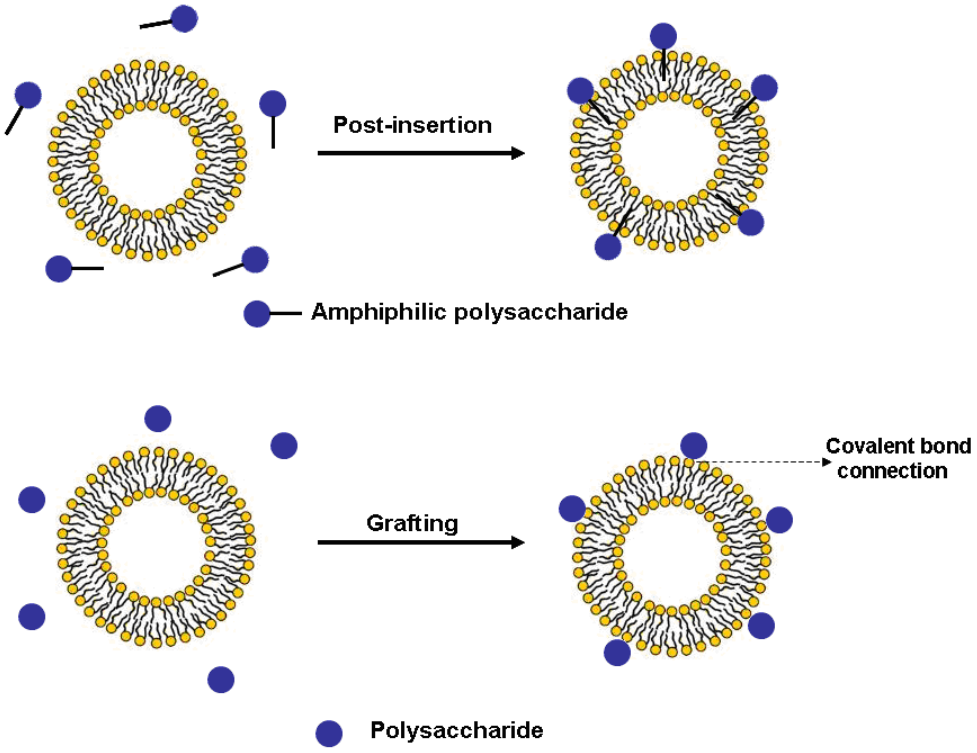

Scheme 1.7. General process of modification of preset capsules.

(1) Post-insertion

In 2008, Richard *et al.* designed dextran-containing lipid nanocapsules through post-insertion process (**Table 1.4, Entry 26**).[155] Lipid nanocapsules (diameter of 59 nm) were prepared using commercial lipids (solutol, labrafac and phospholipon) through phase inversion method. Amphiphilic dextran was generated from modification of Dextran (40 kg/mol) with amine terminal-functionalized Brij 58P by

reductive animation. As evidenced by NMR and TEM, dextran functionalized nanocapsules (diameter of 73 nm) were finally obtained through insertion of modified dextran chains on the preformed nanocapsules at room temperature or 60 °C for 24h (mass incorporation, 5% at room temperature and 10% at 60°C:).

In a same approach, lipid nanocapsules (LNC, diameter of 49 nm) were also prepared by Benoit and co-workers in order to generate chitosan/lipid nanocapsules. Lipochitosan chains (LC, D_{acyl} = 1.3) obtained by modification of chitosan (CS, 4~6 kg/mol) with stearic anhydride, were then inserted within the shell of LNC (through incubation at 37 °C for 24h) to generate chitosan-functionalized nanocapsules (LNC-LC, size from 50 to 62 nm). LNC-LC nanocapsules were post-modified with chitosan and dextran sulphate (6.5~10 kg/mol) by L-b-L deposition to form multi-layered nanocapsules (diameter of 200 nm). Fondaparinux sodium (FP, a heparin-like pentasaccharide) was also incorporated within the shell in the course of the wall construction (**Table 1.4, Entry 27**).[156] More recently, the same group reported a similar post-insertion route to elaborate polysaccharide/lipid nanocapsules using hydroxylamine modified dextran (lipodextran, LD, 40 kg/mol) (**Table 1.4, Entry 28**). In comparison to LNC and LNC-LD, the positively charged LNC-LC showed enhanced uptake by HEK293 cells. Interestingly, post-insertion of polysaccharide chains did not influence the bio-distribution of the nanocapsules in mice.[157]

Tan and co-workers prepared amphiphilic N-palmitoyl chitosan (ChP) from modification of water-soluble chitosan (roughly 30 kg/mol) with palmitoyl chloride.[158] Oleic acid based liposomes (size of 163 nm) were prepared by precise dissolution in a borate buffer and chitosan chains were then anchored on the liposomes. The size of the chitosan-functionalized nanocapsules decreased with the amount of chitosan and the smallest liposomes (size of 130 nm) were obtained when 15% of chitosan was introduced (**Table 1.4, Entry 29**). The authors pointed out that the presence of chitosan on the outer shell improved the integrity and rigidity of the nano-objects.

(2) Grafting strategy

Peer and coworkers described the preparation of hyaluronan-grafted nanocapsules (**Table 1.4, Entry 30**).[159-160] Liposomes were first prepared from the self-organization of 1,2-dilauroyl-sn-glycero-3-phosphoethanolamine (DLPE) and 1,2-dilauroyl-sn-glycero-3-glycerol (DLPG) (molar ratio of DLPE/DLPG is 9/1). Hyaluronan chains (HA, 750 kg/mol) were covalently grafted onto the surface of the liposomes through carbodiimide induced coupling reactions. HA-grafted capsules (diameter of 100 nm) were loaded with anti-cancer drug, i.e. mitomycin C and paclitaxel (efficiency approaching 100%). HA-grafted nanocarriers were proven to enhance the efficacy of drugs and to ensure efficient targeting of CD44 cell surface receptors.

Carboxymethyl chitosan tethered lipid vesicles were reported by Banerjee and co-workers.[161] Amino-functionalized liposomes were first prepared using DPPC and 1,2-distearoyl-sn-glycero-3-phosphoethanolamine (DSPE) applying the thin-film hydration method. Carboxymethyl chitosan (7000 kg/mol) was then grafted at the surface of liposomes through amidation.The resulting nanocapsules (with a size from 200 to 300 nm) allowed for the encapsulation of paclitaxel with an efficiency up to 83.8%. *In vivo* efficacy in subcutaneous model of B16F10 underlined significant improvement of tumour growth inhibition and survival with orally administered paclitaxel-loaded chitosan-decorated vesicles (*vs* lipid vesicles) (**Table 1.4, Entry 31**).

Chitosan-thioglycolic acid (77 and 150 kg/mol) was grafted onto DPPC/ 1,2-dipalmitoyl-sn-glycero-3-phosphoethanolamine-*N*-[4-(p-maleimidomethyl)cyclohe xane-carboxamide] liposomes (D_h = 201 nm) prepared through thin film rehydration method (**Table 1.4, Entry 32**). [162] The grafting of the polysaccharide was performed through maleimide/thiol coupling chemistry. The resulting nanocapsules (D_h = 354 and 590 nm) did not induce immunogenic response after oral administration to rats and were proven to improve the permeation of liposomes in *ex vivo* studies.

1.2.4 Nanoprecipitation

Nanoprecipitation[178], also called as “ouzo effect” or “solvent shifting process”, is a simple technique for preparation of colloids with narrow size distribution avoiding the utilization of ultra-sonication, other high shearing force or surfactants. Since no pre-emulsion is required, this solvent shifting method is more straightforward and simpler than the emulsification approaches.

In nanoprecipitation, a hydrophobic solute (oil, dye, polymer) is dissolved in an organic solvent which is fully miscible with water. Upon addition of water, the solution becomes a non-solvent of the solute which comes out of the solution. Under appropriate conditions, this process spontaneously generates metastable dispersion of nanometer-scale droplets or particles without using surfactants. This process is simple, cheap and applicable to numerous solutes and solvents.

The group of Lecommandoux reported the preparation of glycopolymersomes using the nanoprecipitation technique (see previous sections).[99, 115, 143] However, in these studies, the formation of hollow nano-objects is mostly relying on the features of the amphiphilic carbohydrate-based block copolymers (blocks length, nature of the blocks…) which drive their self-assembly in solution. In other words, the formation of the nanocapsules is not strictly due to the solvent shifting process. From that point of view, to our knowledge, the elaboration of glyconanocapsules (exclusively) induced by the solvent shifting process has not been reported yet.

1.3 Conclusion

Due to the key role of saccharides in biological recognition events, considerable efforts have been devoted to the preparation of tailor-made glycomaterials. In view of generating drug delivery devices not only capable to carry and release therapeutic agents in a controlled manner but also to target specific sites, significant attention has been paid over the last decades on the development of synthetic glyconanocapsules. In this Chapter, we have shown that the generation of such polymer nanocapsules remains a considerable challenge to (physical) chemists. To address this task, soft

matter technologies can effectively produce those via e.g. i) self-assembly of amphiphilic block copolymers into vesicular morphologies, ii) interfacial polymerization in miniemulsion conditions iii) micelles core removal or iv) covalent grafting or layer-by-layer procedures in combination with sacrificial template strategies have been widely exploited. To a lesser extent, approaches based on emulsification techniques, i.e. double emulsification, emulsification-coacervation or polymer coating, have also been reported to generate nanocapsules mostly from polysaccharides. Surprisingly, the nanoprecipitation process which is based on the supersaturation of whatever hydrophobic solute (oil, polymer solids) in a hydrophilic solvent (ethanol, glycerol, acetone…) when adding a far excess of the non-solvent (water) to generate dispersions of small droplets or nanoparticles, has not been used yet to build glyconanocapsules. In this context, one objective of this PhD work will be to explore the feasibility of this last approach to build precisely defined glyconanocapsules in one step (Chapter 4).

1.4 Reference

1. Quintanar-Guerrero, D.; Allemann, E.; Fessi, H. and Doelker, E. *Drug Development and Industrial Pharmacy*, **1998**, *24*, 1113-1128.
2. Mora-Huertas, C. E.; Fessi, H. and Elaissari, A. *Int. J. Pharm.*, **2010**, *385*, 113-142.
3. Sapsford, K. E.; Algar, W. R.; Berti, L.; Gemmill, K. B.; Casey, B. J.; Oh, E.; Stewart, M. H. and Medintz, I. L. *Chem. Rev.*, **2013**, *113*, 1904-2074.
4. Suyetin, M. V. and Vakhrushev, A. V. *Micro & Nano Letters*, **2009**, *4*, 172-176.
5. Savoji, M. T.; Strandman, S. and Zhu, X. X. *Langmuir*, **2013**, *29*, 6823-6832.
6. Mak, W. C.; Bai, J.; Chang, X. Y. and Trau, D. *Langmuir*, **2009**, *25*, 769-775.
7. Kreft, O.; Javier, A. M.; Sukhorukov, G. B. and Parak, W. J. *Journal of Materials Chemistry*, **2007**, *17*, 4471-4476.
8. Qi, W.; Duan, L. and Li, J. B. *Soft Matter*, **2011**, *7*, 1571-1576.
9. Kwon, O. S.; Jang, J. and Bae, J. *Curr. Org. Chem.*, **2013**, *17*, 3-13.
10. Jyothi Sri, S.; Seethadevi, A.; Suria Prabha, K.; Muthuprasanna, P. and Pavitra, P. *Int. J. Pharma Bio Sci.*, **2012**, *3*, 509-531.
11. Couvreur, P.; Barratt, G.; Fattal, E.; Legrand, P. and Vauthier, C. *Critical Reviews in Therapeutic Drug Carrier Systems*, **2002**, *19*, 99-134.
12. Abed, N. and Couvreur, P. *International Journal of Antimicrobial Agents*, **2014**, *43*, 485-496.
13. Mura, S.; Nicolas, J. and Couvreur, P. *Nature Materials*, **2013**, *12*, 991-1003.
14. Nicolas, J.; Mura, S.; Brambilla, D.; Mackiewicz, N. and Couvreur, P. *Chem. Soc. Rev.*, **2013**, *42*, 1147-1235.
15. van Dongen, S. F. M.; de Hoog, H. P. M.; Peters, R.; Nallani, M.; Nolte, R. J. M. and van Hest, J. C. M. *Chem. Rev.*, **2009**, *109*, 6212-6274.
16. De Koker, S.; Hoogenboom, R. and De Geest, B. G. *Chem. Soc. Rev.*, **2012**, *41*, 2867-2884.
17. Damge, C.; Vranckx, H.; Balschmidt, P. and Couvreur, P. *J. Pharm. Sci.*, **1997**, *86*, 1403-1409.
18. Akira, S.; Uematsu, S. and Takeuchi, O. *Cell*, **2006**, *124*, 783-801.
19. Poignard, P.; Saphire, E. O.; Parren, P. and Burton, D. R. *Annual Review of Immunology*, **2001**, *19*, 253-274.
20. Wight, T. N.; Kinsella, M. G. and Qwarnstrom, E. E. *Curr. Opin. Cell Biol.*, **1992**, *4*, 793-801.
21. Kim, B. S.; Hong, D. J.; Bae, J. and Lee, M. *J. Am. Chem. Soc.*, **2005**, *127*, 16333-16337.
22. Kim, B. S.; Yang, W. Y.; Ryu, J. H.; Yoo, Y. S. and Lee, M. *Chemical Communications*, **2005**, 2035-2037.
23. Ryu, J. H.; Lee, E.; Lim, Y. B. and Lee, M. *J. Am. Chem. Soc.*, **2007**, *129*, 4808-4814.
24. Wang, G. Y.; Du, Z. P.; Li, Q. X. and Zhang, W. *Journal of Physical Chemistry B*, **2010**, *114*, 6872-6877.
25. Vivares, D.; Soussan, E.; Blanzat, M. and Rico-Lattes, I. *Langmuir*, **2008**, *24*, 9260-9267.
26. Soussan, E.; Mille, C.; Blanzat, M.; Bordat, P. and Rico-Lattes, I. *Langmuir*, **2008**, *24*, 2326-2330.
27. Moise, M.; Sunel, V.; Holban, M.; Popa, M.; Desbrieres, J.; Peptu, C. and Lionte, C. *Journal of Materials Science*, **2012**, *47*, 8223-8233.
28. Li, X. Y.; Qi, J. P.; Xie, Y. C.; Zhang, X.; Hu, S. W.; Xu, Y.; Lu, Y. and Wu, W. *Int. J. Nanomed.*, **2013**, *8*, 23-32.
29. Lertsutthiwong, P.; Noomun, K.; Jongaroonngamsang, N.; Rojsitthisak, P. and Nimmannit, U. *Carbohydrate Polymers*, **2008**, *74*, 209-214.
30. Lertsutthiwong, P.; Rojsitthisak, P. and Nimmannit, U. *Materials Science & Engineering C-Biomimetic and Supramolecular Systems*, **2009**, *29*, 856-860.
31. Grebinisan, D.; Holban, M.; Sunel, V.; Popa, M.; Desbrieres, J. and Lionte, C. *Cellulose Chemistry and*

Technology, **2011**, *45*, 571-577.

32. Jana, S.; Gangopadhaya, A.; Bhowmik, B. B.; Nayak, A. K. and Mukherjee, A. *Int. J. Biol. Macromol.*, **2015**, *72*, 28-30.

33. Calvo, P.; RemunanLopez, C.; VilaJato, J. L. and Alonso, M. J. *Colloid and Polymer Science*, **1997**, *275*, 46-53.

34. Calvo, P.; VilaJato, J. L. and Alonso, M. J. *Int. J. Pharm.*, **1997**, *153*, 41-50.

35. De Campos, A. M.; Sanchez, A.; Gref, R.; Calvo, P. and Alonso, M. J. *European Journal of Pharmaceutical Sciences*, **2003**, *20*, 73-81.

36. Prego, C.; Fabre, M.; Torres, D. and Alonso, M. J. *Pharmaceutical Research*, **2006**, *23*, 549-556.

37. Goycoolea, F. M.; Valle-Gallego, A.; Stefani, R.; Menchicchi, B.; David, L.; Rochas, C.; Santander-Ortega, M. J. and Alonso, M. J. *Colloid and Polymer Science*, **2012**, *290*, 1423-1434.

38. Vicente, S.; Peleteiro, M.; Diaz-Freitas, B.; Sanchez, A.; Gonzalez-Fernandez, A. and Alonso, M. J. *Journal of Controlled Release*, **2013**, *172*, 773-781.

39. Prego, C.; Torres, D.; Fernandez-Megia, E.; Novoa-Carballal, R.; Quinoa, E. and Alonso, M. J. *Journal of Controlled Release*, **2006**, *111*, 299-308.

40. Torrecilla, D.; Lozano, M. V.; Lallana, E.; Neissa, J. I.; Novoa-Carballal, R.; Vidal, A.; Fernandez-Megia, E.; Torres, D.; Riguera, R.; Alonso, M. J. and Dominguez, F. *European Journal of Pharmaceutics and Biopharmaceutics*, **2013**, *83*, 330-337.

41. Vicente, S.; Goins, B. A.; Sanchez, A.; Alonso, M. J. and Phillips, W. T. *Vaccine*, **2014**, *32*, 1685-1692.

42. Santander-Ortega, M. J.; Peula-Garcia, J. M.; Goycoolea, F. M. and Ortega-Vinuesa, J. L. *Colloids and Surfaces B-Biointerfaces*, **2011**, *82*, 571-580.

43. Santander-Ortega, M. J.; Lozano-Lopez, M. V.; Bastos-Gonzalez, D.; Peula-Garcia, J. M. and Ortega-Vinuesa, J. L. *Colloid and Polymer Science*, **2010**, *288*, 159-172.

44. Sanchez-Moreno, P.; Ortega-Vinuesa, J. L.; Martin-Rodriguez, A.; Boulaiz, H.; Marchal-Corrales, J. A. and Peula-Garcia, J. M. *International Journal of Molecular Sciences*, **2012**, *13*, 2405-2424.

45. Asthana, S.; Jaiswal, A. K.; Gupta, P. K.; Pawar, V. K.; Dube, A. and Chourasia, M. K. *Antimicrobial Agents and Chemotherapy*, **2013**, *57*, 1714-1722.

46. Fernandes, M. M.; Francesko, A.; Torrent-Burgues, J.; Carrion-Fite, F. J.; Heinze, T. and Tzanov, T. *Biomacromolecules*, **2014**, *15*, 1365-1374.

47. Chaubey, P. and Mishra, B. *Carbohydrate Polymers*, **2014**, *101*, 1101-1108.

48. Oyarzun-Ampuero, F. A.; Rivera-Rodriguez, G. R.; Alonso, M. J. and Torres, D. *European Journal of Pharmaceutical Sciences*, **2013**, *49*, 483-490.

49. Preetz, C.; Rube, A.; Reiche, I.; Hause, G. and Mader, K. *Nanomedicine-Nanotechnology Biology and Medicine*, **2008**, *4*, 106-114.

50. Preetz, C.; Hauser, A.; Hause, G.; Kramer, A. and Mader, K. *European Journal of Pharmaceutical Sciences*, **2010**, *39*, 141-151.

51. Liu, Q.; Yin, B. R.; Yang, T. S.; Yang, Y. C.; Shen, Z.; Yao, P. and Li, F. Y. *J. Am. Chem. Soc.*, **2013**, *135*, 5029-5037.

52. Kansal, S.; Tandon, R.; Verma, A.; Misra, P.; Choudhary, A. K.; Verma, R.; Verma, P. R. P.; Dube, A. and Mishra, P. R. *British Journal of Pharmacology*, **2014**, *171*, 4038-4050.

53. Kansal, S.; Tandon, R.; Dwivedi, P.; Misra, P.; Verma, P. R. P.; Dube, A. and Mishra, P. R. *Journal of Antimicrobial Chemotherapy*, **2012**, *67*, 2650-2660.

54. Beloqui, A.; Solinis, M. A.; des Rieux, A.; Preat, V. and Rodriguez-Gascon, A. *Int. J. Pharm.*, **2014**, *468*, 105-111.

55. Landfester, K. *Adv. Mater.*, **2001**, *13*, 765-768.
56. Marie, E.; Landfester, K. and Antonietti, M. *Biomacromolecules*, **2002**, *3*, 475-481.
57. Zhu, A. P.; Pan, Y. N.; Dai, S.; Li, F. J. and Shen, J. *Biomacromolecules*, **2009**, *10*, 1997-2002.
58. Chen, C. K.; Wang, Q.; Jones, C. H.; Yu, Y.; Zhang, H. G.; Law, W. C.; Lai, C. K.; Zeng, Q. H.; Prasad, P. N.; Pfeifer, B. A. and Cheng, C. *Langmuir*, **2014**, *30*, 4111-4119.
59. Zhang, W. J.; Gilstrap, K.; Wu, L. Y.; Bahadur, K. C. R.; Moss, M. A.; Wang, Q. A.; Lu, X. B. and He, X. M. *Acs Nano*, **2010**, *4*, 6747-6759.
60. Jiang, B. B.; Hu, L.; Gao, C. Y. and Shen, J. C. *Acta Biomaterialia*, **2006**, *2*, 9-18.
61. Crespy, D.; Stark, M.; Hoffmann-Richter, C.; Ziener, U. and Landfester, K. *Macromolecules*, **2007**, *40*, 3122-3135.
62. Jagielski, N.; Sharma, S.; Hombach, V.; Mailander, V.; Rasche, V. and Landfester, K. *Macromolecular Chemistry and Physics*, **2007**, *208*, 2229-2241.
63. Sharma, S.; Paiphansiri, U.; Hombach, V.; Mailander, V.; Zimmermann, O.; Landfester, K. and Rasche, V. *Contrast Media & Molecular Imaging*, **2010**, *5*, 59-69.
64. Baier, G.; Musyanovych, A.; Dass, M.; Theisinger, S. and Landfester, K. *Biomacromolecules*, **2010**, *11*, 960-968.
65. Taheri, S.; Baier, G.; Majewski, P.; Barton, M.; Forch, R.; Landfester, K. and Vasilev, K. *Journal of Materials Chemistry B*, **2014**, *2*, 1838-1845.
66. Malzahn, K.; Marsico, F.; Koynov, K.; Landfester, K.; Weiss, C. K. and Wurm, F. R. *Acs Macro Letters*, **2014**, *3*, 40-43.
67. Malzahn, K.; Jamieson, W. D.; Droge, M.; Mailander, V.; Jenkins, A. T. A.; Weiss, C. K. and Landfester, K. *Journal of Materials Chemistry B*, **2014**, *2*, 2175-2183.
68. Baier, G.; Baumann, D.; Siebert, J. M.; Musyanovych, A.; Mailander, V. and Landfester, K. *Biomacromolecules*, **2012**, *13*, 2704-2715.
69. Freichels, H.; Wagner, M.; Okwieka, P.; Meyer, R. G.; Mailander, V.; Landfester, K. and Musyanovych, A. *Journal of Materials Chemistry B*, **2013**, *1*, 4338-4348.
70. Baier, G.; Cavallaro, A.; Vasilev, K.; Mailander, V.; Musyanovych, A. and Landfester, K. *Biomacromolecules*, **2013**, *14*, 1103-1112.
71. Roux, R.; Sallet, L.; Alcouffe, P.; Chambert, S.; Sintes-Zydowicz, N.; Fleury, E. and Bernard, J. *Acs Macro Letters*, **2012**, *1*, 1074-1078.
72. Discher, B. M.; Won, Y. Y.; Ege, D. S.; Lee, J. C. M.; Bates, F. S.; Discher, D. E. and Hammer, D. A. *Science*, **1999**, *284*, 1143-1146.
73. Brinkhuis, R. P.; Rutjes, F. and van Hest, J. C. M. *Polymer Chemistry*, **2011**, *2*, 1449-1462.
74. Li, Z. C.; Liang, Y. Z. and Li, F. M. *Chemical Communications*, **1999**, 1557-1558.
75. Liang, Y. Z.; Li, Z. C. and Li, F. M. *New J. Chem.*, **2000**, *24*, 323-328.
76. Dong, C. M.; Sun, X. L.; Faucher, K. M.; Apkarian, R. P. and Chaikof, E. L. *Biomacromolecules*, **2004**, *5*, 224-231.
77. Dong, C. M. and Chaikof, E. L. *Colloid and Polymer Science*, **2005**, *283*, 1366-1370.
78. You, L. C. and Schlaad, H. *J. Am. Chem. Soc.*, **2006**, *128*, 13336-13337.
79. Hordyjewicz-Baran, Z.; You, L. C.; Smarsly, B.; Sigel, R. and Schlaad, H. *Macromolecules*, **2007**, *40*, 3901-3903.
80. Schlaad, H.; You, L. C.; Sigel, R.; Smarsly, B.; Heydenreich, M.; Mantion, A. and Masic, A. *Chemical Communications*, **2009**, 1478-1480.
81. Murphy, J. J.; Furusho, H.; Paton, R. M. and Nomura, K. *Chemistry-a European Journal*, **2007**, *13*,

8985-8997.
82. Xiao, N. Y.; Li, A. L.; Liang, H. and Lu, J. *Macromolecules*, **2008**, *41*, 2374-2380.
83. Zhou, W.; Dai, X. H. and Dong, C. M. *Macromolecular Bioscience*, **2008**, *8*, 268-278.
84. Dai, X. H. and Dong, C. M. *Journal of Polymer Science Part a-Polymer Chemistry*, **2008**, *46*, 817-829.
85. Dai, X. H.; Dong, C. M. and Yan, D. Y. *Journal of Physical Chemistry B*, **2008**, *112*, 3644-3652.
86. Qiu, S.; Huang, H.; Dai, X. H.; Zhou, W. and Dong, C. M. *Journal of Polymer Science Part a-Polymer Chemistry*, **2009**, *47*, 2009-2023.
87. Pearson, S.; Allen, N. and Stenzel, M. H. *Journal of Polymer Science Part a-Polymer Chemistry*, **2009**, *47*, 1706-1723.
88. Chen, Y.; Espeel, P.; Reinicke, S.; Du, P. F. E. and Stenzel, M. H. *Macromol Rapid Commun*, **2014**, *35*, 1128-1134.
89. Aissou, K.; Pfaff, A.; Giacomelli, C.; Travelet, C.; Muller, A. H. E. and Borsali, R. *Macromolecular Rapid Communications*, **2011**, *32*, 912-916.
90. Du, Z. P.; Wang, L.; Wang, G. Y. and Wang, S. J. *Colloids and Surfaces a-Physicochemical and Engineering Aspects*, **2011**, *381*, 55-60.
91. Huang, J.; Bonduelle, C.; Thevenot, J.; Lecommandoux, S. and Heise, A. *J. Am. Chem. Soc.*, **2012**, *134*, 119-122.
92. Pasparakis, G. and Alexander, C. *Angew. Chem.-Int. Edit.*, **2008**, *47*, 4847-4850.
93. Huang, Y. C.; Arham, M. and Jan, J. S. *European Polymer Journal*, **2013**, *49*, 726-737.
94. Menon, S.; Ongungal, R. M. and Das, S. *Polymer Chemistry*, **2013**, *4*, 623-628.
95. Su, L.; Zhao, Y.; Chen, G. S. and Jiang, M. *Polymer Chemistry*, **2012**, *3*, 1560-1566.
96. Su, L.; Wang, C.; Polzer, F.; Lu, Y.; Chen, G. and Jiang, M. *ACS Macro Lett.*, **2014**, *3*, 534-539.
97. Houga, C.; Le Meins, J. F.; Borsali, R.; Taton, D. and Gnanou, Y. *Chemical Communications*, **2007**, 3063-3065.
98. Houga, C.; Giermanska, J.; Lecommandoux, S.; Borsali, R.; Taton, D.; Gnanou, Y. and Le Meins, J. F. *Biomacromolecules*, **2009**, *10*, 32-40.
99. Schatz, C.; Louguet, S.; Le Meins, J. F. and Lecommandoux, S. *Angew. Chem.-Int. Edit.*, **2009**, *48*, 2572-2575.
100. Otsuka, I.; Fuchise, K.; Halila, S.; Fort, S.; Aissou, K.; Pignot-Paintrand, I.; Chen, Y. G.; Narumi, A.; Kakuchi, T. and Borsali, R. *Langmuir*, **2010**, *26*, 2325-2332.
101. Long, L. X.; Yuan, X. B.; Chang, J.; Zhang, Z. H.; Gu, M. Q.; Song, T. T.; Xing, Y.; Yuan, X. Y.; Jiang, S. C. and Sheng, J. *Carbohydrate Polymers*, **2012**, *87*, 2630-2637.
102. Chiang, W. H.; Lan, Y. J.; Huang, Y. C.; Chen, Y. W.; Huang, Y. F.; Lin, S. C.; Chern, C. S. and Chiu, H. C. *Polymer*, **2012**, *53*, 2233-2244.
103. Pramod, P. S.; Takamura, K.; Chaphekar, S.; Balasubramanian, N. and Jayakannan, M. *Biomacromolecules*, **2012**, *13*, 3627-3640.
104. Liu, K. H.; Chen, S. Y.; Liu, D. M. and Liu, T. Y. *Macromolecules*, **2008**, *41*, 6511-6516.
105. Yin, Y. H.; Xu, S.; Chang, D.; Zheng, H.; Li, J. L.; Liu, X. P.; Xu, P. H. and Xiong, F. L. *Chemical Communications*, **2010**, *46*, 8222-8224.
106. Sun, C. X.; Shu, K.; Wang, W.; Ye, Z.; Liu, T.; Gao, Y. X.; Zheng, H.; He, G. H. and Yin, Y. H. *Int. J. Pharm.*, **2014**, *463*, 108-114.
107. Zhou, C. C.; Wang, M. Z.; Zou, K. D.; Chen, J.; Zhu, Y. Q. and Du, J. Z. *Acs Macro Letters*, **2013**, *2*, 1021-1025.
108. Fan, Y. X.; Liu, Y.; Xi, J. G. and Guo, R. *Journal of Colloid and Interface Science*, **2011**, *360*, 148-153.

109. Liang, X. F.; Li, X. Y.; Chang, J.; Duan, Y. R. and Li, Z. H. *Langmuir*, **2013**, *29*, 8683-8693.
110. Wang, H. J.; Zhao, P. Q.; Liang, X. F.; Gong, X. Q.; Song, T.; Niu, R. F. and Chang, J. *Biomaterials*, **2010**, *31*, 4129-4138.
111. Gupta, P. K.; Jaiswal, A. K.; Kumar, V.; Verma, A.; Dwivedi, P.; Dube, A. and Mishra, P. R. *Molecular Pharmaceutics*, **2014**, *11*, 951-963.
112. Besheer, A.; Hause, G.; Kressler, J. and Mader, K. *Biomacromolecules*, **2007**, *8*, 359-367.
113. Upadhyay, K. K.; Le Meins, J. F.; Misra, A.; Voisin, P.; Bouchaud, V.; Ibarboure, E.; Schatz, C. and Lecommandoux, S. *Biomacromolecules*, **2009**, *10*, 2802-2808.
114. Upadhyay, K. K.; Bhatt, A. N.; Mishra, A. K.; Dwarakanath, B. S.; Jain, S.; Schatz, C.; Le Meins, J. F.; Farooque, A.; Chandraiah, G.; Jain, A. K.; Misra, A. and Lecommandoux, S. *Biomaterials*, **2010**, *31*, 2882-2892.
115. Upadhyay, K. K.; Bhatt, A. N.; Castro, E.; Mishra, A. K.; Chuttani, K.; Dwarakanath, B. S.; Schatz, C.; Le Meins, J. F.; Misra, A. and Lecommandoux, S. *Macromolecular Bioscience*, **2010**, *10*, 503-512.
116. Wu, C. X.; Chu, B.; Kuang, L. Z.; Meng, B. B.; Wang, X. Y. and Tang, S. Q. *Carbohydrate Polymers*, **2013**, *98*, 807-812.
117. Charleux, B.; Delaittre, G.; Rieger, J. and D'Agosto, F. *Macromolecules*, **2012**, *45*, 6753-6765.
118. Ladmiral, V.; Semsarilar, M.; Canton, I. and Armes, S. P. *J. Am. Chem. Soc.*, **2013**, *135*, 13574-13581.
119. Lu, F. Z.; Meng, J. Q.; Du, F. S.; Li, Z. C. and Zhang, B. Y. *Macromolecular Chemistry and Physics*, **2005**, *206*, 513-520.
120. Ting, S. R. S.; Gregory, A. M. and Stenzel, M. H. *Biomacromolecules*, **2009**, *10*, 342-352.
121. Zhang, Q.; Remsen, E. E. and Wooley, K. L. *J. Am. Chem. Soc.*, **2000**, *122*, 3642-3651.
122. Huang, H. Y.; Remsen, E. E.; Kowalewski, T. and Wooley, K. L. *J. Am. Chem. Soc.*, **1999**, *121*, 3805-3806.
123. Samarajeewa, S.; Shrestha, R.; Li, Y. L. and Wooley, K. L. *J. Am. Chem. Soc.*, **2012**, *134*, 1235-1242.
124. Decher, G.; Hong, J. D. and Schmitt, J. *Thin Solid Films*, **1992**, *210*, 831-835.
125. Becker, A. L.; Johnston, A. P. R. and Caruso, F. *Small*, **2010**, *6*, 1836-1852.
126. Liu, W. J.; Chen, G. H.; He, G. H.; He, Z. C. and Qian, Z. *Journal of Materials Science*, **2011**, *46*, 6758-6765.
127. Liu, W. J.; He, G. H. and Qian, Z. *Polymer Bulletin*, **2011**, *67*, 1237-1244.
128. Goethals, E. C.; Elbaz, A.; Lopata, A. L.; Bhargava, S. K. and Bansal, V. *Langmuir*, **2013**, *29*, 658-666.
129. Goethals, E. C.; Shukla, R.; Mistry, V.; Bhargava, S. K. and Bansal, V. *Langmuir*, **2013**, *29*, 12212-12219.
130. Taniguchi, T.; Kunisada, Y.; Shinohara, M.; Kasuya, M.; Ogawa, T.; Kohri, M. and Nakahira, T. *Colloids and Surfaces a-Physicochemical and Engineering Aspects*, **2010**, *369*, 240-245.
131. Kren, B. T.; Unger, G. M.; Sjeklocha, L.; Trossen, A. A.; Korman, V.; Dietheim-Okita, B. M.; Reding, M. T. and Steer, C. J. *Journal of Clinical Investigation*, **2009**, *119*, 2086-2099.
132. Itoh, Y.; Matsusaki, M.; Kida, T. and Akashi, M. *Chemistry Letters*, **2004**, *33*, 1552-1553.
133. Imoto, T.; Kida, T.; Matsusaki, M. and Akashi, M. *Macromolecular Bioscience*, **2010**, *10*, 271-277.
134. Anandhakumar, S.; Mahalakshmi, V. and Raichur, A. M. *Materials Science & Engineering C-Materials for Biological Applications*, **2012**, *32*, 2349-2355.
135. Thomas, M. B.; Radhakrishnan, K.; Gnanadhas, D. P.; Chakravortty, D. and Raichur, A. M. *Int. J. Nanomed.*, **2013**, *8*, 267-273.
136. Zheng, C.; Zhang, X. G.; Sun, L.; Zhang, Z. P. and Li, C. X. *Journal of Materials Science-Materials in Medicine*, **2013**, *24*, 931-939.
137. Gnanadhas, D. P.; Ben Thomas, M.; Elango, M.; Raichur, A. M. and Chakravortty, D. *Journal of Antimicrobial Chemotherapy*, **2013**, *68*, 2576-2586.
138. Shu, S. J.; Sun, C. Y.; Zhang, X. G.; Wu, Z. M.; Wang, Z. and Li, C. X. *Acta Biomaterialia*, **2010**, *6*,

210-217.
139. Shu, S. J.; Zhang, X. G.; Wu, Z. M.; Wang, Z. and Li, C. X. *Biomaterials*, **2010**, *31*, 6039-6049.
140. Liu, Y. X.; Yang, J.; Zhao, Z. Q.; Li, J. J.; Zhang, R. and Yao, F. L. *Journal of Colloid and Interface Science*, **2012**, *379*, 130-140.
141. Guo, H. L.; Guo, Q. Q.; Chu, T. C.; Zhang, X. G.; Wu, Z. M. and Yu, D. M. *Journal of Materials Science-Materials in Medicine*, **2014**, *25*, 121-129.
142. Yu, X. and Pishko, M. V. *Biomacromolecules*, **2011**, *12*, 3205-3212.
143. Bui, L.; Abbou, S.; Ibarboure, E.; Guidolin, N.; Staedel, C.; Toulme, J. J.; Lecommandoux, S. and Schatz, C. *J. Am. Chem. Soc.*, **2012**, *134*, 20189-20196.
144. Liu, N. and Park, H. J. *Colloids and Surfaces B-Biointerfaces*, **2010**, *76*, 16-19.
145. Yang, K. K.; Kong, M.; Wei, Y. N.; Liu, Y.; Cheng, X. J.; Li, J.; Park, H. J. and Chen, X. G. *Journal of Materials Science*, **2013**, *48*, 1717-1728.
146. Klemetsrud, T.; Jonassen, H.; Hiorth, M.; Kjoniksen, A. L. and Smistad, G. *Colloids and Surfaces B-Biointerfaces*, **2013**, *103*, 158-165.
147. Caon, T.; Porto, L. C.; Granada, A.; Tagliari, M. P.; Silva, M. A. S.; Simoes, C. M. O.; Borsali, R. and Soldi, V. *European Journal of Pharmaceutical Sciences*, **2014**, *52*, 165-172.
148. Ge, L. Q. and Ji, J. Y. *Asian Journal of Chemistry*, **2010**, *22*, 66-78.
149. Cuomo, F.; Lopez, F.; Miguel, M. G. and Lindman, B. *Langmuir*, **2010**, *26*, 10555-10560.
150. Cuomo, F.; Lopez, F.; Ceglie, A.; Maiuro, L.; Miguel, M. G. and Lindman, B. *Soft Matter*, **2012**, *8*, 4415-4420.
151. Cuomo, F.; Ceglie, A.; Piludu, M.; Miguel, M. G.; Lindman, B. and Lopez, F. *Langmuir*, **2014**, *30*, 7993-7999.
152. Fukui, Y. and Fujimoto, K. *Langmuir*, **2009**, *25*, 10020-10025.
153. Fukui, Y. and Fujimoto, K. *Chemistry of Materials*, **2011**, *23*, 4701-4708.
154. Chen, M. X.; Li, B. K.; Yin, D. K.; Liang, J.; Li, S. S. and Peng, D. Y. *Carbohydrate Polymers*, **2014**, *111*, 298-304.
155. Richard, A.; Barras, A.; Ben Younes, A.; Monfilliette-Dupont, N. and Melnyk, P. *Bioconjugate Chemistry*, **2008**, *19*, 1491-1495.
156. Hirsjarvi, S.; Qiao, Y.; Royere, A.; Bibette, J. and Benoit, J. P. *European Journal of Pharmaceutics and Biopharmaceutics*, **2010**, *76*, 200-207.
157. Hirsjarvi, S.; Dufort, S.; Bastiat, G.; Saulnier, P.; Passirani, C.; Coll, J. L. and Benoit, J. P. *Acta Biomaterialia*, **2013**, *9*, 6686-6693.
158. Tan, H. W. and Misran, M. *Int. J. Pharm.*, **2013**, *441*, 414-423.
159. Rivkin, I.; Cohen, K.; Koffler, J.; Melikhov, D.; Peer, D. and Margalit, R. *Biomaterials*, **2010**, *31*, 7106-7114.
160. Bachar, G.; Cohen, K.; Hod, R.; Feinmesser, R.; Mizrachi, A.; Shpitzer, T.; Katz, O. and Peer, D. *Biomaterials*, **2011**, *32*, 4840-4848.
161. Joshi, N.; Saha, R.; Shanmugam, T.; Balakrishnan, B.; More, P. and Banerjee, R. *Biomacromolecules*, **2013**, *14*, 2272-2282.
162. Gradauer, K.; Dunnhaupt, S.; Vonach, C.; Szollosi, H.; Pali-Scholl, I.; Mangge, H.; Jensen-Jarolim, E.; Bernkop-Schnurch, A. and Prassl, R. *Journal of Controlled Release*, **2013**, *165*, 207-215.
163. Sunamoto, J.; Iwamoto, K.; Kondo, H. and Shinkai, S. *Journal of Biochemistry*, **1980**, *88*, 1219-1226.
164. Sunamoto, J.; Iwamoto, K. and Kondo, H. *Biochemical and Biophysical Research Communications*, **1980**, *94*, 1367-1373.

165. Potisatityuenyong, A.; Tumcharern, G.; Dubas, S. T. and Sukwattanasinitt, M. *Journal of Colloid and Interface Science*, **2006**, *304*, 45-51.
166. Henriksen, I.; Vagen, S. R.; Sande, S. A.; Smistad, G. and Karlsen, J. *Int. J. Pharm.*, **1997**, *146*, 193-203.
167. Henriksen, I.; Smistad, G. and Karlsen, J. *Int. J. Pharm.*, **1994**, *101*, 227-236.
168. Takeuchi, H.; Matsui, Y.; Sugihara, H.; Yamamoto, H. and Kawashima, Y. *Int. J. Pharm.*, **2005**, *303*, 160-170.
169. Takeuchi, H.; Matsui, Y.; Yamamoto, H. and Kawashima, Y. *Journal of Controlled Release*, **2003**, *86*, 235-242.
170. Gerelli, Y.; Barbieri, S.; Di Bari, M. T.; Deriu, A.; Cantu, L.; Brocca, P.; Sonvico, F.; Colombo, P.; May, R. and Motta, S. *Langmuir*, **2008**, *24*, 11378-11384.
171. Gradauer, K.; Barthelmes, J.; Vonach, C.; Almer, G.; Mangge, H.; Teubl, B.; Roblegg, E.; Dunnhaupt, S.; Frohlich, E.; Bernkop-Schnurch, A. and Prassl, R. *Journal of Controlled Release*, **2013**, *172*, 872-878.
172. Mertins, O. and Dimova, R. *Langmuir*, **2011**, *27*, 5506-5515.
173. Mertins, O. and Dimova, R. *Langmuir*, **2013**, *29*, 14545-14551.
174. Quemeneur, F.; Rinaudo, M. and Pepin-Donat, B. *Biomacromolecules*, **2008**, *9*, 2237-2243.
175. Joraholmen, M. W.; Vanic, Z.; Tho, I. and Skalko-Basnet, N. *Int. J. Pharm.*, **2014**, *472*, 94-101.
176. Kudsiova, L. and Lawrence, M. J. *J. Pharm. Sci.*, **2008**, *97*, 3998-4010.
177. Kudsiova, L.; Arafiena, C. and Lawrence, M. J. *J. Pharm. Sci.*, **2008**, *97*, 3981-3997.
178. Lepeltier, E.; Bourgaux, C. and Couvreur, P. *Adv. Drug Delivery Rev.*, **2014**, *71*, 86-97.

Chapter 2

RAFT Preparation of well-defined Heptyl mannose-based Glycopolymers

Chapter 2 RAFT Preparation of well-defined Heptyl mannose-based Glycopolymers

2.1 Introduction

Adhesion of bacterial pathogens to host cells and tissues, a prerequisite for a majority of infection diseases, is governed by interactions between bacteria surface lectins and complementary carbohydrates displayed at the host cell periphery. To promote adhesion and infection of tissues through multivalent interactions, bacteria such as *Escherichia coli* (*E. coli*) express hundreds of adhesive proteinaceous hair-like organelles, type 1 fimbriae, on their cell surface. These type 1 fimbriae are cylindrical rod-shaped extensions on the *E. coli* cell wall constituted of a major pilin subunit, FimA, and followed by a short, flexible tip fibrillum composed of minor pilins FimF, FimG and the adhesin FimH. The latter is exposed at the extremity of the fimbriae and its lectin domain possesses a mannose-specific receptor site responsible for recognition and binding to host cells.[1] An overgrowth of *E. coli* is associated with infections, *i.e.* urinary tract and bladder infections, inflammatory bowel diseases, sepsis and meningitis, which usually require antibiotic treatments. As bacterial resistance to antibiotics is becoming a serious threat to public health, the anti-adhesive therapy, which lies in the use of drugs capable of preventing bacterial adhesion step with no bactericidal effect, is progressively emerging as a valuable alternative.[2] Because carbohydrate-protein interactions are intrinsically weak (K_d typically in the mM to μM range), the applicability of this approach requires to develop compounds with high affinity towards bacterial lectins so that adhesion (and thus infections) can be prevented at reasonably low concentrations. In this context, extensive research has been carried out on the design of synthetic molecular inhibitors displaying structures that optimize interactions with the lectin sugar-binding site(s) to outmatch interactions with natural ligands. The feasibility of this approach has been demonstrated for *E. coli*. In their pionnering work, Sharon and co-workers showed that mannosides bearing aromatic aglycons are more efficient FimH inhibitors than the methyl mannoside reference.[3] X-ray structure investigations on FimH lectin co-crystallized with butyl α-D-mannoside highlighted that in addition to the hydroxyl groups of D-mannose which establish hydrogen bonds with the amino acids

located at the bottom of the FimH binding pocket, the butyl group develops strong hydrophobic interactions at the entrance (of the binding pocket), the so-called tyrosine gate (Tyr48, Ile52 and Tyr137).[4] Optimization of the alkyl chain length led to the discovery of *n*-heptyl α-D-mannose (HM), a nanomolar FimH antagonist (binding affinity of 5 nM recorded by SPR).[4] These findings greatly impacted the development of FimH antagonists paving the way to the discovery of other potent compounds with biphenyl,[5-7] indolinyl phenyl,[8] or squarate aglycones[9] for the potential treatment of *E. coli*-induced urinary tract infections. Recently, it was also showed that thiazolylaminomannosides,[10] a new family of FimH antagonists, could extend the anti-adhesive concept to the treatment of specific inflammatory bowel diseases such as Crohn's disease (CD), in which adherent-invasive *Escherichia coli* (AIEC) can play a key role in the inflammation process.[11-12] Targeting the cause of the inflammation is a promising alternative to the current marketed CD drugs essentially based on lowering tumor necrosis factor (TNF) levels.[13]

Another conventional route for the design of high-affinity ligands consists in the incorporation of several epitopes on a common scaffold (multivalent molecule, dendrimer or polymer chain).[14-23] Such derivatives can display noticeable enhancement in activity compared to their monovalent counterparts on a per mole of epitope basis on a wide range of lectins. This trend is often referred to as the "cluster glycoside" effect.[24] Multivalent FimH antagonists have been reported by several research groups. In seminal works, Lindhorst[25] and Roy[26-27] developed multivalent FimH inhibitors from dendrimer scaffolds whereas Gouin and Bouckaert recently introduced HM ligands on functionalized hydrophilic cyclodextrin-based scaffolds and observed substantial cluster effects *in vitro*[28-29] and *in vivo*.[30]

In this chapter, we will describe the preparation of macromolecular anti-adhesives of type 1 piliated *E. coli* through the association of a judicious ligand selection with the presentation of multiple ligands on a polymeric scaffold. More precisely, we will firstly focus on the design and synthesis of model macromolecular inhibitors of type-1 fimbriae bacterial adhesion based on the incorporation of multiple copies of n-heptyl

α-D-mannose (HM), one of the strongest molecular binder of the monovalent lectin domain of FimH, as pendent motifs, to build series of multivalent HM-based polymers with various chain lengths and topologies for assessment of the influence of HM valency and spatial presentation of the epitopes. In addition, in order to investigate the influence of HM density and of the relative position of HM groups on the polymer chains, the synthesis of series of well-defined glyco(co)polymers with tunable compositions and microstructures will be described in this chapter.

2.2 Synthesis of mannosylated monomers

2.2.1 Synthesis of *N*-[7-(α-D-mannopyranosyloxy)heptyl] methacrylamide (HMM)

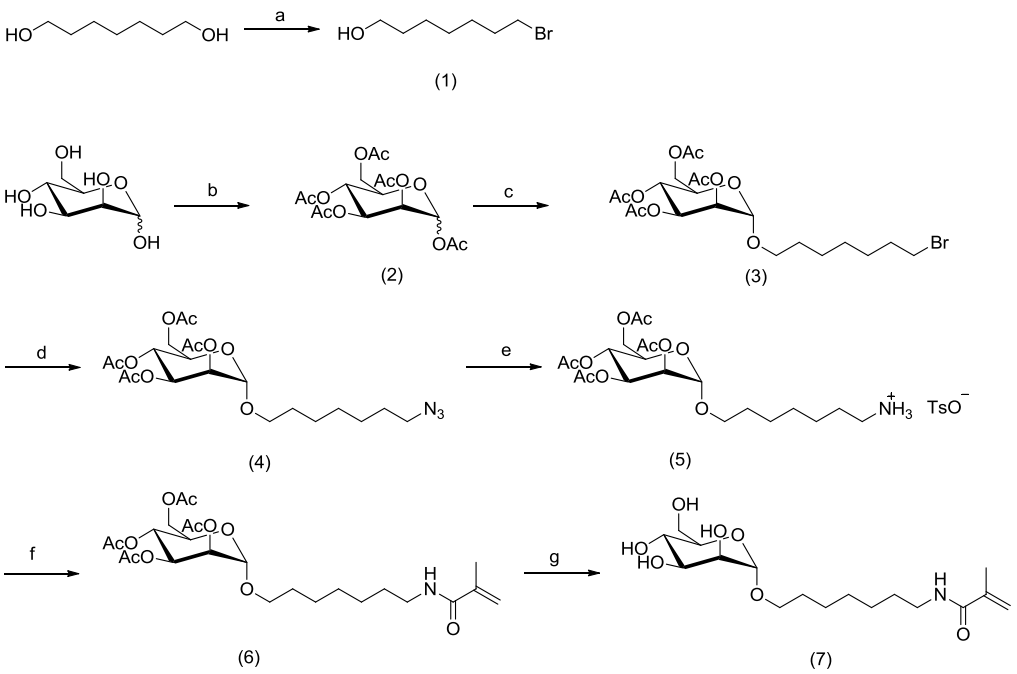

Scheme 2.1: Preparation of HMM. Reagents and conditions: a) HBr, toluene (reflux); b) anhydrous NaOAc, acetic anhydride, 100 °C; c) $SnCl_4$, CF_3CO_2Ag, CH_2Cl_2; d) NaN_3, DMF, 70 °C; e) H_2, Pd/C, p-TsOH, EtOH; f) methacryloyl chloride, CH_2Cl_2, Et_3N; g) NaOMe, MeOH.

Owing to its nanomolar affinity toward FimH lectin (K_d = 5 nM as measured by SPR)[4], heptyl mannoside (HM) is a promising building block for constructing potent anti-adhesive glycopolymers. To design a HM-based glycomonomer (HMM), a

multi-step synthetic strategy was developed (7 steps, **Scheme 2.1**). To build the spacer between the carbohydrate and the group to polymerize, 7-bromoheptan-1-ol (**1**) was first generated from 1,7-heptanediol and HBr.[31] D-mannose was then fully acetylated using anhydrous NaOAc and acetic anhydride at high temperature. The resulting α-peracetyl-mannose (**2**) was then engaged in a glycosylation reaction to attach the heptyl chain to the sugar moiety. The crude product (**3**) was subsequently reacted with sodium azide and the resulting azide group of (**4**) was then converted in a primary amine through catalytic hydrogenation. **5** was reacted with methacryloyl chloride to incorporate the polymerizable group through the formation of a stable amide bond. *N*-[7-(α-D-mannopyranosyloxy)heptyl] methacrylamide (HMM, compound **7** in scheme 2.1) was finally obtained after quantitative deprotection of the mannose under basic conditions. The NMR and ESI spectra of intermediate derivatives are given in Chapter 5 (experimental methods). The ^{1}H and ^{13}C NMR of HMM are given in **Figure 2.1**. The presence of the mannoside is clearly assessed by the peaks between 3.5 and 4 ppm and the peak at 4.91 ppm corresponding to the anomeric proton. ^{13}C spectrum further confirms the presence of the mannoside (typical signature of the anomeric carbon of mannose at 99.7 ppm, peak l). Peaks e-i belonging to the heptyl linker are observed between 1.4 and 1.7 ppm whereas the formation of the methacrylamide group is highlighted by the presence of the peaks a-c at 1.98, 5.48 and 5.71 ppm in ^{1}H NMR (peaks a-c at 17.75, 120.52 and 139.44 ppm in ^{13}C NMR). The preparation of HMM is further confirmed by ESI-MS analysis. Experimental mass for the main population at 384.1980 m/z are in excellent agreement with the theoretical mass of $(M+Na)^+$ ($[C_{17}C_{31}NO_7Na]^+$ at 384.1993 m/z) (see **Figure 2.2**).

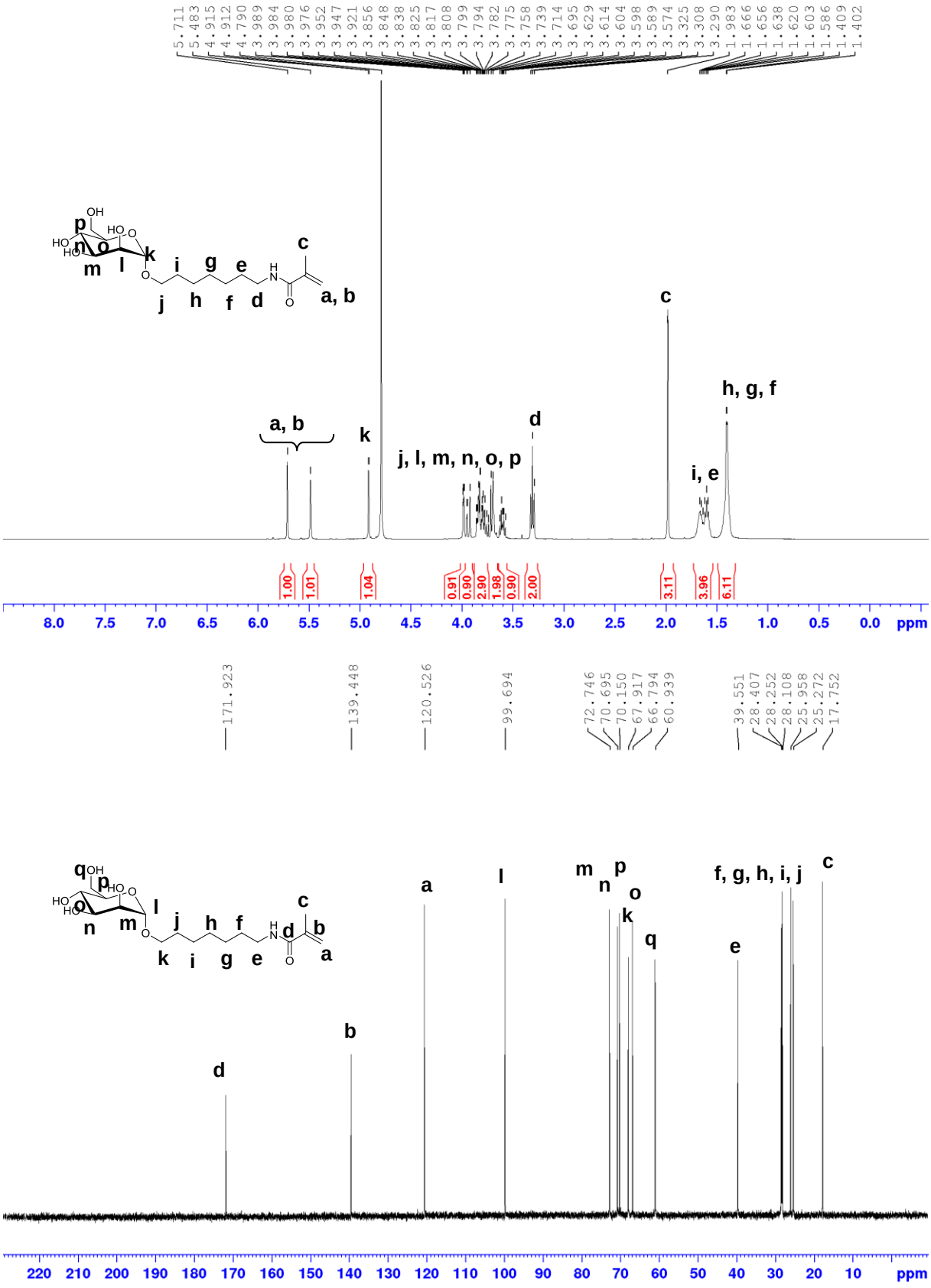

Figure 2.1. ^{1}H NMR and ^{13}C NMR spectra of HMM (D_2O, r.t.).

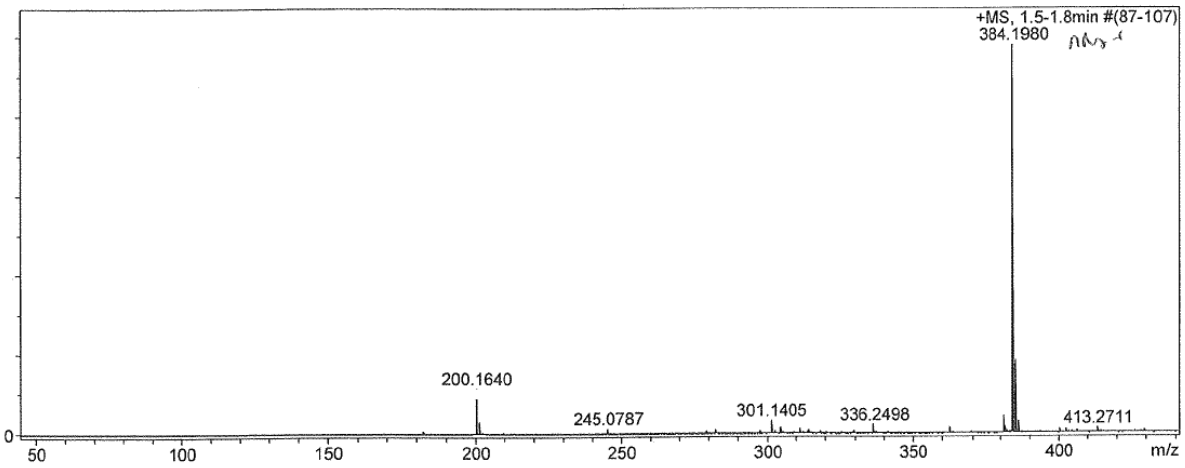

Figure 2.2. ESI-MS spectrum of HMM.

2.2.2 Synthesis of *N*-[2-(α-D-mannopyranosyloxy)ethyl] methacrylamide (EMM)

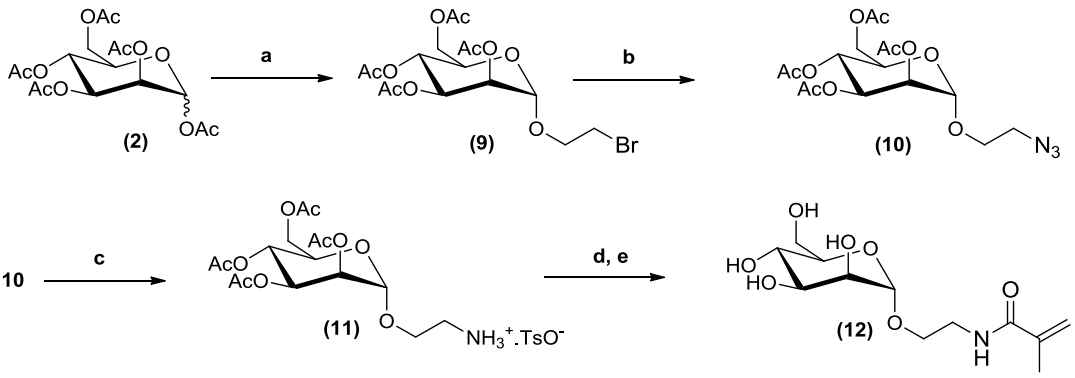

Scheme 2.2: Preparation of EMM. Reagents and conditions: a) $SnCl_4$, CF_3CO_2Ag, CH_2Cl_2; b) NaN_3, DMF, 70 °C; c) H_2, Pd/C, p-TsOH, EtOH; d) methacryloyl chloride, CH_2Cl_2, Et_3N; e) NaOMe, MeOH.

To further probe the influence of the spacing between the mannose and the polymer backbone on anti-adhesive properties of the glycopolymers, a second glycomonomer, *N*-[2-(α-D-mannopyranosyloxy)ethyl] methacrylamide (EMM), having a short ethyl linker between the mannose and the methacrylamide group was prepared. The synthesis of EMM was directly adapted from the procedure described for the preparation of HMM (**Scheme 2.2**). Briefly, 2-bromoethanol was first reacted with α-peracetyl-mannose through glycosylation and a methacrylamide group was introduced through sequential azidation, hydrogenation and methacrylation steps.

The NMR and ESI spectra of intermediate derivatives are given in Chapter 5. The ^{1}H and ^{13}C NMR spectra of this second glycomonomer after deprotection are given in **Figure 2.3**. The synthesis of EMM was confirmed by NMR analyses. Again, characteristic peaks of mannose moieties were clearly distinguished, especially the ones corresponding to anomeric proton (4.82 ppm) and carbon (100.3 ppm). The incorporation of polymerizable double bond group was ascertained by the presence of peaks at 1.89, 5.42 and 5.65 ppm for ^{1}H NMR and 18.35, 121.69 and 139.71 ppm for ^{13}C NMR. ESI-MS analysis gave further evidence of the preparation of EMM with the detection of a main population at 314.1204 m/z matching with the theoretical mass for $(M+Na)^+$ ($[C_{12}C_{21}NO_7Na]^+$ 314.1210 m/z) (see **Figure 2.4**).

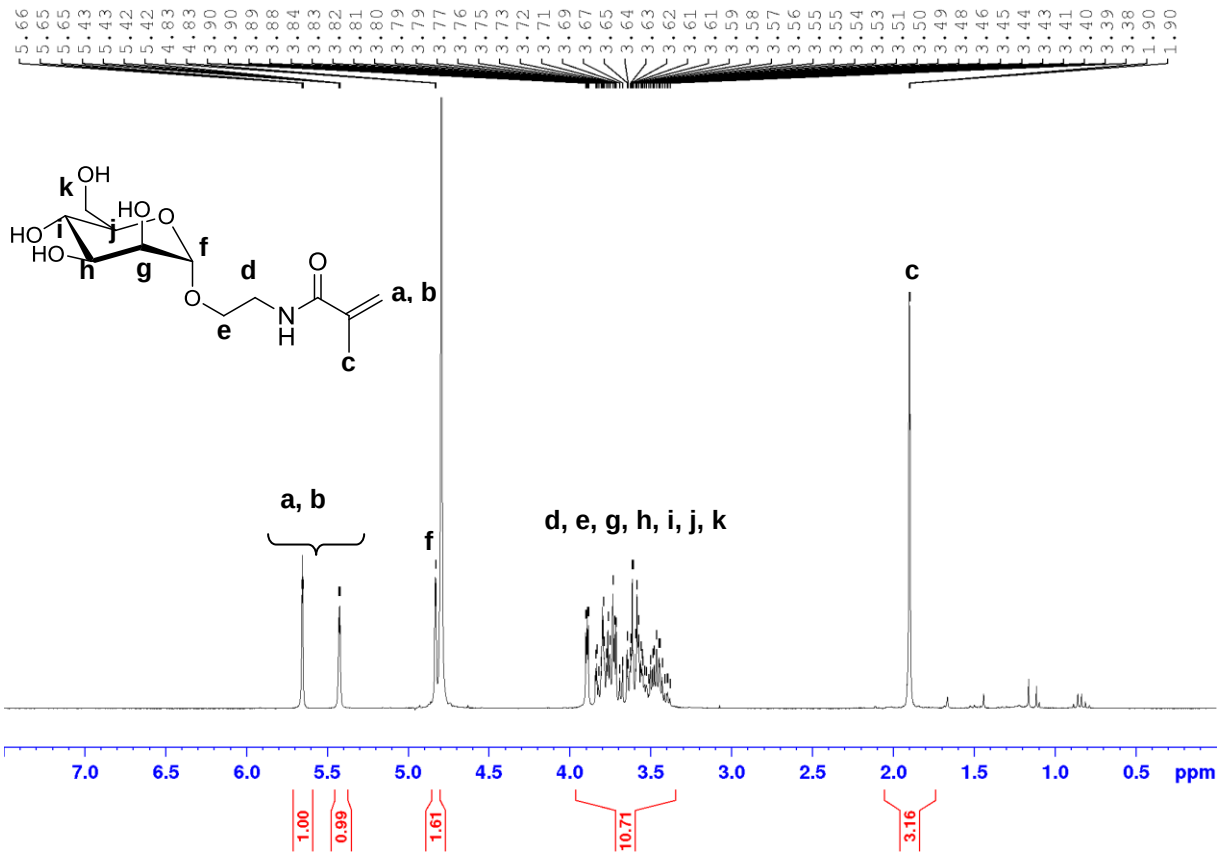

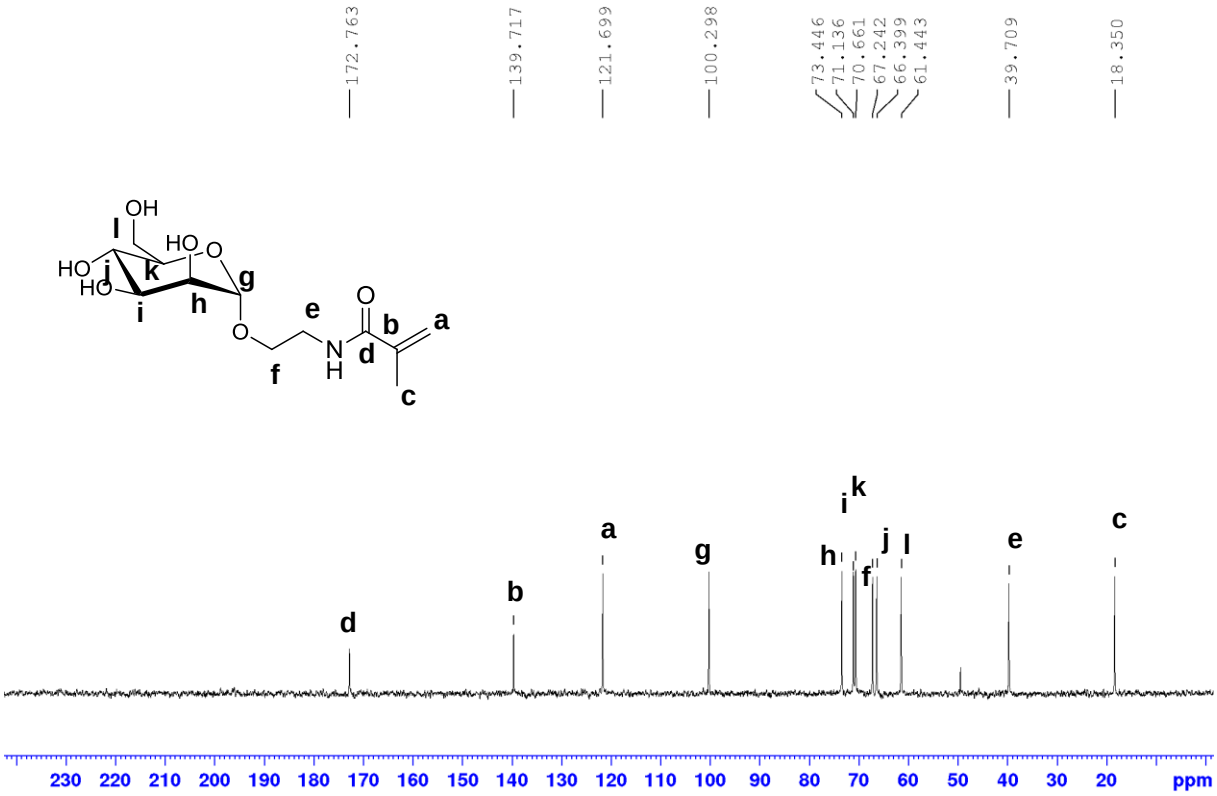

Figure 2.3. ^{1}H NMR and ^{13}C NMR spectra of EMM (D_2O, r.t.).

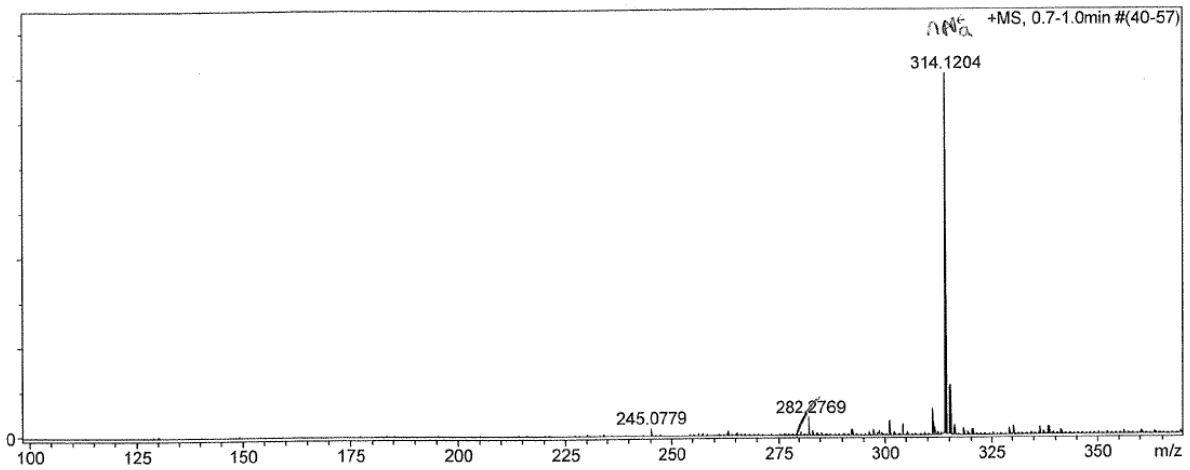

Figure 2.4. ESI-MS spectrum of EMM.

2.3 Design of multifunctional RAFT agents for the preparation of star-shaped glycopolymers

In the quest for the generation of highly potent macromolecular FimH antagonists based on HM, the influence of several parameters such as the degree of polymerization and polymer topology (linear versus 3-arm and 8-arm glycopolymers)

was investigated. To generate a series of well-defined macromolecules, we decided to employ a controlled/living radical technique, the reversible addition-fragmentation chain transfer polymerization (RAFT) which has proven to be extremely valuable for the construction of glycopolymers.[32-35] Whereas precisely defined linear glycopolymers can be straightforwardly generated by polymerizing HMM in the presence of commercially available chain transfer agents (such as 4-cyano-4-(phenylcarbonothioylthio) pentanoic acid, CPADB), the preparation of well-defined star-shaped glycopolymers requires the design of multifunctional RAFT agents. With this goal in mind, we synthesized two original RAFT agents bearing three or eight dithiobenzoate mediating groups (see **Scheme 2.3**) where the core of the multifunctional molecule constitutes the leaving group (R group) of the RAFT agent (see Chapter 5 for details on the principle of RAFT polymerization). In the presence of such RAFT agents, the arms grow directly from the multifunctional core. Practically, the multifunctional RAFT agents were synthesized in two steps (**Scheme 2.3**). The carboxyl group of CPADB was first activated through reaction with N-hydroxysuccinimide (NHS) to favor amidification over aminolysis of the dithiobenzoate.[36] The resulting RAFT agent was then added in slight excess (typically 1.1 eq. per amine) to a solution containing the polyamines, tris(2-aminoethyl)amine or Octa Ammonium POSS to afford trifunctional and octafunctional RAFT agents (**14** and **15**). ^{1}H and ^{13}C NMR spectra of multi-functional RAFT agents after purification by column chromatography (see details in experimental part) are given in **Figures 2.5** and **2.7**.

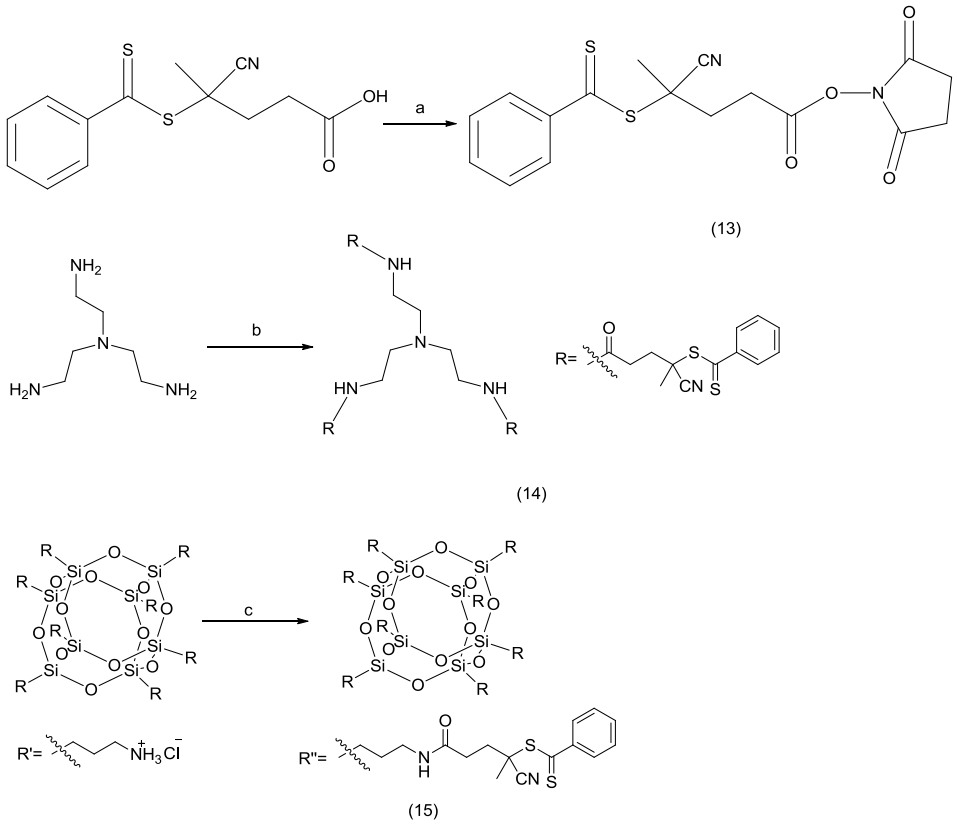

Scheme 2.3: Preparation of multifunctional RAFT agents. a) DCC, NHS, Chloroform; b) 13, MeOH/THF; C) 13, DIPEA, MeOH/THF.

Characteristic peaks of dithiobenzoate groups are present at 7.35, 7.53 and 7.86 ppm in ^{1}H NMR as well as at 126.8, 128.7, 133.2, 144.6 and 222.9 ppm in ^{13}C NMR spectra. The formation of amide bonds connecting CPADB to the core, *i.e.* tris(2-aminoethyl)amine, is also confirmed by the presence of a peak at 6.93 ppm in ^{1}H NMR spectra. The peak g belonging to the tri-functional core shows up at 3.29 ppm. The respective integration of the peaks of the dithiobenzoate and tris(2-aminoethyl)amine segments (for instance, by comparison of peaks c and g) underlines that a CPADB molecule has been coupled with each amine of the core. Therefore, the NMR spectra give evidence of the generation of CPADB-based trifunctional RAFT agent. Consistent with the NMR data, ESI-MS analysis shows a major population at 930.2409 m/z corresponding to $(M+H)^{+}$ (theoretical mass for $[C_{45}H_{52}N_7O_3S_6]^{+}$ is 930.2450) and a minor one at 465.6270 m/z corresponding to $(M+2H)^{2+}$ (see **Figure 2.6**).

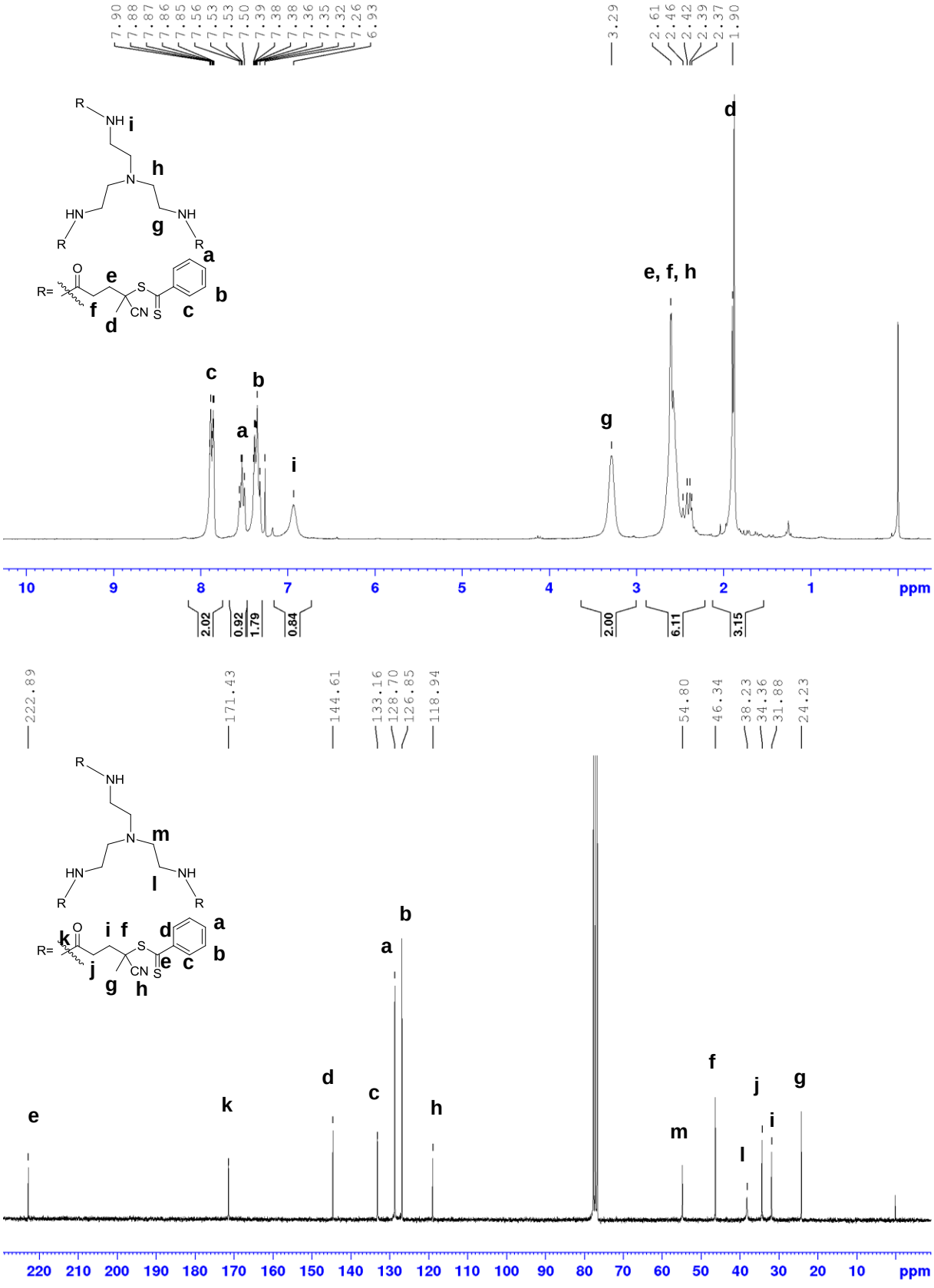

Figure 2.5. ^{1}H NMR and ^{13}C NMR spectra of CPADB-based trifunctional RAFT agent ($CDCl_3$, r.t.).

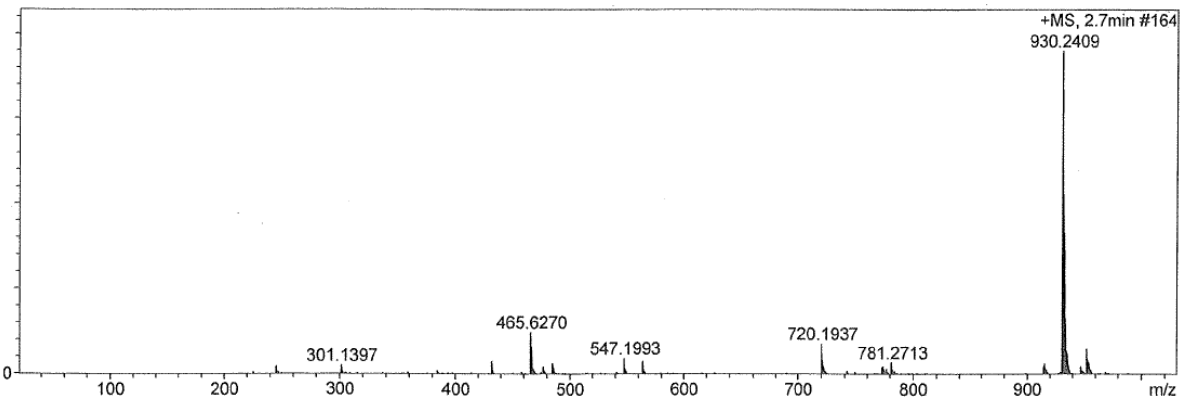

Figure 2.6. ESI-MS of CPADB-based trifunctional RAFT agent.

For CPADB based octafunctional RAFT agent, the peaks at 7.37, 7.54 and 7.88 ppm in ^{1}H NMR and 222.9 ppm in ^{13}C NMR confirms the presence of dithiobenzoate groups on the POSS cage. The peaks due to the POSS end groups are observed between 0.52-0.78, 2.24-2.75 and 3.22-3.45 ppm. The formation of amide linkages between the CPADB units and the POSS cage is confirmed by the presence of a peak at 6.56 ppm in ^{1}H NMR. The comparison of the integration of peaks c and h (**Fig 2.7**) gives clear evidence of the generation of the CPADB-based octafunctionalized RAFT agent. ESI-MS analysis reveals one major population at 1485.2639 m/z which is attributed to $(M+2H)^{2+}$ (theoretical mass of $(M+2H)^{2+}$, i.e. $C_{128}H_{154}N_{16}O_{20}S_{16}Si_8$, is 2970.5200 (see **Figure 2.8**).

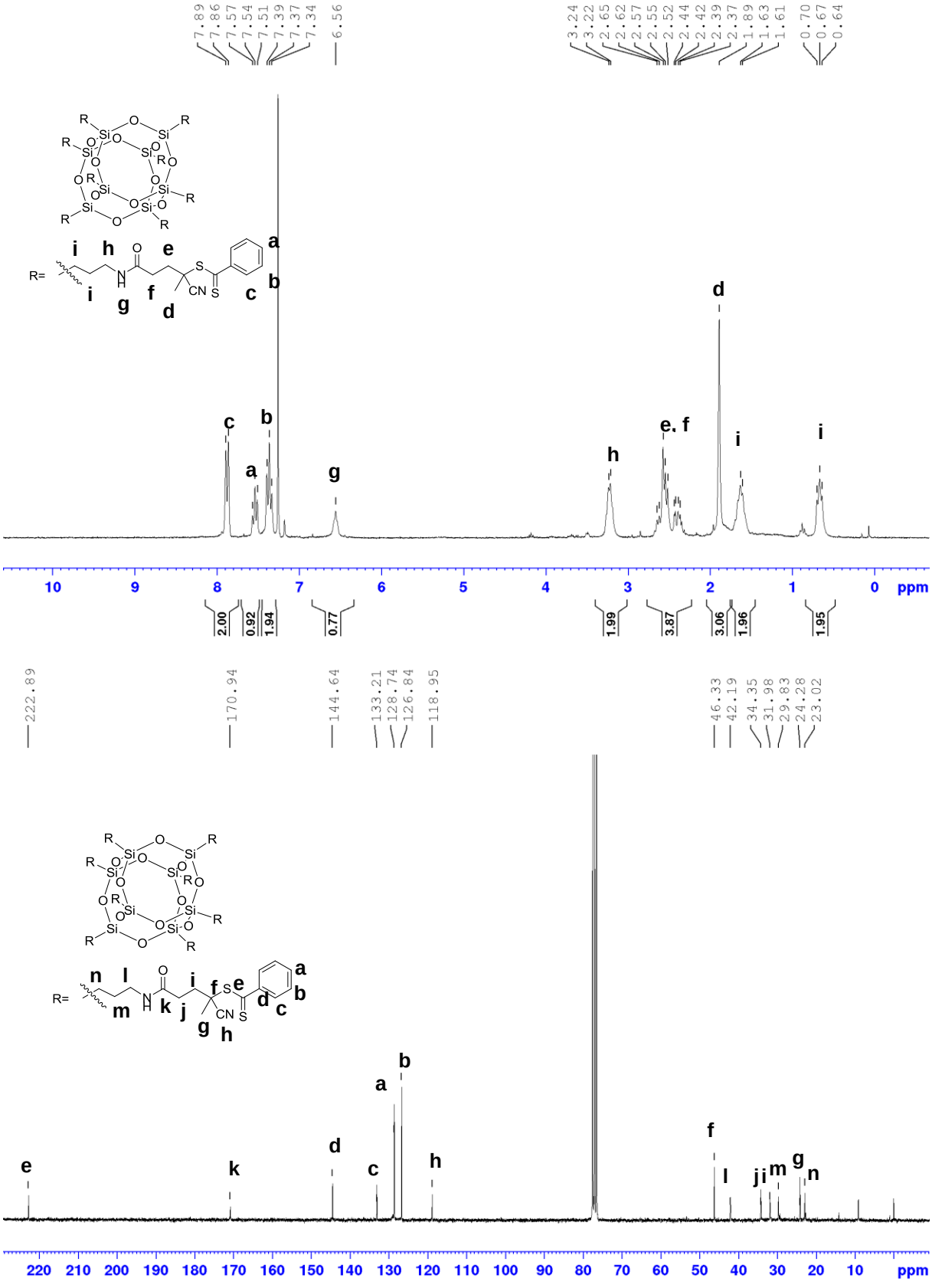

Figure 2.7. ^{1}H NMR and ^{13}C NMR spectra of CPADB-based octafunctional RAFT agent ($CDCl_3$, r.t.).

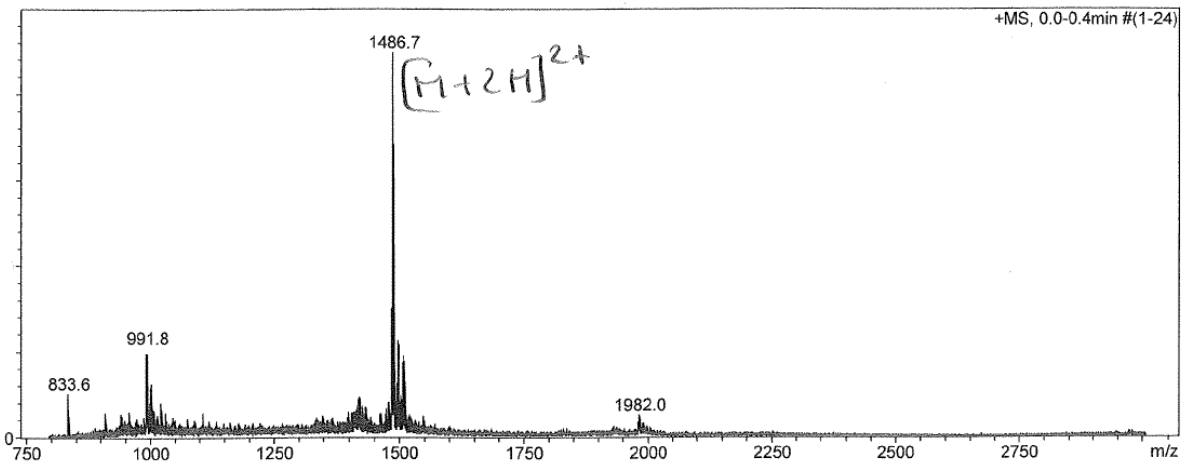

Figure 2.8. ESI-MS of CPADB-based octafunctional RAFT agent.

2.4 RAFT preparation of linear/star-shaped PHMM glycopolymers

2.4.1 Preparation of PHMM

Considering the influence of valency on carbohydrate/lectin interactions, a prerequisite for accurately studying FimH/glycopolymers interactions is to generate a set of glycopolymers with precise control over the topology and the degree of polymerization. To do so, HMM was thus polymerized at 70 or 80°C in the presence of CPADB or multifunctional analogues (**14** or **15**) at different [HMM]/[RAFT agent]/[Initiator] ratio (see Scheme 2.4 and Table 2.1).

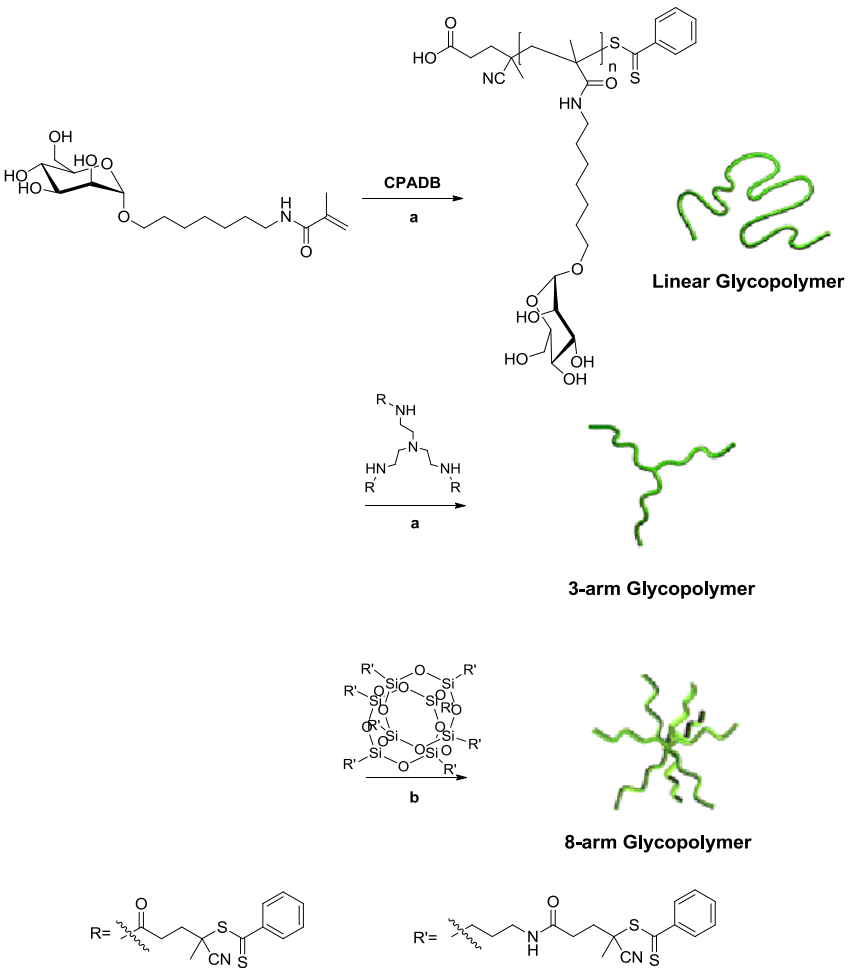

Scheme 2.4: Preparation of linear and star glycopolymers. a) ACPA, DMSO/D_2O (1/1, v/v), 70 °C; b) AIBN, DMSO, 70 or 80 °C.

Depending on the solubility of the mediating agent, polymerizations were carried out in 1/1 (v/v/) water/DMSO mixtures (CPADB or **14**) or in pure DMSO (**15**) in the presence of ACPA or AIBN as initiators. To address potential polymerization control issues, kinetics studies on the homopolymerization of the HMM glycomonomer via the RAFT process were systematically conducted. The semi-logarithmic plots of monomer conversion versus time for RAFT polymerization of HMM in solution are given in **Figure 2.9**. No inhibition or very short inhibition period was observed. Polymerization rates were comparable in the presence of CPADB and **14** and significantly lower in the presence of **15** as mediating agent. Importantly, homopolymerizations proceeded with pseudo-first-order kinetics whatever the nature of the RAFT agent suggesting that the concentration of propagating species is

constant during the whole process.

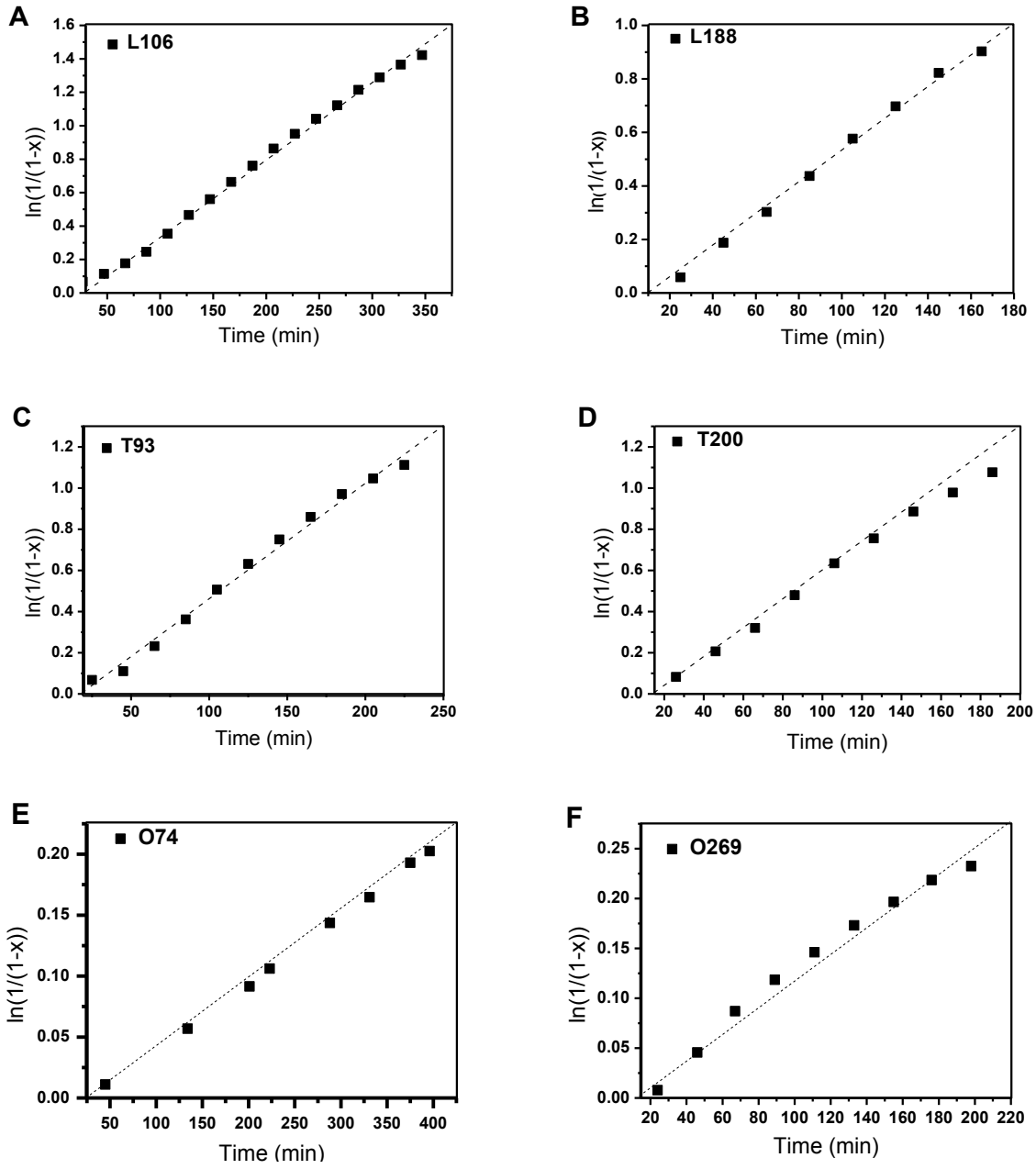

Figure 2.9. Semi-logarithmic plots of monomer conversion versus time for RAFT polymerization of HMM for CPADB, 14 and 15. (Conditions of polymerization given in Table 2.1) .

After purification steps to remove residual monomer, we looked at the evolution of the glycopolymer chain molecular weight with conversion by ^{1}H NMR (**Fig 2.10**, ^{1}H NMR spectrum of L47 as an example) from relative integration of the aromatic protons of the terminal RAFT agent between 7.20~8.20 ppm and protons from polymer backbone at 2.90~4.10 ppm. Consistent with a controlled/living process, number

average molecular weights determined from NMR were proven to increase with conversion and a good agreement between theoretical (calculated from HMM conversion and initial [HMM]/[RAFT] ratio, see **Table 2.1**) and experimental values was observed (**Fig 2.10** ^{1}H NMR of L47 as an example).

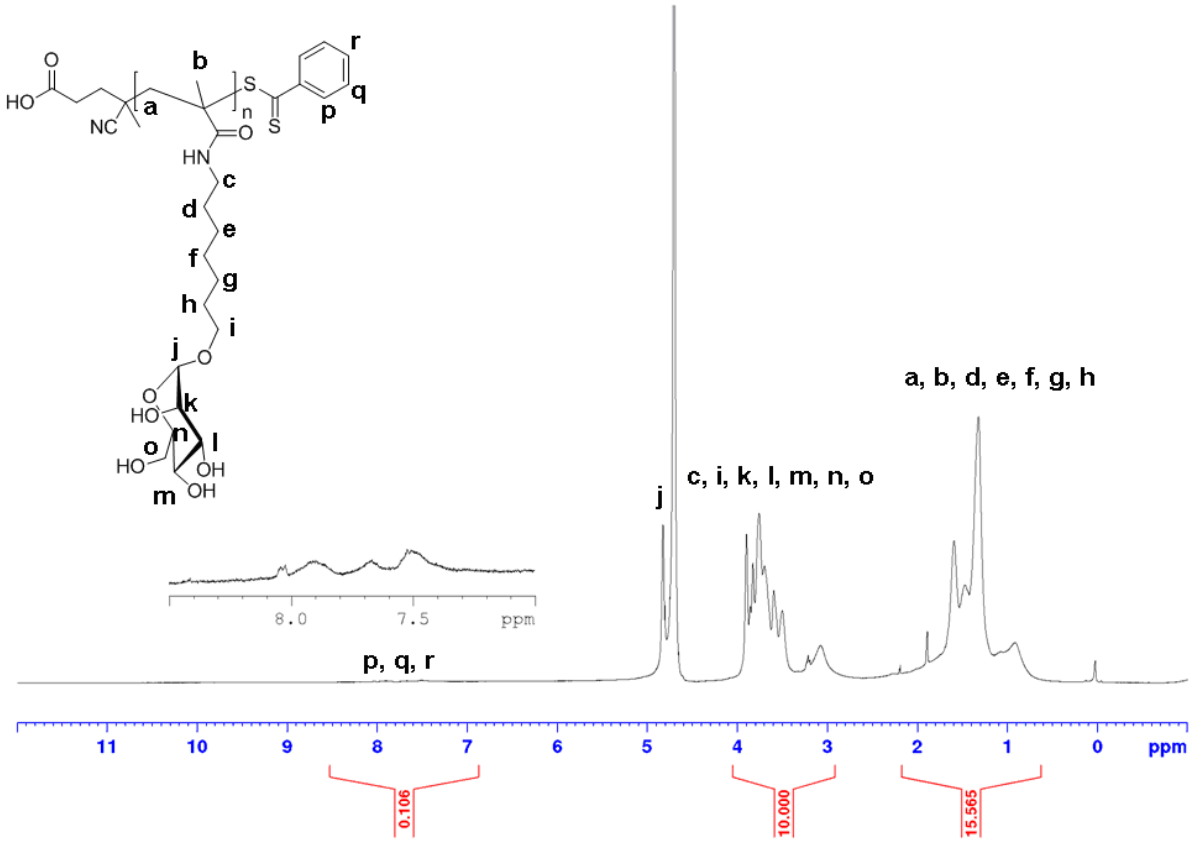

Figure 2.10 ^{1}H NMR spectrum of L47 (D_2O, r.t.).

Characterization of the (unprotected) glycopolymers by SEC was proven challenging. No peak could be observed by analyzing the glycopolymers using pure water or DMF/LiBr (0.05 M) as eluents possibly due to interactions with the columns or similar refractive index values for these polymer/solvent systems. SEC experiments were finally performed in a $NaNO_3$/NaOH aqueous solution (pH =7) with a double RI/light scattering detection. Whereas high molecular weight linear PHMM (L188) and star shaped PHMM (T51, T74, T93, T200, O74 and O269) were prone to aggregate under such conditions and could not be adequately characterized, absolute molecular weight of the other samples (from L31 to L106 and L221) were determined (see **Table 2.1**). The obtained values were slightly higher but again in reasonable agreement with

theoretical molecular weight. A further evidence of the controlled character of the CPADB-mediated polymerization of HMM was given by the molecular weight distributions which were below 1.10. To get a full picture of our glycopolymer library, a fraction of each glycopolymer was subsequently acetylated and analyzed by SEC in THF. A progressive shift of the SEC traces towards high molecular weight on consumption of HMM was observed (See **Fig 2.11**) and the molecular weight distributions of all the acetylated glycopolymers were narrow (*Đ* equal or below 1.15 with the exception of O269). It is worth noting that despite quantitative acetylation of the glycopolymers, molecular weights determined by SEC in THF were significantly lower than theoretical values as a consequence of the PS calibration.

Table 2.1. Library of linear and star homoglycopolymers

Ligand	[M]/[CTA]/[I]	[M] (mM)	$M_{n\ th}$ [d] (kg.mol^{-1})	$M_{n\ NMR}$ [e] (kg.mol^{-1})	M_w [f] (kg.mol^{-1})	$M_{n\ SEC}$ [h] (kg.mol^{-1})	DP_n [e]	D_h [j] (nm)
L31[a]	32/1/0.2[k]	0.45	8.7	11.5	15.0 (1.04)	14.0 (1.06)[i]	31	4.2
L47[a]	50/1/0.33[k]	0.45	15.6	17.2	24.0 (1.03)	17.9 (1.07)[i]	47	5.0
L55[a]	74/1/0.33[k]	0.45	17.8	20.2	26.4 (1.06)	18.4 (1.06)[i]	55	5.2
L69[a]	94/1/0.5[k]	0.45	23.5	25.3	29.2 (1.07)	21.2 (1.08)[i]	69	5.9
L106[a]	123/1/0.5[k]	0.45	34.2	38.6	45.5 (1.06)	25.5 (1.09)[i]	106	6.5
L188[a]	300/1/0.5[k]	0.90	64.5	68.4	n.d[g]	30.2 (1.15)[i]	188	7.9
L 221[a]	500/1/0.2[k]	1.13	80.1	81.2	102.5 (1.02)		221	8.9
T51[b]	74/1/0.33[k]	0.45	14.4	19.6	n.d[g]	20.4 (1.12)[i]	51	5.9
T74[b]	99/1/0.5[k]	0.45	22.8	28.0	n.d[g]	22.9 (1.13)[i]	74	6.4
T93[b]	123/1/0.5[k]	0.45	30.7	34.8	n.d[g]	27.6 (1.12)[i]	93	6.5
T200[b]	300/1/0.5[k]	0.90	72.1	73.2	n.d[g]	32.1 (1.13)[i]	200	8.0
O74[c]	123/1/1[k]	0.45	20.3	29.7	n.d[g]	17.2 (1.10)[i]	74	6.4

O269[c]	500/1/1[l]	0.70	78.8	100.4	n.d[g]	21.6 (1.34)[i]	269	9.1
PEMM	250/1/0.5[k]	0.45	53.6	54.6	n.d[g]		183	

[a]: Linear homopolymers; [b]: 3-arm star homopolymers; [c]: 8-arm star homopolymers; [d]: Calculated from monomer conversion; [e]: Determined from relative integration of the aromatic chain end group and polymer backbone peaks; [f]: Determined from SEC with RI/light scattering detection in $NaNO_3$/NaOH aqueous solution (pH =7); [g]: not determined due to aggregation in $NaNO_3$/NaOH aqueous solution; [h]: Determined from SEC analysis in THF and PS calibration (after acetylation); [i]: *Đ* from SEC analysis in THF and PS calibration (after acetylation); [j]: determined from DLS analysis in pure water; [k]: Polymerization carried at 70°C; [l]: Polymerization carried out at 80°C.

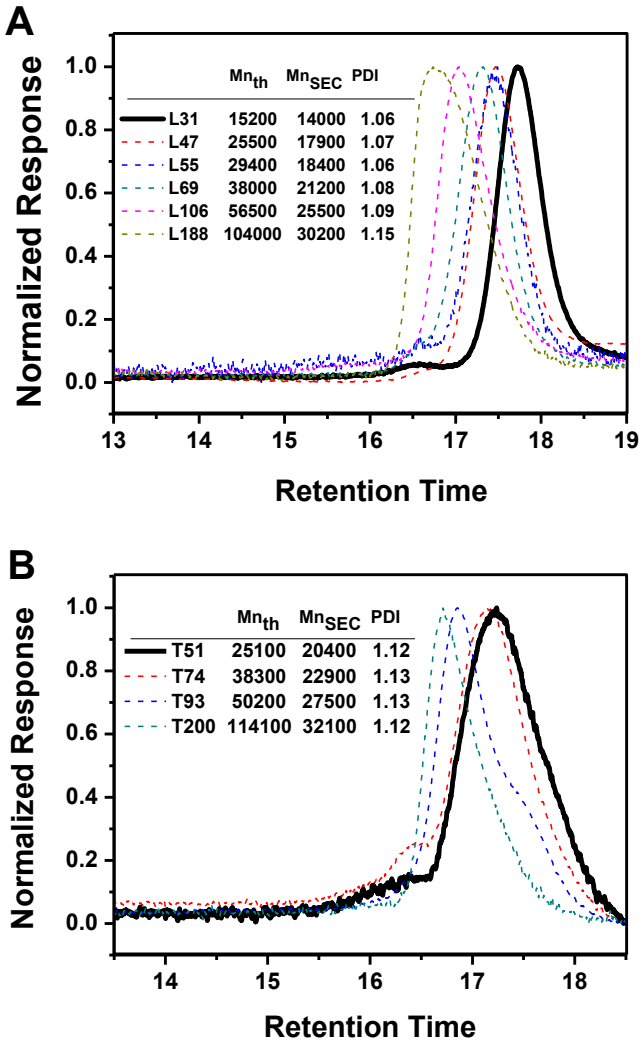

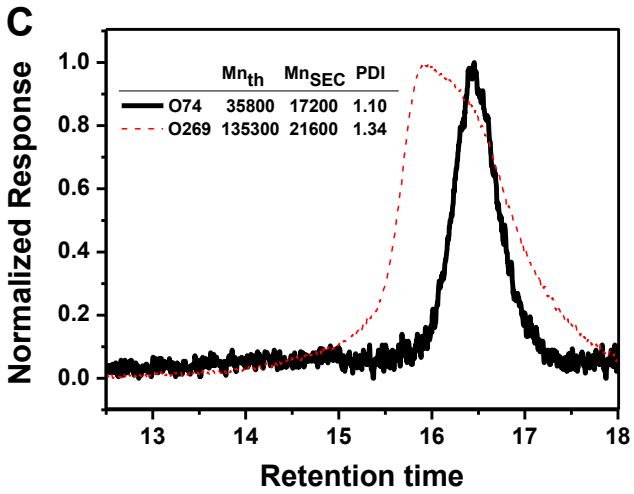

Figure 2.11. Evalution of the GPC traces for the synthetic acetylated glycopolymers. A) Linear glycopolymer; B) 3-arms glycopolymer; C) 8-arms glycopolymer. (Use of PS calibration in THF)

The glycopolymers were subsequently studied by dynamic light scattering analysis (DLS) in pure water (at 1mg/mL). With the exception of L55 and L69, no aggregation was observed in these conditions. A single population was observed for the glycopolymers and the hydrodynamic diameters typically comprised of values between 4.2 nm for the shortest linear glycopolymer (L31) to 9.1 nm for the longest 8-arm star (O269). (**Figure 2.12**).

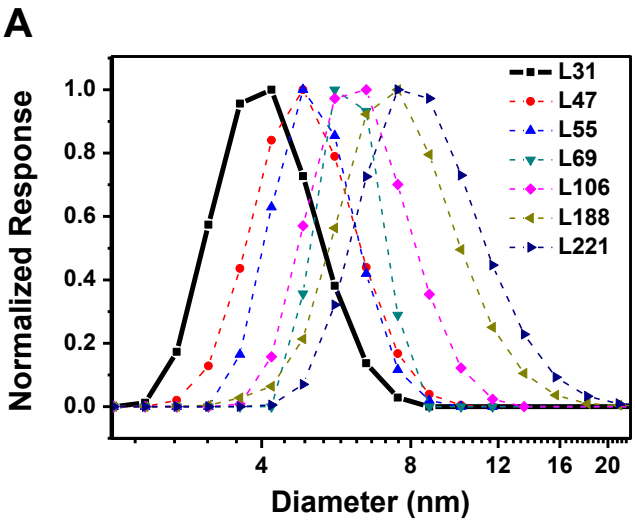

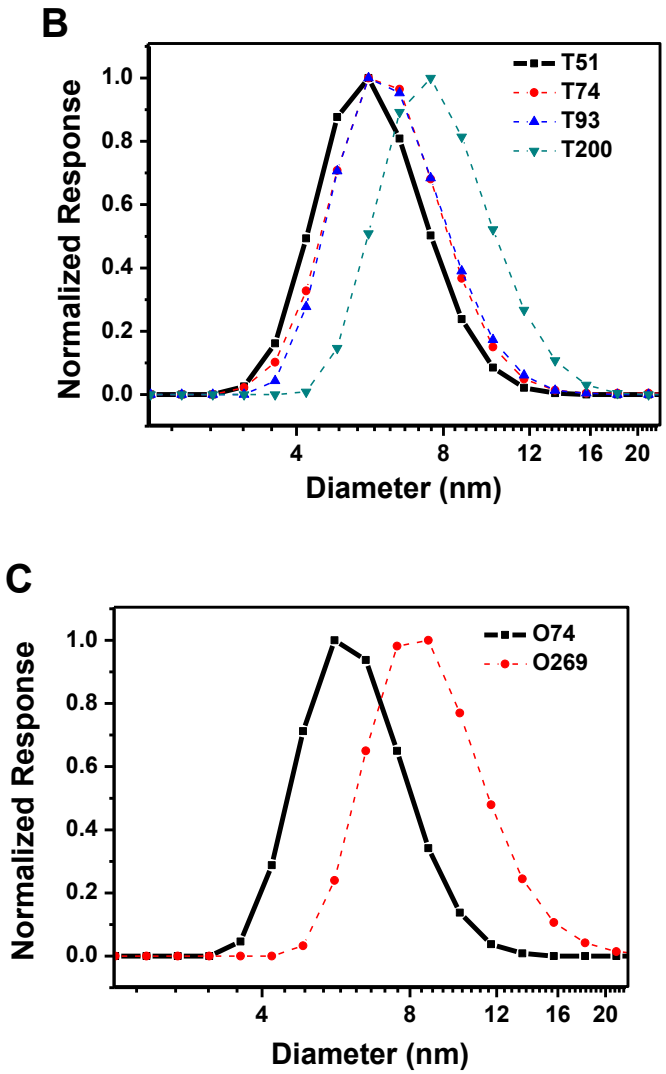

Figure 2.12. DLS of PHMM glycopolymers (see Table 2.1). A) Linear glycopolymers; B) 3-arms glycopolymers; C) 8-arms glycopolymers. The volume weighted sizes were obtained from measurements performed with 1 mg/mL glycopolymer aqueous solution.

2.4.2 Synthesis of glycopolymer PEMM

In addition to this library of PHMM glycopolymers, a mannosylated glycopolymer with a short ethyl linker, poly(*N*-[2-(α-D-mannopyranosyl-oxy)ethyl] methacrylamide) (PEMM, M_n = 53 600 kg.mol^{-1} , DP_n = 183, and $Đ$ = 1.17, see Table 2.1) was also prepared by RAFT polymerization in the presence of CPADB (see **Scheme 2.5**) in order to further evaluate the influence of the alkyl spacer on the interactions within the sugar-binding pocket of the FimH adhesin and *in fine* on inhibition of bacterial adhesion.

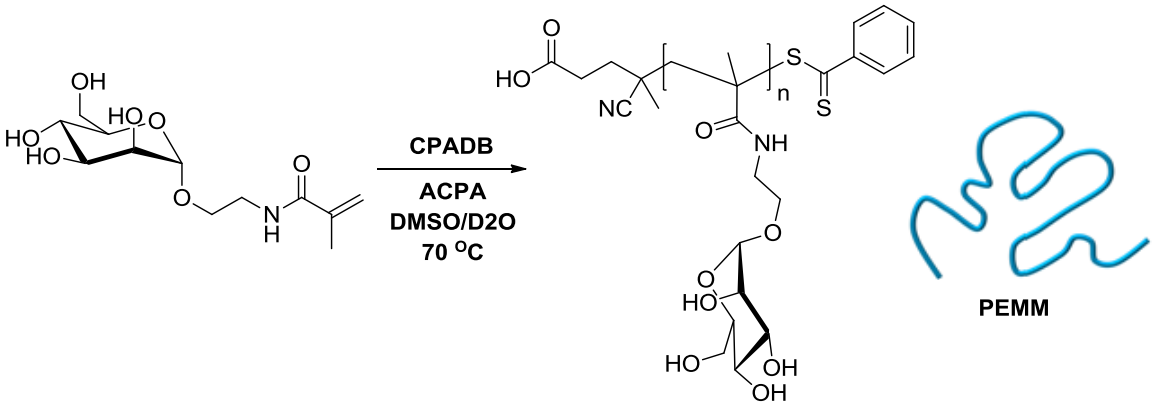

Scheme 2.5: Preparation of PEMM.

2.4.3 Chain-end modification of glycopolymers

In view of using the PHMM glycopolymers for biomedical applications *in vitro* and *in vivo* conditions, toxicity issues needed to be addressed. As discussed by Bulmus and co-workers, end-capping of glycopolymers (or other polymers) with dithiobenzoate moiety results in significant cytotoxicity.[37-38] To overcome these problems, the dithiobenzoate functionality at the ϖ-chain was quantitatively removed through aminolysis (addition of an excess of primary amine) and the resulting thiol was reacted with *N*-isopropylacrylamide (thio-Michael addition) to avoid chain coupling reactions through the formation of disulfides (**Scheme 2.6**). Destruction of the dithiobenzoate moiety was first assessed by the disappearance of the characteristic pink color of DTB-end-functionalized polymers. After dialysis and freeze drying, white fluffy powders were obtained. The removal of DTB was further assessed by ^{1}H NMR with the disappearance of a typical aromatic peak at around 8 ppm and the appearance of a new peak at 4.18 ppm confirming the incorporation of an isopropyl group on the chain (**see Annex A7**). Accordingly, the disappearance of the typical band due to absorption of the thiocarbonyl group in the near UV range (π-π transition) further demonstrated the efficacy of the removal (**Fig 2.13**). No shift of the SEC traces was observed after chain-end modification confirming the absence of disulfide formation during the DTB removal process (See **Fig 2.13**).

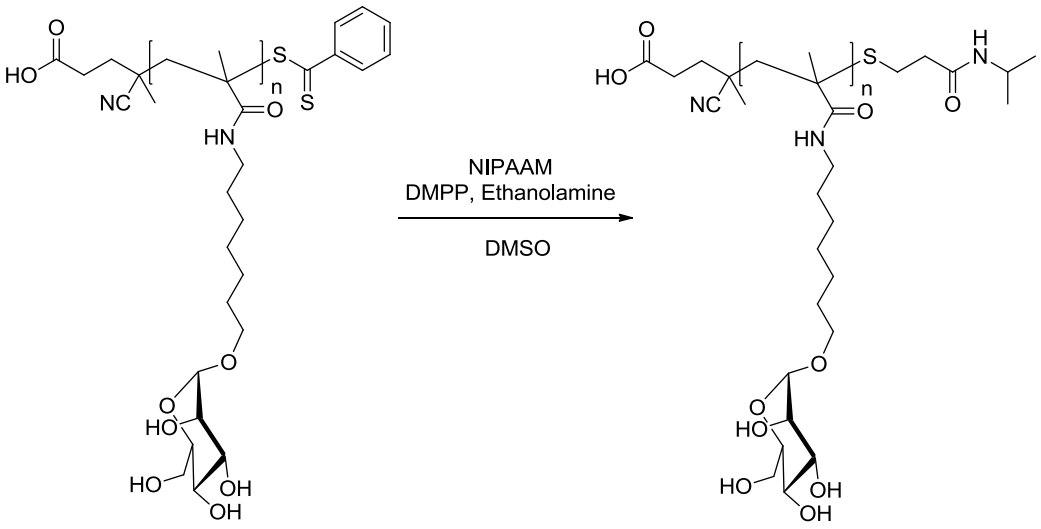

Scheme 2.6. Chain-end modification of glycopolymers.

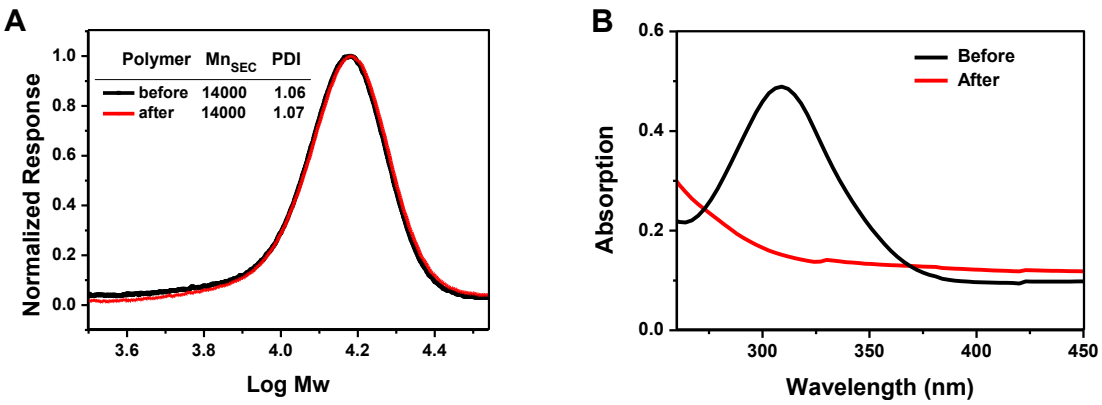

Figure 2.13. A) SEC trace for peracetylated L31 between before and after chain-end modification (Use of PS calibration in THF); B) UV-vis absorption spectra between before and after chain-end modification.

To study the effect of the DTB-free glycopolymers on cellular viability, control cytotoxicity tests were carried out on human intestinal epithelial Caco-2 cells. As can be seen on **Figure 2.14**, when the cells are co-incubated with 100 nM of PHMM (a glycopolymer concentration far higher than the ones used in the frame of the adhesive tests), no toxic effect is observed.

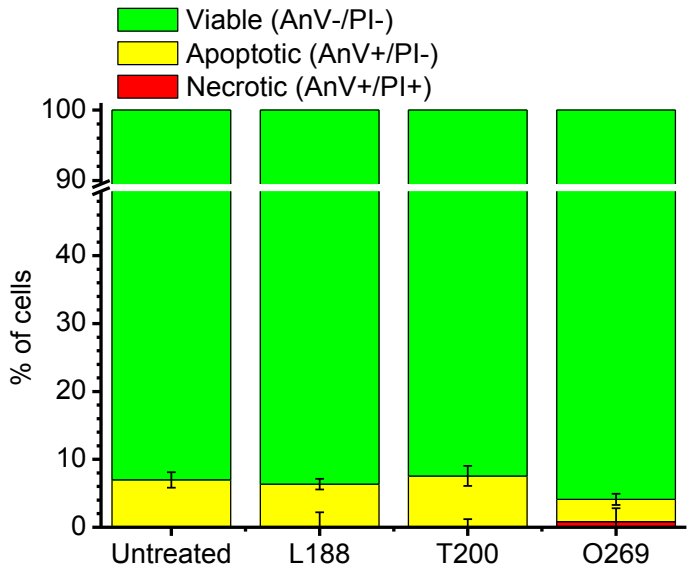

Figure 2.14: PHMM cytotoxicity tests on human intestinal epithelial Caco-2 cells after 48h of co-incubation with 100 nM of indicated glycopolymer

2.5 Elaboration of library of PHMM/PGMA glyco(co)polymers with tunable compositions and microstructures

In order to investigate the influence of carbohydrate density and of the relative position of the carbohydrates on the polymer backbone, we subsequently focused on the RAFT preparation of copolymers based on HMM and glycidyl methacrylate (GMA) (**Scheme 2.7**). HMM was evidently selected to promote interactions with FimH adhesion and GMA was chosen to allow for post-modification of the glycopolymers through ring opening with various amines to gain insight into the influence of pendent groups adjacent to the carbohydrates on anti-adhesive properties.

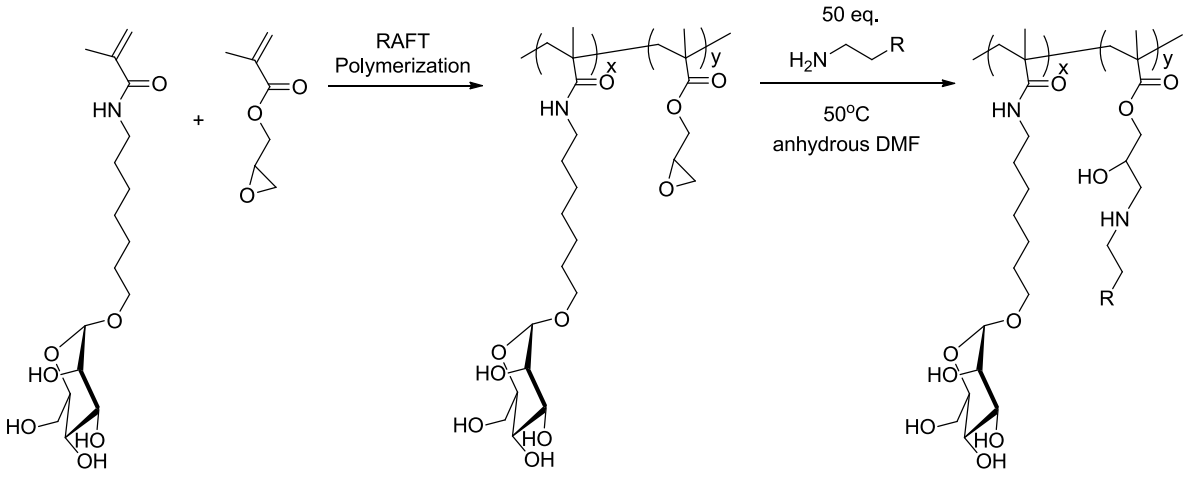

Scheme 2.7: General approach for the preparation of HMM-based glyco-copolymers.

In order to get a clear picture of the composition and monomer sequence distribution of glycopolymers generated in statistical copolymerization, the reactivity ratios of HMM and GMA in radical polymerization were first evaluated. Polymerizations were carried out in DMSO in the presence of CPADB as mediating agent. The reactivity ratios of this copolymerization system were estimated utilizing two different methods: the Jaacks method[39] and the usual Kelen-Tüdos method[40-41] (experimental details given in Chapter 5). Analogous values of reactivity ratios were obtained for both methods. The reactivity ratio of HMM and the reactivity ratio of GMA were determined to be 0.14/0.13 and 2.82/2.77 respectively (**Figure 2.14 A** and **B**).

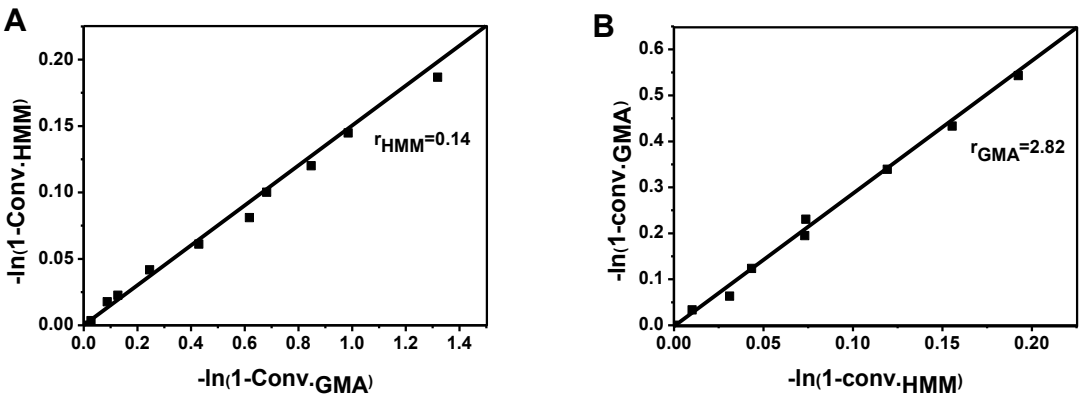

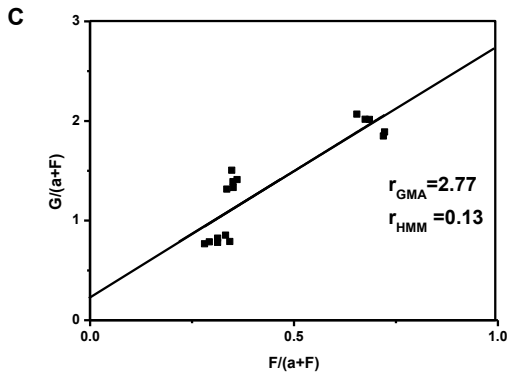

Figure 2.14. (A) Jaacks plots of the RAFT polymerization obtained for $[HMM]_0$:$[GMA]_0$=34; (B) Jaacks plots of the RAFT polymerization obtained for $[HMM]_0$:$[GMA]_0$=0.028; (C) Kelen-Tudös plot for the RAFT copolymerization of HMM and GMA in DMSO at 35 °C (α=0.57).

These disparate reactivity ratios indicate that GMA is consumed at a significantly higher rate than HMM and that the monomer feed and copolymer composition progressively drift with conversion (increase of f_{HMM} and F_{HMM}). As a consequence, when the batch copolymerization of HMM and GMA is not carried out at the azeotropic composition, the microstructure of the resulting chains evolves from the α-end to the ϖ-end of the chain to become more and more rich in HMM (gradient microstructure). In order to prepare glycopolymers with tunable compositions and microstructures, 3 different protocols of (co)polymerization were thus explored: i) sequential polymerizations of HMM and GMA leading to block copolymers ii) batch copolymerizations (as described above) spontaneously leading to gradient copolymers and iii) semi-batch copolymerizations where GMA is continuously added to the monomer feed to obtain a more uniform distribution of GMA units within the chains. For each methodology, three different GMA/HMM molar compositions (1/2, 1/1, 2/1) and a constant global degree of polymerization of 200 were targeted.

Table 2.2. Library of glyco-copolymers

Entries	Polymer	T (°C)	[M]/[CTA]/[I]	$[HMM]_0$ (M)	$[GMA]_0$ (M)	$[GMA]_{sp}$ [f] (M)	Solvent	Conv. (%)	$M_{n\ th}$ [a] ($g.mol^{-1}$)	$M_{n\ NMR}$ [b] ($g.mol^{-1}$)	$M_{n\ SEC}$ [c] ($g.mol^{-1}$)	$Đ$ [d]
1	$PGMA_{65}$	40	100/1/0.25		0.40		Toluene	61	8900	9500	11500	1.31
2	$PGMA_{65}$-*b*-$PHMM_{133}$	70	200/1/0.33	0.55			DMSO	64	55100	57500	51000	1.20
3	P(GMA_{66}-*grad*-HMM_{130})	70	220/1/0.4	0.90	0.39		DMSO	87	55400	56600	52900	1.18
4	P(GMA_{63}-*stat*-HMM_{134})	70	220/1/0.5	1.23	0.17[e]	0.84	DMSO	88	56700	57600	54800	1.15
5	$PGMA_{100}$	40	150/1/0.25		0.40		Toluene	61	13300	14500	20900	1.25
6	$PGMA_{100}$-*b*-$PHMM_{107}$	70	140/1/0.33	0.73			DMSO	68	50300	53900	48500	1.19
7	P(GMA_{103}-*grad*-HMM_{108})	70	220/1/0.5	0.90	0.39		DMSO	83	45900	53900	48800	1.17
8	P(GMA_{95}-*stat*-HMM_{107})	70	220/1/0.5	1.10	0.30[e]	1.50	DMSO	82	47100	52400	48300	1.18
9	$PGMA_{136}$	40	200/1/0.25		0.40		Toluene	64	18500	19600	28900	1.15
10	$PGMA_{136}$-*b*-$PHMM_{65}$	70	90/1/0.33	0.55			DMSO	69	41700	42800	48500	1.15
11	P(GMA_{134}-*grad*-HMM_{66})	70	220/1/0.5	0.52	0.97		DMSO	92	42200	43200	48100	1.11
12	P(GMA_{134}-*stat*-HMM_{66})	70	220/1/0.5	0.70	0.43[e]	2.15	DMSO	88	41200	43200	48100	1.17

[a]: Calculated from monomer conversion; [b]: Determined from relative integration of the aromatic chain end group and polymer backbone peaks; [c]: Determined from SEC analysis in THF and PS calibration (after acetylation); [d]: *Đ* from SEC analysis in THF and PS calibration (after acetylation); [e]: concentration of GMA in the initial batch; [f]: concentration of GMA in the pump-controlled syringe.

2.5.1 RAFT Preparation of PGMA-*b*-PHMM block copolymers

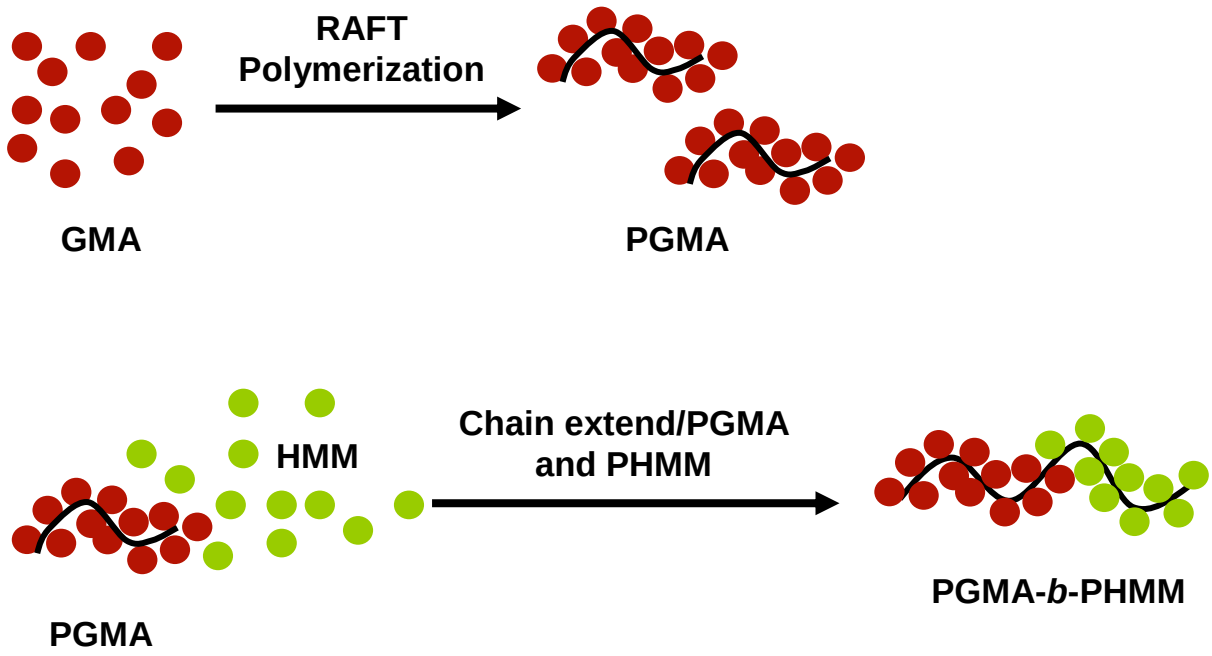

Scheme 2.8. Construction of block glyco-copolymers.

Sequential polymerizations of HMM and GMA were carried out to generate three diblock copolymers with different molar compositions (**Scheme 2.8**). Conditions of polymerization and macromolecular characteristics of the PGMA and PGMA-*b*-PHMM block copolymers are gathered in Table 2.2 (Entries 1-2, 5-6 and 9-10) and supplementary characterizations are given in Chapter 5. For clarity's sake, only the preparation of $PGMA_{65}$-*b*-$PHMM_{133}$ is described hereafter. The first block was prepared by polymerizing GMA at 40°C in the presence of CPADB in toluene using V70 as initiator ([GMA]/[CPADB]/[V70] = 100/1/0.25, $[GMA]_0$ = 0.40 M). A linear relationship between *-(ln [1-x])* and *t* was observed for the RAFT polymerization of GMA (**Figure 2.15 A**). Consistent with a controlled/living process, the experimental number average molecule weight of the resulting PGMA (9.5 kg/mol), determined from integration of protons of the dithiobenzoate (located at the ϖ chain end) at 7.4~7.9 ppm and protons of the repetitive unit at 4.3 ppm (see **Fig 2.16**) agreed with the theoretical number average molecule weight (determined from monomer conversion) 8.9 kg/mol. The SEC analysis (THF, PS calibration) revealed a monomodal trace and a relatively narrow molecular weight distribution (M_n = 11.5

kg.mol, *Đ* = 1.31). The chain extension of PGMA macroRAFT agent with HMM was then carried in anhydrous DMSO at 70°C ([HMM]/[PGMA]/[ACPA] = 200/1/0.33, $[HMM]_0$ = 0.55 M). Again, pseudo-first order kinetic plots were observed for the polymerization of HMM (**Figure 2.15 B**). As can be seen in **Figure 2.17**, chain extension with HMM resulted in a clear shift of the SEC trace toward higher molecular weight region confirming the growth of the PHMM block (M_n = 51.0 kg/mol, *Đ* = 1.20, SEC analysis performed in THF with PS calibration after acetylation of the block glycopolymer, **see Fig 2.17**). Importantly, no low molecular weight shoulder could be observed suggesting that the majority of the PGMA chains are involved in the copolymerization process. Composition of the resulting diblock was finally determined by ^{1}H NMR from integration of dithiobenzoate group (7.8 ppm) and protons from polymer backbone at 4.0~5.1 ppm (Attribution was given in **Fig 2.16**). An excellent agreement between experimental and theoretical GMA/HMM molar composition (determined from conversion of HMM) was observed confirming that an excellent control of the final GMA/HMM molar composition can be obtained for PGMA-*b*-PHMM block copolymers.

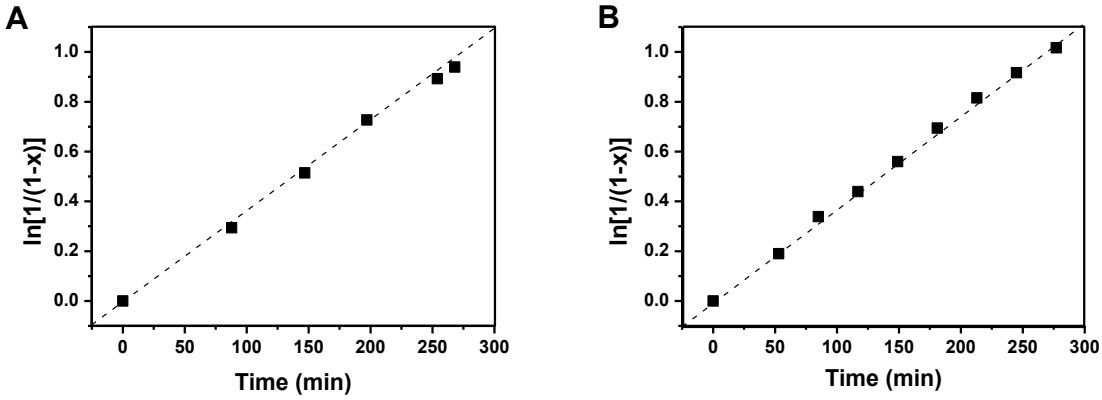

Figure 2.15. Pseudo first-order kinetic plots for sequential polymerizations of GMA and of HMM. (Conditions of polymerization given in Entries 1 (for A) and 2 (for B) of Table 2.2.

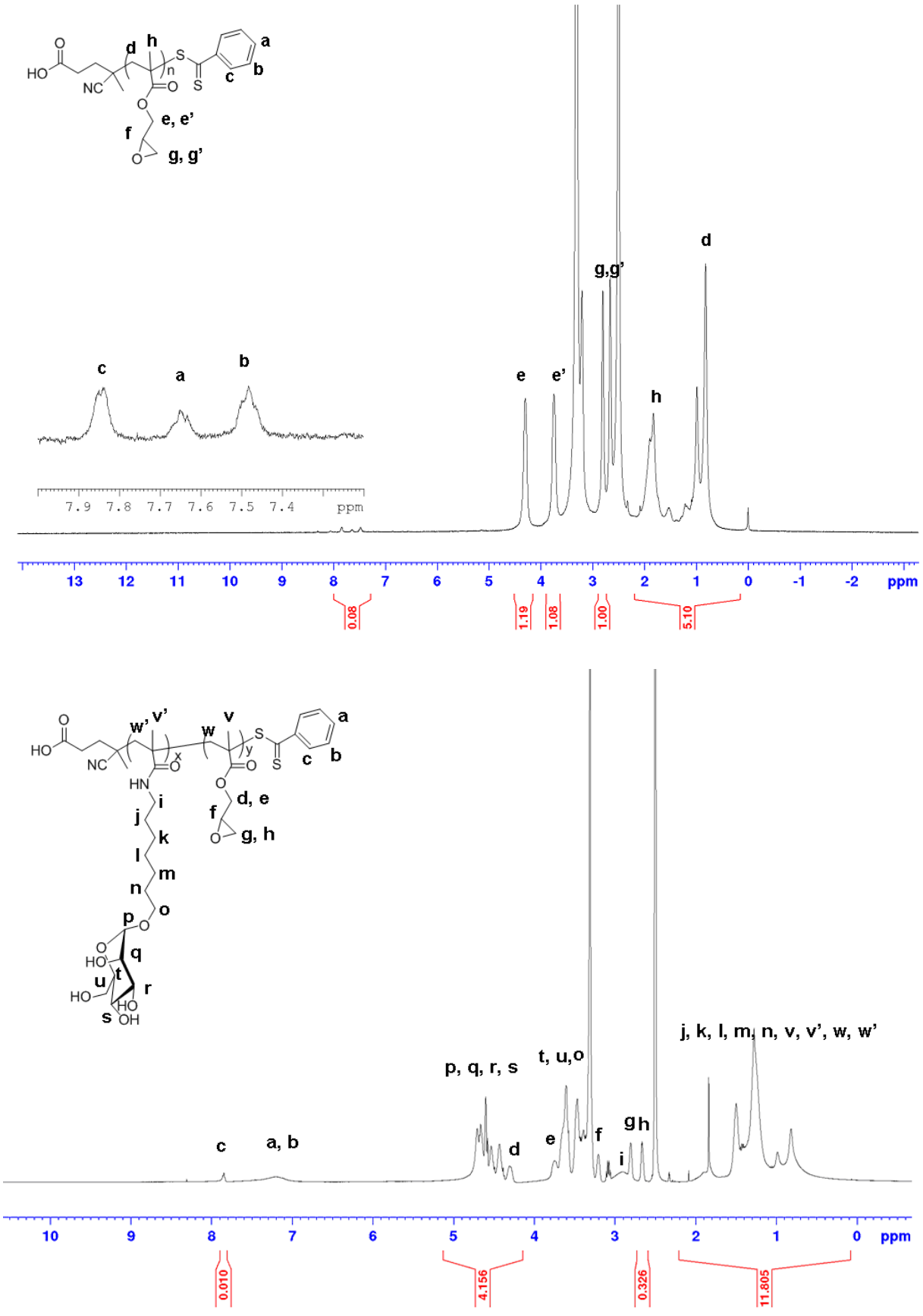

Figure 2.16. ^{1}H NMR spectra of block copolymer PGMA $_{65}$ and PGMA$_{65}$-*b*-PHMM$_{133}$ (DMSO-d6,

r.t.).

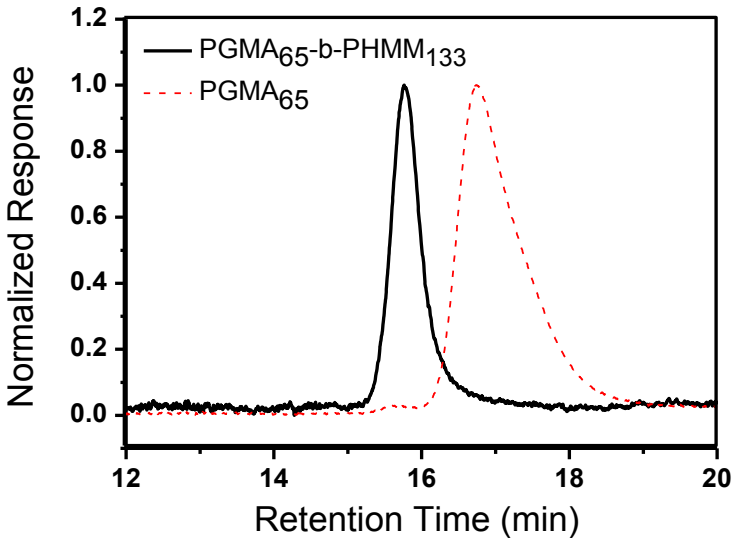

Figure 2.17. SEC traces of $PGMA_{65}$ and $PGMA_{65}$-*b*-$PHMM_{133}$ after acetylation (PS calibration, THF as eluent).

2.5.2 RAFT Preparation of PGMA-*grad*-PHMM copolymers through batch copolymerization

Considering the high difference in reactivity between GMA and HMM (polymerization of GMA is much faster than that of HMM), copolymers with a gradient profile composition should be generated through batch copolymerization due to progressive increase of the molar fraction of HMM in the monomer mixture **(Scheme 2.9)**.

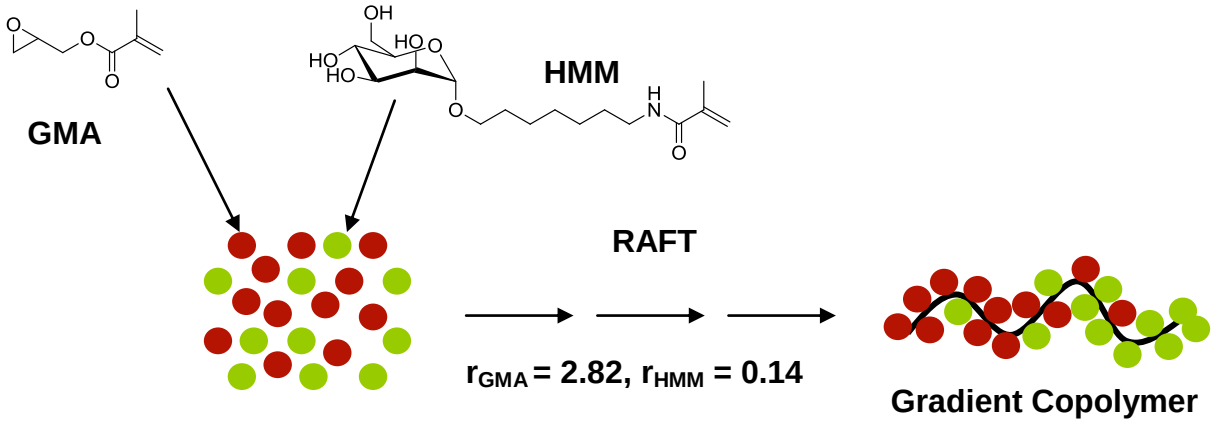

Scheme 2.9. Construction of gradient glyco-copolymers.

Conditions of polymerization and macromolecular characteristics of the PGMA-*grad*-PHMM copolymers are presented in Table 2.2 (Entries 3, 7 and 11) and supplementary characterizations are given in Chapter 5. The preparation of $PGMA_{66}$-*grad*-$PHMM_{130}$ is discussed below. Copolymerization of HMM and GMA ($[HMM]_0/[GMA]_0$ = 2.3, $[GMA]_0$ = 0.39 M) was carried out in anhydrous DMSO-d6 using a Young NMR Tube for in-situ NMR monitoring of the copolymerization at 70 °C in the presence of CPADB and ACPA as initiator. **Figure 2.18A** shows the first-order kinetic plot of the batch copolymerization, which was in an agreement with the theoretical prediction (simulated from the reactivity ratios of two monomers). Consistent with the values of r_{HMM} and r_{GMA}, consumption of GMA was significant faster than that of HMM resulting in an increase of F_{HMM} with conversion (herein, F_{HMM} means the average HMM molar fraction in the copolymer), see **Figure 2.18B**. After purification, the composition and the number average molecular weight of the gradient copolymer were evaluated by ^{1}H NMR (**Figure 2.19**). The final composition of the copolymer (~33.6% of GMA and 66.4% of HMM) is in good agreement with the initial composition in monomers and experiment molecular weights are close to the theoretical values calculated from the overall conversion in monomers (see Table 2.2). SEC analysis of $PGMA_{66}$-*grad*-$PHMM_{130}$ after acetylation revealed one single sharp trace suggesting a good control of the copolymerization (M_n = 52.9 kg/mol, $Đ$ = 1.18) (**see Fig 2.20**).

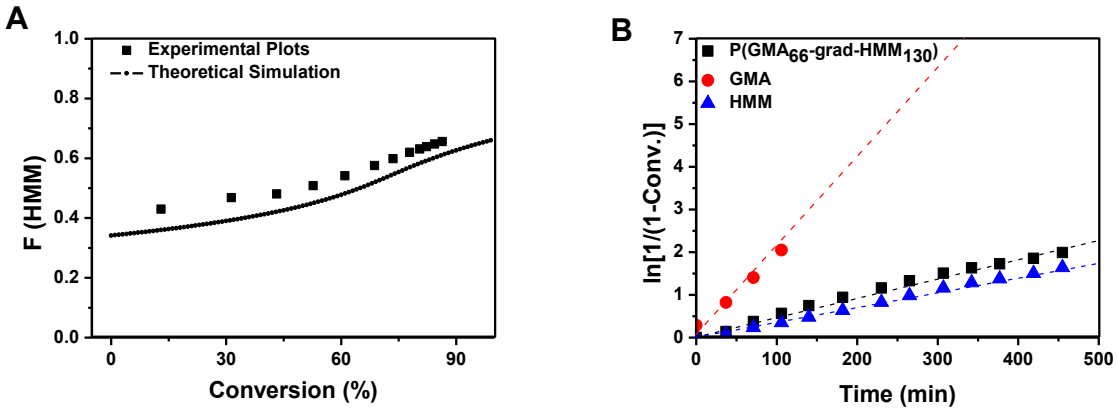

Figure 2.18. (A) The fraction of HMM on copolymer chain during propagation in RAFT polymerization of P(GMA_{66}-*grad*-HMM_{130}); (B) Pseudo first-order kinetic plots for copolymerization

of GMA and HMM. (Entry 3, Table 2.2).

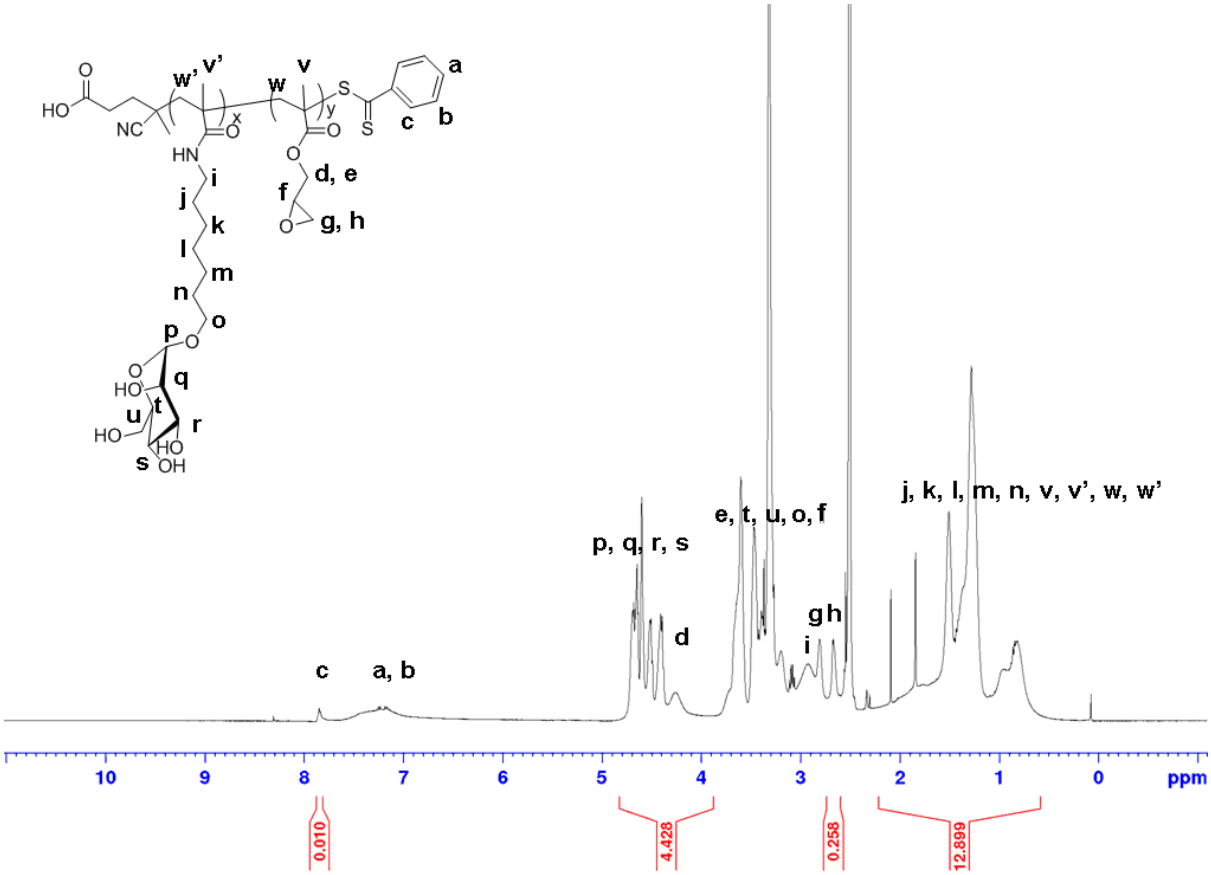

Figure 2.19. ^{1}H NMR of gradient copolymer P(GMA_{66}-*grad*-HMM_{130}) (DMSO-d6, r.t.).

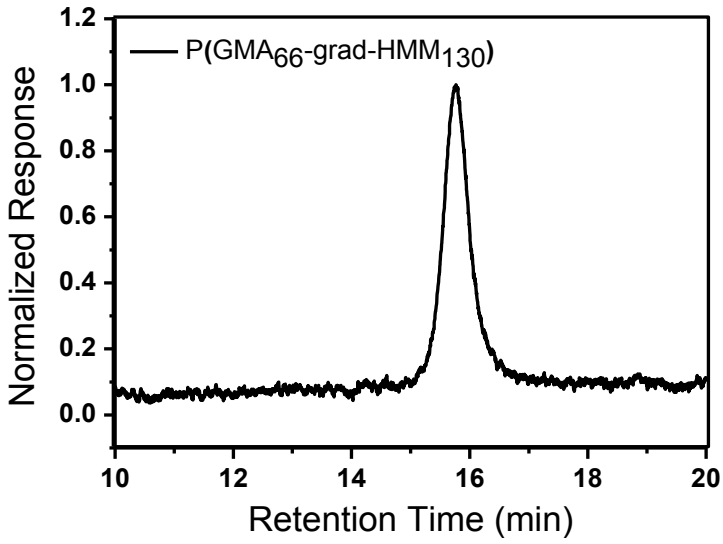

Figure 2.20. SEC analysis of P(GMA_{66}-*grad*-$PHMM_{130}$) after acetylation (PS calibration, THF as eluent).

2.5.3 RAFT Preparation of PGMA-*stat*-PHMM copolymers through semi-batch copolymerization

The procedure for semi-batch copolymerization as shown in **Scheme 2.10** was adapted from a paper of Billon and co-workers.[42]

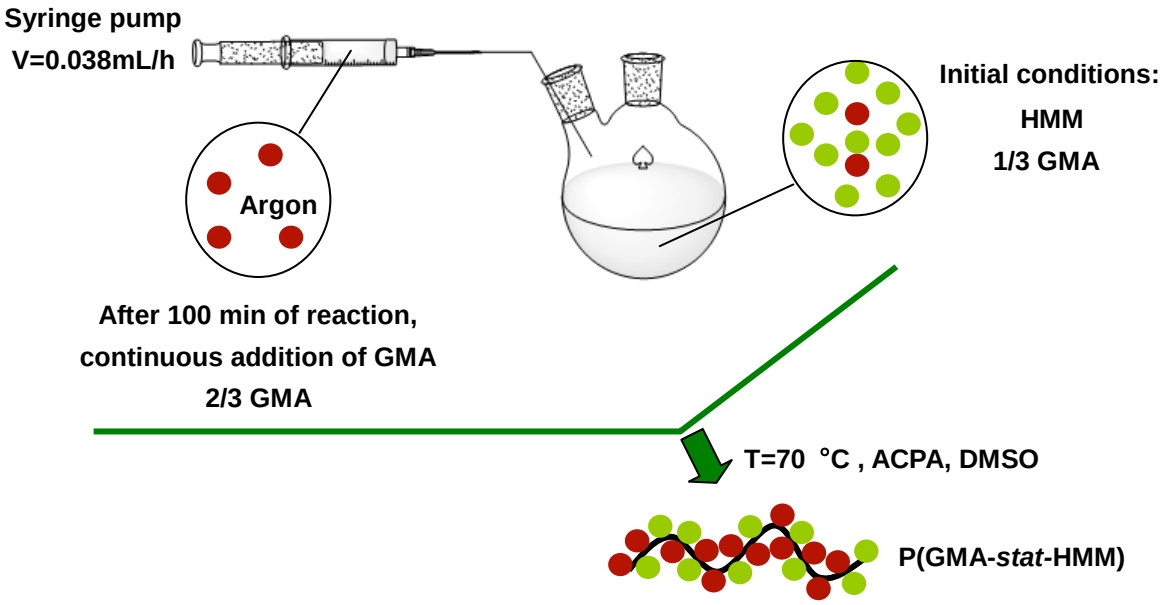

Scheme 2.10 RAFT Preparation of PGMA-*stat*-PHMM copolymers using a semi-batch procedure

The preparation of P(GMA_{63}-*stat*-HMM_{134}) through semi-batch copolymerization is described below to illustrate the general procedure. In brief, one third of the GMA (to be engaged in the polymerization) was initially mixed with HMM, CPADB and ACPA in anhydrous DMSO. Copolymerization was carried out at 70 °C (see Entry 4 in Table 2.2). After 100 min of copolymerization, 92% of GMA was consumed as well as 38% of HMM (at this stage, the copolymer is then composed of 76% of HMM) (**Figure 2.21A**). Then, a solution of GMA in DMSO (1.4 mL, 0.84 M) was progressively added under argon with the help of a syringe pump at a rate of 0.038mL/h. The RAFT copolymerization (see Figure **2.21B**) exhibits pseudo-first order kinetics (for both GMA and HMM). As can be observed in **Fig 2.21A**, contrary to the batch copolymerization of GMA and HMM which results in a significant composition drift due to reactivity ratio disparities between the two monomers, the semi-batch procedure with progressive

addition of GMA in the course of the copolymerization allows for maintaining the copolymer composition almost constant over conversion (from 70 to 76% of HMM in the copolymer chain at 44% and 88% of conversion respectively, which is in good agreement with the overall [HMM]/[GMA] ratio: 2.5/1). After purification, the number average molecule weight was determined by ^{1}H NMR (**Figure 2.22**) which was comparable with theoretical result. The SEC analysis of glyco-copolymers were subsequently acetylated and analyzed by SEC (M_n = 54.8 kg/mol, $Đ$ = 1.15) in THF (**see Fig 2.23**).

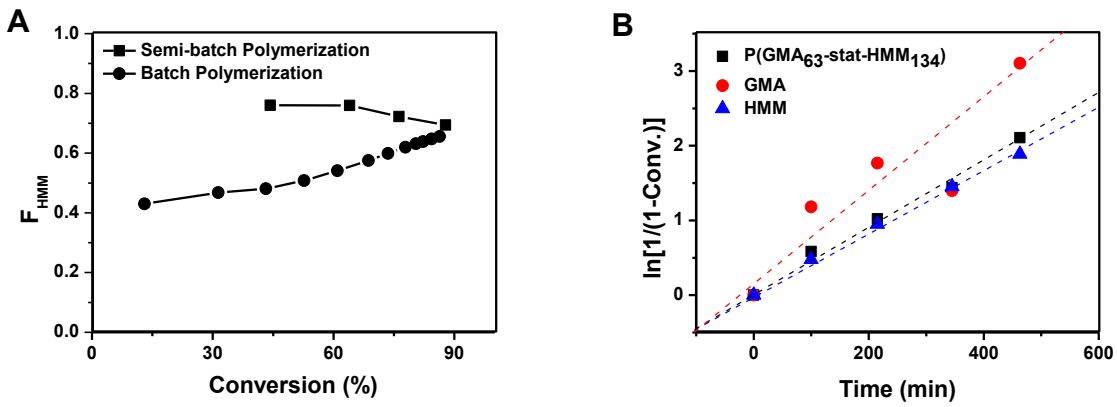

Figure 2.21. (A) Evolution of F_{HMM} with overall monomer conversion for preparation of P(GMA_{63}-*stat*-HMM_{134}); (B) Pseudo first-order kinetic plots for the copolymerization of HMM and GMA (Entry 4, Table 2.2)

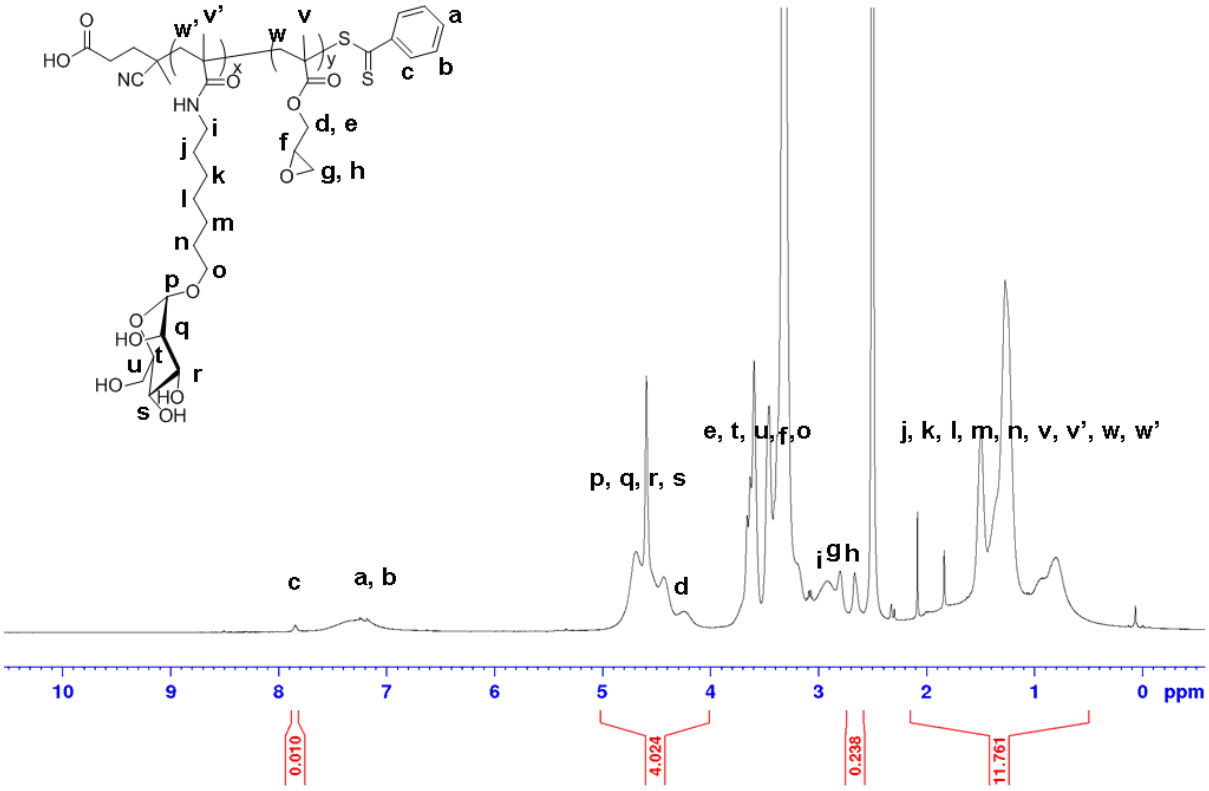

Figure 2.22. ^{1}H NMR spectrum of statistical copolymer P(GMA_{63}-*stat*-HMM_{134}) (DMSO-d6, r.t.).

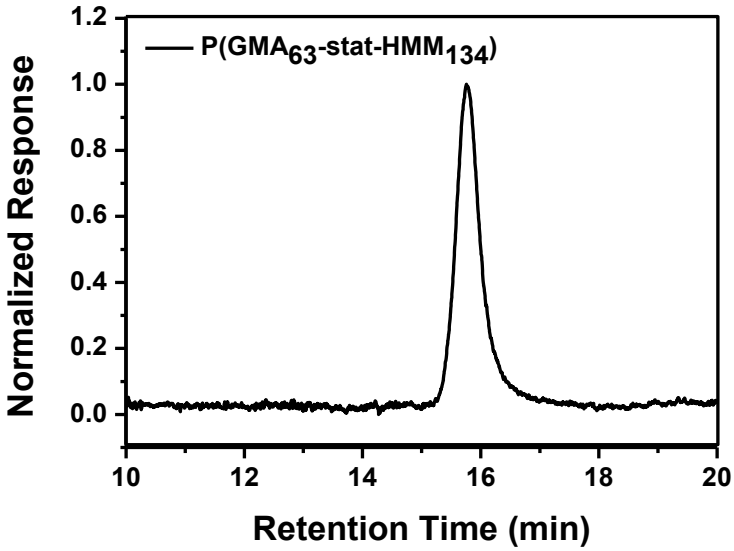

Figure 2.23. SEC analysis of P(GMA_{63}-*stat*-HMM_{134}), SEC was performed after acetylation. (Use of PS calibration in THF, figures for other statistic copolymers were given in annex 6)

In addition to the evolution of the copolymer composition over conversion which supports the synthesis of glyco-copolymers with different microstructures using a batch or a semi-batch copolymerization procedure (PGMA-*grad*-PHMM *vs* PGMA-*stat*-PHMM), we attempted to gain further insight into the chain microstructure through NMR spectroscopy. ^{1}H and ^{13}C NMR spectra of the homopolymers (PGMA and PHMM) and of glyco-copolymers exhibiting similar chemical compositions (PGMA$_{65}$-*b*-PHMM$_{133,}$ PGMA$_{66}$-*grad*-PHMM$_{130}$ and PGMA$_{63}$-*stat*-PHMM$_{134}$) are stacked in Figures **2.24** and **2.25**. Because the repeating units generated by HMM and GMA are chemically very comparable, no information can be collected on the diad, triad or tetrad sequence distributions. However, slight spectral differences can be observed for the three types of glyco-copolymers. As expected, the NMR spectrum of the block copolymer perfectly matches with the superimposition of the two homopolymers spectra. The broadening of the peaks observed on the ^{1}H NMR spectra of PGMA$_{66}$-*grad*-PHMM$_{130}$ and, to a larger extent of PGMA$_{63}$-*stat*-PHMM$_{134}$ clearly reflects the presence of different types of monomer sequences in these two copolymers. Accordingly, signals also showed much more complex splittings in the 170-180 ppm domain of the ^{13}C NMR (corresponding to -*C*=O) of PGMA$_{66}$-*grad*-PHMM$_{130}$ and PGMA$_{63}$-*stat*-PHMM$_{134}$.

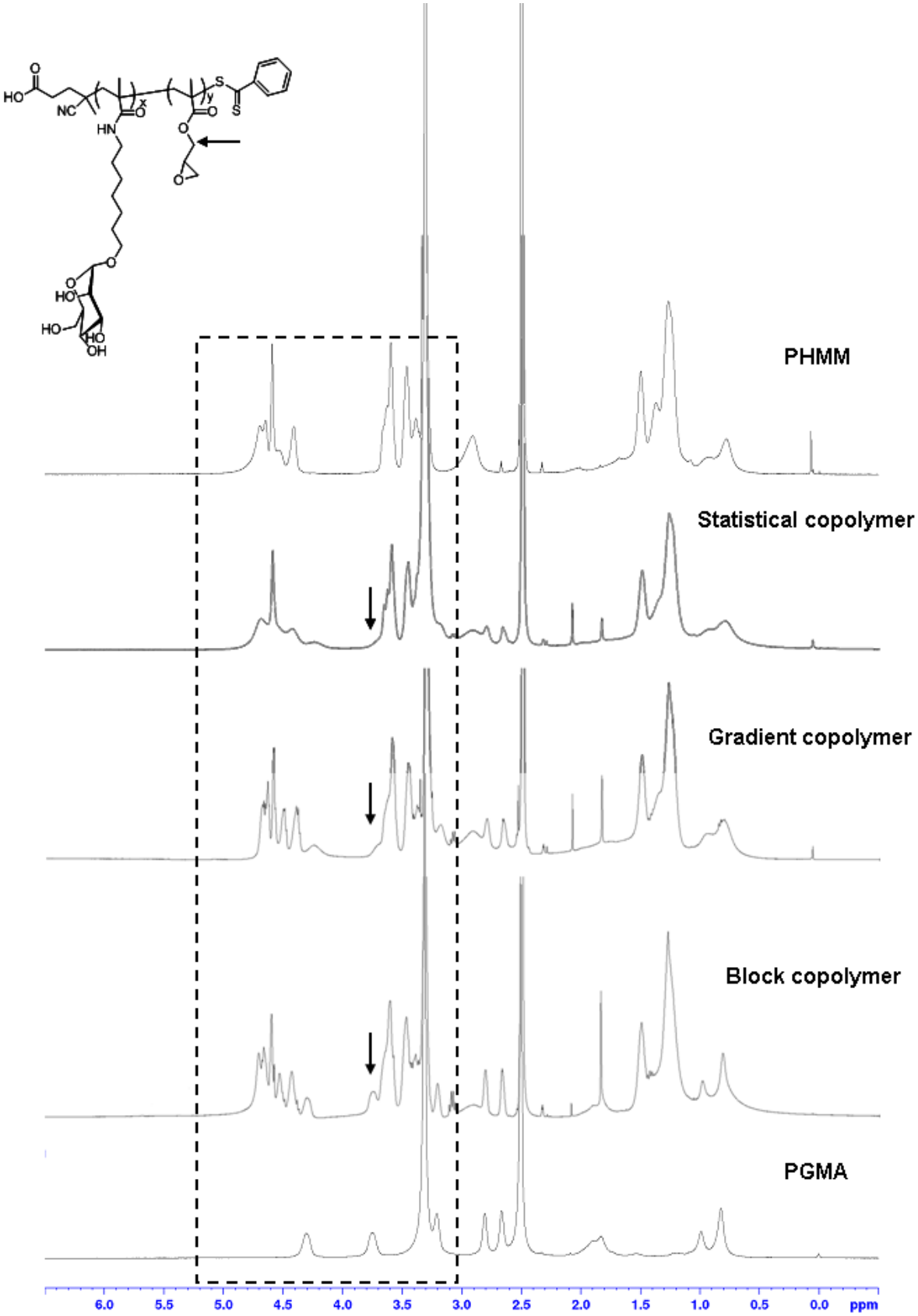

Figure 2.24. ^{1}H NMR spectra (in DMSO-d6 at r.t.) of PHMM and PGMA homopolymers and of statistical, gradient and block copolymers having similar HMM/GMA composition (HMM/GMA ≈

2/1).

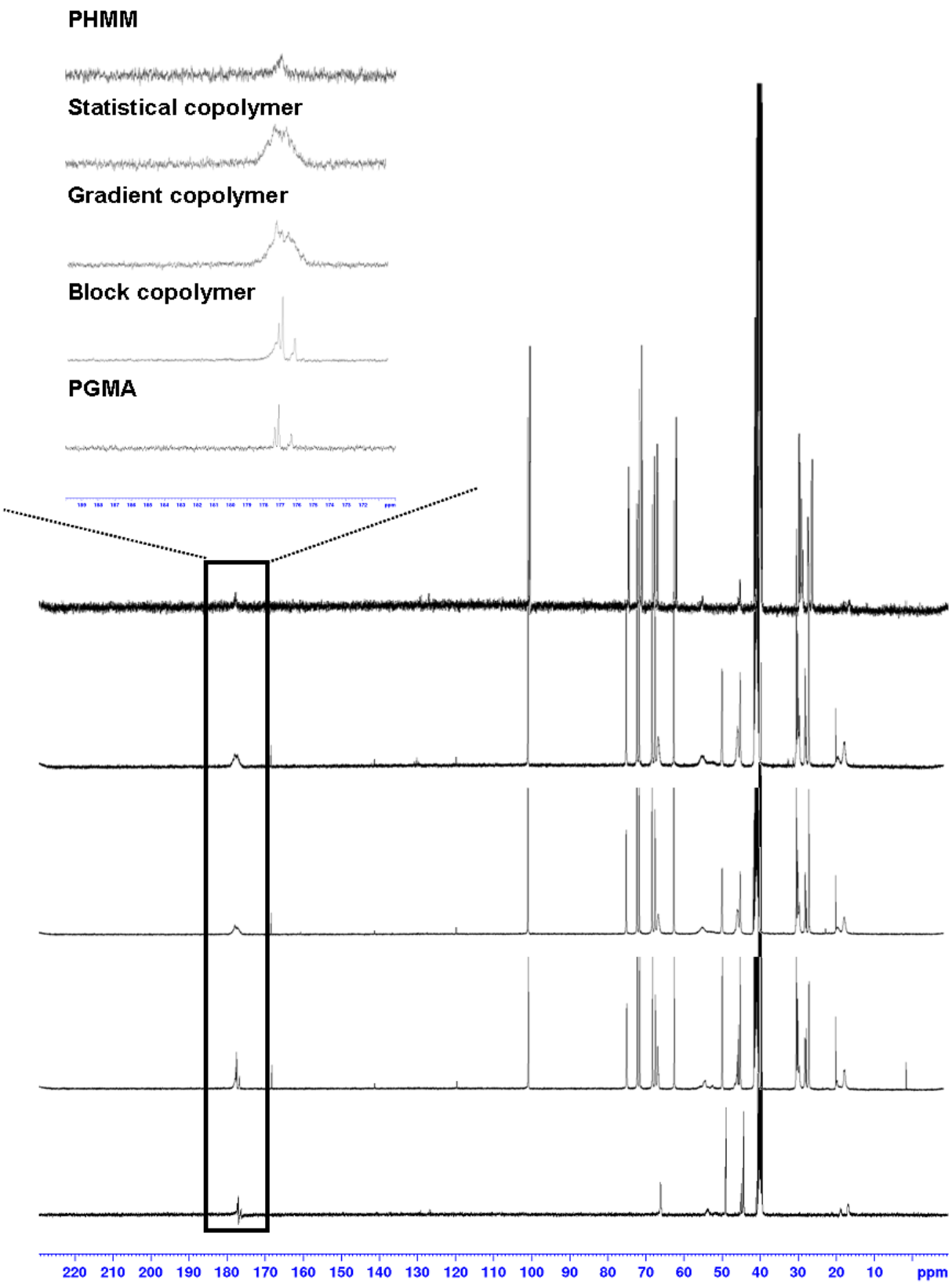

Figure 2.25. ^{13}C NMR spectra (in DMSO-d6 at r.t.) of of PHMM and PGMA homopolymers and of

statistical, gradient and block copolymers having similar HMM/GMA composition (HMM/GMA ≈ 2/1).

2.5.4 Post-modification of the copolymers with various amines

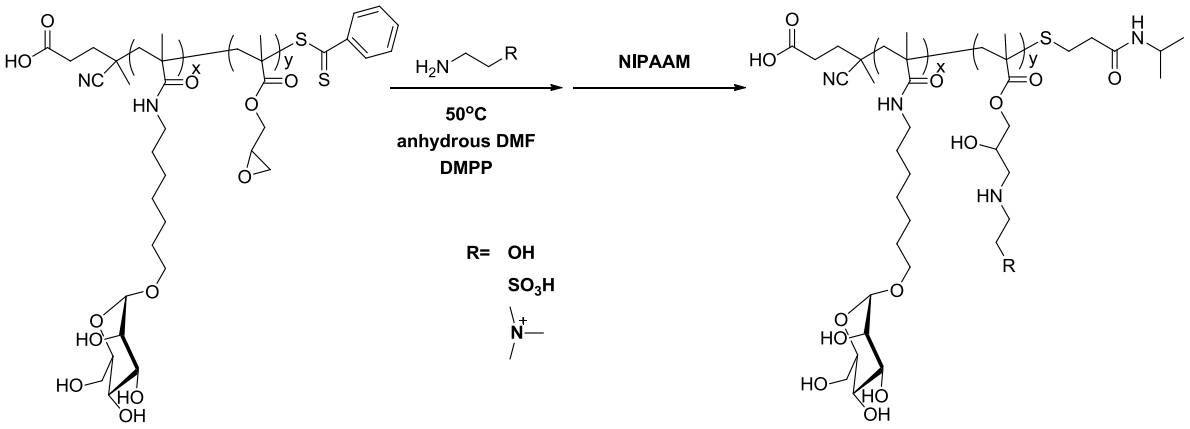

Scheme 2.11. Post-modification of GMA containing copolymers.

The reactive pendant epoxy groups were subsequently engaged in post-polymerization modifications[43-44] to introduce various functional groups along the copolymer backbone through ring opening with primary amines and to further investigate the impact of the post-modification on the anti-adhesive properties of the glyco-copolymers. Post-polymerization modifications were carried out with ethanolamine, taurine and (2-aminoethyl)trimethylammonium (see **Scheme 2.11**). To avoid undesired cross-linking of the chains due to the coupling of secondary amines (formed after reaction of a primary amine with an epoxy) with unreacted epoxy groups, the post-modifications were carried out in anhydrous conditions in the presence of a very large excess of amine (50 equivalents of amine per epoxy ring, glycopolymer solution added drop by drop into the solution containing the primary amine). DMPP and NIPAAM were also engaged in the reaction to simultaneously ensure effective chain end capping of the copolymers. After dialysis and freeze-drying, white fluffy powders were obtained. The success of the post-modification and the removal of dithiobenzoate were confirmed by combining ^{1}H NMR and ^{13}C NMR (**Figure 2.26 and 2.27**, ethanolamine modified P(GMA_{63}-*stat*-HMM_{134}) was used as an example). The disappearance of the peaks of dithiobenzoate (about 8 ppm in ^{1}H NMR) directly

confirmed the removal of the DTB group. The disappearance of the peaks of the epoxy ring (2.6 ppm and 2.8 ppm ^{1}H NMR, 49 ppm in ^{13}C NMR) and of the adjacent methylene (66 ppm in ^{13}C NMR) gave evidence of the success of the epoxy-ring opening reactions. The generation of ethanolamine functionalized copolymer was finally proved by the appearance of a new peak at 61 ppm corresponding to NH-CH_2-CH_2-OH in ^{13}C NMR. In SEC analysis, the shift of a peak towards the higher molecular weights (M_{nSEC} = 63.3 kg/mol, $Đ$ = 1.19) also confirmed the success of the post-modification (**Figure 2.27**).

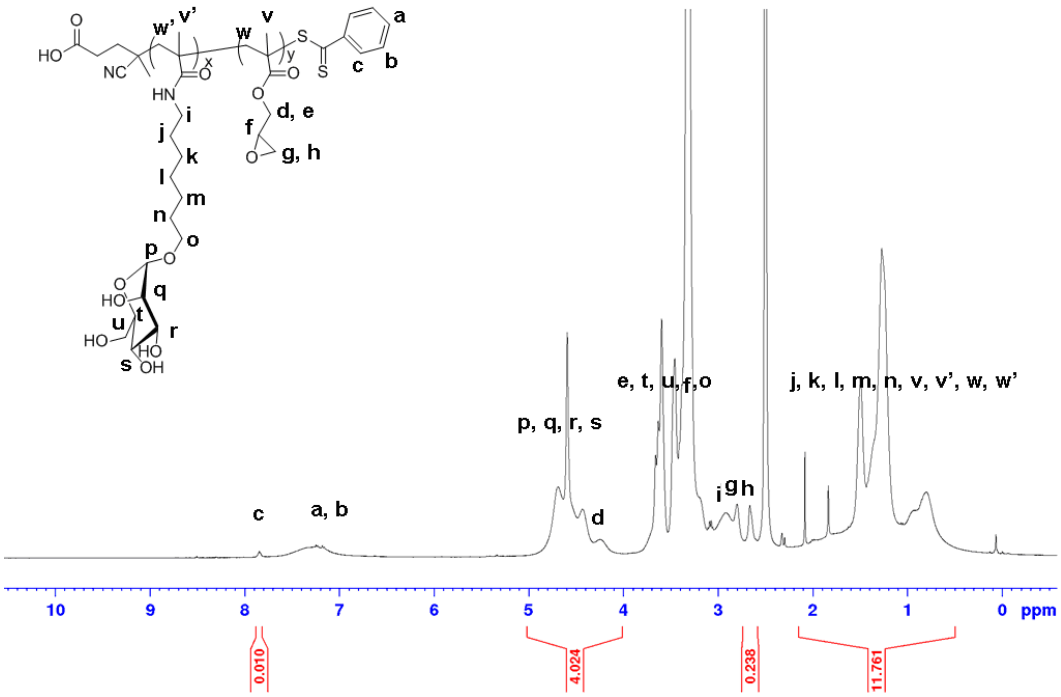

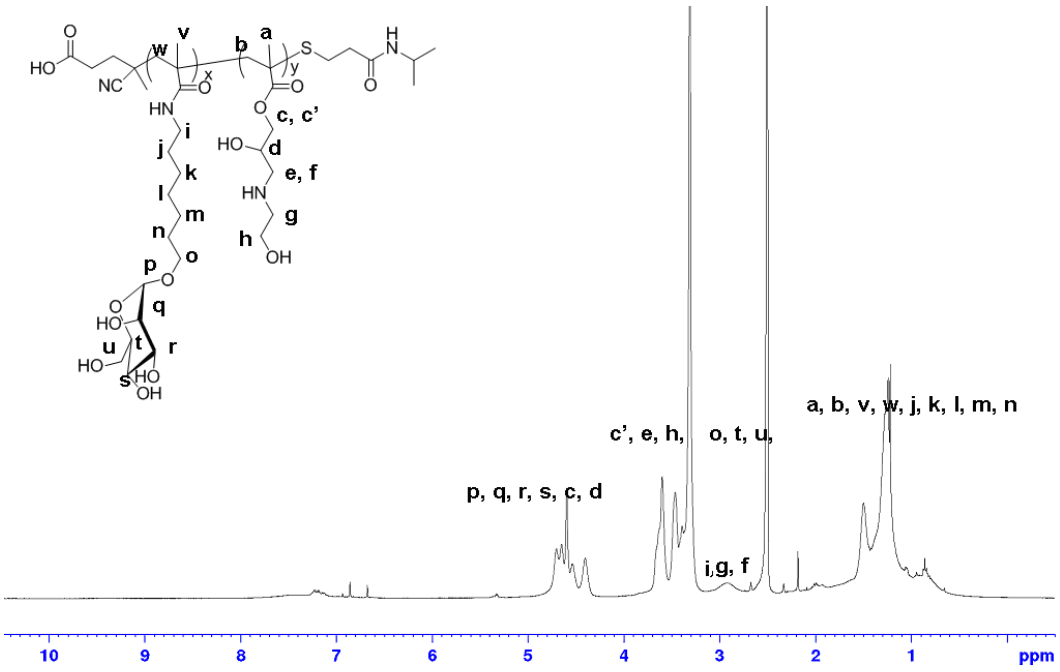

Figure 2.26. ^{1}H NMR spectra of ethanolamine modified glyco-copolymer using P(GMA_{63}-*stat*-HMM_{134}) as precursor.

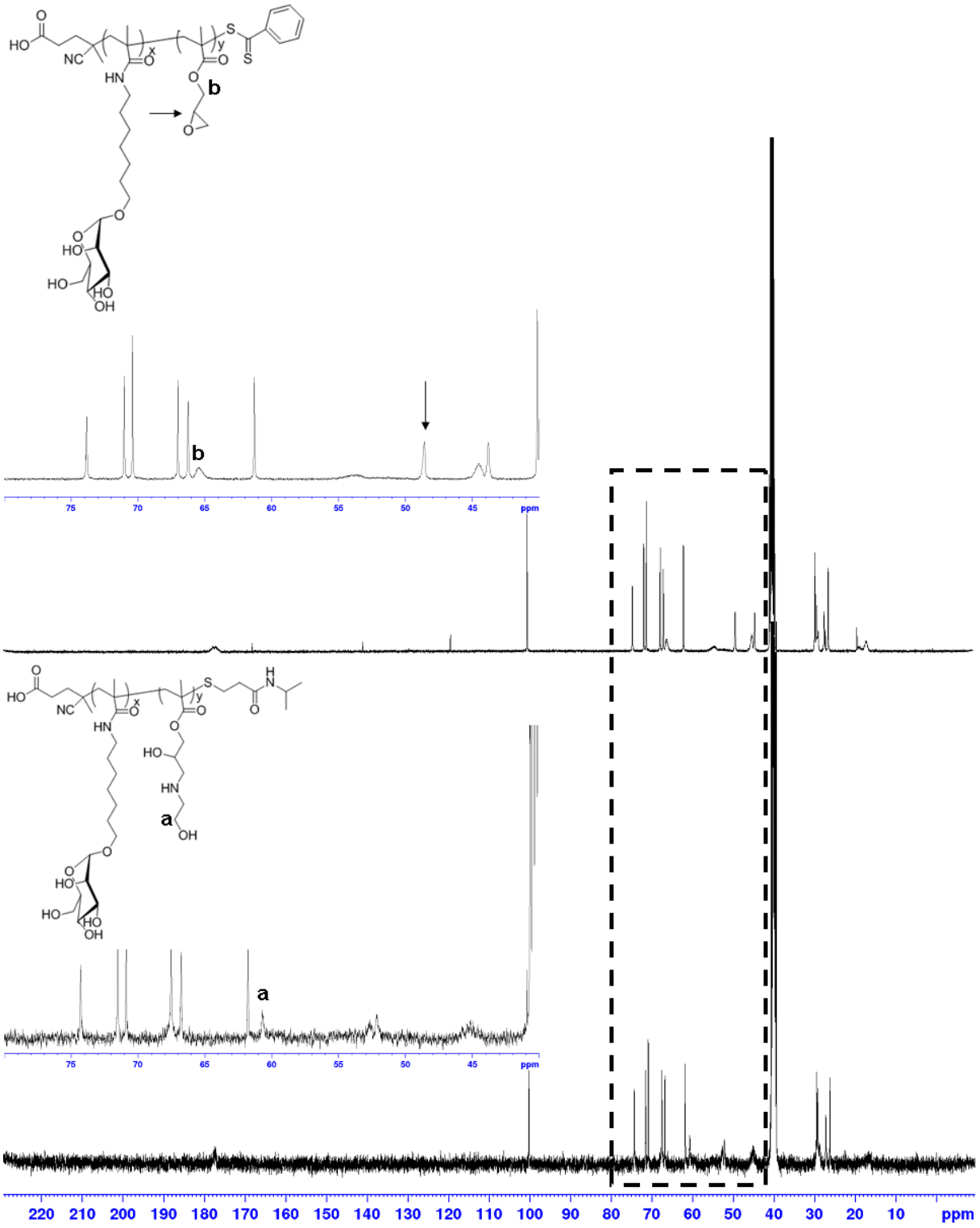

Figure 2.26. ^{13}C NMR spectra of ethanolamine modified glyco-copolymer using P(GMA_{63}-*stat*-HMM_{134}) as precursor.

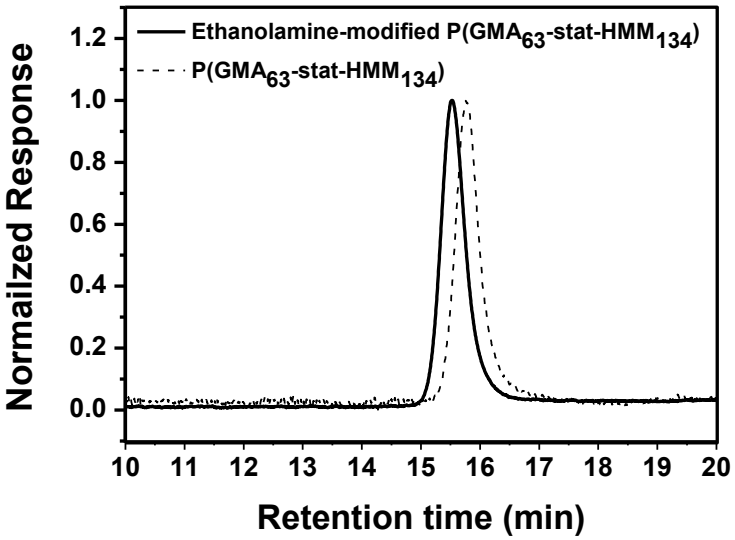

Figure 2.27. SEC trace for post-modification of statistical copolymers, the SEC was performed after acetylation. (Use of PS calibration in THF).

The modified glycopolymers were subsequently studied by dynamic light scattering analysis (DLS) in pure water (concentration at 1 mg/mL). The results are given in **Table 2.3.** After modification, several copolymers, especially those modified with taurine or (2-aminoethyl)trimethylammonium and having a low HMM content tend to form large aggregates in water possibly due to unwanted cross-linking side reactions between epoxy rings or straightforward self-assembly of the copolymers in solution. The other copolymers are observed as unimers (Entries 6EA, 6AA, 7EA, 8EA……) or as small aggregates (Entries 1AA, 1TR, 3EA, 4AA……).

Table 2.3. DLS studies of post-modified copolymers.

Entries	Copolymers	Diameter (nm)[a]		
		Ethanolamine (EA)	(2-aminoethyl) trimethylammonium (AA)	Taurine (TR)
1	$PGMA_{65}$-*b*-$PHMM_{133}$	15	21	25
2	$P(GMA_{66}$-*grad*-$HMM_{130})$	18	13	15
3	$P(GMA_{63}$-*stat*-$HMM_{134})$	20	17	17
4	$PGMA_{100}$-*b*-$PHMM_{107}$	15	25	n.d[b]

5	P(GMA_{103}-*grad*-HMM_{108})	10	14	n.d[b]
6	P(GMA_{95}-*stat*-HMM_{107})	8	9	n.d[b]
7	$PGMA_{136}$-*b*-$PHMM_{65}$	9	16	n.d[b]
8	P(GMA_{134}-*grad*-HMM_{66})	8	n.d[b]	n.d[b]
9	P(GMA_{134}-*stat*-HMM_{66})	16	n.d[b]	n.d[b]

[a]: determined from DLS analysis in pure water (1mg/mL); [b]:not determined due to aggregation.

2.6 Conclusion

Aiming at generating glycopolymers with anti-adhesive properties, we have designed and prepared series of linear and star-shaped multi-valent homoglycopolymers by RAFT polymerization based on heptyl mannoside (HM), a nanomolar FimH antagonist. In order to investigate the influence of carbohydrate density and of the relative position of the carbohydrates on the polymer backbone, the glyco(co)polymers composed of HMM and GMA have been prepared with tunable compositions and microstructures. Neutral, positively charged and negatively charged modified copolymers have then been prepared through a epoxy ring opening procedure. Glycopolymer/FimH interactions and anti-adhesive properties of the glycopolymers described in this chapter are presented in Chapter 3.

2.7 Reference

1. Choudhury, D.; Thompson, A.; Stojanoff, V.; Langermann, S.; Pinkner, J.; Hultgren, S. J. and Knight, S. D. *Science*, **1999**, *285*, 1061-1066.

2. Sharon, N. *Biochimica Et Biophysica Acta-General Subjects*, **2006**, *1760*, 527-537.

3. Firon, N.; Ashkenazi, S.; Mirelman, D.; Ofek, I. and Sharon, N. *Infection and Immunity*, **1987**, *55*, 472-476.

4. Bouckaert, J.; Berglund, J.; Schembri, M.; De Genst, E.; Cools, L.; Wuhrer, M.; Hung, C. S.; Pinkner, J.; Slattegard, R.; Zavialov, A.; Choudhury, D.; Langermann, S.; Hultgren, S. J.; Wyns, L.; Klemm, P.; Oscarson, S.; Knight, S. D. and De Greve, H. *Molecular Microbiology*, **2005**, *55*, 441-455.

5. Han, Z. F.; Pinkner, J. S.; Ford, B.; Obermann, R.; Nolan, W.; Wildman, S. A.; Hobbs, D.; Ellenberger, T.; Cusumano, C. K.; Hultgren, S. J. and Janetka, J. W. *Journal of Medicinal Chemistry*, **2010**, *53*, 4779-4792.

6. Han, Z. F.; Pinkner, J. S.; Ford, B.; Chorell, E.; Crowley, J. M.; Cusumano, C. K.; Campbell, S.; Henderson, J. P.; Hultgren, S. J. and Janetka, J. W. *Journal of Medicinal Chemistry*, **2012**, *55*, 3945-3959.

7. Klein, T.; Abgottspon, D.; Wittwer, M.; Rabbani, S.; Herold, J.; Jiang, X. H.; Kleeb, S.; Luthi, C.; Scharenberg, M.; Bezencon, J.; Gubler, E.; Pang, L. J.; Smiesko, M.; Cutting, B.; Schwardt, O. and Ernst, B. *Journal of Medicinal Chemistry*, **2010**, *53*, 8627-8641.

8. Jiang, X. H.; Abgottspon, D.; Kleeb, S.; Rabbani, S.; Scharenberg, M.; Wittwer, M.; Haug, M.; Schwardt, O. and Ernst, B. *Journal of Medicinal Chemistry*, **2012**, *55*, 4700-4713.

9. Sperling, O.; Fuchs, A. and Lindhorst, T. K. *Organic & Biomolecular Chemistry*, **2006**, *4*, 3913-3922.

10. Brument, S.; Sivignon, A.; Dumych, T. I.; Moreau, N.; Roos, G.; Guerardel, Y.; Chalopin, T.; Deniaud, D.; Bilyy, R. O.; Darfeuille-Michaud, A.; Bouckaert, J. and Gouin, S. G. *Journal of Medicinal Chemistry*, **2013**, *56*, 5395-5406.

11. Darfeuille-Michaud, A.; Neut, C.; Barnich, N.; Lederman, E.; Di Martino, P.; Desreumaux, P.; Gambiez, L.; Joly, B.; Cortot, A. and Colombel, J. F. *Gastroenterology*, **1998**, *115*, 1405-1413.

12. Darfeuille-Michaud, A.; Boudeau, J.; Bulois, P.; Neut, C.; Glasser, A. L.; Barnich, N.; Bringer, M. A.; Swidsinski, A.; Beaugerie, L. and Colombel, J. F. *Gastroenterology*, **2004**, *127*, 412-421.

13. Boettner, B. *SciBX*, **2013**, *6*, 1-2.

14. Bernardi, A.; Jimenez-Barbero, J.; Casnati, A.; De Castro, C.; Darbre, T.; Fieschi, F.; Finne, J.; Funken, H.; Jaeger, K. E.; Lahmann, M.; Lindhorst, T. K.; Marradi, M.; Messner, P.; Molinaro, A.; Murphy, P. V.; Nativi, C.; Oscarson, S.; Penades, S.; Peri, F.; Pieters, R. J.; Renaudet, O.; Reymond, J. L.; Richichi, B.; Rojo, J.; Sansone, F.; Schaffer, C.; Turnbull, W. B.; Velasco-Torrijos, T.; Vidal, S.; Vincent, S.; Wennekes, T.; Zuilhof, H. and Imberty, A. *Chemical Society Reviews*, **2013**, *42*, 4709-4727.

15. Becer, C. R. *Macromolecular Rapid Communications*, **2012**, *33*, 742-752.

16. Kanai, M.; Mortell, K. H. and Kiessling, L. L. *Journal of the American Chemical Society*, **1997**, *119*, 9931-9932.

17. Kitov, P. I.; Sadowska, J. M.; Mulvey, G.; Armstrong, G. D.; Ling, H.; Pannu, N. S.; Read, R. J. and Bundle, D. R. *Nature*, **2000**, *403*, 669-672.

18. Kitov, P. I.; Mulvey, G. L.; Griener, T. P.; Lipinski, T.; Solomon, D.; Paszkiewicz, E.; Jacobson, J. M.; Sadowska, J. M.; Suzuki, M.; Yamamura, K. I.; Armstrong, G. D. and Bundle, D. R. *Proceedings of the National Academy of Sciences of the United States of America*, **2008**, *105*, 16837-16842.

19. Kumar, J.; McDowall, L.; Chen, G. J. and Stenzel, M. H. *Polymer Chemistry*, **2011**, *2*, 1879-1886.

20. Richards, S. J.; Jones, M. W.; Hunaban, M.; Haddleton, D. M. and Gibson, M. I. *Angewandte Chemie-International Edition*, **2012**, *51*, 7812-7816.

21. Polizzotti, B. D. and Kiick, K. L. *Biomacromolecules*, **2006**, *7*, 483-490.

22. Grunstein, D.; Maglinao, M.; Kikkeri, R.; Collot, M.; Barylyuk, K.; Lepenies, B.; Kamena, F.; Zenobi, R. and Seeberger, P. H. *Journal of the American Chemical Society*, **2011**, *133*, 13957-13966.
23. Pasparakis, G.; Cockayne, A. and Alexander, C. *Journal of the American Chemical Society*, **2007**, *129*, 11014-+.
24. Lundquist, J. J. and Toone, E. J. *Chemical Reviews*, **2002**, *102*, 555-578.
25. Lindhorst, T. K.; Kieburg, C. and Krallmann-Wenzel, U. *Glycoconjugate Journal*, **1998**, *15*, 605-613.
26. Nagahori, N.; Lee, R. T.; Nishimura, S.; Page, D.; Roy, R. and Lee, Y. C. *Chembiochem*, **2002**, *3*, 836-844.
27. Touaibia, M.; Wellens, A.; Shiao, T. C.; Wang, Q.; Sirois, S.; Bouckaert, J. and Roy, R. *Chemmedchem*, **2007**, *2*, 1190-1201.
28. Gouin, S. G.; Wellens, A.; Bouckaert, J. and Kovensky, J. *Chemmedchem*, **2009**, *4*, 749-755.
29. Almant, M.; Moreau, V.; Kovensky, J.; Bouckaert, J. and Gouin, S. G. *Chemistry-a European Journal*, **2011**, *17*, 10029-10038.
30. Bouckaert, J.; Li, Z. L.; Xavier, C.; Almant, M.; Caveliers, V.; Lahoutte, T.; Weeks, S. D.; Kovensky, J. and Gouin, S. G. *Chemistry-a European Journal*, **2013**, *19*, 7847-7855.
31. Chong, J. M.; Heuft, M. A. and Rabbat, P. *Journal of Organic Chemistry*, **2000**, *65*, 5837-5838.
32. Godula, K.; Rabuka, D.; Nam, K. T. and Bertozzi, C. R. *Angewandte Chemie-International Edition*, **2009**, *48*, 4973-4976.
33. Ahmed, M. and Narain, R. *Biomaterials*, **2012**, *33*, 3990-4001.
34. Min, E. H.; Ting, S. R. S.; Billon, L. and Stenzel, M. H. *Journal of Polymer Science Part a-Polymer Chemistry*, **2010**, *48*, 3440-3455.
35. Wu, Y. Y.; Wang, M.; Sprouse, D.; Smith, A. E. and Reineke, T. M. *Biomacromolecules*, **2014**, *15*, 1716-1726.
36. Bathfield, M.; D'Agosto, F.; Spitz, R.; Charreyre, M. T. and Delair, T. *Journal of the American Chemical Society*, **2006**, *128*, 2546-2547.
37. Deng, Z. C.; Ahmed, M. and Narain, R. *Journal of Polymer Science Part a-Polymer Chemistry*, **2009**, *47*, 614-627.
38. Pissuwan, D.; Boyer, C.; Gunasekaran, K.; Davis, T. P. and Bulmus, V. *Biomacromolecules*, **2010**, *11*, 412-420.
39. Jaacks, V. *Makromol. Chem.*, **1972**, *161*, 161-172.
40. Kelen, T.; Tudos, F.; Turcsanyi, B. and Kennedy, J. P. *J. Polym. Sci., Polym. Chem. Ed.*, **1977**, *15*, 3047-3074.
41. Dube, M. A. and Penlidis, A. *Polymer*, **1995**, *36*, 587-598.
42. Escale, P.; Ting, S. R. S.; Khoukh, A.; Rubatat, L.; Save, M.; Stenzel, M. H. and Billon, L. *Macromolecules*, **2011**, *44*, 5911-5919.
43. Barbey, R.; Kauffmann, E.; Ehrat, M. and Klok, H. A. *Biomacromolecules*, **2010**, *11*, 3467-3479.
44. Sung, D.; Park, S. and Jon, S. *Langmuir*, **2012**, *28*, 4507-4514.

Chapter 3

Glycopolymers for Anti-adhesive Treatment of *E. coli*-Induced Inflammatory Diseases

Chapter 3 Glycopolymers for Anti-adhesive Treatment of *E. coli*-Induced Inflammatory Diseases

3.1 Introduction

In the previous chapter, we described the preparation of precisely defined glycopolymers having multiple copies of *n*-heptyl α-D-mannose (HM), as pendent motifs. Through the association of a judicious ligand selection with the presentation of multiple ligands on a polymeric scaffold, we expect to generate highly potent macromolecular inhibitors of type-1 fimbriae bacterial adhesion. In the present Chapter, we will thus evaluate the capability of precisely defined HM-based glycopolymers to efficiently bind to FimH lectin domains of *E. coli* strains (UTI 89 and AIEC LF82 clinically isolated from patients with urinary tract infections and Crohn's disease respectively). Practically, we will first investigate FimH adhesin/glycopolymers interactions through dynamic and static light scattering analyses. We will then evaluate the ability of the glycopolymers to associate with *E. coli* strains. Finally we will estimate the capability of the glycopolymers to inhibit recognition and binding of adherent-invasive *E. coli* with live epithelial cells or to disrupt adherent-invasive *E. coli* adhesion with live epithelial cells *in vitro* and *ex vivo* (**Scheme 3.1**).

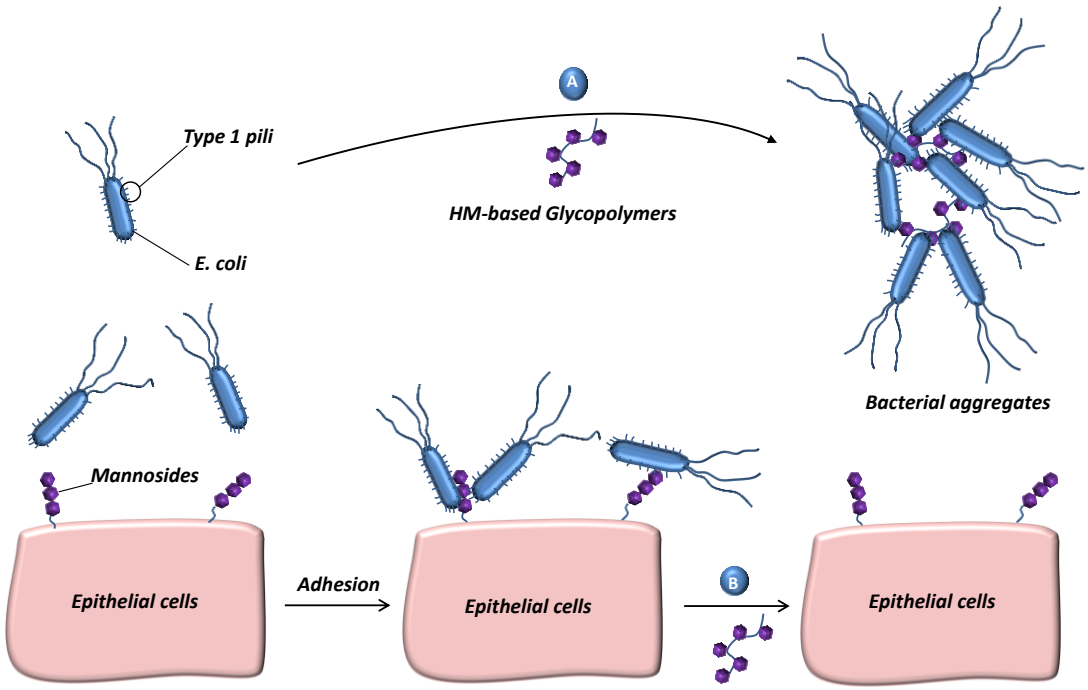

Scheme 3.1: Principle of HM-based glycopolymers anti-adhesive action; **A**: Sequestration of free bacteria in the lumen of the gut; **B**: Disruption of established *E coli*-cell interactions

3.2 Multivalent FimH antagonists

The macromolecular FimH antagonists with different size and topology (described in Chapter 2) have been designed to assess the influence of HM valency and spatial presentation of the epitopes. We hypothesized that the polymeric antagonists would generate stronger multivalent interactions, on a valency-corrected basis, by recruiting a higher number of bacterial pili, mimicking more accurately *E. coli* attachment to the glycocalyx of the host cells.

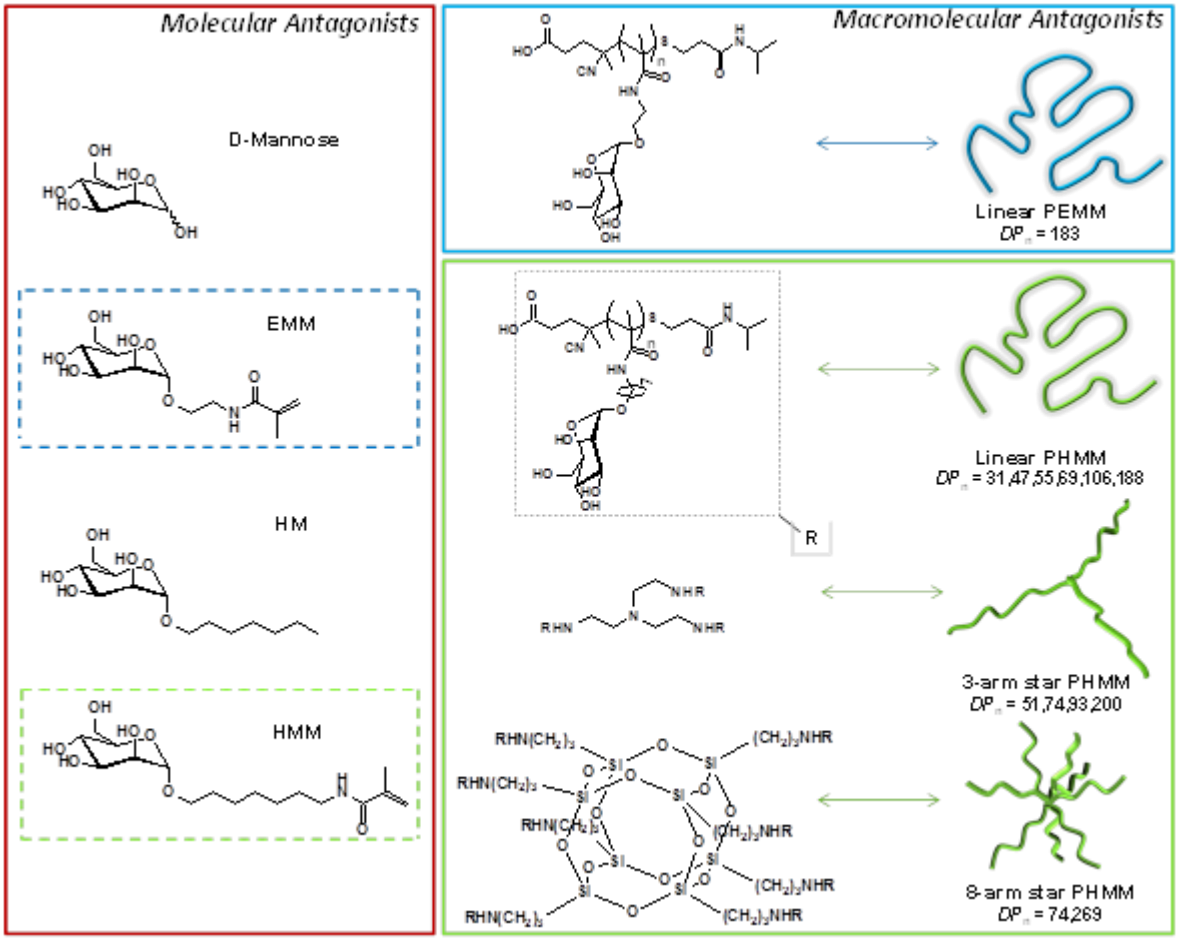

Scheme 3.2: Molecular and macromolecular FimH antagonists explored in this study.

3.3 Glycopolymer/FimH interactions

To gain preliminary insight into type 1 piliated *E. coli* bacteria/PHMM interactions, association of FimH adhesin and glycopolymer chains was investigated by dynamic light scattering (DLS). To closely apprehend the initial conditions, DLS was first

carried out on FimH adhesin (83 µM) on the one hand and PHMM (L188, 15 µM) on the other hand (**Figure 3.1A**, blue and black curves, respectively). The D_h-values, 4.2 ± 0.1 and 825 ± 33 nm are obtained for FimH adhesin and 10.7 ± 0.3 and 259 ± 2 nm for L188, corresponding to free macromolecules and pre-assembled ones.[1] The distributions shown in **Figure 3.1A** are mass-weighted. When converting them into number-weighted distributions, we get $N_{small} \sim 10^3$-10^5 N_{big}, meaning that the number of free macromolecules (N_{small}) is in fact much larger than that of pre-assembled ones (N_{big}). A polymer suspension of L188 (20 µL at 15 µM) was subsequently added in a single step to a suspension of FimH adhesin (350 µL at 83 µM, [Man]/[FimH] ~ 2).

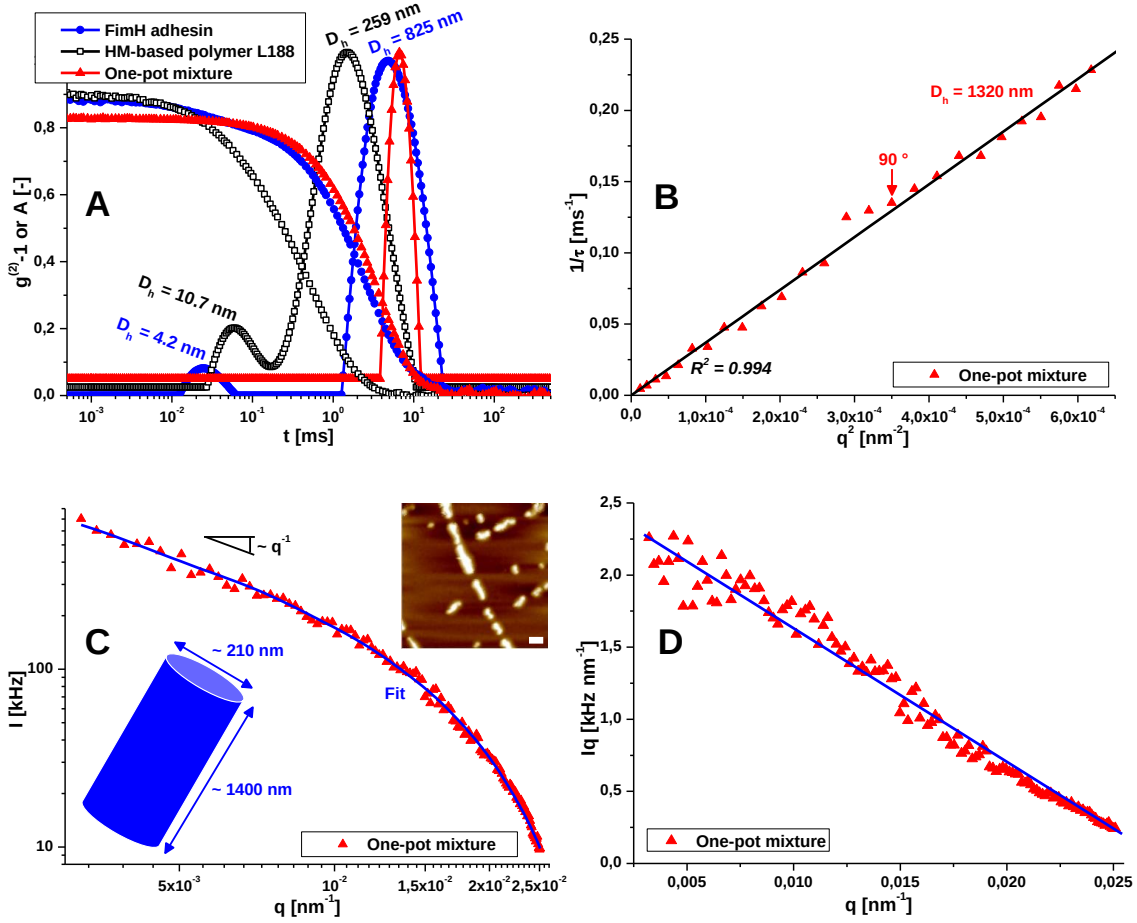

Figure 3.1: A) DLS, autocorrelation function ($g^{(2)}$-1) and relaxation time distribution (A) at 90°; B) DLS, inverse of the relaxation time distribution maximum (1/τ) on squared wave vector modulus (q^2) between 15 and 140° by step of 5° (hydrodynamic diameter (D_h) and correlation coefficient (R^2)); C) SLS, scattering intensity (I) on wave vector modulus (q) between 14 and 143° by step of

1°; Inset: AFM picture of FimH-L188 complexes (scale bar: 1 μm) D) SLS, corresponding Kratky plot. All measurements were carried out in HEPES buffer (20 mM, pH 7.4) containing NaCl (150 mM).

The above-mentioned populations almost instantaneously disappear upon addition, replaced by a new single narrow-sized population (**Figure 3.1A**, red curve), which can be reasonably attributed to the formation of FimH adhesin/PHMM complexes. These self-assemblies were probed by DLS at various scattering angles from 15 to 140 ° (**Figure 3.1B**).The inverses of the relaxation time distribution maxima (1/τ) exhibit a proportional dependency with q^2 (squared wave vector modulus), displaying Brownian diffusive motion of objects characterized by the D_h-value of 1320 nm. Static light scattering (SLS) was carried out on this peculiar mixture (**Figure 3.1C**). Experimental scattering intensity perfectly fits with the form factor of uniform cylinder of length *ca.* 1400 nm and diameter *ca.* 210 nm (blue solid line, **Figure 3.1C**). Accordingly, a single linear regime is observed on the Kratky representation (**Figure 3.1D**). These results are further corroborated by atomic force microscopy (AFM) measurements where the cylinder length and diameter in the dried state coincide with the values determined by SLS in aqueous solution (see inset **Figure 3.1C**). The formation of these original supramolecular cylinders thus demonstrates the capability of each glycopolymer chain to accommodate a large number of FimH adhesin molecules.

In addition to the one-shot addition procedure described above, PHMM/FimH interactions were also investigated for a stepwise addition procedure (see **Figure 3.2**). Specifically, PHMM Hepes solution (L188, 15 μM) was sequentially added into FimH Hepes solution (83 μM) to finally reach the same composition as the one obtained for the one-shot addition procedure. Again, the populations present in the solution were probed by DLS. For clarity's sake, we exclusively focus herein on L188/FimH system (however, association of FimH adhesin with PHMM chains was also confirmed for the other glycopolymers, see Chapter 5). In contrast to the one-shot addition procedure which resulted in the formation of a unique population of supramolecular cylinders, the sequential addition of glycopolymer aliquots in solution led to a far more complex

picture. All along the addition of glycopolymers, three different populations were detected.

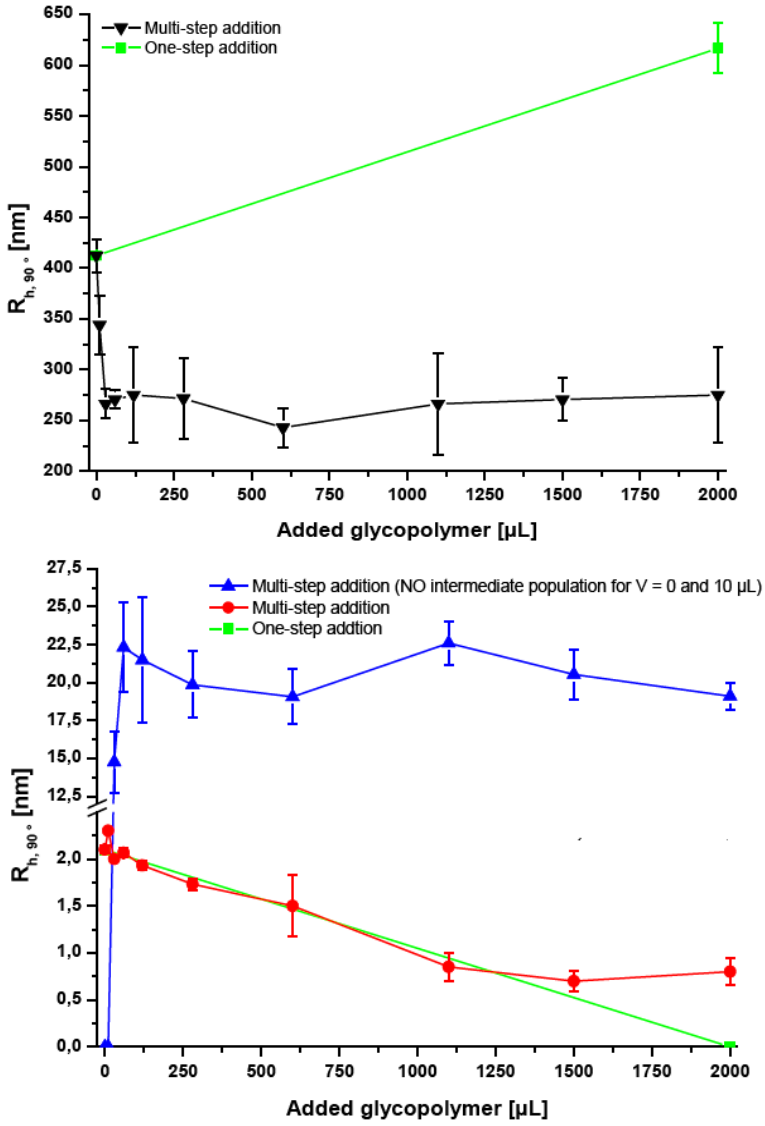

Figure 3.2: Comparison plots between one-shot and stepwise addition.

A first population observed at very low R_h was attributed to free/self-assembled FimH. The dimensions of this population progressively decreased with glycopolymer content (from 2nm to 1nm) but contrary to the one-shot addition procedure, this population remained present even after complete addition of the glycopolymer. These data suggest that when the glycopolymer chains are sequentially incorporated in the FimH solution, it is not possible to quantitatively complex the adhesin with the pendent mannosides (in spite of a favorable HM/FimH ratio).

A second population with a R_h that rapidly stabilizes at about 20 nm was also systematically detected. The proportion of these objects seems to increase with glycopolymer content. Finally a third population with a R_h starting from 400 nm and rapidly dropping to about 250 nm is detected. This last population could be either a "reservoir" of aggregated FimH (its proportion is decreasing upon addition of glycopolymers) or FimH/L188 aggregates. In this context of multimodal distribution, no SLS analysis was performed for this experiment.

3.4 Glycopolymer/Bacteria interactions

The capability of PHMM chains to bind FimH in their natural environment, *i.e.* when the lectin is located to the extremity of bacteria pili, was then investigated. In this view, a bacterial suspension of type 1 piliated *E. coli* strain UTI89 (OD_{650nm}=1.3) was subjected to PHMM chains at concentrations ranging from 1 to 3 μM of L188 (See **Figure 3.3**). As shown in **Figures 3.3B** and **3.3C**, PHMM acts as a powerful glue to agglutinate *E. coli* bacteria. Introduction of PHMM results in the formation of bacterial clusters whose size increases with the concentration of ligands (50 x 98 μm after adding 3μM) confirming that the glycopolymer chains induce multiple binding events with the bacteria-bound FimHs and that one glycopolymer chain is capable to establish cross-linking interactions with FimH adhesins expressed by multiple bacteria.

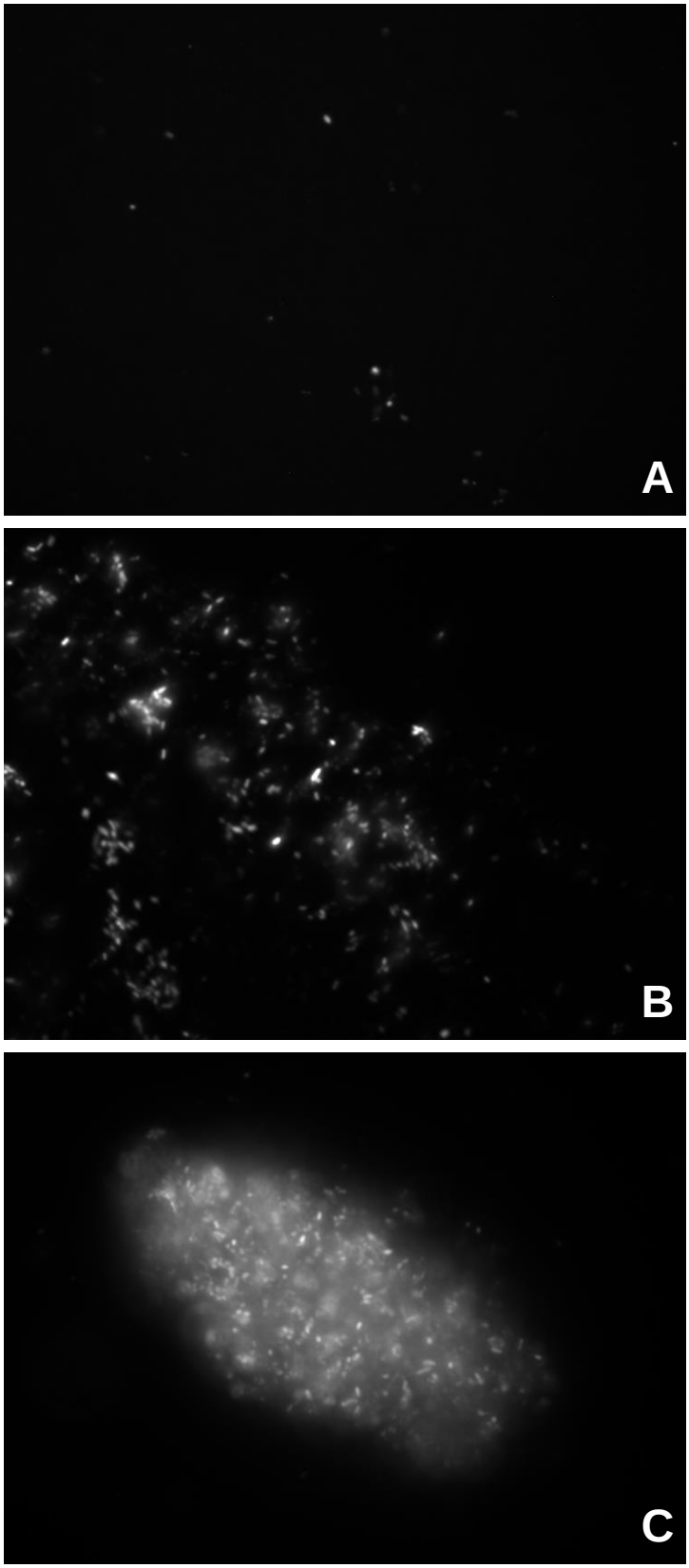

Figure 3.3: Glycopolymer-induced agglutination of type 1 fimbriated *E. coli* (strain UTI89). (A) Fluorescence microscopy pictures of Katushka-expressing type 1 fimbriated *E. coli* UTI89 (reference and details in Supporting Information); (B) exposed to 1μM of L188; (C) to 3μM of L188

and resulting in a “bacterial egg” agglomerate with approximate dimensions 98 x 51 µm.

3.5 Adhesion Tests

The propensity of the glycopolymers to prevent attachment of *E. coli* to host cells was further investigated through adhesion assays. Infections of intestinal epithelial T84 cells were performed with AIEC reference strain LF82 previously incubated with a series of mannosides (HMM, HM and α-D-mannose) or PHMM (pre-incubation protocol). Poly(*N*-[2-(α-D-mannopyranosyl-oxy)ethyl] methacrylamide) (PEMM, M_n = 53 600 kg.mol^{-1} and $Đ$ = 1.17), a mannosylated glycopolymer with a short ethyl linker, was also tested to evaluate the influence of the alkyl spacer on bacterial adhesion inhibition (See **Scheme 3.2**). T84 cells were selected due to their high level of expression of CEACAM6 glycoprotein, an established receptor for AIEC bacteria adhesion on intestinal host cells in Crohn’s disease patients.[2] Pre-incubation assays were primarily performed at 0.1 µM (on mannose unit basis) of FimH antagonists. Levels of AIEC LF82 bacteria adhering to the cells in the presence of antagonists were expressed in percentages of residual bacteria, 100% corresponding to adhesion in absence of any compound. At such concentrations, no monovalent reference efficiently impedes the binding of AIEC LF82 to T84 cells (residual adhesion over 80% for α-D-mannose and HM) even though noticeable decrease of adhesion level is observed with HMM (59%). In the presence of the multivalent PHMM chains, the residual percentage of AIEC LF82 bound to T84 cells considerably drops (levels of adhesion typically ranging from 17 to 43%). Inhibitory activities tend to increase with chain length for linear glycopolymers (39, 23 and 17% for L31, L106 and L188 respectively) and to slightly decrease with the number of arms for the star-shaped glycopolymers (20 and 26 % for T200 and O269). More generally, consistent with previous work of Stenzel and co-workers on concanavaline A and glucosylated polymers, no enhancement of activity is observed for star-shaped glycopolymers.[3] In contrast to PHMM, PEMM shows no inhibitory activity at 0.1 µM (**Figure 3.5**). This result confirms that the presentation of multiple binding sites on a polymer scaffold is not sufficient for designing effective anti-adhesive polymers and that optimization of

the interactions between the ligand and the binding pocket within the FimH adhesin domain is of crucial importance.[4] Dose-dependent effects were further explored for compounds of each polymer group (L31, L188, T51, T200, O98 and monovalent ligands as references, see **Figure 3.4**). No significant anti-adhesive properties were observed below a concentration of 1 µM for monovalent mannosides (HMM, HM). Polymer ligands, especially linear and 3-arm stars PHMM, display greater inhibitory activity than monovalent ligands. Whereas 1 µM of HMM, the most effective monovalent ligand, is required to inhibit significantly the attachment of AIEC LF82 to T84 cells (residual adhesion ~ 45%), the presence of 10 nM of PHMM with the highest valency (L188 or T200) results in similar levels of adhesion (45 and 50%). This 100 times increase in inhibitory potency (valency-corrected) clearly highlights the benefits of multivalent polymeric inhibitors over monovalent ligands.

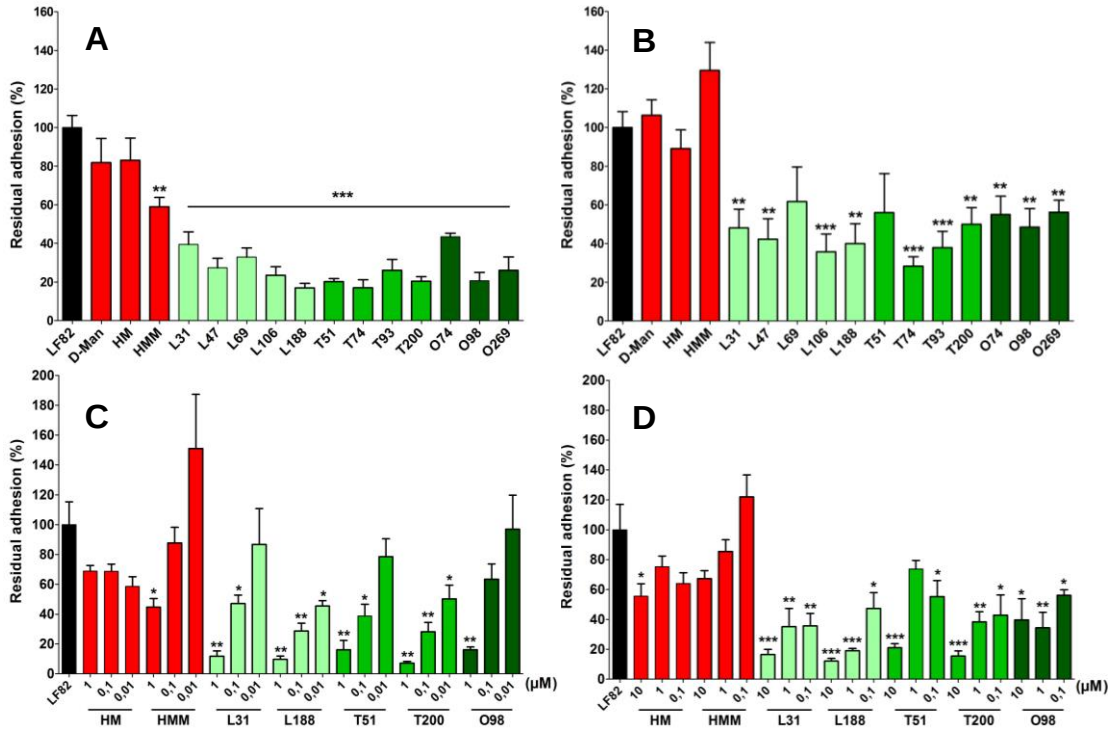

Figure 3.4 : A) Residual adhesion of the bacterial strain AIEC LF82 to T84 cells at a concentration of 0.1 µM of inhibitors (on mannose unit basis) in pre-incubation experiments. B) Residual adhesion of the bacterial strain AIEC LF82 to T84 cells at a concentration of 1 µM of inhibitors (on mannose unit basis) in post-incubation experiments. C) Inhibitory effects of mannosides or glycopolymers (at 0.01, 0.1 and 1 µM) on AIEC LF82 adhesion levels to T84 cells in pre-incubation experiments. D) Inhibitory effects of mannosides or glycopolymers (at 0.1, 1 and 10 µM) on AIEC

LF82 adhesion levels to T84 cells in post-incubation experiments. Results are expressed as percentages of adherent bacteria, AIEC LF82 adhesion in absence of inhibitors was considered as 100% (means ±SEM). *P<0.05, **P<0.01, ***P<0.001.

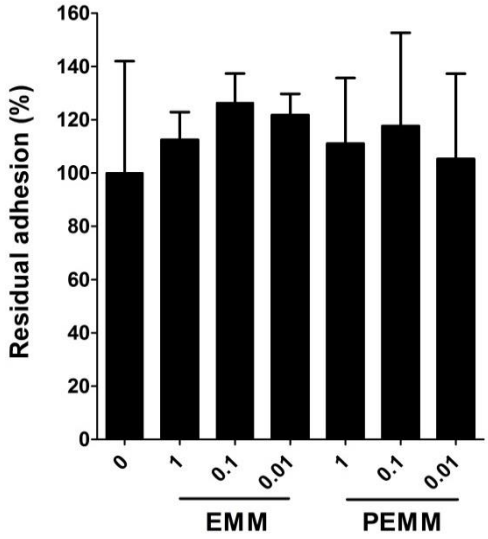

Figure 3.5: Residual adhesion of AIEC strain LF82 to T84 cells at a concentration of 1, 0.1 and 0.01 µM of EMM or PEMM inhibitors (on mannose unit basis) in pre-incubation experiments. Results are expressed as percentages of adherent bacteria, AIEC LF82 adhesion in absence of inhibitors was considered as 100%

Post-incubation experiments were subsequently performed to evaluate the aptitude of HM-based compounds to disrupt pre-established interactions between T84 intestinal epithelial cells and AIEC LF82 bacteria. Thus, T84 cells were first infected by bacteria, extensively washed to eliminate non-adhering bacteria and subsequently incubated with monovalent or macromolecular FimH antagonists for 3h. No efficient detachment of bacteria was observed upon addition of molecular inhibitors less than 10 µM (55 and 67 % of residual adhesion for HM and HMM). In contrast, most of AIEC bacteria are washed out when a concentration of 0.1 µM (on mannose basis) of the most potent glycopolymers is added (36, 47 and 43% of residual adhesion for L31, L188 and T200). These results demonstrate that PHMM chains are not only capable to efficiently inhibit recognition events in a prophylactic approach but also to disrupt established interactions between epithelial cell receptors and FimH adhesion

domains.

3.6 Ex-vivo tests

Based on the pre- and post-incubation assays data, L188 was finally selected for testing PHMM anti-adhesive properties in *ex vivo* conditions. More specifically, the ability of this macromolecular antagonist to prevent AIEC LF82 adhesion was tested on a model of colonic loops of transgenic CEABAC10 mice expressing CEACAM6.

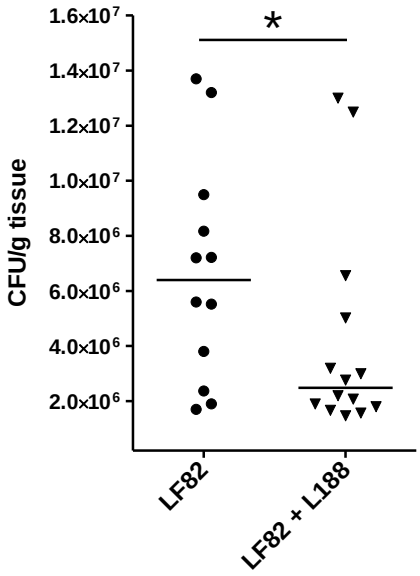

Figure 3.6: Inhibitory effect of glycopolymer L188 on the adhesion level of the AIEC LF82 strain to intestinal tissue from transgenic CEABAC10 mice expressing human CEACAM6. Bacteria were pre-incubated 15 min with the inhibitor at a dose of 3.4 µmol of mannose units, then a volume of 100 µL of bacteria/inhibitor mixture was injected into colonic loops (~0.6 cm for 1h). Results are expressed as percentages of bacteria adherent to the colonic mucosa (means ± sem, n=5 to 8 mice). 100% corresponds to the bacterial adhesion in absence of any treatment (NT for non-treated). *: $P<0.05$.

With that aim, LF82 bacteria (6 x 10^5 CFU) or a mix of LF82 bacteria (6 x 10^5 CFU) and L188 (3.4 µmol of mannose units) were injected into the loops and incubated for one hour. After washing steps, LF82 adhesion levels to the intestinal tissue in the presence or absence of inhibitor were estimated (See **Figure 3.6**). As observed *in vitro* on T84 cells, L188 actively prevents AIEC attachment to the colonic tissues (6.4 x 10^6 CFU/g of tissue for PHMM-free experiment vs 2.5 x 10^6 CFU/g of tissue in the

presence of PHMM, 61% decrease of bacteria adhering to colonic mucosa).

3.7 ELLSA tests

Competitive Enzyme-Linked Lectinosorbent assays (ELLSA) were finally carried out to gain further knowledge on the association of the glycopolymers to FimH (as a function of the HM valency and topology). Briefly, the principle of this assay lies in the competition between FimH/glycopolymers and FimH/RNAseB interactions, RNAseB being a protein (coated on the immunosorbent plates) which displays a mixture of oligomannose glycans ($Man_5GlcNAc_2$, $Man_7GlcNAc_2$, and $Man_8GlcNAc_2$) capable to strongly bind to FimH (see technical details in Chapter 5). The intensity of FimH binding to the substrate represented by the optical density of chromophore absorbance at 450 nm was measured for a dilution series of glycopolymers as well as for α-D-mannose, methyl α-D-mannoside and HM as molecular references to build dose-response inhibition profiles (See **Figure 3.7**). In contrast to the conclusions drawn from the adhesion tests, the highest level of inhibition (IC_{50} = 0.11 μM) was obtained for HM. Thanks to the favoured binding of FimH to pendent HM ligands, the glycopolymers also efficiently disrupt FimH/RNAseB association but no gain of affinity is observed with macromolecular inhibitors (IC_{50} = 0.40-1.5 μM Man) owing to the monovalent nature of the FimH binding site. The apparent affinity of the pendent HM bound to the polymeric structure is indeed lower than the one observed for the free HM reference probably due to steric hindrance.

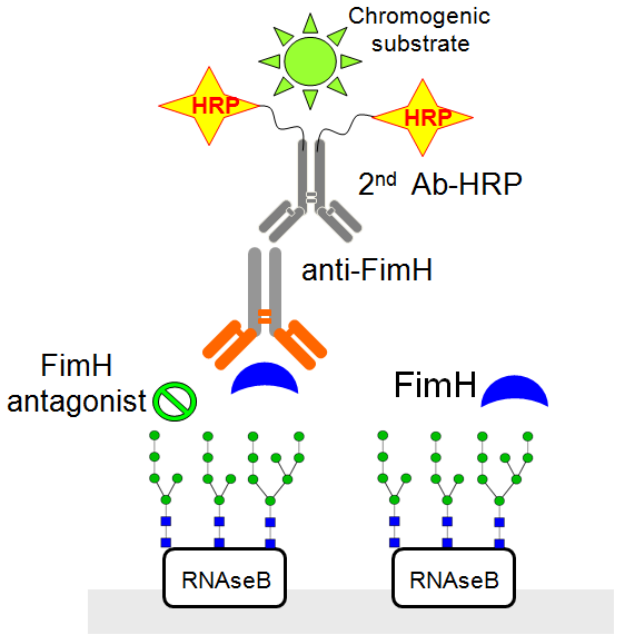

Ligand	MIC50 nM (of PHMM)
L31[a]	12,9
L47[a]	12,27
L55[a]	10,07
L69[a]	9,46
L106[a]	9,10
L188[a]	6,55
T51[b]	29,5
T74[b]	9,8
T93[b]	10,6
T200[b]	6,62
O74[c]	10,92
O269[c]	4,42

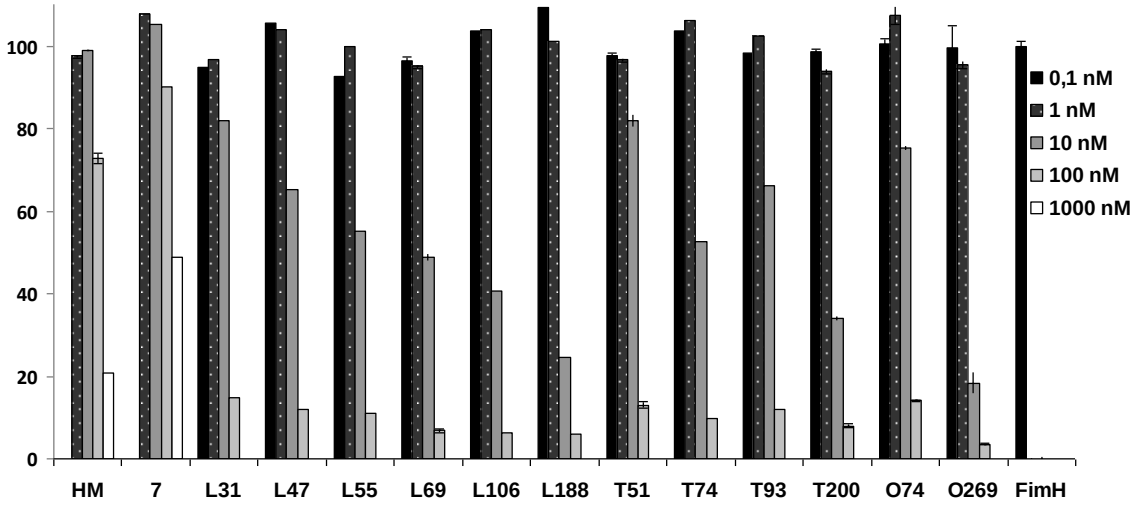

Figure 3.7: (Top left) Principle of competitive lectin ELLSA assays (Bottom and Top left) Affinity testing of glycopolymers toward oligomannose glyco-epitopes using ELLSA. a: linear glycopolymers; b: 3-arms glycopolymers; c: 8-arms glycopolymers.

As a general trend, the activity of the glycopolymers (on a mannose unit basis) slightly decreases with DP_n whereas topology has barely any influence. Importantly, the glycopolymer chains still display considerably higher affinity for FimH than α-D-mannose or methyl α-D-mannoside (IC_{50} = 38.4 and 12 μM respectively) confirming the importance of the heptyl group between the mannosides and the

polymer backbone. Taken together, these results suggest that the significant enhancement in activity over monovalent ligands (highlighted by the anti-adhesive tests) is not related to a higher intrinsic affinity of the polymer bound ligands for FimH, but to the capability of the glycopolymers to undergo multiple cross-linking interactions with living bacteria and to generate large aggregates in which only peripheral bacteria can adhere to the cells.

3.8 Preliminary results on copolymers anti-adhesive properties

Adhesion tests were also performed on the post-modified PHMM/PGMA copolymers described in the Chapter 2. In pre-incubation tests, infections of intestinal epithelial T84 cells were performed on AIEC reference strain LF82 which were previously incubated with a series of copolymers with different compositions, microstructures and pendent groups (see Table 2.2 and 2.3 in Chapter 2 for details). To establish comparisons between homopolymers and copolymers, one of the most potent homopolymers (L188) was used as control (52%). Pre-incubation assays were performed at 0.1 µM (on mannose unit basis) of FimH antagonists (**Figure 3.8**). Inhibitory activities tended to slightly increase with ethanolamine content (48~58% for 1EA~3EA, 40~42% for 4EA to 6EA, 30~50% for 7EA~9EA) and to significantly decrease with the incorporation of positively charged trimethylammonium (60~100%). No specific influence is observed for negatively charged copolymers (49~52%, 1T~3T). These results suggest that when it comes to (glyco)copolymers, the nature of the comonomer plays an important role on the anti-adhesive properties. The influence of the copolymers microstructure and HM density was far more difficult to unravel since no clear correlation between these features and the residual adhesion could be established. Post-incubation experiments were subsequently performed at a concentration of 0.1 µM (on mannose basis). Again, copolymer 7EA was the most potent inhibitor (35% vs 45% for L188). No enhancement of activity was observed for the other copolymers.

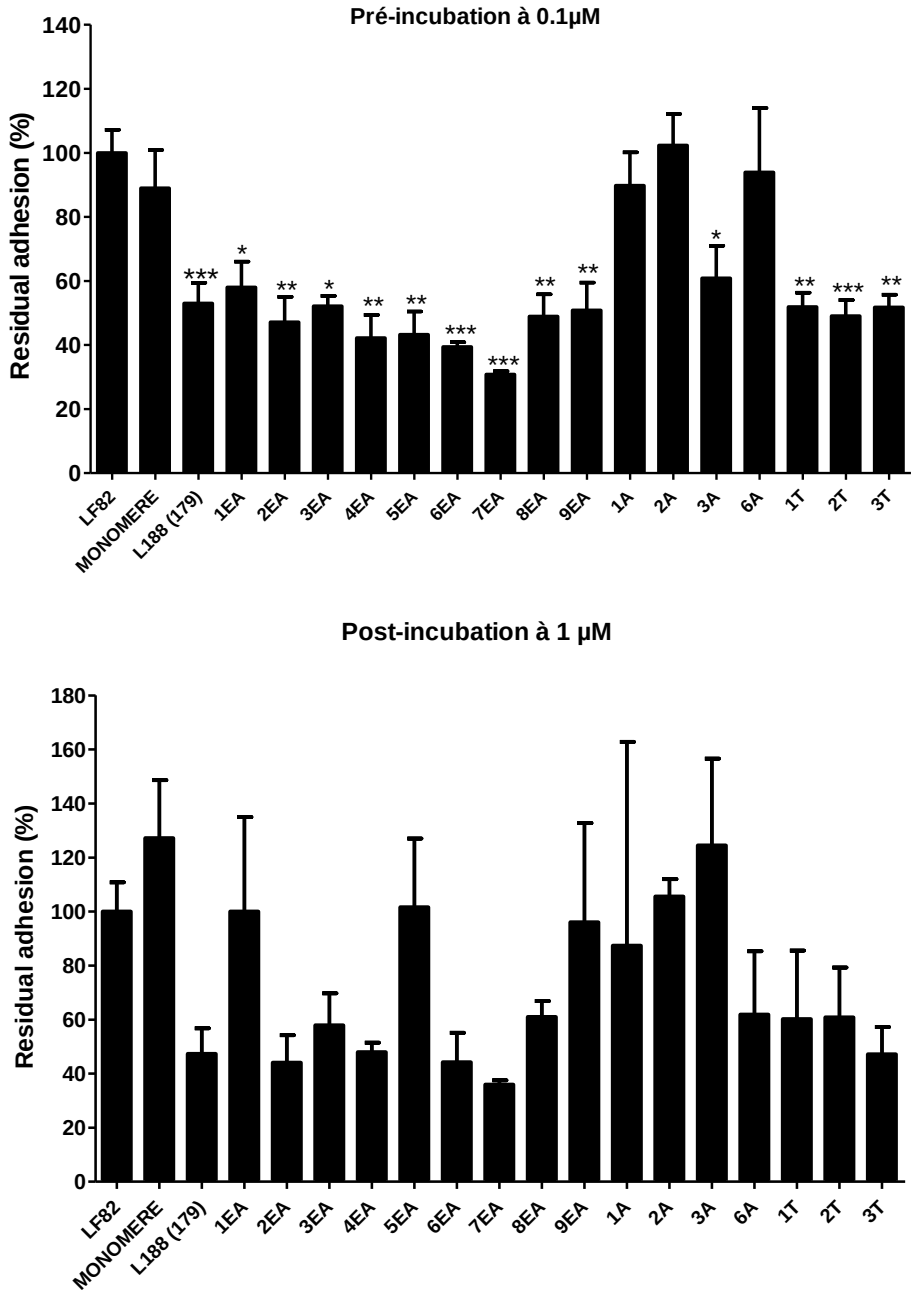

Figure 3.8 : (Up) Residual adhesion of the bacterial strain AIEC LF82 to T84 cells at a concentration of 0.1 µM of inhibitors (on mannose unit basis) in pre-incubation experiments; (Bottom) Residual adhesion of the bacterial strain AIEC LF82 to T84 cells at a concentration of 1 µM of inhibitors (on mannose unit basis) in post-incubation experiments. Results are expressed as percentages of adherent bacteria, AIEC LF82 adhesion in absence of inhibitors was considered as 100% (means ±SEM). *P<0.05, **P<0.01, ***P<0.001.

3.9 Conclusions

In summary, in this Chapter we have evaluated the potential interest of the multivalent approach in preventing/disrupting adherent-invasive *E. coli* adhesion implied in Crohn's disease inflammation. Investigation of AIEC strain LF82 adhesion to T84 cells in the presence of molecular and macromolecular antagonists highlighted the remarkable anti-adhesive capacities of HM-based glycopolymers *in vitro*. Compared to the monovalent HM reference, HM-based glycopolymers were more than 100-fold more potent (valency corrected basis) in preventing/disrupting AIEC attachment to intestinal epithelial cells. The anti-adhesive effect was further evidenced *ex vivo*, in the colon of a transgenic mouse model of CD. As evidenced by the lower IC_{50}'s observed for macromolecular inhibitors in ELLSA assays performed with recombinant FimH, the enhancement in activity is not due to a greater intrinsic affinity for FimH targets but rather to crosslinking interactions and aggregation of the bacteria as suggested by DLS and fluorescence microscopy analyses on HM-based glycopolymers and FimH and bacteria/glycopolymer mixtures. These disparities between ELLSA and adhesion assays also indicate that in the quest for highly efficient pathogen anti-adhesives, classically performed carbohydrate-lectin interactions studies such as ELLSA, ITC or SPR, should be interpreted with caution when they do not account for pathogen aggregation that significantly impact the cell-adhesive properties. Importantly, the *in vitro* and *ex vivo* results reported here illustrate the strong potential of the multivalent concept to prevent/disrupt AIEC attachment to the gut and may constitute an important step towards an anti-adhesive treatment of *E. coli*-induced inflammatory diseases. To validate this last point, the most promising glycopolymers (L188) are currently tested on model mice in a laboratory of INSERM Clermont-Ferrand (Team of Dr Nicolas Barnich/Pr Arlette Darfeuille-Michaud) in *in vivo* conditions.

3.10 References

1. The diameter of gyration (D_g) of 68.4 kg.mol^{-1} glycopolymer (DP_n = 188) in Θ-solvent conditions is crudely given, taking into account the polymer pending groups, by: $D_g = 2\sqrt{\frac{DP_n b^2}{6}} \sim 12\,\text{nm}$ where b gives the segment length (b ~ 7 × 0.154 nm). This calculated value is compatible with the experimental value 10.7 nm, thus showing the presence of single molecule coils. The molar mass of FimH adhesin (16.9 kg.mol^{-1}) is also coherent with the experimental value 4.2 nm and data given in reference 5.

2. Barnich, N. ; Carvalho, F. A. ; Glasser, A-L.; Darcha, C.; Jantscheff, P.; Allez, M.; Peeters, Bommelaer, G.; Desreumaux, Colombel, J-F.; Darfeuille-Michaud, A. J. *Clin. Invest.*, **2007**, *117*, 1566-1574.

3. Chen, Y. ; Chen, G. ; Stenzel, M. H. *Macromolecules* **2010**, *43*, 8109-8114.

4. Richards, S-J.; Jones, M. W.; Hunaban, M.; Haddleton, D.M, Gibson, M. I. *Angew. Chem. Int. Ed.*, **2012**, *51*, 7812-7816.

5. Bouckaert, J.; Li, Z.; Xavier, C.; Almant, M.; Caveliers, V.; Lahoutte, T.; Weeks, S. D.; Kovensky, J.; Gouin, S. G. *Chem. Eur. J*., **2013**, *19*, 7847-7855.

Chapter 4

Simple but Precise Engineering of Functional Nanocapsules through Nanoprecipitation

Chapter 4 Simple but Precise Engineering of Functional Nanocapsules through Nanoprecipitation

4.1 Introduction

The nanoprecipitation technique, is a simple means for generating narrow size distribution colloids without using ultra-sonication or high shear mechanical mixing methods. The principle of the technique lies in the supersaturation of whatever hydrophobic solute (oil, polymer, dye…) primarily dissolved in a hydrophilic solvent (e.g. acetone, THF……) when a large excess of water is added. Upon addition of water, the solution turns to be a non-solvent of the hydrophobic solute, inducing spontaneous emulsification. For certain proportions of solute, solvent and non-solvent, submicronic droplets or particles are generated (**Scheme 4.1**).[1]

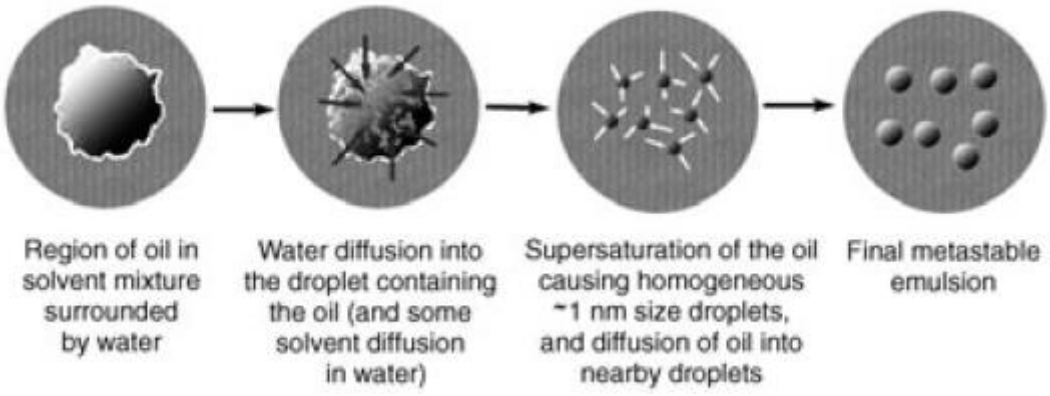

Scheme 4.1. Schematics of the liquid–liquid nucleation process of Ouzo effect[1].

In this chapter, we wil aim at developing an undemanding method for the construction of multifunctional, oil-filled nanocapsules in a simple and straightforward batch experiment. In contrast to the general applications of nanoprecipitation in the preparation of particles.[2] we will intend to find experimental conditions allowing for the encapsulation of liquids by a polymer using the Ouzo effect. To identify a domain of composition in which narrowly dispersed core-shell nano-objects can be elaborated, we will first establish phase diagrams and will then focus on the production of nanocapsules decorated with biorelevant molecules within the shell and loaded with hydrophobic molecules in a simple one-pot procedure.

4.2 Determination of phase diagram

For preparing the carbohydrate-based membrane of the capsules, 2 water soluble linear glycopolymers (PHMM1 and PHMM2) were prepared by RAFT polymerization using agent CPADB as RAFT agent. The polymerization proceeded smoothly to yield polymers exhibiting molar masses of 24 and 102 kg mol^{-1} and *Đ* values below 1.10 (**Figure 4.4A**). Dynamic light scattering was performed to evaluate the hydrodynamic diameter of individual chains (below 10 nm) in pure water solution (**Figure 4.4B**).

Table 4.1: Glycopolymers obtained by RAFT polymerization

Polymer	$M_{n\ th}$ [a] ($kg.mol^{-1}$)	$M_{n\ NMR}$ [b] ($kg.mol^{-1}$)	M_w [c] ($kg.mol^{-1}$)	*Đ* [d]	DP_n [b]	D_h [e] (nm)
PHMM1	15.6	17.4	24.0	1.03	47	5.0
PHMM2	80.1	81.2	102.5	1.02	221	8.9

[a)] calculated from monomer conversion; [b)] determined from relative integration of the aromatic chain end group and polymer backbone peaks; [c)] determined from SEC with RI/light scattering detection in $NaNO_3$/NaOH aqueous solution (pH =7); [d)] *Đ* from SEC analysis in $NaNO_3$/NaOH aqueous solution; [e)] determined from DLS analysis in pure water.

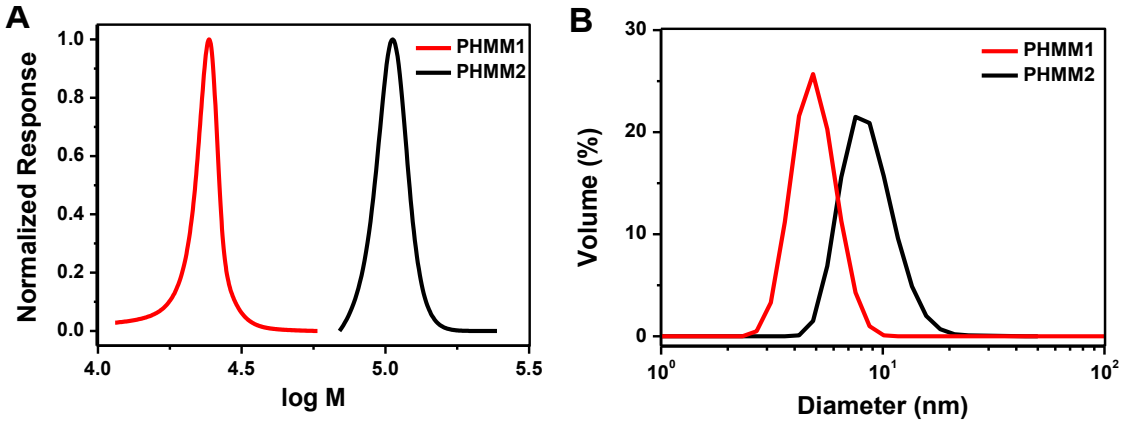

Figure. 4.4. (A) SEC traces of glycopolymers in $NaNO_3$/NaOH aqueous solution (pH =7); (B) Hydrodynamic diameters as measured by DLS in pure water (1mg/mL).

4.2.1 Cloudy point boundary of PHMM in water/acetone mixtures

As a first step towards the preparation of nanocapsules, phase diagrams for polymer/ water (solvent)/ acetone (non-solvent) and hexadecane (HD)/ acetone(solvent)/ water (non- solvent) ternary systems were determined. The cloud point boundary for the polymer/water/acetone ternary system was readily determined by titrating aqueous solutions of polymer with acetone (non solvent). It can basically be described by a straight line at a constant mass fraction of acetone (**Figure 4.5**). Noteworthy, the boundary is slightly shifted to lower mass fraction of solvent when the titration is performed with the polymer possessing the highest molar mass. Below this boundary, the polymer is fully dissolved in the solvent mixture whereas above it the glycopolymer chains generate large aggregates.

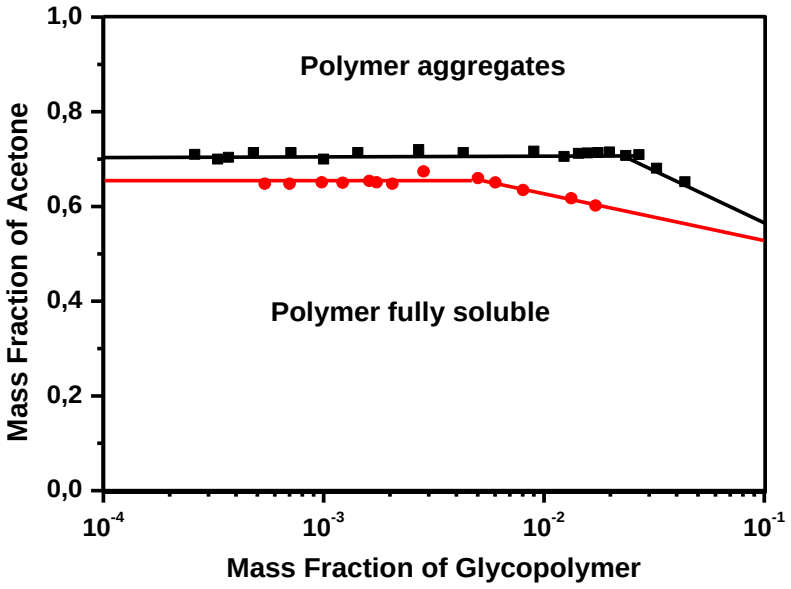

Figure 4.5. Phase diagram of PHMM1 (red) and PHMM2 (black) in water/acetone mixtures. The content of water is deduced from the two other weight fractions.

4.2.2 Ouzo domain of Hexadecane/Acetone/Water ternary system

Similar to the determination of the cloudy point boundary for PHMM/acetone/water mixtures, the binodal curve for the HD/acetone/water system was determined by titration of HD/acetone solution with water. The Ouzo limit, beyond which large droplets are formed, was determined by dynamic light scattering. Special

requirements were made here to ensure reproducible measurements of the Ouzo limit: i) a non-ionic surfactant (Brij56) was added in the organic phase to stabilize the HD droplets once formed; ii) after adding the required content of water for emulsification, an extra load of water was rapidly poured to dilute the samples and avoid Ostwald ripening. The Ouzo limit was determined by measuring the number of counts by DLS, before and after filtrating the mixture with 1.20 µm polyethersulfone filters. Identical numbers of counts corresponded to homogeneous emulsions of HD droplets (Ouzo conditions), whereas a decrease of it indicates a loss of large HD droplets on the filter (out of Ouzo conditions) (**Figure 4.6**).

The two curves were finally overlapped to obtain the Ouzo domain of HD, where monodisperse hexadecane nanodroplets can be generated in a reproducible manner without addition of surfactant.

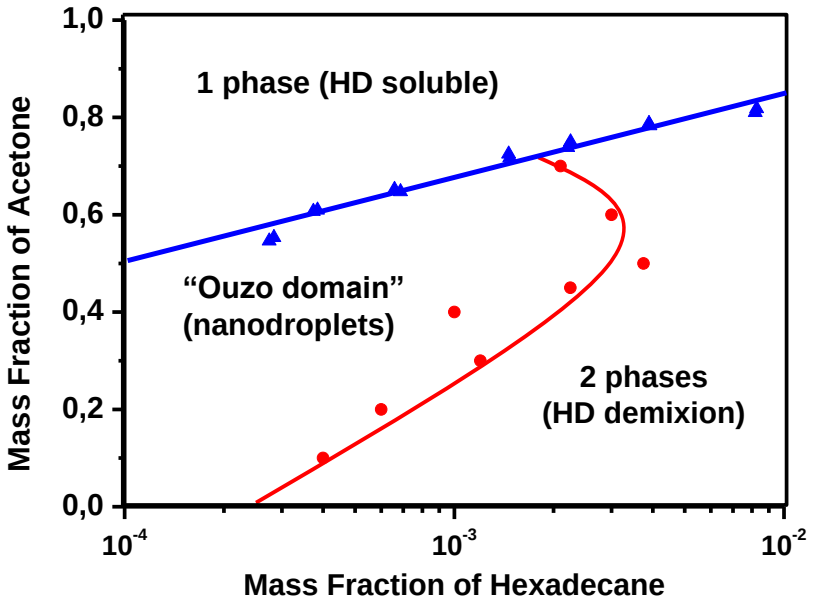

Figure 4.6. Phase diagram of HD shifting in acetone/water mixture, showing the binary curve (in blue) and the Ouzo limit (in red).

4.3 Preparation of glyco-nanocapsules through Nanoprecipitaion

4.3.1 Phase diagram for nanocapsules preparation

The phase diagrams of glycopolymer/water/acetone and HD/water/acetone ternary

systems were then overlapped (Figure 4.7), to identify conditions where nanocapsules with narrow size distribution can be built. A prerequisite for the generation of glyconanocapsules is to work in a domain of composition where HD will generate exclusively nanodroplets (in the Ouzo domain) and at the meantime where polymer chains preferentially stick at the surface of the nanodroplets.

After overlapping of the 2 phase diagrams, 6 regions can be distinguished (a~e). In zones a, b and c, PHMM is fully soluble forbidding the formation of a polymeric shell. In zones d, e and f, PHMM generates aggregates. HD is fully soluble in zones c and d, demixes in zones a and c, and generates metastable emulsion in zones b and f. The domain f is the only one in which well-defined nanocapsules can be built through the conjoint precipitation of HD and glycopolymer (domain f given in green in Figure 4.7). Practically, PHMM2 which leads to a cloudy point boundary for lower content of acetone (Figure 4.5), was preferred over PHMM1 in order to widen the domain of application.

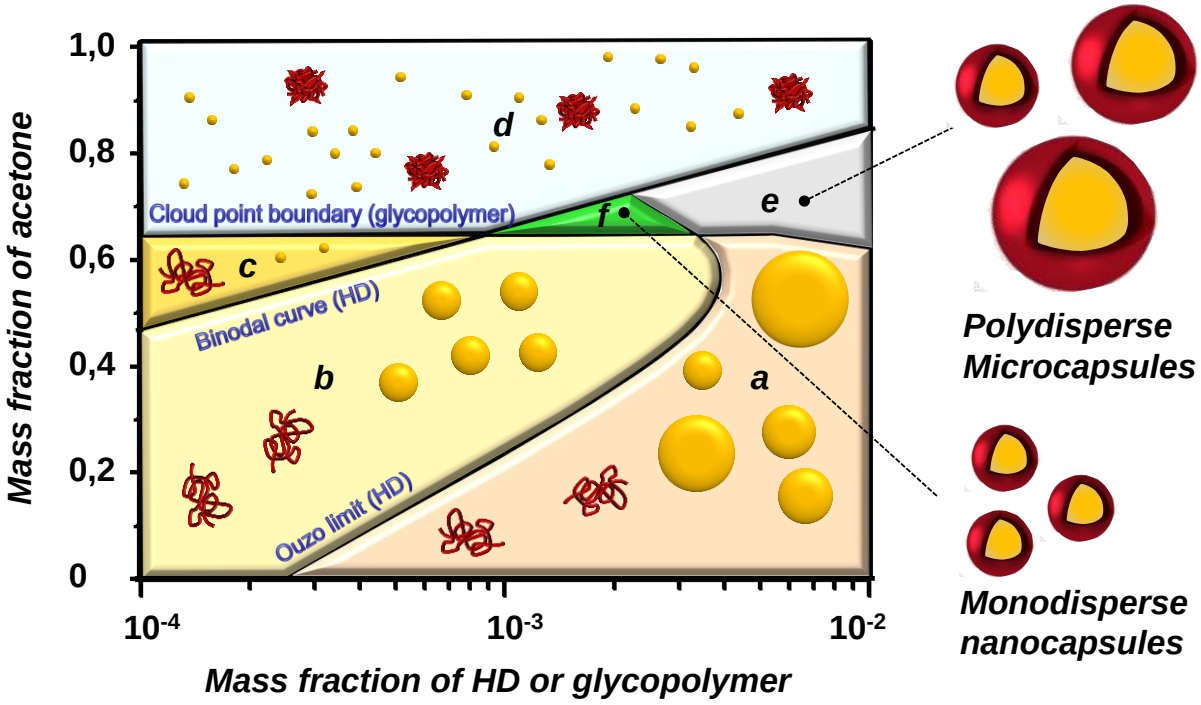

Figure 4.7. Overlapped phase diagrams of PHMM and HD in acetone/water mixtures. PHMM is soluble in *a*, *b*, *c*, and micellizes in *d*, *e* and *f*; HD is fully dissolved in *c* and *d*, generate metastable emulsions in *b* and *f*, and demixes in *a* and *e*. The domain *f* in which well-defined nanocapsules

are built through conjoint precipitation of HD and glycopolymer is shown in green. (●) HD molecule, (●) HD droplet, (●) swollen polymer chain, (●) polymer coil, (●) core-shell HD/glycopolymer capsule.

To prepare the glyconanocapsules, the content of acetone should be between 65 and 70 wt%, with a final weight fraction of HD around 0.2 wt%. In a preliminary test, PHMM2 (1mg) was dissolved in 350 mg of water, whereas 2 mg of HD were dissolved in 650 mg acetone separately. Aqueous solution of PHMM2 was then poured into the acetone solution all at once, and the transparent solution turned to be milky immediately. Dynamic light scattering (DLS) of the resulting dispersion highlighted the presence of a single population with diameter (D_z) of 135 nm and a polydispersity index of 0.11 (Figure 4.8A). However, after evaporation of the acetone, the population corresponding the nanocapsules totally disappeared and a new one corresponding to individual chains of PHMM2 (Diameter ~10nm) appeared. Besides, the nanocapsules (in water/acetone mixture) do not survive to TEM analysis (Figure 4.8B). HD leaked out of the droplets and dark dots of precipitated glycopolymers were observed (similar morphologies were observed when aqueous solution of PHMM2 were directly casted). As a consequence, we decided to maintain the morphology of the nanocapsules through cross-linking of the shell.

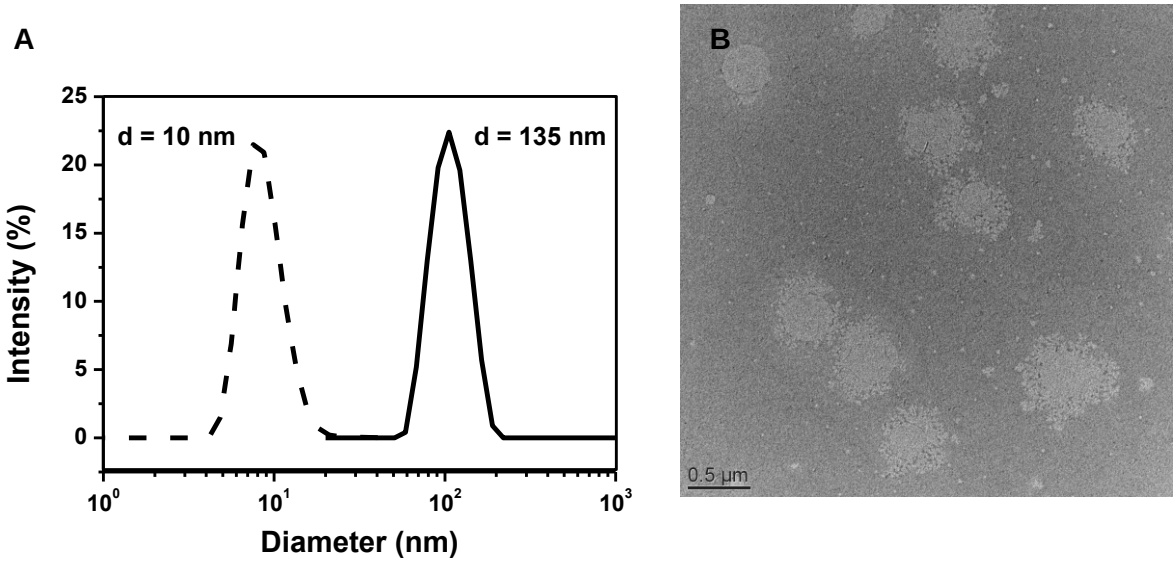

Figure 4.8. (A) DLS of non-crosslinked HD-filled glyconanocapsules (**right, black curve**) obtained by dissolving **PHMM2** (1mg) in water (0.35g), dissolving HD (2mg) in acetone (0.65g) and pouring

PHMM2 aqueous solution into acetone solution all at once, mass fraction of acetone=0.65 and DLS of the solution after evaporation of acetone (**left, dash curve**) that underlines the presence of the glycopolymer unimers. (B) TEM picture showing that if the membranes are not cross-linked, HD droplets spread under the microscope vacuum into “octopuses’ like’ structure, though retaining a spherical shape.

4.3.2 Capsules’ stabilization using cross-linking strategy

For “freezing” the structure of capsules and simultaneously promoting their functionalization, isophorone diisocyanate (IPDI), a low water-sensitive cross-linker, was initially added to the organic solution. In **Figure 4.9** are given the TEM pictures of a series of nano-objects of increasing complexity. The first attempt of shell cross-linking with 0.5 equivalent of IPDI per chain failed at efficiently stabilizing the formed glyconanocapsules. (see Figure 4.8B and 4.9B). Upon the addition of 1 equivalent of IPDI per chain, the D_z value of the capsules increased to 248 nm (PDI = 0.07), and the formation of a thin, fragile and deformable membrane was observed by TEM at the surface of the droplets (**Figure 4.9**). HD domains and glycopolymer nanoparticles (from self-assembly of the free unreacted chains during sample casting) were however still present. A further increase in IPDI content resulted in progressive shrinkage of the capsule membranes as a result of cross-linking reaction between PHMM chains, and the D_z value of nanocapsules dropped to 200 nm and 150 nm upon the addition of 5 and 24 equivalents, respectively. The nano-objects gradually evolved to robust and perfectly spherical glyconanocapsules. Accordingly, leakage of HD was suppressed, and the polymer membranes are sufficiently robust not to be broken during the TEM process (casting/analysis).

A

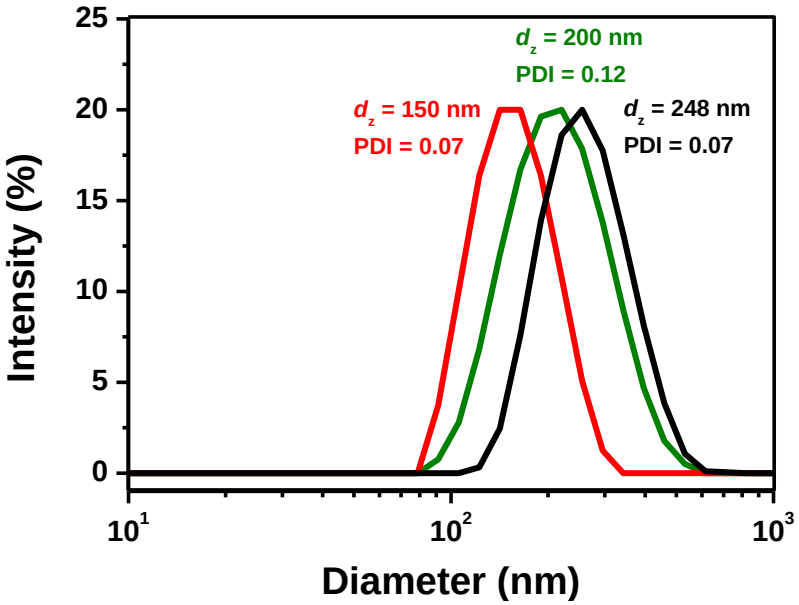

B

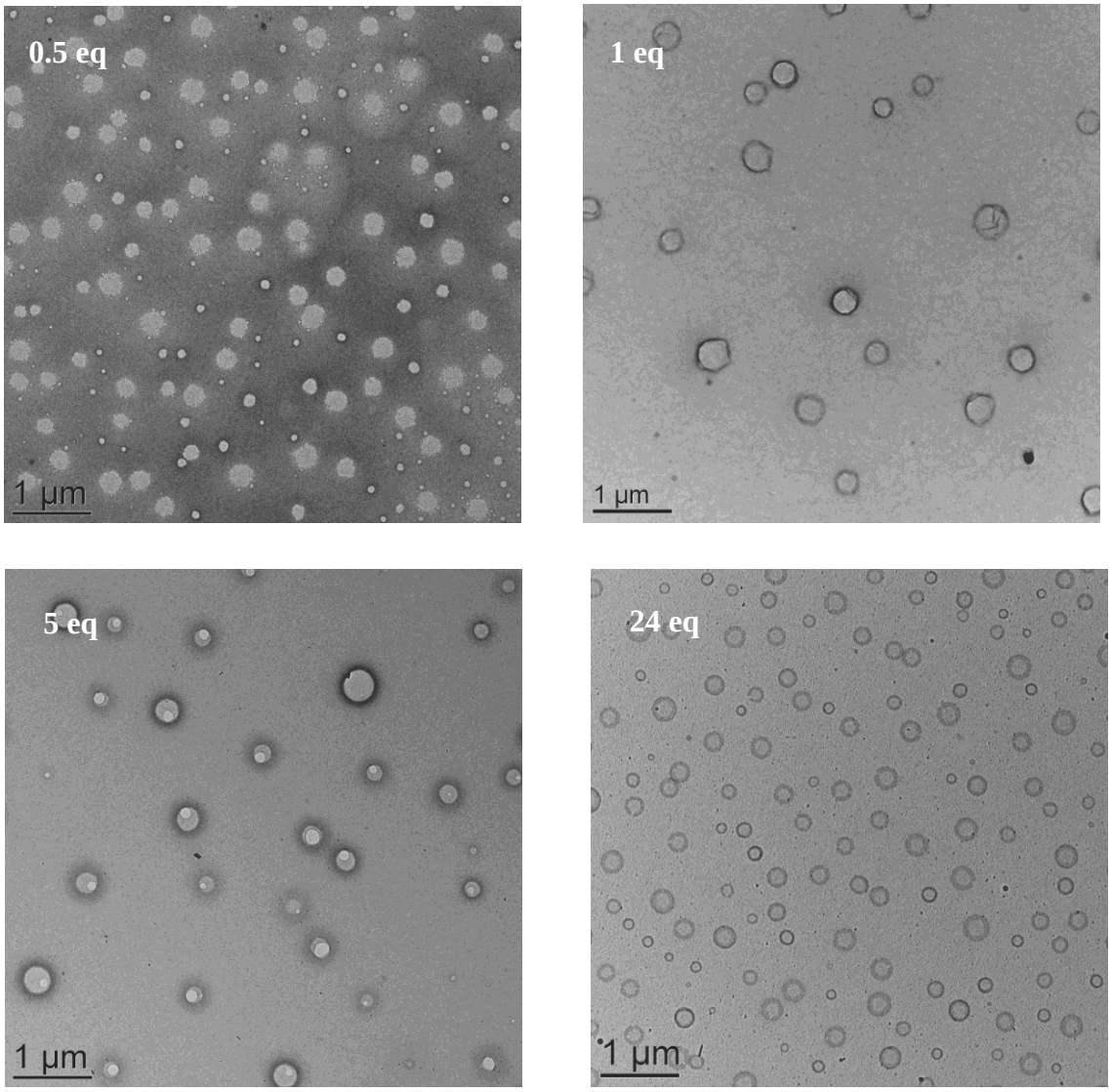

Figure 4.9. (A) DLS of glyconanocapsules cross-linked with 1 (black), 5 (green) and 24 (red)

equivalents of IPDI (per PHMM chain). (B) Selected TEM pictures of glyconanocapsules cross-linked with 0.5, 1, 5 and 24 eq. of IPDI.

To confirm our assumptions on the domain of applicability of this process, experiments were subsequently performed out of the domain f. As expected, solvent shifting in the domain b does not allow formation of nanocapsules. Under such conditions, droplets are not covered by the glycopolymer chains so that, despite IPDI addition, emulsion droplets destabilize with time. In a similar manner (and for the same reason), no nanocapsules are observed in the domain a. Interestingly, experiments in the domain e, give rise to the formation of microcapsules together with submicronic capsules (Figure 4.10).

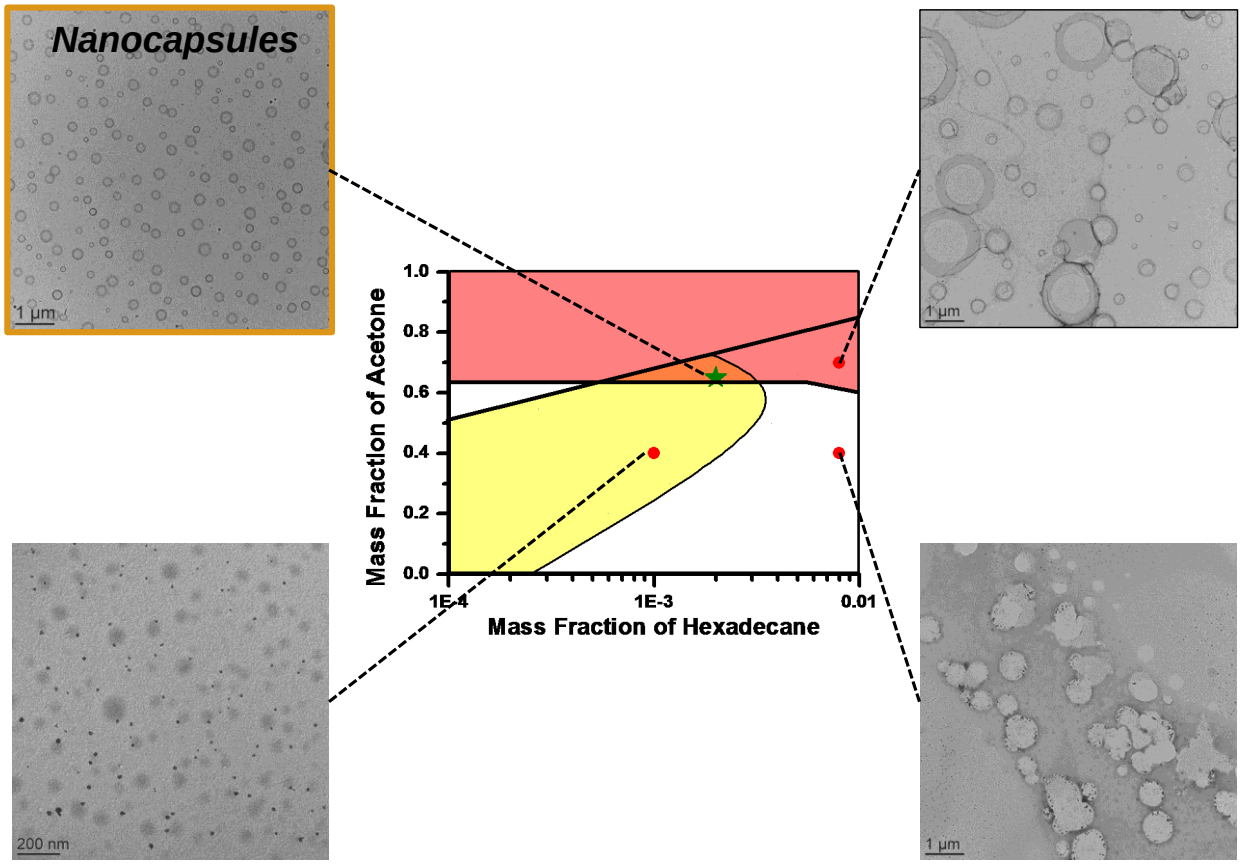

Figure 4.10. Morphologies observed for different HD/Acetone/water compositions after solvent shifting and IPDI polymer cross-linking.

4.4 Functionalization and loading of glyconanocapsules

To extend the scope of our procedure leading to the straightforward preparation of

glyconanocapsules, we subsequently explored the sequestration of hydrophobic molecules withiin the liquid core of the capsules and the covalent attachment of molecules of biological interest (ligands, fluorescent tags……) on the nanocapsules' shell (**Scheme 4.2**).

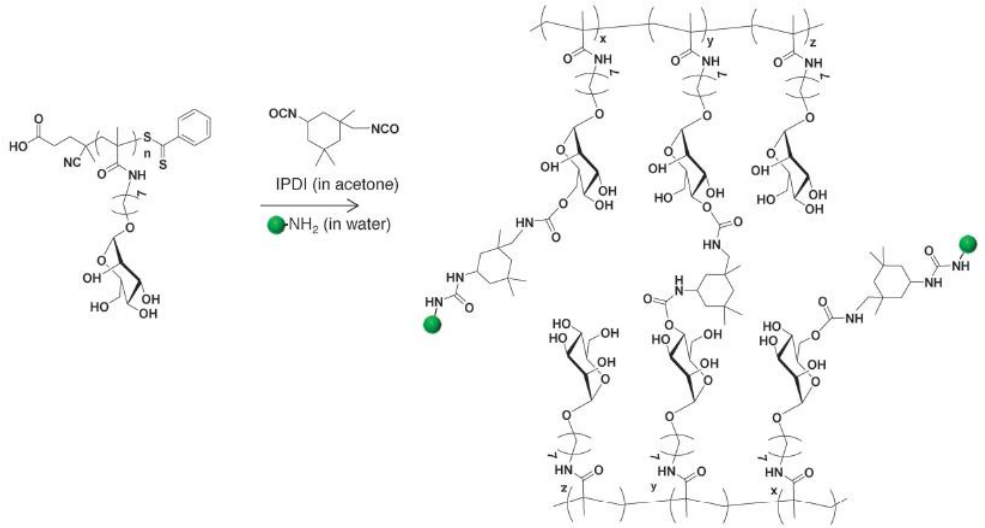

Scheme 4.2. One-pot cross-linking and functionalization of the polymer shell.

4.4.1 Post-Functionalization of glyco-nanocapsules by amino-functionalized molecules

A simple amine, octylamine (1 equivalent per polymer chain), was added 2h after solvent shifting to consume the remaining isocyanate groups and quench the cross-linking reactions occuring within the shell. After such treatment, capsules with D_z = 283 nm (PDI = 0.09) were finally obtained, whereas overnight cross-linking resulted in the preparation of nanocapsules with D_z~248 (PDI = 0.07). (**Figure 4.11**).

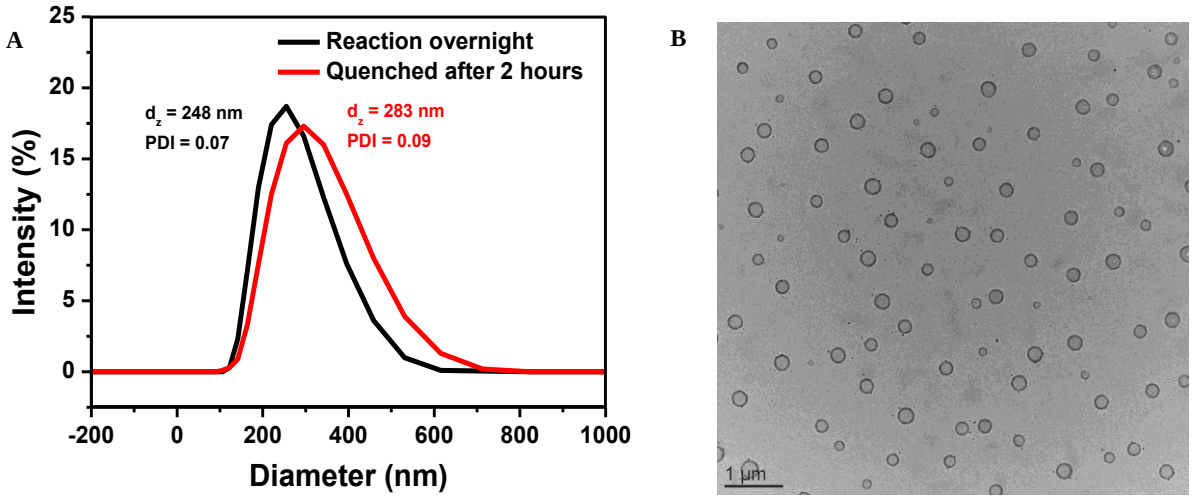

Figure 4.11. (A) Size distribution of IPDI-cross-linked nanocapsules and octylamine-functionalized nanocapsules in water (B) TEM picture of the octylamine-functionalized glyconanocapsules.

4.4.2 Functionalization of the glyconanocapsules using biological molecules

The glyconanocapsules generated through nanoprecipitation are potential candidates for drug delivery systems. It is therefore of crucial importance to demonstrate that surface functionalization of the nanocapsules with molecules paving the way to imaging or targeting (dyes, ligands) can be undertaken. Incorporation of biotin in the course of the preparation of the nanocapsules was thus explored. In this view, an amino functionalized biotin (2 eq. per PHMM chain) was dissolved together with the glycopolymer in the aqueous solution, and the nanoprecipitation was carried out as previously described (24 equivalent per chain) to afford functionalized nanocapsules with a D_z~246 nm (PDI = 0.12). Consistent with a successful functionalization, biotinylated nanocapsules were proven to disrupt 4'-hydroxyazobenzene-2-carboxylic acid (HABA)-avidin complexes thanks to the favored binding of avidin to biotin (Kd =10-15 M vs 5.8 x 10-6 M for HABA-avidin, **Figure 4.12**). To confirm the presence of biotin at the surface of the nanocapsules, avidin, a tetrameric biotin-binding protein was added to a solution of biotinylated nanocapsules. The obvious shift in DLS measurement confirmed the formation of large aggregates (967 nm) upon addition of tetravalent avidin (0.125 eq. per chain) to biotinylated nanocapsules (D_z = 246 nm, PDI = 0.12)

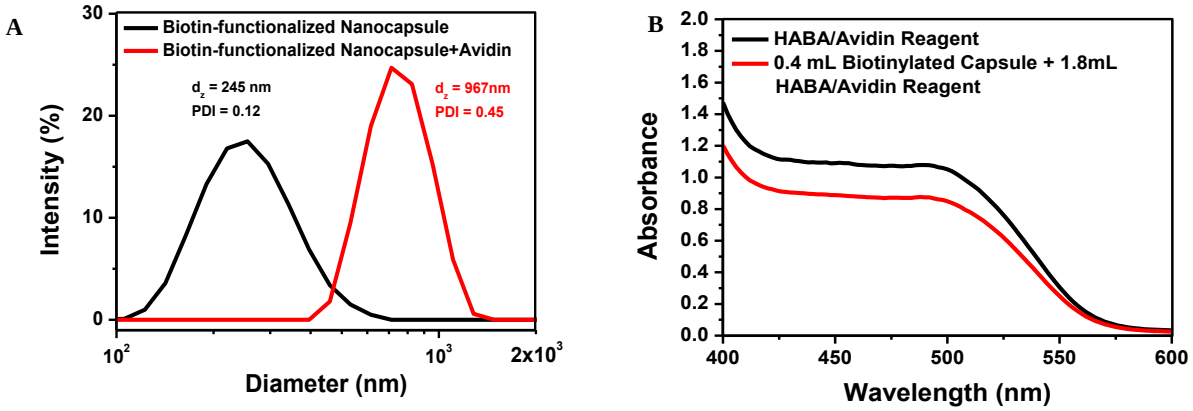

Figure 4.12. (A) Size distribution of biotin-functionalized glyconanocapsules in water before and after conjugation to avidin; (B) UV-absorption spectra of biotinylated and non–biotinylated nanocapsule. HABA test results were calculated using absorbances measured at 500nm.

4.4.3 Functionalization of glyconanocapsule using Fluorescence probes

Fluorescence imaging is a common and practical technique for investigating and tracking of the delivery system *in vitro* and *in vivo*. Herein, a methodology for fluorescence labeling was explored to generate glyco-nanocapsules suitable for *in vitro* or *in vivo* imaging.

Fluorophores were attached to the polymer shell in the course of nanocapsules preparation by incorporating an amino-functionalized fluorescein (Fc) tag (2 equivalent per polymer chain) in the initial aqueous solution before the solvent shifting procedure (24 eq. of IPDI). The addition of Fc had no impact on the nanoprecipitation and cross-linking processes. Fc-labeled nanocapsules with a z-average diameter of 210 nm (PDI = 0.07) were generated. The covalent attachment of Fc tags to the polymer shell during the nanoprecipitation process was confirmed by a characteristic fluorescence emission at 518 nm (**Figure 4.13**).

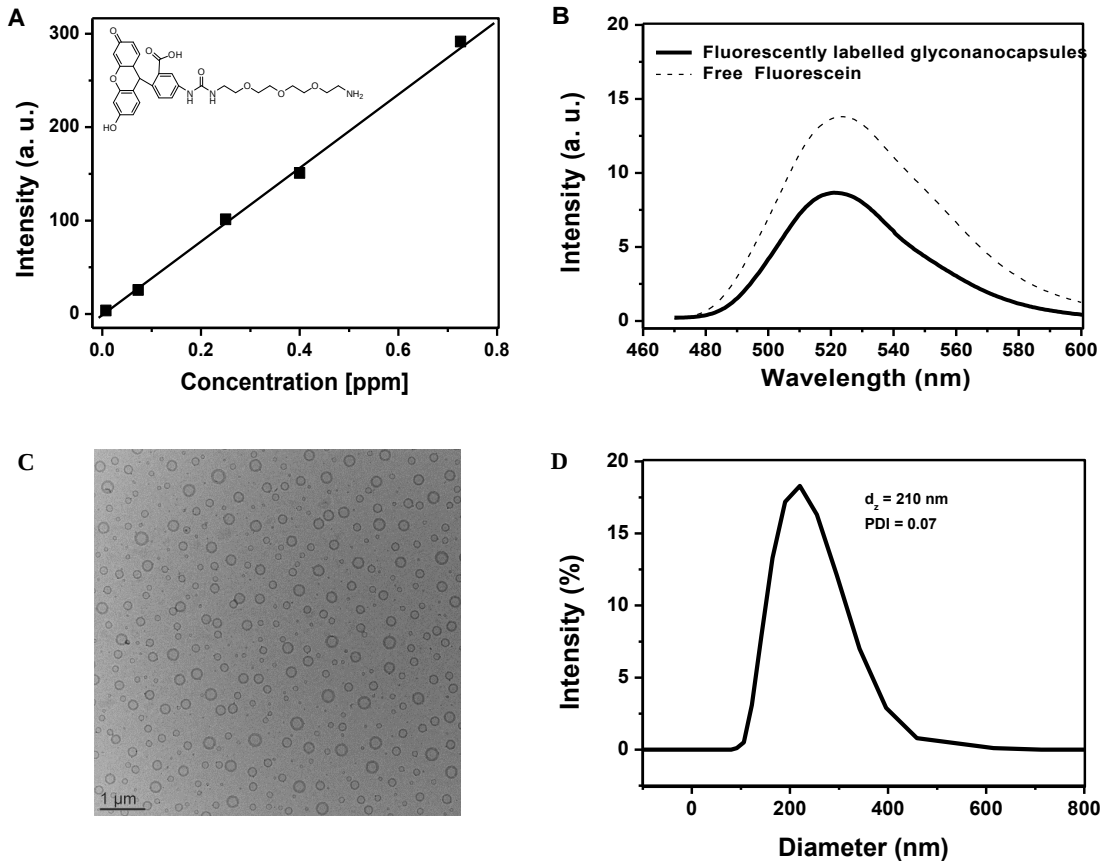

Figure 4.13. (A) Calibration curve of amino-functionalized fluorescein (Fc) in water. (B) Fluorescence emission spectra of fluorescein-labelled glyconanocapsules (λ_{ex}=450 nm). (C) TEM picture of fluorescein-labelled glyconanocapsules. (D) Size distribution of Fc-functionalized glyconanocapsules in water.

4.4.4 Encapsulation of hydrophobic probes within the core of the nanocapsules

To prepare dye-loaded nanocapsules, hydrophobic probes (e.g. pyrene) were directly added to the organic solution (HD with 2.5 % pyrene inside) prior to the nanoprecipitation procedure (24 eq. IPDI). The encapsulation of pyrene was assessed by the fluorescence emission spectrum of the resulting dispersion. The spectrum showed an ensemble of monomeric peaks (between 375 nm and 410 nm) and an additional broad unstructured band (from 425 to 550 nm) due to excited-stat-dimer (excimer) emission, which reflects the spatial proximity of the fluorophores in the nanocapsule cavity. (**Figure 4.14**)

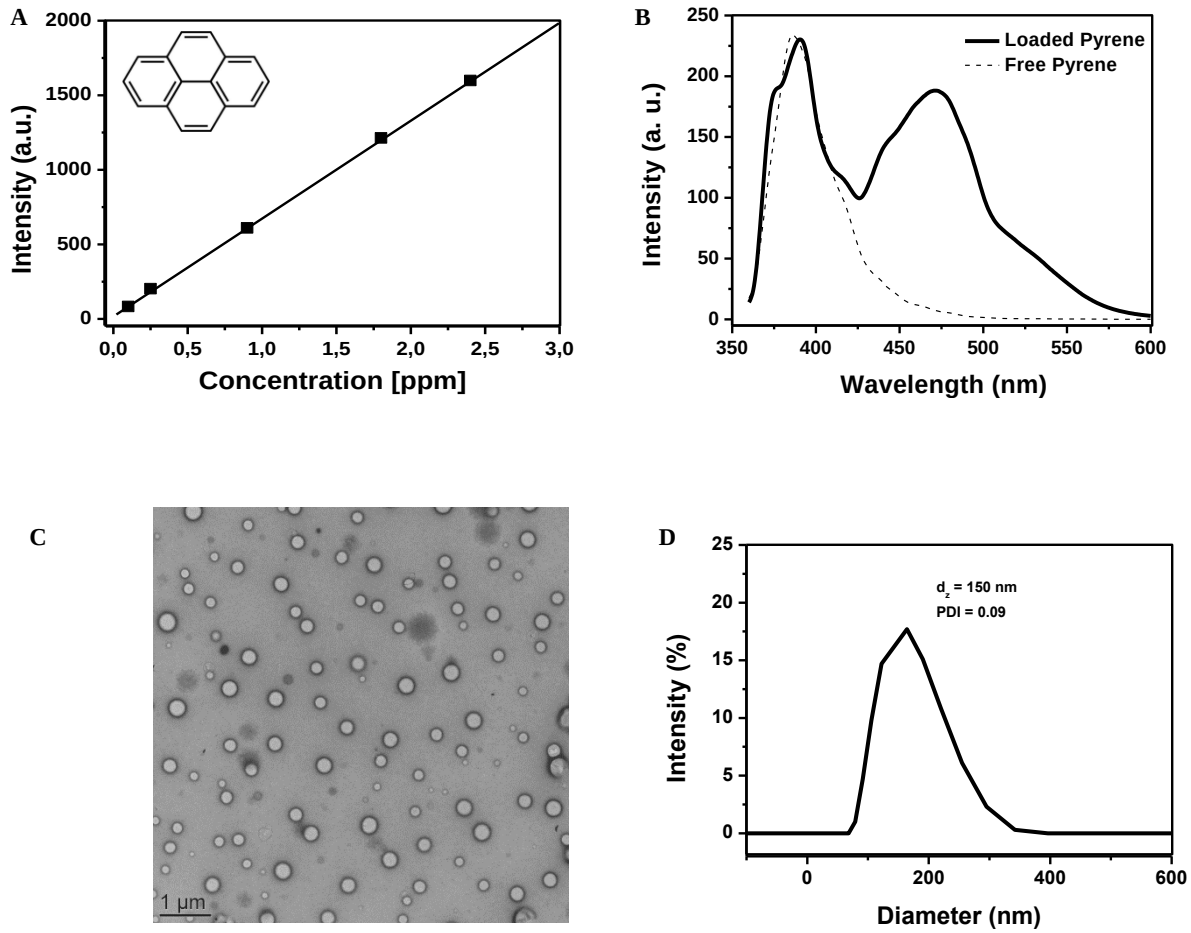

Figure 4.14. (A) Calibration curve of pyrene in hexadecane (λ_{ex} = 335 nm). (B) Fluorescence emission spectra of Pyrene-loading glyconanocapsules. The straight line shows the loaded pyrene glyconanocapsules with concentration at 0.32 ppm, the dash line corresponds to the reference (free pyrene at same concentration in hexadecane). The presence of a clear excimer peak (from 460 nm to 550 nm) for the pyrene-loaded sample confirms the hydrophobic environnement of pyrene molecules embedded in HD oil. (C) TEM picture of pyrene-loaded glyconanocapsules. (D) Size distribution of pyrene-loaded glyconanocapsules in water.

4.4.5 Multi-functionalization of glyconanocapsule using one-pot strategy

One pot procedure allowing for the preparation of well-defined nanocapsules and concomitant surface functionalization and loading of actives within the liquid core was then investigated. As a proof of concept, the preparation of biotinylated nanocapsules loaded with pyrene was explored. Practically, amino-functionalized biotin (2 equivalents per polymer chain) was dissolved with glycopolymer in water, and pyrene (2.5 % in HD) was added in the organic solution to perform the one-pot

nanoprecipitation (24 eq. of IPDI). The encapsulation of pyrene was assessed by the fluorescence emission spectrum exhibiting characteristic bands of loaded pyrene (**Figure 4.15**), whereas the formation of large aggregates (635 nm) upon addition of tetravalent avidin (0.125 eq. per chain) to resulting nanocapsules (D_z = 287 nm, PDI = 0.09) confirmed the incorporation of biotin moieties on the shell.

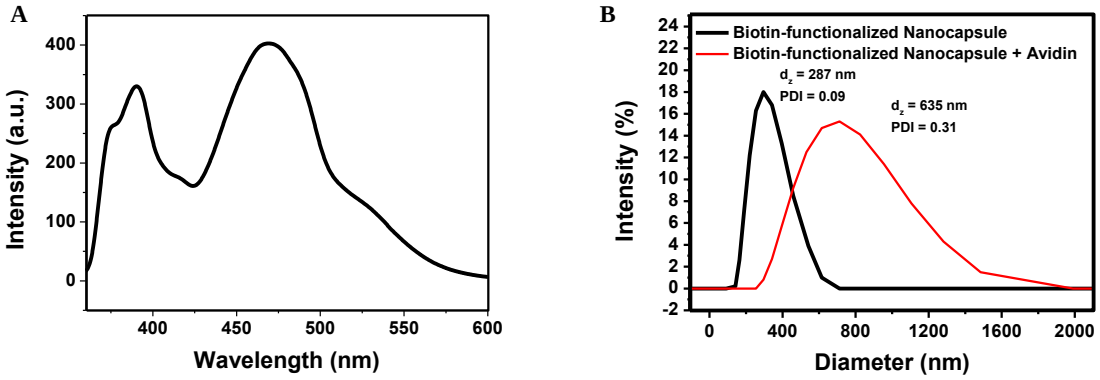

Figure 4.15. (A) Fluorescence emission spectra of pyrene-loading glyconanocapsules. (B) Size distribution of biotin-functionalized glyconanocapsules in water before and after conjugation to avidin.

4.4.6 Fabrication of NP coated glyconanocapsules

Besides the grafting of functions on the surface of nanocapsules and loading of hydrophobic actives within the core, the incorporation of metal nanoparticles could be of interest for biomedical application (imaging, therapy……). Preliminary experiments were carried out with commercially available dodecanethiol-functionalized gold nanoparticles (3~5 nm, AuNP) dispersed in the HD (2 wt%) and then in acetone. Owing to their long alkyl grafts, the AuNPs were expected to be loaded within HD core during the nanoprecipitation process. This procedure afforded the incorporation of AuNP within the nanocapsules but contrary to our assumption, the AuNP were finally located in the shell of the nanocapsules and not inside the nanocapsules (**Figure 4.16**). Again, the addition of nanoparticles had very limited impact on the colloidal properties of the nanocapsules. Using the same approach, nanocapsules with dodecanethiol-functionalized iron oxide nanoparticles (5 nm) within the shell were straightforwardly obtained (**Figure 4.17**).

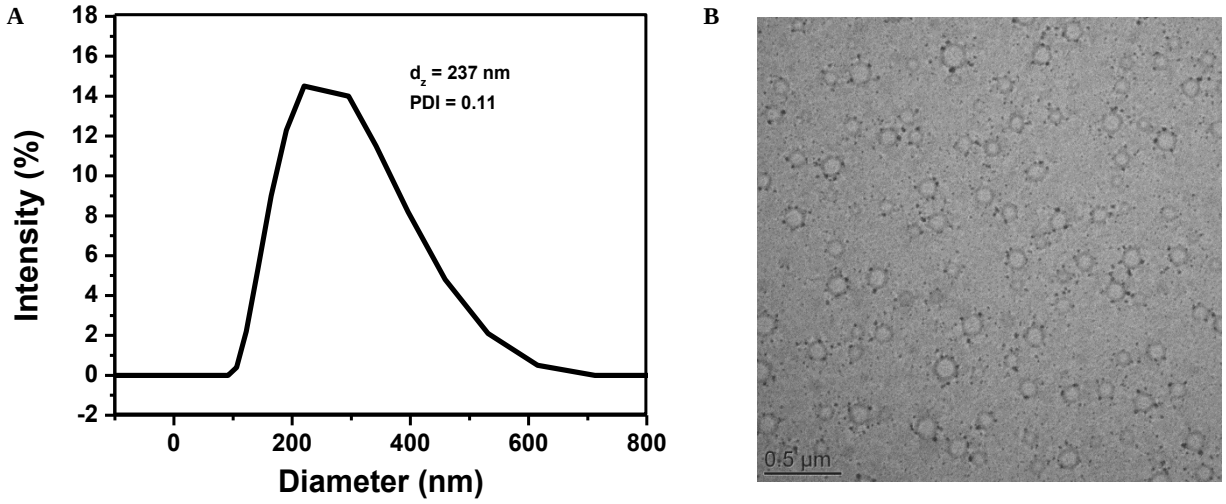

Figure 4.16. (A) DLS and (B) TEM picture of AuNP-coated glyconanocapsules obtained using a one-pot procedure .

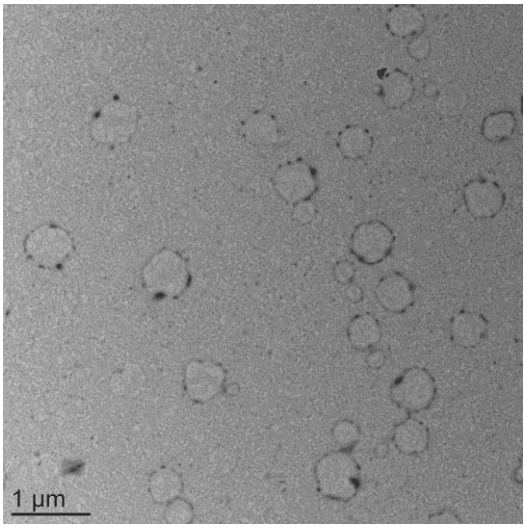

Figure 4.17. TEM picture of iron oxide NP-coated glyconanocapsules obtained using a one-pot procedure.

4.5 Investigation of the scope of the approach

4.5.1 Generation of PEMM based nanocapsules through nanoprecipitation

For emphasizing the general applicability of this method, we finally explored the preparation of nanocapsules from a different oil, miglyol 812 (more environment-friendly and biocompatible), and another synthetic glycopolymer (poly

(N-[2-(α-D-mannopyranosyloxy)ethyl] methacrylamide), PEMM) which presents a much shorter alkyl spacer between the chain backbone and the mannoside (and thus a less pronounced amphiphilic character). As for PHMM based nanocapsules, we first established the phase diagrams for miglyol/water/acetone and PEMM/water/acetone ternary systems. By overlapping the two diagrams, we found out that PEMM-based nanocapsules could possibly be built with mass fraction of acetone around 0.46 and a mass fraction of miglyol equal to $5 \cdot 10^{-4}$. In analogy with the PHMM/water/acetone/HD system, well-defined miglyol-filled glyconanocapsules were generated (**Figure 4.18**), but a smaller diameter and lower polydispersity index (D_z = 130 nm, PDI = 0.04) were observed.

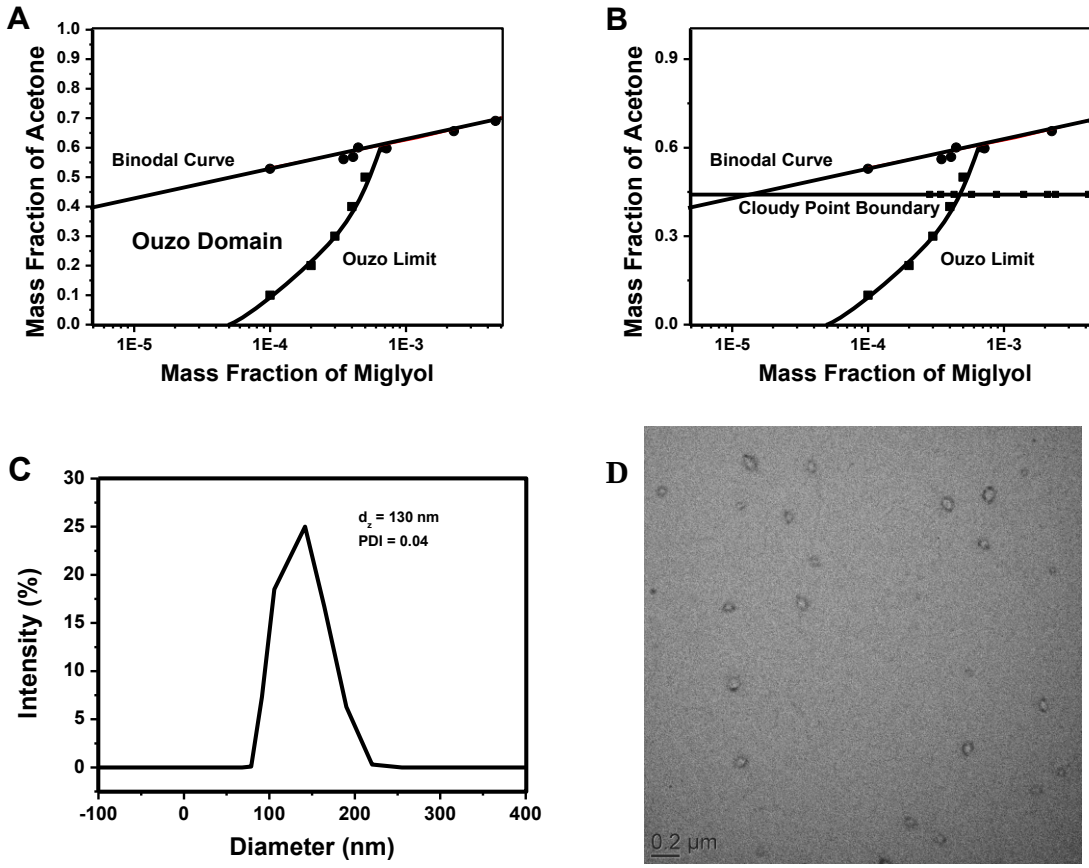

Figure 4.18. A) Phase diagrams of miglyol/acetone/water. (B) Overlapped phase diagrams of PEMM and miglyol/acetone/water. (C) Size distribution of IPDI-cross-linked PEMM based nanocapsules in water (D) TEM picture of the resulting glyconanocapsules.

4.5.2 Generation of P(HMM-*co*-PGMA) based nanocapsules through nanoprecipitation

As epoxy pendent groups are attractive for post-nanoprecipitation modification of the nanocapsules (with amino or thiol functionalized compounds for instance), we further attempted to build epoxy-functionalized glyconanocapsules from P(HMM-*co*-PGMA) copolymer having an homogeneous distribution of epoxy groups along the chains (to avoid the formation of micelles of copolymer in aqueous conditions). A new copolymer, P(HMM_{206}-*co*-GMA_{17}) was then constructed using the semi-batch process described in Chapter 2.

Table 4.2: Glycopolymer obtained by RAFT polymerization

Polymer	$M_{n\ th}$ [a] (kg.mol^{-1})	$M_{n\ NMR}$ [b] (kg.mol^{-1})	M_w [c] (kg.mol^{-1})	$Đ$ [d]	D_h [e] (nm)
P (HMM_{206}-*co*-GMA_{17})	**74.0**	**77.1**	**42.5**	**1.10**	**13**

[a)] calculated from monomer conversion; [b)] determined from relative integration of the aromatic chain end group and polymer backbone peaks; [c)] determined of acetylated polymer from SEC with RI/light scattering detection in THF solution using PS calibration; [d)] $Đ$ determined of acetylated polymer from SEC analysis in THF solution using PS calibration; [e)] determined from DLS analysis in pure water.

4.5.3 Determination of phase diagram

The cloudy point boundary for this glyco-copolymer in water (solvent)/acetone (nonsolvent) mixtures was first determined (see **Figures 4.19** for the establishment of phase diagrams) as previously described. Interestingly, the incorporation of around 10% mol of GMA units within the glycopolymer chains leads to a significant shift of the cloud point boundary to lower fraction of acetone (from 0.65 for PHMM to 0.58 for copolymer). By overlapping the two phase diagrams (See Scheme 4.3), one can immediately see the importance of this shift that allows for widening the tiny domain in which miglyol-filled epoxy-functionalized glyconanocapsules can be obtained.

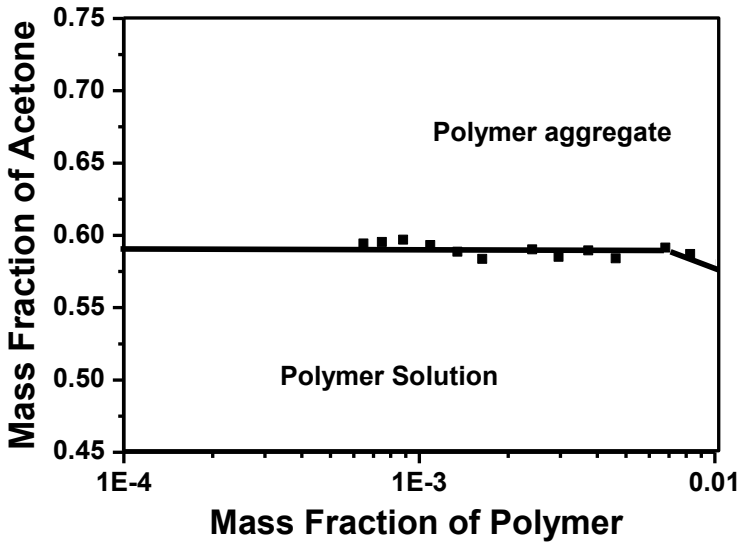

Figure 4.19. (A) Phase diagram of copolymer in water/acetone mixtures. The content of water is deduced from the two other weight fractions. (B) Phase diagram of Miglyol shifting in acetone/water mixture, showing the binary curve and the Ouzo limit.

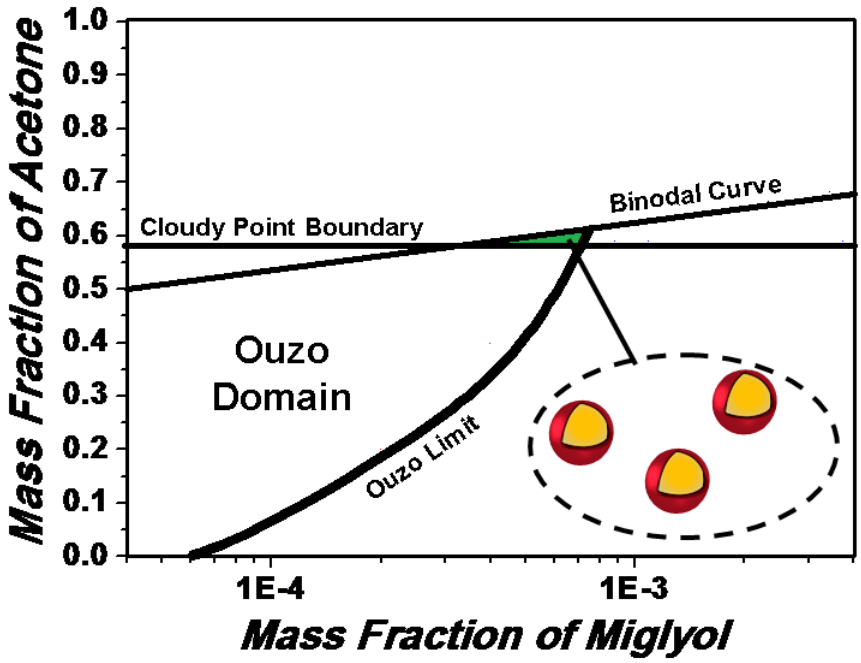

Scheme 4.3. Overlapped phase diagrams of Copolymer and Miglyol 812 in acetone/water mixtures.

4.5.4 Preparation of glyconanocapsules through nanoprecipitation

We first considered cystamine as a potential cross-linking agent in order to maintain the morphology of the objects without inducing any toxicity and at the meantime, to confer a degradable character of the nanocapsules (through reduction of the disulfide bond by glutathione or DTT). Unfortunately, under conditions of cross-linking ([cystamine]/[epoxy]=9/1, from 25 to 35°C), which preserve the stability of the emulsion, disparate results were observed, and efficient cross-linking as shown in Figure 4.20 could not be obtained in a reproducible manner. As a consequence, this route was finally given up and IPDI was further used as a cross-linking agent.

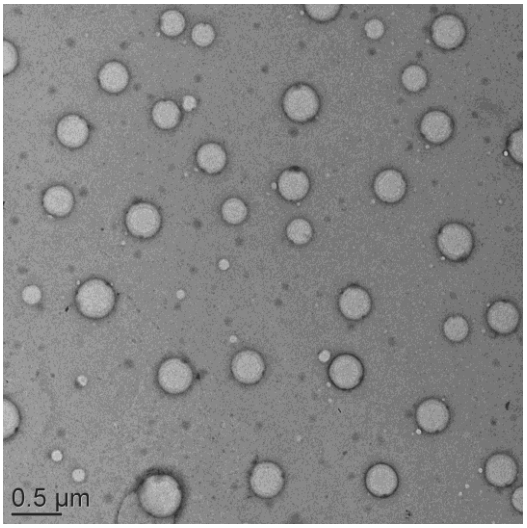

Figure 4.20. TEM pictures of glyconanocapsules cross-linked 9 equivalent cystamine.

In contrast to the PHMM/HD system, efficient cross-linking of the nanocapsules required the addition of 48 equivalents of IPDI. This trend may be due to the need to work at very low concentrations of polymer (0.1 wt% for PHMM and 0.025 wt% for copolymer) and/or due to the presence of more impurities in miglyol. As confirmed by TEM analysis (**Figure 4.21**), mechanically stable spherical nanocapsules (D_z = 117 nm, PDI = 0.03) were generated upon addition of 48 equivalents of IPDI and no leakage of miglyol was observed during the TEM procedure.

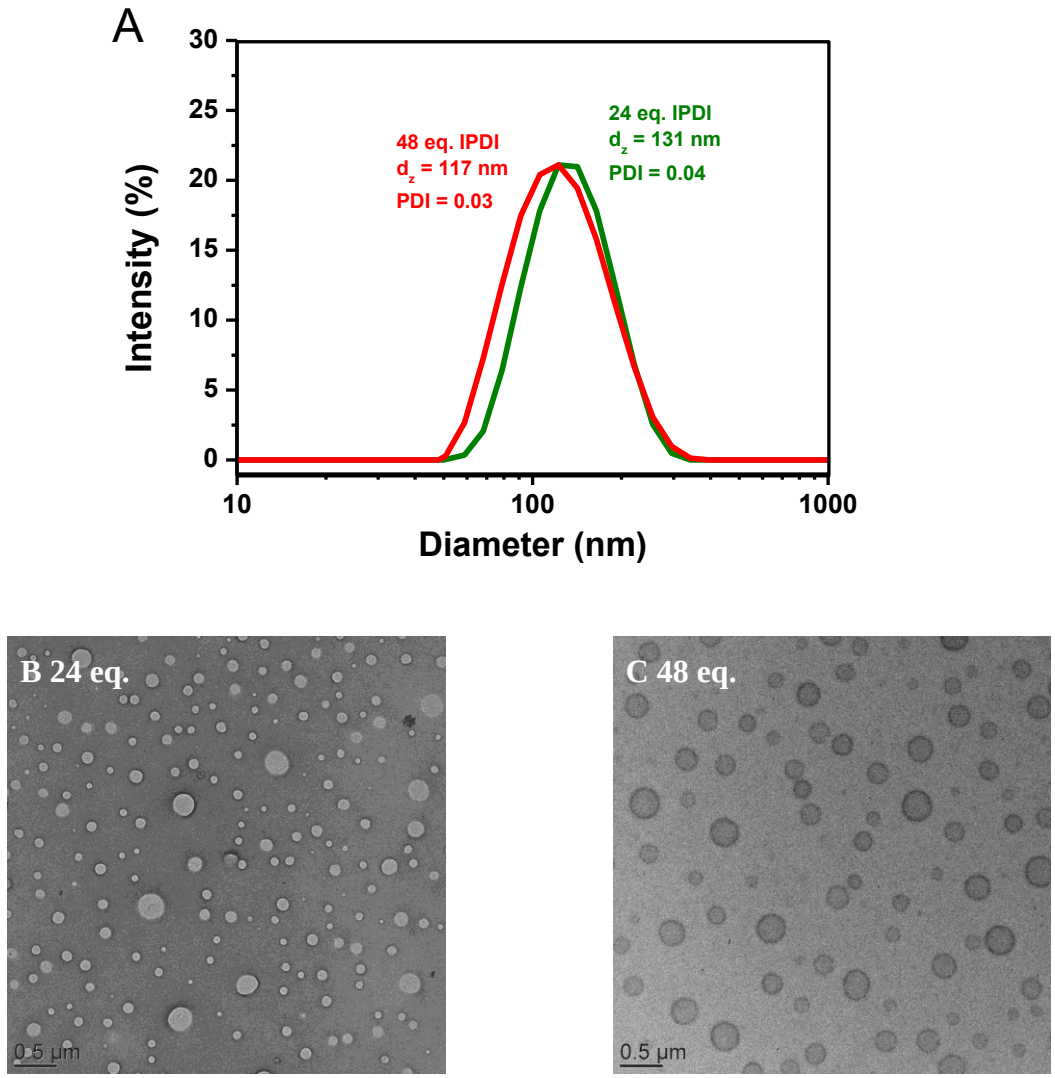

Figure 4.21. (A) DLS of glyconanocapsules cross-linked with 24 (green) and 48 (red) equivalents of IPDI (per polymer chain). (B) and (C) Selected TEM pictures of glyconanocapsules cross-linked with 24 and 48 eq. of IPDI.

4.5.5 Post-nanoprecipitation modification of nanocapsules

After elaboration of the nanocapsules through nanoprecipitation and cross-linking of the polymeric shell, the presence of epoxy moieties of the surface of the nanocapsules was exploited to introduce new functional groups. The avidin-biotin system was investigated as a model of protein-ligand interaction with the broad application like tumor pretargeting clinical diagnostics and so on. Biotin ethylenediamine (1 eq. per polymer chain) was thus added into a mixture of capsules

and the solution was heated overnight at 40°C. The surface decoration does not impact the dimensions of the nano-objects (D_z = 111 nm). After dialysis, the biotinylated nanocapsules were mixed with an aqueous solution of avidin (0.25 eq per chain), resulting in the formation of very large aggregation of nanocapsules owing to strong interaction between avidin and grafted biotin (**Figure 4.22A**). Accordingly, the characteristic UV based of pre-established HABA/Avidin complexes at 500 nm in water (see Figure 4.22B) rapidly dropped when modified capsules was added thanks to the strong affinity of avidin for biotin moieties.

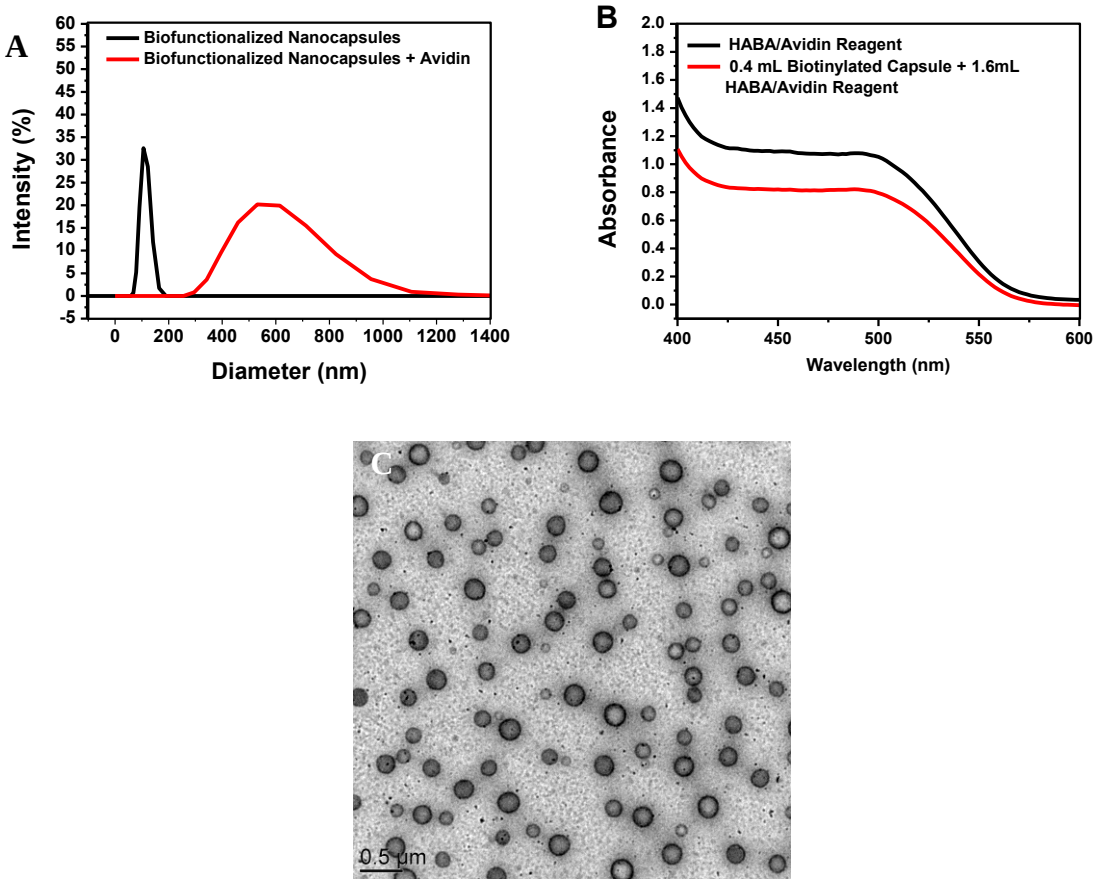

Figure 4.22. (A) Size distribution of biotinylated nanocapsules in water before and after conjugation to avidin. (B) UV-absorption spectra of biotinylated and non–biotinylated nanocapsules. HABA test results were calculated using absorbances measured at 500nm. (C) TEM picture of the biotin-functionalized glyconanocapsules.

Fluorophores were also attached to the polymer shell through post-nanoprecipitation modification by incorporating Alexa Fluor® 555 Cadaverine (1 eq. per chain) into the

solution of capsules (overnight reaction at 40°C). Alexa-labeled nanocapsules with D_h of 123 nm (PDI = 0.27) were generated. After dialysis, Alexa probe functionalized nanocapsules exhibited a characteristic fluorescence emission at 566 nm (Figure 4.23).

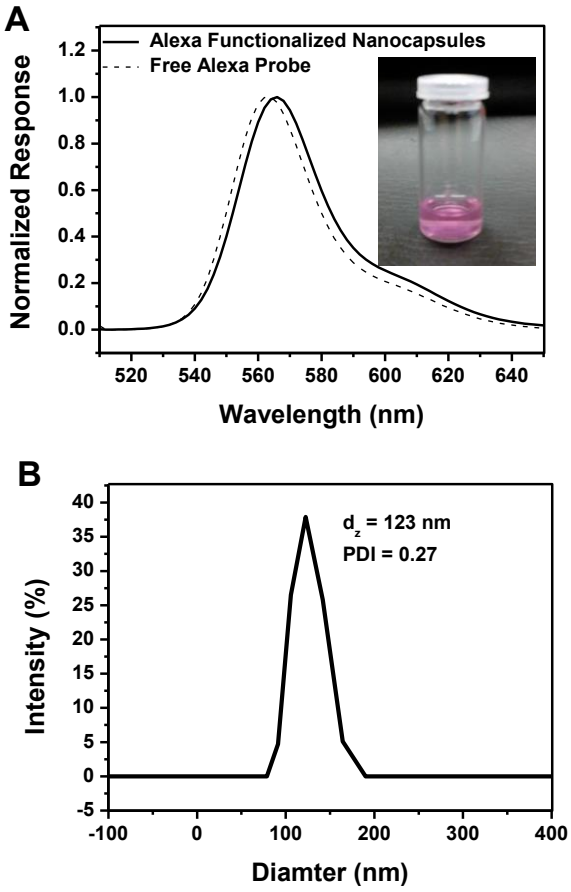

Figure 4.23. (A) Fluorescence emission spectra of Alexa-functionalized glyconanocapsules. (B) Size distribution of Alexa-functionalized nanocapsules.

Finally, we also attempted to covalently anchor magnetic cobalt nanoparticles at the surface of the nanocapsules shell through epoxy-amine reactions. Epoxy-functionalized glyconanocapsules were thus reacted overnight at 40 °C with commercially available amino functionalized magnetic nanoparticles (Turbobeads®, D_z = 30 nm) dispersed in water. Incorporation of magnetic nanoparticles was highlighted by TEM microscopy and the modified nanocapsules responded to the presence of a magnet. The size of the resulting objects was almost the same as epoxy-functionalized nanocapsules even though the size distribution slightly

broadened after modification with magnetic nanoparticles (**Figure 4.24**).

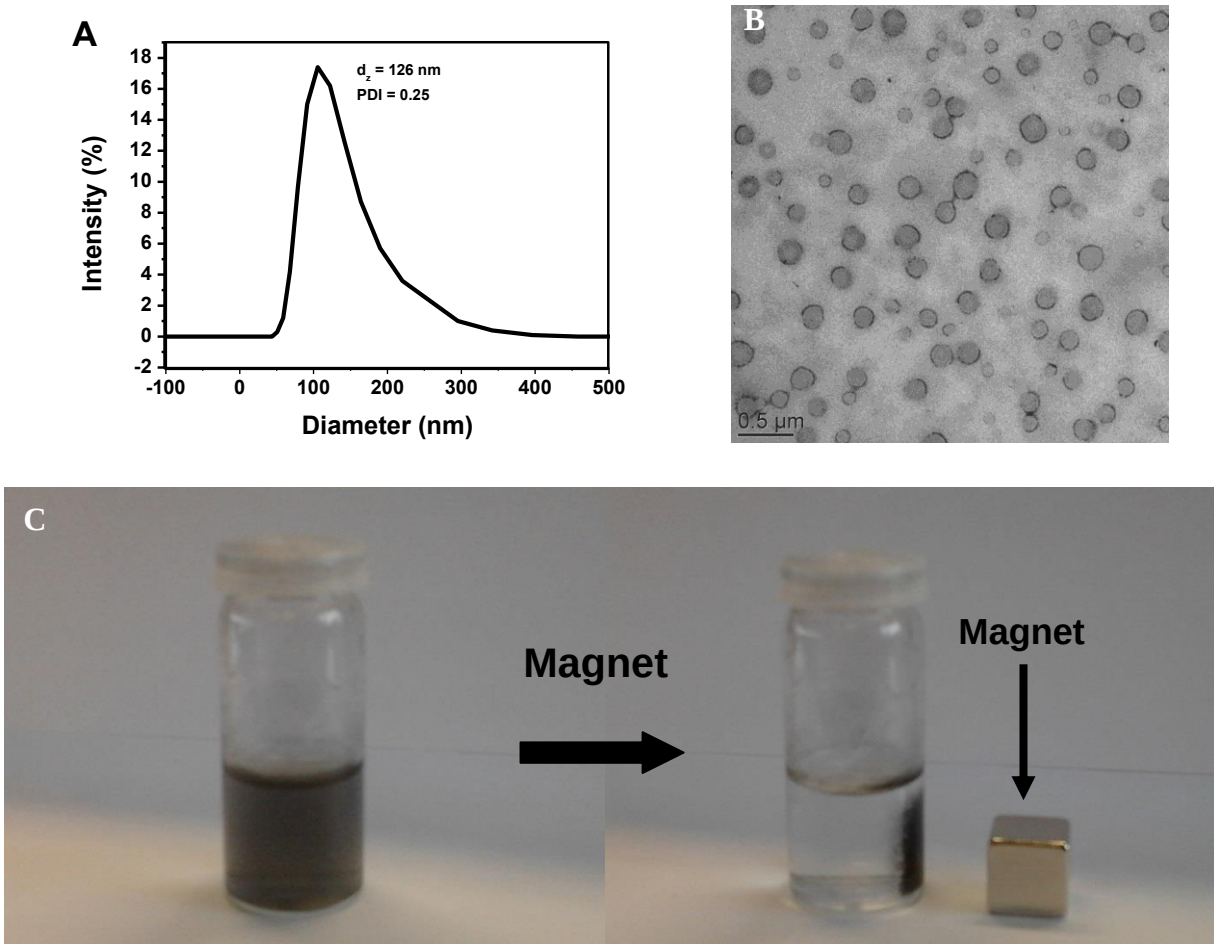

Figure 4.24. (A) Size distribution of magnetic NP-grafted nanocapsules. (B) TEM picture of the magnetic NP-grafted glyconanocapsules. (C) Behavior of magnetic NP-grafted glyconanocapsules in the presence of a magnet

4.5.6 Specific interaction with *E. coli* AIEC LF82

In the previous chapter, we have shown that HM-based glycopolymer chains are capable to interact with FimH adhesins and aggregate *E. Coli* bacteria. In this context, we decided to evaluate the capability of P(HMM-co-GMA) glyconanocapsules to capture *E. Coli* AIEC LF82 bacteria in aqueous solution and form large bacteria/capsules aggregates. To study nanocapsules-bacteria interactions, green fluorescent GFP-marked AIEC LF82 strains (emission at ~ 520 nm) were cultured overnight to produce a solution of bacteria (OD_{600nm} = 0.6). An aqueous solution of glyconanocapsules was concentrated to 33 and 66 µM (concentration of

glyco-copolymers in aqueous solution). As a reference, we first looked at the solution of green fluorescent bacteria. As can be seen in **Figure 4.25A**, the bacteria were proven to freely swim in the solution and no aggregation was observed after three hours. Important changes were observed when bacteria were mixed with glyconanocapsules for 3h. In the presence of 33 µM of glyconanocapsules, numerous small-size aggregates were visualized after 3h of exposure (**Figure 4.25**). Increase of nanocapsule content to 66 µM led to the formation of very large clusters of nanocapsules and bacteria (**Figure 4.25 C)**.

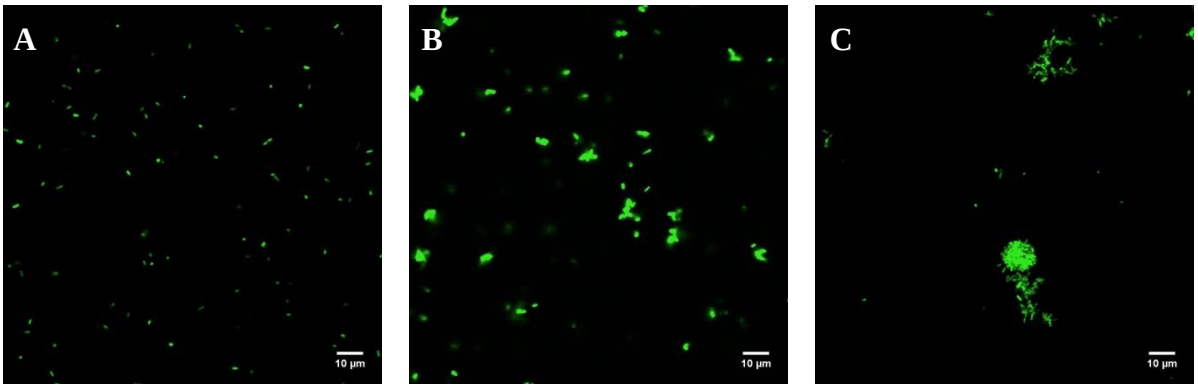

Figure 4.25. Confocal fluorescence microscopy pictures of (A) *E. Coli* AIEC LF82 bacteria. (B) Glyconanocapsules (33 µM)-bacteria aggregates. (C) Glyconanocapsules (66 µM)-bacteria aggregates.

The kinetics of clusters formation was also investigated. The aggregation behavior was observed after 30 min, 1h, 2h and 3h for the solution of GFP-marked *E. Coli* (OD_{600nm} = 0.6) exposed to glyconanocapsules (66 µM). As seen in **Figure 4.26 A**, nanocapsules/bacteria aggregates are rapidly formed after addition of the nano-objects. After 30 min of co-incubation, small aggregates (with size lower than 10 µm) are detected. Increasing the time of exposure leads to a further growth of the clusters. After 3h of exposure, very large aggregates with size up 40 µm are indeed visualized (**Figure 4.26D**).

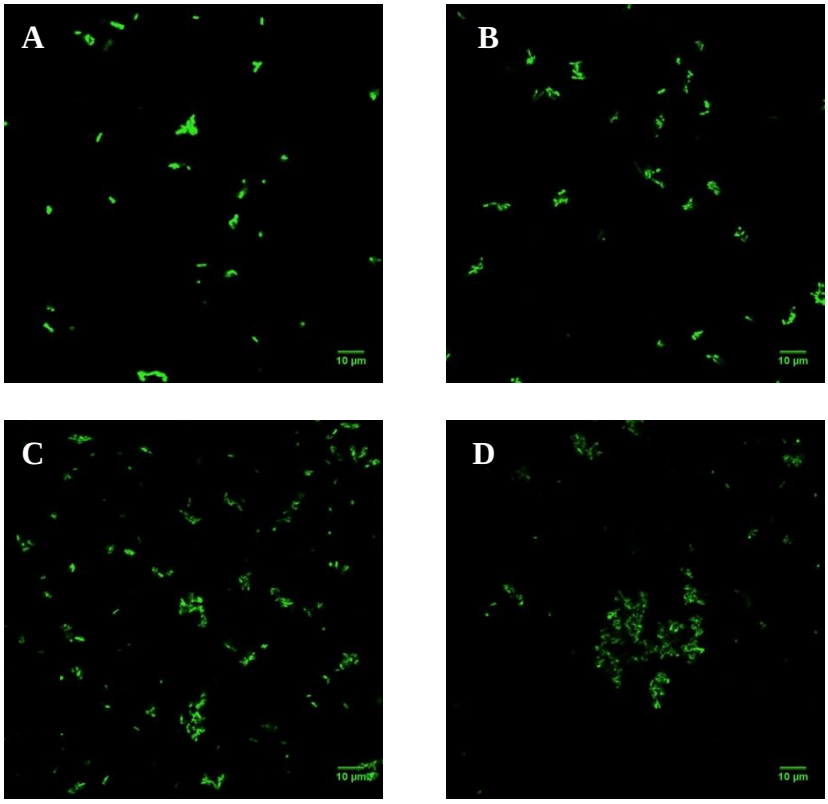

Figure 4.26. Kinetic study of aggregation between glyconanocapsules and bacteria (A) 30 min, (B) 1h, (C) 2h and (D) 3h.

4.6 Conclusions

In this chapter, we have demonstrated that the exploitation of phase diagrams of different solutes solvent-shifted by the ouzo effect enables the generation of well-defined nanocapsules by an extremely fast and straightforward method. The nanocapsules from PHMM can be shell-cross-linked, shell-functionalized, and loaded with actives at the same time in a one-pot procedure. This simplified route to functional nanocapsules is general and can be readily transposed to other systems to design new materials of practical applicability in different fields in which colloids are used. For instance, the generation of glyconanocapsules from P(HMM-co-GMA) leads to a convenient platform for post-nanoprecipitation modification, resulting in multi-functional nanocapsules. The glyconanocapsules exhibits the strong affinity towards *E coli* bacteria leading to the formation of huge bacteria/capsules aggregates.

4.7 References

1. Ganachaud, F. and Katz, J. L. *Chemphyschem*, **2005**, *6*, 209-216.

2. Aubry, J.; Ganachaud, F.; Addad, J. P. C. and Cabane, B. *Langmuir*, **2009**, *25*, 1970-1979.

Chapter 5

Experimental Part

Chapter 5 Experimental Part

5.1 Material preparation and general characterization methods

Materials

4-Cyano-4-(phenylcarbonothioylthio) pentanoic acid (CPADB), 4,4'-Azobis (4-cyanovaleric acid) (ACPA), isophorone diisocyanate (IPDI), hexadecane, water (HPLC), deuterium oxide (D_2O), avidin from egg white, and pyrene were purchased from Sigma Aldrich, and used without further purification. Dodecanethiol-functionalized gold nanoparticles (Sigma-Aldrich, particle size 3-5 nm, 2% w/v in toluene) were dispersed in hexadecane and toluene was removed under vacuum. Iron oxide (II, III) magnetic nanoparticles (Sigma Aldrich, particle size 10nm, 5mg/mL in Toluene) were dispersed in hexadecane and toluene was removed under vacuum. Amino-functionalized fluorescein (Fc) was obtained from protonated Fluorescein-PEG3-Amine TFA (Broadpharm) by adding 1.5 eq. of triethylamine (Sigma Aldrich) in water for 2 days. Amino-functionalized biotin was obtained from protonated biotin ethylenediamine hydrobromide (Sigma Aldrich) by adding 1.5 eq. of triethylamine (Sigma Aldrich). Miglyol 812 was purchased from SASOL (Germany). Acetone, methanol, DMSO and petroleum ether were purchased from Carlo Erba. Dialysis membranes (Mw cut-off 1000 Da) were purchased from Spectrum Laboratories, Inc. Other reactants were purchased from Sigma-Aldrich. 7-bromoheptan-1-ol (**1**) was prepared as described in the litterature.[1] Human intestinal epithelial cell line T84 were purchased from American Type Culture Collection (ATCC, CCL-248) and maintained in the culture medium recommended by ATCC in an atmosphere containing 5% of CO_2 at 37°C.

Intestinal epithelial cells

Human intestinal epithelial cell line T84 and human cervical adenocarcinoma cell line HeLa were purchased from American Type Culture Collection (ATCC, CCL-248; ATCC, CCL-2) and maintained in the culture medium recommended by ATCC in an atmosphere containing 5% of CO_2 at 37°C. Human colorectal adenocarcinoma cell line Caco-2 was obtained from the Cell Culture Collection of the Department of

Structural and Functional Glycobiology, Faculty of Biology, University of Science and Technology of Lille 1. Cells were cultured in EMEM medium supplemented with 20% fetal bovine serum (FBS) and penicillin/streptomycin.

Construction of fluorescent strain UTI89 nadB::cat-kat

The strain LF82 nadB::cat-kat was constructed with the recombination system reported by Datsenko and Wanner[2] except that the linear fragments used were long homologous recombinant sequences amplified from pDONR221-nadB-catkat derived from pDONR221-nadB[3]. Briefly, the recombinant plasmid pDONR221-nadB-cat was constructed first by amplification of the chloramphenical gene from pKD3[2] using the primers EcatF GCAAT**GAATTC**TAGAGAATAGGAACTTCGGAAT and EBcatR (ATTGC**GAATTC*GGATCC***AAGTATAGGAACTTCGGCGCGCCTA), enzymatic digestion by *EcoRI* and ligation into pDONR221-nadB. The katushka gene *kat* were amplified with primers KatF, containing the BamHI site and em7 promoter sequences (CGC***GGATCC***TGTTGACAATTAATCATCGGCATAGTATATCGGCATAGTATAATA CGACAAGGTGAGGAACTAAACCATGGTGGGTGAGGATAGCGTGCTGA) and KatR (CGC***G GATCC***GCATTAGCTGTGCCCCAGTTT) from pTurboFP-635C (Evrogen). The fragments and the pDONR221-nadB-cat were digested using *BamH1*. Upon ligation, the plasmid pDONR221-nadB-cat-kat was obtained. The plasmid was transformed into *E. coli* LF82 and clones containing the plasmid selected on kanamycin/chloramphenicol LB-agar during an overnight incubation at 37 degrees. Incubation during another four days at room temperature showed pinki colonies, confirming the expression of the katushka near-infra red fluoresent protein.

Enzyme-linked lectinosorbent assay

Enzyme-linked lectinosorbent assay (ELLSA) was performed using microplate reader BioTek-ELx800. RNAse B proteins (Sigma, R-7884) were used as a substrate of oligomannose glycans. For detection of FimH binding towards nature glycans were used rabbit anti-FimH polyclonal antibodies (Eurogentec) and goat anti-rabbit HRP-labeled secondary antibody (Enzo Life Sciences).

E. coli strain LF82 isolated from an ileal biopsy of a CD patient was used as AIEC reference strain.[4] Bacteria were grown overnight at 37 °C in Luria Bertani (LB) broth. A bacterial suspension was prepared in phosphate buffer saline (PBS) for in vitro adhesion assays or ex vivo assays on colonic mucosa from CEABAC10 mice.

Methods

Nuclear magnetic resonance (NMR) spectra were recorded on a Bruker DRX 250 spectrometer (250 MHz) in $CDCl_3$ (for monomer precursors and multifunctional RAFT agents) or D_2O solutions (glycomonomers, glycopolymers) at 298K and referenced to residual solvent peaks. Peak multiplicity is reported as: singlet (s), doublet (d), triplet (t), quartet (q), multiplet (m), and broad (br).

ESI-MS spectra (m/z) of monomer precursors, glycomonomers and RAFT agents were measured on a Thermo-FinniganMat 95XL. High resolution mass spectra HRMS were obtained by Electrospray Ionisation (ESI) on a Micromass-Waters Q-TOF Ultima Global.

Aqueous size exclusion chromatography (SEC) analysis of glycopolymers from HMM was performed in a 0.1 M $NaNO_3$ aqueous solution (pH adjusted to 7 by addition of NaOH) at a flow rate of 0.5 mL/min at 35°C on a Waters 510 apparatus equipped with a refractive-index detector Waters 410 and a laser light scattering (Wyatt Technology) dual detection and fitted with Waters Ultrahydrogel columns. For light scattering measurements, dn/dc coefficients were calculated with a laser source operating at 633 nm. dn/dc values were determined from the slopes of curves plotting the variation of the refractive index as a function of the concentration (dn/dc = 0.172). Acetylated glycopolymers were analyzed with a SEC apparatus running in THF at 25°C (flow rate: 1 $mL.min^{-1}$) and equipped with a Viscotek VE 1121 automatic injector, three columns (Waters HR2, HR1 and HR0.5), and a differential refractive index detector (Viscotek VE3580). The average molar masses of the glycopolymers were derived from a calibration curve based on a series of PS standards.

Dynamic light scattering. Particle size measurements were carried out by dynamic

light scattering (DLS) using a Malvern Instruments Zetasizer nano series instrument and using the cumulant method. The aqueous solutions were prepared at 1mg/mL, at least five measurements were made for each sample. Equilibration times of 10 minutes were respected before each measurement.

The light scattering study on FimH/L188 interactions was performed using an ALV/CGS-8FS/N069 apparatus (from ALV) equipped with an ALV/LSE-5004 multiple τ digital correlator with a 125 ns initial sampling time (from ALV) and a 35 mW red helium-neon linearly polarized laser operating at a wavelength of 632.8 nm (from JDSU). Both suspensions and their resulting mixture were used unfiltered. The studied systems were loaded in 10 mm diameter cylindrical cells, immerged in a toluene bath and thermostated at a temperature of 25.0 ± 0.1 °C prior to measurements. Data were collected at different scattering angles ranging from 14 to 143° by step of 1° for a counting time of typically 60 s using the digital ALV correlator control software. In dynamic light scattering (DLS), the relaxation time distribution was obtained using the Contin analysis of the autocorrelation function ($g^{(2)}$-1). In static light scattering (SLS), the scattering intensity was corrected by the solvent signal and normalized by the toluene signal. The scattering volume change with observation angle was also taken into account.

Additional DLS experiments on Glycopolymer/FimH interaction were performed by a Malvern Instruments Zetasizer nano series instrument using the cumulant method with aqueous solution of glycopolymer and FImH (specific conditions were given in Annex 7) in Hepes buffer at 20 °C. Specifically, FimH aqueous solution (83 μM) were prepared and measured by DLS with protein workspace mode. The glycopolymer aqueous solution was progressively added into FimH solution, DLS data was recorded after each addition to follow the formation of Glycopolymer/FimH aggregates. At least three measurements were made for each sample. Equilibration times of 5 minutes were respected before each measurement.

AFM Microscopy. In order to perform Atomic Force Microscopy measurements, silicon substrates (approximately 1 x 1 cm^2) were cleaned by ozonolysis treatment.

Samples were prepared by spin-coating (4000 rpm, 30 s) from aqueous solutions (L188 at 15 µM) and dried under vacuum. AFM images were acquired in air at room temperature using a Nanoscope IIIa Multimode (Digital Instruments/VEECO, CA). Intermittent contact imaging (i.e., tapping mode) was performed at a scan rate of 1 Hz. Uncoated silicon probes with a resonant frequency between 280 and 405 kHz, a spring constant 20 and 80 N/m, length of 115-135 µm, width of 30-40 µm and nominal tip radius of curvature less than 10 nm are used. Images were displayed and analyzed using the Nanoscope 6.14R1 software.

Optical rotations were measured on a 343 Perkin Elmer at 20°C in a 1cm cell in the stated solvent; $[\alpha]_D$ values are given in 10^{-1} deg.cm^2.g^{-1} (concentration *c* given as g/100mL).

TEM images were obtained on a Philips CM120 electronic microscope, by observations in transmission at an accelerating voltage of 80 kV. Samples were made by placing a drop of sample (1mg/mL) onto Formvar-coated copper grid. Excess solution was carefully blotted off using filter paper and samples were dried for a few minutes before analysis.

Fluorescent microscopy was performed with fixed slides under a Carl Zeiss AxioImager A1 DIC/fluorescent microscope (Oberkochen, Germany) using 0.4NA 10×, 0.75 NA 40× air, and 1.3 NA 100× oil immersion objectives. Fluorescent images were taken by a Zeiss AxioCam MRmIII cooled digital CCD camera under constant exposure. Fluorescence of katushka was evaluated at red channel (610 nm emission was obtained at 532 nm excitation) and at similar conditions the emission at NIR channel (700 nm) was detected. Zeiss AxioVision and ImageJ software were used for image analysis.

Fluorescence spectroscopy analyses were performed using a JASCO FP-8000 series spectrofluorometer. For building calibration curves, five different concentrations of fluorophores in water (amino-functionalized fluorescein, from 7.26 10^{-3} to 7.26ppm) or hexadecane (pyrene, from 0.1 to 2.4ppm) were prepared. The fluorescence

intensity for each solution was set at λ_{ex} = 450 and 335 nm, respectively.

5.2 Monomer synthesis (HMM and EMM)

5.2.1 Synthesis of *N*-[7-(α-D-mannopyranosyloxy)heptyl] methacrylamide (HMM)

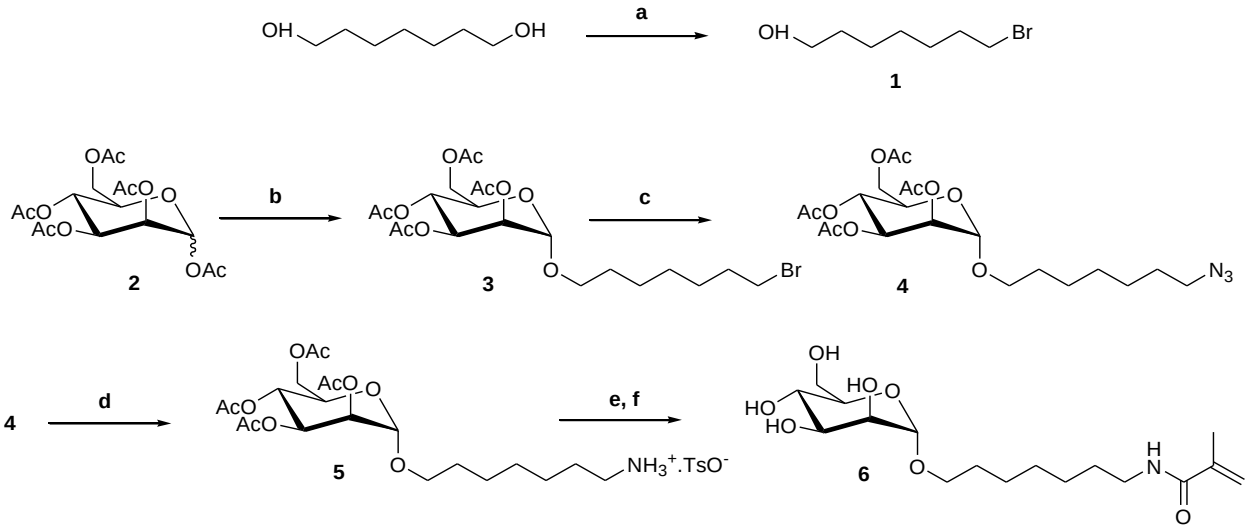

Scheme 5.1: Preparation of HMM. Reagents and conditions: a) HBr, toluene (reflux); b) **1**, $SnCl_4$, CF_3CO_2Ag, CH_2Cl_2; c) NaN_3, DMF; d) H_2, Pd/C, p-TsOH, EtOH; e) methacryloyl chloride, CH_2Cl_2, Et_3N; f) NaOMe, MeOH.

Synthesis of azido-fuctionalized mannoside (4).

$SnCl_4$ (1M in CH_2Cl_2, 154mL, 154mmol) was added dropwise (within 30 min) at room temperature to a solution of 7-bromoheptan-ol (**1**) (15.2g, 77.91mmol), peracetylated D-mannose (**2**) (20g, 51.2mmol) and silver trifluoroacetate (17.0g, 76.8mmol) in freshly distilled dichloromethane (250mL). Disappearance of the starting material was observed within 3h and the mixture became pale pink. Saturated aqueous $NaHCO_3$ (600mL) was added to adjust pH above 8, and the solution was vigorously stirred for 20min. A biphasic system formed upon addition of aqueous $NaHCO_3$ with a white suspension in the aqueous layer. The biphasic solution was diluted with 500mL of water and the aqueous layer was extracted with CH_2Cl_2 (3×300mL). The organic layers were combined, washed successively with saturated aqueous $NaHCO_3$ (150mL), water (3×300mL), brine (2×300mL) and dried over $MgSO_4$. After solvent

removal by evaporation, the crude product (**3,** pale yellow gum) was dissolved in anhydrous DMF (200mL), sodium azide (16.6g, 255mmol) and tetra-n-butyl ammonium iodide (18.9g, 51.2mmol) were added. The mixture was stirred at 70 °C under argon for 24h, cooled to room temperature, filtered and the solid was washed with EtOAc (3×300mL). The filtrate was diluted with EtOAc to reach a total volume of 1L. The organic layer was washed with aq. $NaHCO_3$ (3×500mL), water (3×500mL), brine (500mL) and dried. After concentration, the resulting product (yellow gum) was purified by column chromatography (petroleum ether/ethyl acetate, 7/1, v/v) to afford the corresponding azido-fuctionalized glycoside (**4**)**.** Final yield: 12.6 g (50%) obtained as a colorless gum.

$[\alpha]_D$ = +11 (c= 0.35, Chloroform). ^{1}H NMR (300 MHz, $CDCl_3$) δ 5.32-5.11 (m, 3H, H-2, -3, -4), 4.73 (d, *J* = 1.5 Hz,1H, H-1), 4.20 (dd, *J* = 5.4, 12.3 Hz, 1H, H-6), 4.03 (dd, *J* = 2.4, 12.3 Hz, 1H, H-6'), 3.90 (m, 1H, H-5), 3.68-3.54 (m, 1H, H-OCH*H*CH_2), 3.44-3.33 (m, 1H, OC*H*HCH_2), 3.21 (t, *J* = 6.9 Hz, 2H, N_3C*H*$_2CH_2$), 2.09, 2.04, 1.98, 1.93 (s, 4×3H, 4×C*H*$_3$CO), 1.64-1.46 (m, 4H, C*H*$_2(CH_2)_3$*CH*$_2CH_2N_3$), 1.30 (s, 6H, CH_2(C*H*$_2$)$_3$$(CH_2)_2N_3$);^{13}C NMR ($CDCl_3$) δ 170.1, 170.1, 169.7, 169.9, (O*C*OCH_3), 97.5 (C-1), 69.7 (C-2), 69.0 (C-3), 68.4 (C-5, O*C*$H_2(CH_2)_5$), 66.2 (C-4), 62.5 (C-6), 51.4 (*C*H_2N_3), 29.1, 28.9, 28.7, 26.6, 26.0, (OCH_2(*C*H$_2$)$_5$$CH_2N_3$), 20.9, 20.7, (OCO*C*$H_3$); ESI-MS: m/z calculated for $[C_{21}H_{33}N_3NaO_{10}]^+$, 510.2058, found 510.2051.

Synthesis of HMM (compound 6).

4 (12.6g, 25.8mmol), p-toluenesulfonic acid (5.41g, 28.4mmol) and 10% palladium on activated charcoal (2g) as the catalyst were stirred overnight in ethanol (240mL) at room temperature under 1 atm of hydrogen. The solution was filtered over celite and evaporated to obtain a colorless gum **(5)**. The resulting product was directly engaged in the next step without further purification. **5** was dissolved in a solution of anhydrous CH_2Cl_2 (150mL) containing triethylamine (10.5mL, 75.9mmol). Methacryloyl chloride (3.8mL, 32.9mmol) was added dropwise into the solution in an ice bath. The solution was stirred for 1h at room temperature. After reaction, the solution was washed with water (2×200mL), dried over $MgSO_4$ and the solvent was removed. The acetylated

monomer was finally purified by column chromatography (petroleum ether/ethyl acetate, 3/1, v/v). Yield: 7.4 g (55%) of a colorless gum.

[[α]$_D$ = +10 (c= 0.4, Chloroform). ^{1}H NMR (300 MHz, $CDCl_3$) *δ* 5.89 (s, 1H, NH), 5.65 (s, 1H, CC*H*$_2$), 5.39-5.17 (m, 4H, H-3, CC*H*$_2$, H-4, H-2), 4.78 (d, *J* =1.5 Hz, 1H, H-1), 4.35-4.20 (dd, *J* = 5.1, 12.3 Hz,1H, H-6), 4.16-4.05 (m, 1H, H-6'), 4.02-3.91 (m, 1H, H-5), 3.67 (m, 1H, OC*H*$_2$CH$_2$), 3.50 (m, 1H, OC*H*$_2$CH$_2$), 3.28 (q, *J* =6.3 Hz, 2H, NHC*H*$_2$CH$_2$), 2.15, 2.09, 2.03, 1.98, (s, 4×3H, 4×C*H*$_3$CO), 1.95 (s, 3H, CC*H*$_3$), 1.67-1.46 (m, 4H, C*H*$_2$(CH$_2$)$_3$*CH*$_2$CH$_2$NH), 1.34 (s, 6H, CH$_2$(C*H*$_2$)$_3$(CH$_2$)$_2$NH); ^{13}C NMR ($CDCl_3$) *δ* 170.8, 170.3, 170.1, 169.9, (O*C*OCH$_3$), 168.6 (NH*C*O), 140.4 (CO*C*(CH$_3$)CH$_2$), 119.2 (COC(CH$_3$)*C*H$_2$), 97.7 (C-1), 69.8 (C-2), 69.3 (C-3), 68.5 (C-5, O*C*H$_2$(CH$_2$)$_5$), 66.4 (C-4), 62.6 (C-6), 39.8 (*C*H$_2$NHCO), 29.6, 29.2, 29.1, 26.8, 26.1, (OCH$_2$(*C*H$_2$)$_5$CH$_2$NH), 21.1, 20.8 (OCO*C*H$_3$), 18.9 (CO*C*(*CH*$_3$)CH$_2$). ESI-MS: m/z calculated for [$C_{25}H_{39}NNaO_{11}$]$^+$, 552,2415, found 552.2417.

The protected monomer (6.1g, 11.5mmol) was finally deacetylated in methanol (250 mL), using 1M NaOMe/MeOH solution (5.1mL). The solution was stirred at room temperature for 3h. The pH of the solution was adjusted to 5, the solution was then filtrated and the solvent was removed to obtain the pure monomer (**HMM**) as a colorless gum. 4.1 g (98% yield).

[α]$_D$ = +11 (c= 0.4, Methanol). ^{1}H NMR (300 MHz, D_2O) *δ* 5.71 (s, 1H, CC*H*$_2$), 5.48 (s, 1H, CC*H*$_2$), 4.91 (d *J* =1.5 Hz, 1H, H-1), 4.00-3.50 (m, 8H, OC*H*$_2$CH$_2$, H-2, -3, -4, -5, -6, -6'), 3.30 (t *J* = 6.9 Hz, 2H, NHC*H*$_2$CH$_2$), 1.98 (s, 3H, CC*H*$_3$), 1.73-1.54 (m, 4H, C*H*$_2$(CH$_2$)$_3$*CH*$_2$CH$_2$NH), 1.40 (s, 6H, CH$_2$(C*H*$_2$)$_3$(CH$_2$)$_2$NH); ^{13}C NMR (D_2O) *δ* 171.9 (NH*C*O), 139.5 (CO*C*(CH$_3$)CH$_2$), 120.5 (COC(CH$_3$)*C*H$_2$), 99.7 (C-1), 72.8 (C-2), 70.70(C-3), 70.2 (C-5), 67.9 (O*C*H$_2$(CH$_2$)$_5$), 66.8 (C-4), 60.9 (C-6), 39.6 (*C*H$_2$NHCO), 28.4, 28.3, 28.1, 25.9, 25.3 (OCH$_2$(*C*H$_2$)$_5$CH$_2$NH), 17.8 (CO*C*(*CH*$_3$)CH$_2$); ESI-MS: m/z calculated for [$C_{17}H_{31}N\ O_7Na$]$^+$, 384.1993, found 384.1980.

5.2.2 Synthesis of *N*-[2-(α-D-mannopyranosyloxy)ethyl] methacrylamide (EMM)

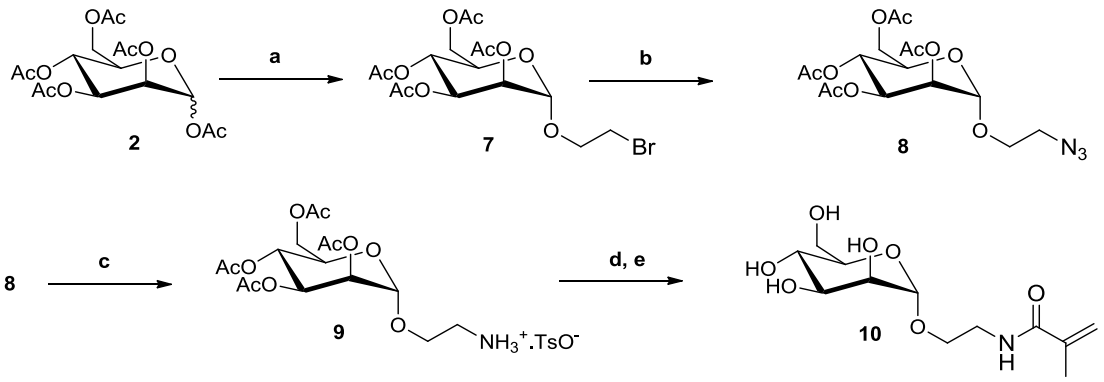

Scheme S1: Preparation of HMM. Reagents and conditions: a) $SnCl_4$, CF_3CO_2Ag, CH_2Cl_2; b) NaN_3, DMF; c) H_2, Pd/C, p-TsOH, EtOH; d) methacryloyl chloride, CH_2Cl_2, Et_3N; e) NaOMe, MeOH.

Synthesis of azido-fuctionalized mannoside (8).

$SnCl_4$ (1M in CH_2Cl_2, 38.4mL, 38.4mmol) was added dropwise (within 30 min) at room temperature to a solution of 2-bromoethnol (1.5mL, 19.2mmol), peracetylated D-mannose (**2**) (5g, 12.8mmol) and silver trifluoroacetate (4.24g, 38.4mmol) in freshly distilled dichloromethane (120mL). Disappearance of the starting material was observed within 3h and the mixture became pale pink. Saturated aqueous $NaHCO_3$ (200mL) was added to adjust pH above 8, and the solution was vigorously stirred for 20min. A biphasic system formed upon addition of aqueous $NaHCO_3$ with a white suspension in the aqueous layer. The biphasic solution was diluted with 300mL of water and the aqueous layer was extracted with CH_2Cl_2 (3×300mL). The organic layers were combined, washed successively with saturated aqueous $NaHCO_3$ (150mL), water (3×300mL), brine (2×300mL) and dried over $MgSO_4$. After solvent removal by evaporation, the crude product (**7,** pale yellow gum) was dissolved in anhydrous DMF (150mL), sodium azide (4.16g, 63.9mmol) and tetra-n-butyl ammonium iodide (4.73g, 12.8mmol) were added. The mixture was stirred at 70 °C under argon for 24h, cooled to room temperature, filtered and the solid was washed with EtOAc (3×300mL). The filtrate was diluted with EtOAc to reach a total volume of 1L. The organic layer was washed with aq. $NaHCO_3$ (3×300mL), water (3×300mL), brine (300mL) and dried. After concentration, the resulting product (yellow gum) was

purified by column chromatography (petroleum ether/ethyl acetate, 7/1, v/v) to afford the corresponding azido-fuctionalized glycoside (**8**)**.** Final yield: 4.1 g (76%) obtained as a colorless gum.

^{1}H NMR (300 MHz, $CDCl_3$) δ 5.40-5.20 (m, 3H, H-2, -3, -4), 4.85 (d, *J* = 1.5 Hz,1H, H-1), 4.20 (dd, *J* = 5.1, 12.3 Hz, 1H, H-6), 4.10 (dd, *J* = 2.4, 12.3 Hz, 1H, H-6'), 4.05 (m, 1H, H-5), 3.90-3.82 (m, 1H, H-OCH*H*CH_2), 3.69-3.62 (m, 1H, OC*H*HCH_2), 3.55-3.30 (m, 2H, N_3C*H*$_2CH_2$), 2.14, 2.09, 2.03, 1.98 (s, 4×3H, 4×C*H*$_3$CO); ^{13}C NMR ($CDCl_3$) δ 170.7, 170.1, 169.9 (O*C*OCH_3), 97.8 (C-1), 69.5 (C-2), 68.9(C-3), 67.1 (C-5, O*C*H_2CH_2 N_3), 66.1 (C-4), 62.5 (C-6), 50.4 (*C*H_2N_3), 20.9, 20.8 (OCO*C*H_3).

Synthesis of EMM (compound 10).

8 (4.1g, 9.8mmol), p-toluenesulfonic acid (2.05g, 10.8mmol) and 10% palladium on activated charcoal (1g) as the catalyst were stirred overnight in ethanol (240mL) at room temperature under 1 atm of hydrogen. The solution was filtered over celite and evaporated to obtain a colorless gum **(9)**. The resulting product was directly engaged in the next step without further purification. **9** was dissolved in a solution of anhydrous CH_2Cl_2 (50mL) containing triethylamine (3.71mL, 26.6mmol). Methacryloyl chloride (1.08mL, 11.5mmol) was added dropwise into the solution in an ice bath. The solution was stirred for 1h at room temperature. After reaction, the solution was washed with water (2×200mL), dried over $MgSO_4$ and the solvent was removed. The acetylated monomer was finally purified by column chromatography (petroleum ether/ethyl acetate, 3/1, v/v). Yield: 2.1g (51%) of a colorless gum.

$[\alpha]_D$ = +13 (c= 0.3, Chloroform). ^{1}H NMR (300 MHz, $CDCl_3$) δ 6.28 (s, 1H, NH), 5.69 (s, 1H, CC*H*$_2$), 5.39-5.17 (m, 4H, H-3, CC*H*$_2$, H-4, H-2), 4.80 (d, *J* =1.5 Hz, 1H, H-1), 4.26-4.19 (dd, *J* = 5.7, 12.3 Hz,1H, H-6), 4.13-4.05 (dd, *J* = 2.4, 12.3 Hz, 1H, H-6'), 4.00-3.90 (m, 1H, H-5), 3.85-3.76 (m, 1H, OC*H*$_2CH_2$), 3.64-3.30 (m, 3H, OC*H*$_2CH_2$, NHC*H*$_2CH_2$), 2.13, 2.07, 2.02, 1.98, (s, 4×3H, 4×C*H*$_3$CO), 1.95 (s, 3H, CC*H*$_3$); ^{13}C NMR ($CDCl_3$) δ 170.7, 170.1, 169.7 (O*C*OCH_3), 168.5 (NH*C*O), 139.8 (CO*C*(CH_3)CH_2), 120.0 (COC(CH_3)*C*H_2), 97.7 (C-1), 69.4 (C-2), 69.1 (C-3), 68.8 (C-5),

67.3 (O*C*H_2), 66.1 (C-4), 62.5 (C-6), 39.3 (*C*H_2NHCO), 20.9, 20.8 (OCO*C*H_3), 18.7 (CO*C*(*C*H_3)CH_2).

The protected monomer (2.1g, 4.46mmol) was finally deacetylated in methanol (87 mL), using 1M NaOMe/MeOH solution (1.8mL). The solution was stirred at room temperature for 3h. The pH of the solution was adjusted to 5, the solution was then filtrated and the solvent was removed to obtain the pure monomer (**EMM**) as a colorless gum. 1.2 g (92% yield).

$[\alpha]_D$ = +17 (c= 0.3, Methanol). ^{1}H NMR (300 MHz, D_2O) δ 5.65 (s, 1H, CC*H*$_2$), 5.42 (s, 1H, CC*H*$_2$), 4.82 (d *J* =1.5 Hz, 1H, H-1), 3.90-3.37 (m, 10H, OC*H*$_2$$CH_2$, NHC*H*$_2$$CH_2$, H-2, -3, -4, -5, -6, -6'), 1.89 (s, 3H, CC*H*$_3$); ^{13}C NMR (D_2O) δ 172.7 (NH*C*O), 139.7 (CO*C*(CH_3)CH_2), 121.7 (COC(CH_3)*C*H_2), 100.3 (C-1), 73.4 (C-2), 71.1 (C-3), 70.7 (C-5), 67.2 (O*C*$H_2$$CH_2$), 66.4 (C-4), 61.4 (C-6), 39.7 (*C*H_2NHCO), 18.4 (CO*C*(*C*H_3)CH_2); ESI-MS: m/z calculated for [$C_{12}H_{21}N$ O_7Na]$^+$, 314.1204, found 314.1210.

5.3 Synthesis of CPADB-based multi-functional RAFT agents

Synthesis of CPADB-based trifunctional RAFT agent.

Typically, in an argon conditioned Schlenk tube, 4-cyano-4-(phenylcarbonothioylthio) pentanoic acid (CPADB, 297mg, 1mmol) was dissolved in chloroform (20 mL). After cooling to 0°C, *N*-hydroxysuccinimide (115mg, 1mmol) and *N*,*N*′-dicyclohexylcarbodiimide (206mg, 1mmol) were successively added. After one hour at 0°C, the solution was stirred overnight at room temperature. The solution was filtrated and the solvent was evaporated to afford the activated RAFT agent as a pink powder (95%, 357 mg). ^{1}H NMR (250 MHz, $CDCl_3$) δ 7.91 (d, *J* = 7.5 Hz, 2H, phenyl), 7.58 (t, *J* = 7.5 Hz, 1H, phenyl), 7.41 (t, *J* = 7.5 Hz, 2H, phenyl), 3.11-2.45 (m, 8H, C*H*$_2$C*H*$_2$CO and CC*H*$_2$C*H*$_2$C), 1.96 (s, 3H, C*H*$_3$). ^{13}C NMR ($CDCl_3$) δ 220.01, 168.93, 167.22, 144.52, 133.31, 128.76, 126.87, 118.28, 45.59, 32.88, 27.05, 25.71, 24.38 (Spectra given in Fig S5).

The activated RAFT agent (1.24g, 3.3mmoL) was dissolved in THF (100mL) and a solution of tris(2-aminoethyl)amine (146 mg, 1mmol) in methanol (10mL) was added dropwise at room temperature. The solution was stirred for 1h. After reaction, the solvent was evaporated and the crude product was purified by column chromatography (CH_2Cl_2/Methanol, 30/1, v/v). 520mg (41%) as pink powder. ^{1}H NMR (250 MHz, $CDCl_3$) δ 7.86 (m, 6H, phenyl), 7.53 (m, 3H, phenyl), 7.35 (m, 6H, phenyl), 6.93 (s, 3H, N*H*), 3.29 (s, 6H, NHCH_2CH_2N), 2.88-2.21 (m, 18H, CH_2CH_2CO and NHCH_2CH_2N), 1.90 (m, 9H, CH_3).^{13}C NMR ($CDCl_3$) δ 222.89 (S*C*S), 171.43 (*C*ONH), 144.61, 133.16 , 128.70, 126.85 (phenyl), 118.94 (*C*N), 54.80 (N*C*H_2CH_2), 46.34 (CH_3*C*CN), 38.23 (NCH_2*C*H_2NH), 34.36 (CO*C*H_2CH_2), 31.88 (CH_2*C*H_2C), 24.23 (*C*H_3) (Spectra given in Fig S6). ESI-MS: *m*/*z* calculated for $C_{45}H_{52}N_7O_3S_6$ $[M+H]^+$ 930.2450, found 930.2409.

Synthesis of CPADB-based octafunctional RAFT agent. To a solution of Octa Ammonium POSS purchased from Hybrid Plastics (200 mg, 0.17mmol) in methanol (10mL) was added 0.33mL of DIPEA (2 mmol)). After 2h under stirring, the solution was introduced drop by drop in a solution of activated RAFT agent (650mg, 1.7mmoL in 100mL) of THF. After 1h of reaction, the solvent was evaporated and the RAFT agent was finally purified by column chromatography (CH_2Cl_2/Methanol, 30/1, v/v), obtained pink powder 151mg (30%).^{1}H NMR (250 MHz, CDCl3) δ 7.88 (d, *J* = 7.5 Hz, 16H, phenyl), 7.54 (t, *J* = 7.5 Hz, 8H, phenyl), 7.37 (t, *J* = 7.5 Hz, 16H, phenyl), 6.56 (s, 8H, N*H*), 3.45-3.22 (m, 16H, CH_2CH_2NH), 2.75-2.24 (m, 32H, CH_2CH_2CO), 1.89 (s, 24H, CH_3), 1.78-1.45 (m, 16H, SiCH_2CH_2), 0.78-0.52 (m, 16H, SiCH_2CH_2). ^{13}C NMR (CDCl3) δ 222.89 (S*C*S), 170.94 (*C*ONH), 144.64, 133.21, 128.74, 126.84 (phenyl), 118.95 (*C*N), 46.33 (CH_3*C*CN), 42.19 (NH*C*H_2CH_2), 34.35 (CO*C*H_2CH_2), 31.98 (CH_2*C*H_2C), 29.83 (CH_2*C*H_2CH_2), 24.28 (*C*H_3), 23.02 (CH_2CH_2*C*H_2). (Spectra given in Fig S7)

ESI-MS: *m*/*z* calculated for $C_{128}H_{154}N_{16}O_{20}S_{16}Si_8$ $[M+2H]^{2+}$ 1485.2600, found 1485.2639.

5.4 Preparation of GIcopolymer (PHMM and PEMM)

RAFT polymerization of HMM

In a typical experiment (**L47**), a Schlenk flask (10 mL) was charged with HMM (100 mg, 2.8×10^{-4} mol) dissolved in 0.35 mL of water, 4,4'-azobis (4-cyanovaleric acid) (ACPA, 0.52 mg, 1.85×10^{-6} mol), and 4-cyano-4-(phenylcarbonothioylthio) pentanoic acid (1.56 mg, 5.55×10^{-6} mg) dissolved in 0.35 mL of DMSO. After mixing, the pink solution was deoxygenated by three consecutive freeze-pump-thaw cycles. After the last cycle, the Schlenk flask was filled with nitrogen, allowed to warm to room temperature and finally immersed in an oil bath at 70 °C. After polymerization (conversion at 84%), the Schlenk flask was plunged into iced water and the solution was then freeze-dried overnight. The crude product was redissolved in a minimal quantity of methanol and precipitated in an acetone/petroleum ether mixture (Volume ratio at 7/3) to remove unreacted monomer and initiator. The resulting pink powder was dried overnight under vacuum to give 60 mg **L47** as a pale pink solid.

Polymerizations of HMM in the presence of CPADB-based trifunctional RAFT agent were carried out in similar conditions. Polymerizations of HMM in the presence of CPADB-based octafunctional RAFT agent were carried out in pure DMSO using AIBN as initiator owing to the poor solubility of the RAFT agent in water. Kinetics of polymerization and SEC traces of the resulting star-shaped glycopolymers are given in Figures S1 and S2

RAFT Polymerization of EMM

The polymerization procedure was adapted from the one described above for HMM. In brief, solution polymerization of EMM (150mg) was performed in DMSO (0.5mL) and mediated by 4-cyano-4-(phenylcarbonothioylthio) pentanoic acid using 4,4'-azobis (4-cyanovaleric acid) as initiator ($[M]_0$/[CTA]/[ACPA]=250/1/0.3). The solution was deoxygenated by three consecutive freeze-pump-thaw cycles and the Schlenk flask was finally filled with nitrogen, allowed to warm to room temperature and finally immersed in an oil bath at 70 °C. After polymerization (73% of conversion), the

Schlenk flask was plunged into iced water and the solution was then freeze-dried overnight. The crude product was redissolved in a minimal quantity of DMSO and precipitated in an acetone/petroleum ether mixture (Volume ratio at 7/3) to remove unreacted monomer and initiator. The powder was dried overnight under vacuum to give 90 mg of PEMM as a pale pink solid. PEMM (M_w = 96 kg.mol-1, $Đ$ = 1.17) was characterized by SEC with RI/LS detection in $NaNO_3$/NaOH aqueous solution (pH =7).

Removal of the dithiobenzoate chain ends. HM-based glycopolymer (L47, 40mg, 2.32×10^{-6} mol) was dissolved in a 1mL of DMSO (1mL). The solution was deoxygenated by three consecutive freeze-pump-thaw cycles. Ethanolamine (1.4 mg 10 eq) was added in solution and the pink color immediately disappeared. NIPAAm (13.2 mg, 50eq) and dimethylphenylphosphine (0.3 mg 1eq) were then incorporated and the solution was stirred overnight at room temperature. Water (2 x 100 mL) and dichloromethane (200 mL) were added to the solution. The aqueous phase was collected, dialyzed against deionized water for 2 days and freeze-dried to afford a fluffy white powder (36 mg, 90%).

Acetylation of HM-based glycopolymers for SEC analysis in THF. The glycopolymer (L47, 2mg, 1.16×10^{-7} mol) was dissolved in a solution of anhydrous DMF (1mL) containing pyridine (4.3 mg, 2 eq. per hydroxyl group). Acetic anhydride (14.0 mg, 5 eq. per hydroxyl group) was incorporated into the solution. The solution was heated overnight at 50°C. After reaction, 150 mL of dichloromethane was added. The solution was washed with water (2×200mL), dried by $MgSO_4$ and the solvent was evaporated to obtain the acetylated glycopolymer (yield~ 90%) as a beige paste.

5.5 Preparation of Glyco-copolymer

Determination of Reactivity ratios of HMM and GMA

Jaacks method

The Jaacks method was perfomed as high monomer feed ratio ($[HMM]_0/[GMA]_0$ = 34 and 0.028, respectively). Specifically, HMM (122 mg, 3.40×10^{-4} mol) and GMA (1.4 mg, 1.00×10^{-4} mol) were dissolved in anhydrous DMSO (0.7 mL), CPADB (2 mg, 7.16×10^{-6} mol) was engaged as RAFT agent and V70 (0.43, 1.39×10^{-6} mol) was used as initiator. Ran the polymerization at 40 °C, kinetics studies on the polymerization for each monomer via entire RAFT process were systematically conducted. Using $-\ln(1-Conv._{HMM})$ as y-axis and $-\ln(1-Conv._{GMA})$ as x-axis to make the graph, the results was treated with linear simulation, the reactivity ratio of HMM was just the slope. r_{GMA} could be determined applying the reverse condition.

Kelen-Tüdös method

Kelen-Tüdös method needs three kinetic experiments were performed. The monomer feed ratio ($[HMM]_0/[GMA]_0$) was used at 0.25, 1 and 2. CPADB was selected as RAFT agent using V70 as initiator ([HMM+GMA]/[CTA]/[Initiator] = 50/1/0.2). Performed the polymerization at 40 °C, kinetics studies on each copolymerization were systematically conducted. Using G/(α+F) as y-axis and F/(α+F) as x-axis to do the graph, the results was treated with the linear simulation. r_{GMA} was the G/(α+F) as the F/(α+F) equaled to 1, and r_{HMM} was the product of α×|intercept|. α is used to distribute uniformly and symmetrically the experimental points between 0 and 1.

$$F = \frac{(m_1/m_2)^2}{dm_1/dm_2} \qquad G = \frac{m_1/m_2}{dm_1/dm_2}(dm_1/dm_2 - 1)$$

$$a = \sqrt{F_m F_M}$$

Preparation of Block copolymers

In a typical experiment, two step RAFT homopolymerization was employed. In the first polymerization, a Schlenk flask (10 mL) was charged with monomer GMA (200 mg, 14.1×10^{-4}mol) dissolved in 2 mL of DMSO, V70 (1.08 mg, 3.50×10^{-6} mol), and CPADB (3.92 mg, 14.1×10^{-6} mol) dissolved in 1.5 mL of DMSO. After mixing, the pink solution was deoxygenated by three consecutive freeze-pump-thaw cycles. After the last cycle,

the Schlenk flask was filled with nitrogen, allowed to warm to room temperature and finally immersed in an oil bath at 70 °C. After polymerization (conversion at 61%), the crude product was precipitated in an Et_2O to remove unreacted monomer and initiator. The resulting pink powder was dried overnight under vacuum to give 100 mg of $pGMA_{65}$ as a pale pink solid. $M_{n\ SEC}$ =11.5 kg.mol^{-1}, $Đ$ = 1.31(using PS calibration in THF).

In the second step, a Schlenk flask (10 mL) was charged with monomer HMM (140 mg, 3.87×10^{-4}mol dissolved in 0.5 mL of DMSO, ACPA **(**0.18 mg, 0.64×10^{-6} mol), $pGMA_{65}$ (19 mg, 2.0×10^{-6} mol) dissolved in 0.2 mL of DMSO. After mixing, the pink solution was deoxygenated by three consecutive freeze-pump-thaw cycles. After the last cycle, the Schlenk flask was filled with nitrogen, allowed to warm to room temperature and finally immersed in an oil bath at 70 °C. After polymerization (conversion at 64%), the Schlenk flask was plunged into iced water and the solution was then freeze-dried overnight. The crude product was redissolved in a minimal quantity of solvent (methanol/DMSO, v/v, 20/1) and precipitated in an acetone/petroleum ether mixture (v/v, 7/3) to remove unreacted monomer and initiator. The resulting pink powder was dried overnight under vacuum to give 80 mg of $pGMA_{65}$-*b*-$pHMM_{133}$ as a pale pink solid. $M_{n\ SEC}$ =51.0 kg.mol^{-1}, $Đ$ = 1.20. (after acetylation, using PS calibration in THF).

Preparation of Gradient copolymers

In a typical experiment, a Schlenk flask (10 mL) was charged with monomer HMM (130 mg, 3.60×10^{-4}mol) and GMA (22 mg, 1.54×10^{-4}mol) dissolved in 0.3 mL of anhydrous DMSO, ACPA (0.26 mg, 0.93×10^{-6} mol), and CPADB (0.65 mg, 2.34×10^{-6} mol) dissolved in 0.1 mL of DMSO. After mixing, the pink solution was deoxygenated by three consecutive freeze-pump-thaw cycles. After the last cycle, the Schlenk flask was filled with nitrogen, allowed to warm to room temperature and finally immersed in an oil bath at 70 °C. After polymerization (conversion at 87%), the Schlenk flask was plunged into iced water and the solution was then freeze-dried overnight. The crude product was redissolved in a minimal quantity of solvent (methanol/DMSO, v/v, 20/1)

and precipitated in an acetone/petroleum ether mixture (v/v, 7/3) to remove unreacted monomer and initiator. The resulting pink powder was dried overnight under vacuum to give 110 mg of p(GMA_{66}-*grad*-HMM_{130}) as a pale pink solid. $M_{n\ SEC}$ =52.9 kg.mol^{-1}, $Đ$ = 1.18. (after acetylation, using PS calibration in THF).

Preparation of Statistical copolymers

In a typical experiment, a Schlenk flask (10 mL) was charged with monomer HMM (150 mg, 4.15×10^{-4}mol) and GMA (8 mg, 0.56×10^{-4}mol) dissolved in 0.25 mL of water, ACPA (0.38 mg, 1.35×10^{-6} mol), and CPADB (0.75 mg, 2.70×10^{-6} mol) dissolved in 0.07 mL of DMSO. After mixing, the pink solution was deoxygenated by three consecutive freeze-pump-thaw cycles. After the last cycle, the Schlenk flask was filled with nitrogen, allowed to warm to room temperature and finally immersed in an oil bath at 70 °C. After 100 min, a DMSO solution (0.14 mL) of the GMA (0.84 M) was progressively added under argon by syring pump at a rate of 0.038 mL/h. After polymerization (conversion at 88%), the Schlenk flask was plunged into iced water and the solution was then freeze-dried overnight. The crude product was redissolved in a minimal quantity of solvent (methanol/DMSO, v/v, 20/1) and precipitated in an acetone/petroleum ether mixture (v/v, 7/3) to remove unreacted monomer and initiator. The resulting pink powder was dried overnight under vacuum to give 125 mg of p(GMA_{63}-*stat*-HMM_{134}) as a pale pink solid. $M_{n\ SEC}$ =54.8 kg.mol^{-1}, $Đ$ = 1.15 (after acetylation, using PS calibration in THF).

5.6 Bio-assay for anti-adhesive of piliated *E.Coli*

Cytotoxicity tests

The cytotoxicity tests were performed using FACS Calibur flow cytometer (BD Biosciences, San Jose, CA, USA) according to manufactures' instructions and generally accepted procedures. Propidium iodide (PI) was used to counterstain necrotic cells (PI+). Apoptotic cells were detected as Annexin-V-FITC+/PI- cells.

Competitive Enzyme-Linked Lectinosorbent Assay (ELLSA)

Immunosorbent microplates (Nunc, Maxisorp) were coated with 100 µl of 5 mg/ml

solution of RNAse-B in 100 mM carbonate/bicarbonate buffer pH 9.6. Plates were incubated at 4°C overnight and then washed (300 µl/well) three times with 10 mM phosphate – buffered saline (PBS) containing 0.15% Tween – 20. All wells were blocked with 200 µl 3% bovine serum albumin (BSA) in 10 mM phosphate – buffered saline (PBS) containing 0.15% Tween – 20 (PBST) and incubated at 37 °C 2 h. Then washed three times with PBST. Thiazole-bearing mannosides were dissolved in PBST at the concentrations indicated on graphs and added to the microwells. FimH was diluted in PBST to 0.07µM and added to each well of plate and incubated for 1h at room temperature. Wells were washed three times with PBST. Wells were incubated with 100 µl of rabbit-anti-FimH antibodies IgG (aFimH) diluted 1:5000 in PBST for 1h at room temperature. Wells were washed 3 times with PBST and incubated with 100 µl of goat-anti-rabbit HRP-labeled secondary antibody, Enzo Life Sciences (2ndAb-HRP) diluted 1:10000 in PBST for 1h at room temperature. The wells were washed three times with PBST and 100 µl of 3,3′,5,5′-Tetramethylbenzidine (TMB) were added to each well and incubated in darkness for 5 – 15 min. The reaction was stopped with 100 µl/well of 1N sulfuric acid. Plate absorbance was analysed at 450 nm using microplate reader BioTek-ELx800.

Adhesion tests

Detailed procedures on experiments with Katushka UTI89+L188 and with Caco-2 /HeLa with LF82 and L188

To evaluate the effectiveness of synthesized glycopolymers were used the model of co-incubation of Crohn-disease provoking strain LF82 of *E.coli* bacteria with human epithelia cells of Caco-2 and HeLa cell lines. Cells were grown on the glass. Before adding of a bacterial suspension, cells were washed three times by fresh culture medium (without antibiotic). 4 µl of bacterial suspension of type 1 piliated *E. coli* strain LF82 (OD=1.3) were added to cells. L188 inhibitor was added at concentration of 500 nM. After 2h of co-incubation of cells with bacteria (under the presence or absent of L188 inhibitor), samples were analyzed by fluorescent microscopy.

Adhesion assays of AIEC LF82 strain on intestinal epithelial cells T84.

The intestinal epithelial cells T84 were seeded in 48-well tissue culture plates at a density of 1.5 x 10^5 cells/well and were incubated at 37 °C for 48h. For pre-incubation protocol, AIEC LF82 bacteria were incubated for 1 h with mannoside derivatives (α-D-Mannose, HM or **HMM**) or HM-based glycopolymers at final concentrations of 1; 0.1 and 0.01 µM (in mannose unit basis) then cells were infected with the mixture at a multiplicity of infection (MOI) of 10 bacteria per cell for 3 h. Monolayers were washed 3 times with phosphate buffer (PBS) and lysed with 1% Triton X-100 (Sigma) in deionized water. Samples were diluted and plated onto LB agar plates to determine the number of colony-forming units (CFU). For the post-incubation protocol, cells were infected with AIEC LF82 bacteria at a MOI of 10 for 3 h, then monolayers were extensively washed with PBS and inhibitory compounds were added at final concentrations of 10, 1 and 0.1 µM (in mannose unit basis) onto the cells for an additional 3 hours-period.

Ex vivo assay : Adhesion assays of AIEC LF82 strain on colonic tissues from CEABAC10 mice

Adhesion assay of AIEC LF82 bacteria were performed using colonic tissues from transgenic mice expressing the human CEACAM6 protein.[5] Briefly, 10 to 12-week-old FVB/N CEABAC10 transgenic mice were anesthetized, euthanized by cervical dislocation and colons were removed. Colons were washed twice in phosphate buffer saline (PBS) and segmented in independent loops of ≈ 0.6 cm. A volume of 100 µL containing 6×10^5 CFU of LF82 bacteria in PBS in the presence or absence of 3.4 µmol of the glycopolymer L188 were injected into the loops. Loops were incubated 4 h at 37°C in Krebs-Ringer bicarbonate buffer (Sigma) in an atmosphere containing 5% of CO_2, and then opened and washed 4 times in PBS. Tissues were homogenized, appropriately diluted and plated onto Luria-Bertani agar plates containing ampicillin (100 µg/mL) and erythromycin (20 µg/mL) to select AIEC LF82 bacteria.

5.7 Preparation of glyconanocapsules through nanoprecipitation

5.7.1 Homopolymer

Phase diagrams' determination

Cloud point boundary. This equilibrium limit corresponds to the solubility limit of the polymer in acetone-water mixtures. The method consists of titrating with acetone various aqueous solutions of glycopolymer unimers (**L47** or **L221**) until the mixtures turn milky (generation of swollen micelles). Compositions at the cloud point line are deduced from the mass of acetone added at the onset of turbidity and at a given glycopolymer initial concentration.

Binodal curve. This equilibrium limit corresponds to acetone/water compositions where the HD is not soluble anymore. The method consists of titrating with water acetonic solutions of hexadecane of increased concentrations until the mixture turned milky, or even phase separates, through the generation of droplets.

"Ouzo limit". This boundary curve separates the Ouzo domain, where stable HD nanodroplets can be formed, from the high concentration region where HD phase-separates from the mixture. Special requirements were made here to ensure reproducible measurements of the Ouzo limit: i) a non-ionic surfactant (Brij56) was added in the organic phase to stabilize the HD droplets once formed; ii) just after the required content of water, an extra load of water was rapidly pourred to dilute the samples and avoid Ostwald ripening. The Ouzo limit was determined by measuring the number of counts by DLS, before and after filtrating the mixture with 1.20 µm polyethersulfone filters. Identical numbers of counts before and after filtration correspond to homogeneous emulsions of HD droplets, whereas a decrease of it indicates a loss of big, numerous HD droplets on the filter.

Preparation of PHMM-based glyconanocapsules

Typically, **L221** (1mg) was dissolved in 350 mg H_2O, whereas 2 mg HD were poured in 650 mg acetone separately. **L221** aqueous solution was then poured into the acetone solution all at once, the transparent solution turned to be milky immediately. After shaking for seconds, the solution was immediately characterized by DLS and TEM (Figure S4). To prepare cross-linked nanocapsules, various contents of IPDI

were added primarily in the acetone phase prior solvent shifting. The solutions were left overnight and then characterized by DLS and TEM.

Preparation of PEMM-based nanocapsules

PEMM (0.5 mg) was dissolved in 540 mg of water, whereas 0.5 mg miglyol 812 and IPDI (0.05 mg, 24 eq.) were poured in 460 mg acetone. Polymer aqueous solution was then incorporated into the acetone solution all at once. The transparent solution turned to be milky immediately. The solution was left overnight and then characterized by DLS and TEM.

Glyconanocapsules' functionalization

Post-functionalization of glyconanocapsules using a simple amine. After 2h of cross-linking (1 eq. IPDI per PHMM chain), 0.0016mg of octylamine (1 eq. comparing to IPDI) was introduced into the milky mixture solution. After shaking for seconds, the solution was left overnight before being observed by TEM and DLS analyses.

Functionalization of glyconanocapsule using amino-functionalized biotin. L221 (1mg) and 0.007mg amino-functionalized biotin (2 eq per PHMM chain) was dissolved in 350 mg of water. 2 mg of HD and 0.06 mg IPDI (24eq per PHMM chain) were dissolved in 650 mg acetone. The **L221** aqueous solution was then poured into the acetone solution to generate functionalized glyconanocapsules. The solution was left overnight. After dialysis for 3 days, 0.125 eq. avidin in 0.5 mL water was added into the glyconanocapsule solution and the evolution of the aggregated complex was analyzed by DLS. In the meantime, the dialyzed sample was measured by UV-Vis after introducing HAVA/Avidin reagent for determining the efficiency of biotin grafting reaction.

Fluorescence tags and assays

One-pot functionalization of glyconanocapsule by amino-functionalized fluorescein. L332 (1mg) and 0.015 mg amino-functionalized fluorescein (2 eq per PHMM chain) were dissolved in 350 mg of water. 2 mg of HD and 0.06 mg IPDI (24 eq

per PHMM chain) were dissolved in 650 mg of acetone. The aqueous polymer solution was then poured into the acetone solution and the solution was left overnight. After dialysis for 3 days, the glyconanocapsule solution was analyzed by fluorescence spectroscopy, DLS and TEM. No signal was observed for blank experiments with fluorescein.

Pyrene-Loading experiment. L221 (1 mg) was dissolved in 350 mg H_2O. On the other hand, 2 mg hexadecane containing 2.5% wt pyrene and IPDI (0.06 mg, 24eq.) were added to 650 mg of acetone.The aqueous polymer solution was poured into acetone solution and the solution was left for overnight. After dialysis for 3 days, the glyconanocapsule solution was analyzed by Fluorescence spectroscopy, DLS and TEM.

One-pot preparation of pyrene-loaded biotinylated nanocapsules

L221 (1 mg) and 0.007mg of amino-functionalized biotin (2 eq per PHMM chain) were dissolved in 350 mg of water. 2 mg of HD with 2.5% wt pyrene and IPDI (0.06 mg, 24eq.) were added to 650 mg of acetone. The aqueous solution was then poured into the acetone solution and the solution was left for overnight. After dialysis for 3 days, the glyconanocapsule solution was analyzed by Fluorescence spectroscopy and DLS.

AuNP-coated glyconanocapsules.

L221 (1 mg) was dissolved in 350 mg of H_2O. On the other hand, 2 mg hexadecane (with 2% wt dodecanethiol functionalized gold nanoparticles) were mixed with IPDI (0.06 mg, 24eq.) in 650 mg acetone. PHMM2 aqueous solution was poured into acetone solution and the solution turned immediately milky. The solution was left overnight and further analyzed by DLS and TEM.

Iron oxide NP-coated glyconanocapsules.

NP coated nanocapsules

L221 (1 mg) was dissolved in 350 mg of H_2O. 2 mg of HD containing 0.6% wt of iron oxide nanoparticles and IPDI (0.06 mg, 24eq.) were added to 650 mg of acetone. The

aqueous solution was poured into the acetone solution and the solution was left for overnight. The solution was further analyzed by TEM.

5.7.2 Copolymer

Glycopolymer/Water/Acetone system*:*

Cloud point boundary. This equilibrium limit corresponds to the solubility limit of the polymer in acetone-water mixtures. The method consists of titrating with acetone various aqueous solutions of glycopolymer unimers until the mixtures turn milky (generation of swollen micelles). Compositions at the cloud point line are deduced from the mass of acetone added at the onset of turbidity and at a given glycopolymer initial concentration.

Miglyol/water/acetone system*:*

Binodal curve. This equilibrium limit corresponds to acetone/water compositions where the Miglyol 812 is not soluble anymore. The method consists of titrating with water acetonic solutions of miglyol of increased concentrations until the mixture turned milky, or even phase separates, through the generation of droplets .

“Ouzo limit”. This boundary curve separates the Ouzo domain, where stable Miglyol nanodroplets can be formed, from the high concentration region where Miglyol phase-separates from the mixture. Special requirements were made here to ensure reproducible measurements of the Ouzo limit: i) a non-ionic surfactant (Brij56) was added in the organic phase to stabilize the Miglyol droplets once formed; ii) just after the required content of water, an extra load of water was rapidly pourred to dilute the samples and avoid Ostwald ripening. The Ouzo limit was determined by measuring the number of counts by DLS, before and after filtrating the mixture with 1.20 µm polyethersulfone filters. Identical numbers of counts before and after filtration correspond to homogeneous emulsions of Miglyol droplets, whereas a decrease of it indicates a loss of big, numerous Miglyol droplets on the filter (**Figure S3**).

Preparation of glyconanocapsules

Typically, Glyco-copolymer (2.5 mg) was dissolved in 4100 mg H_2O, whereas 5 mg miglyol was dissolved in 5900 mg acetone. The polymer aqueous solution was then poured into the acetone solution all at once, the transparent solution turned to be milky immediately. To prepare cross-linked nanocapsules, various contents of IPDI were added primarily in the acetone phase prior solvent shifting. The solutions were left overnight and then characterized by DLS and TEM.

Glyconanocapsules' functionalization

Functionalization of glyconanocapsule using amino-functionalized biotin. Glycopolymer (2.5 mg) was dissolved in 4100 mg of water. 5 mg of Miglyol and 0.34 mg IPDI (48 eq per polymer chain) were dissolved in 5900 mg acetone. The **polymer** aqueous solution was then poured into the acetone solution to generate glyconanocapsules. After overnight, the 0.01 mg amino-functionalized biotin (1 eq per PHMM chain) was added into solution and reacted at 40 °C for overnight. After dialysis for 3 days, 0.125 eq. avidin in 0.5 mL water was added into the glyconanocapsule solution and the evolution of the aggregated complex was analyzed by DLS. In the meantime, the dialyzed sample was measured by UV-Vis after introducing HAVA/Avidin reagent for determining the efficiency of biotin grafting reaction.

Functionalization of glyconanocapsule using amino-magnetic particle. Glycopolymer (2.5 mg) was dissolved in 4100 mg of water. 5 mg of Miglyol and 0.34 mg IPDI (48 eq per polymer chain) were dissolved in 5900 mg acetone. The **polymer** aqueous solution was then poured into the acetone solution to generate glyconanocapsules. After overnight, the 0.030 mL amino-turbobead was added into solution and reacted at 40 °C for overnight, and then characterized by DLS and TEM.

Functionalization of glyconanocapsule using cadaverine functionalized Alexa 555 probe. Glycopolymer (2.5 mg) was dissolved in 4100 mg of water. 5 mg of Miglyol and 0.34 mg IPDI (48 eq per polymer chain) were dissolved in 5900 mg. The **polymer** aqueous solution was then poured into the acetone solution to generate

glyconanocapsules. After overnight, the cadaverine functionalized Alexa 555 probe 0.03 mg amino-functionalized biotin (1 eq per polymer chain) was added into solution and reacted at 40 °C for overnight, and then characterized by DLS, fluorescent spectra and TEM.

Glyconanocapsules induced *E.Coli* aggregation.

E. Coli AIEC LF82 marked with GFP was incubated in the medium to produce a batch of bacteria solution (OD = 0.6). After evaporation of acetone, the aqueous solution of glyconanocapsules is concentrated to 33 and 66 μM. 10μL of capsules solution was added into 10μL bacteria solution with soft shaking. After 3h incubation, the solution was observed by confocal microscopy.

Kinetic study on capsules/bacteria aggregation was also performed in the similar process as above. 10μL of 66 μM capsules solution was added into 10μL bacteria solution with soft shaking. The observation of aggregates by confocal microscopy was performed after incubation for 30 min, 1 h, 2 h and 3 h.

5.8 Reference

1. Chong, J. M.; Heuft M. A.; Rabbat, P. *J. Org. Chem.* **2000**, *65*, 5837-5838.

2. Datsenko, K. A.; Wanner, B. L. *Proc Natl Acad Sci U S A*, **2000**, *97*, 6640-6645.

3. Li, Z.; Bouckaert, J.; Deboeck, F.; De Greve, H.; Hernalsteens, J. P. *Microbiology* **2012**, *158*, 736-745.

4. Darfeuille-Michaud, A.; Neut, C.; Barnich, N.; Lederman, E.; Di Martino, P.; Desreumaux, P.; Gambiez, L.; Joly, B.; Cortot, A.; Colombel, J.F. *Gastroenterology* **1998**, *115*, 1405-1413.

5. Chan, C. H.; Stanners, C.P. *Mol Ther*. **2004**, *9*, 775-785

General Conclusion

General Conclusion

In the frame of the fight against antibiotic resistance, this PhD work was dedicated to the rational design of *n*-heptyl α-D-mannose-based macromolecular anti-adhesives of type 1 piliated *E. coli* and to the evaluation of the capability of these glycomaterials to block bacterial adhesion.

In the first Chapter dedicated to the state of art in the field of carbohydrate-functionalized nanocapsules, we reviewed all the chemical and physical processes enabling to build synthetic glyconanocapsules from glycopolymers and polysaccharides. We highlighted that emulsification routes, self-assembly of amphiphilic copolymers or template strategies are routinely employed to generate such morphologies. We also pointed out that the nanoprecipitation process had not been used yet to build glyconanocapsules.

In Chapter 2, we described the preparation of well-defined linear and star-shaped glycopolymers. A first series of well-defined linear and star-shaped (3-arms and 8-arms) glycopolymers with multiple HM epitopes and different chain length (DP_n from 31 to 269) was generated via RAFT polymerization. To further investigate the influence of carbohydrate density and of the relative position of the carbohydrates on the polymer backbone on the anti-adhesive properties, a series of precise-defined glyco(co)polymers with 3 different microstructures (block, gradient and statistical) and compositions (molar ratios of GMA/HMM are about 2/1, 1/1 and 1/2) was also constructed. The presence of pendent oxirane groups allowed post-modification via epoxy-amine reaction to introduce new functionalities or ionic charges on the copolymers.

In Chapter 3, we investigated the capability on the glycopolymers described in Chapter 2 to block bacterial adhesion. We explored glycopolymer/FimH and glycopolymer/bacteria interactions and showed that HM-based glycopolymers efficiently inhibit bacterial adhesion and disrupt established cell-bacteria interactions in vitro at very low concentration (0.1 µM). On a valency corrected basis, HM-based

glycopolymers were proven to be respectively 10^2 and 10^6 times more potent than HM and D-mannose for their capacity to disrupt the binding of adherent-invasive *E. coli* to T84 intestinal epithelial cells. Anti-adhesive capacities of HM-based glycopolymers were finally demonstrated *ex vivo* in the colonic loop of a transgenic mouse model of CD.

In Chapter 4, we reported a simple and precise route to multi-functional glyconanocapsules constituted of anti-adhesive glycopolymers through nanoprecipitation. The phase diagrams of different solutes (hexadecane, miglyol 812 and glycopolymers) were precisely determined leading to the generation of monodisperse oil-filled and glycopolymer coated nanocapsules. The proposed route allows for elaborating the nanocapsules' walls, cross-linking and functionalizing the walls and encapsulating active compounds in a rapid one-pot procedure. Importantly, this approach to functional nanocapsules is not limited to PHMM homopolymers and can be transposed to other polymer systems to design new materials of practical applicability in different fields. For instance, miglyol-filled glyconanocapsules were conveniently built from P(HMM-co-GMA) and the presence of the oxirane groups was further exploited to carry out post-nanoprecipitation modifications with bio-relevant molecules (amino-functionalized biotin, fluorescent probes) or magnetic nanoparticles. As PHMM polymer chains, HMM-containing glyconanocapsules were proven to interact strongly with *E. coli* leading to the formation of large bacteria/nanocapsules clusters.

To pursue this work dealing with the preparation of potent multivalent FimH antagonists, it would be of particular interest to synthesize a new generation of glycomonomers based on thiazolylaminomannosides.[1] Indeed, our close collaborators, Sébastien G. Gouin, Julie Bouckaert and Arlette Darfeuille-Michaud recently demonstrated that this class of monovalent FimH antagonists leads to a 100 times increase in inhibitory potency compared to HM. It would also be valuable to explore other routes to multivalent inhibitors. Instead of recoursing to controlled radical polymerization techniques, the antagonists could be directly attached onto

biodegradable reactive polysaccharide backbones. As the HM-based glycopolymers have shown good results *in vitro* and *ex vivo*, it would be interesting to study more in details their anti-adhesive properties in *in vivo* conditions

In order to extend the scope of HM-based nanocapsules in drug delivery applications, we should first solve the problem of biodegradability of the present polymer shell. To overcome this issue, we propose to incorporate biodegradable groups into the glycopolymer backbones. For instance, it has been shown by Julien Nicolas and co-workers that controlled radical copolymerization of cyclic ketene acetals with common monomers such methacrylates or styrene affords the preparation of well-defined macromolecules with cleavable ester links within the chain.[2] Copolymerization of cyclic ketene acetals with HMM could thus give birth to biodegradable glycopolymers and could pave the way to the generation of biodegradable HM-based glyconanocapsules. Furthermore, it is also interesting to explore the preparation of multi-component nanocapsules through nanoprecipitation. Taking advantage of the simple and straightforward process described in Chapter 4, polymers sharing a same domain of nanoprecipitation could be simultaneously coprecipitate to form multi-component nanocapsules. The success of this approach would extremely simplify the techniques to prepare multi-component nanocapsules, and accelerate the progress in the development of multi-functional nanocapsules.

1. Brument, S.; Sivignon, A.; Dumych, T. I.;Moreau, N.; Roos, G.; Guerardel, Y.; Chalopin, T.;Deniaud, D.;Bilyy, R. O.; Darfeuille-Michaud, A.;Bouckaert, J.; Gouin, S.G. *J. Med. Chem.*, 2013, **56**, 5395-5406.

2. Tardy, A.; Delplace, V.; Siri, D.; Lefay, C.; Harrisson, S.; de Fatima Albergaria Pereira, B.; Charles, L.; Gigmes, D.; Nicolas, J.; Guillaneuf, Y. *Polym. Chem.* 2013, **4**, 4776-4787.

Annex

Annex

Annex 1. NMR Spectrums

Figure A1. ^{1}H NMR and ^{13}C NMR of azido-functionalized mannoside (4, $CDCl_3$)

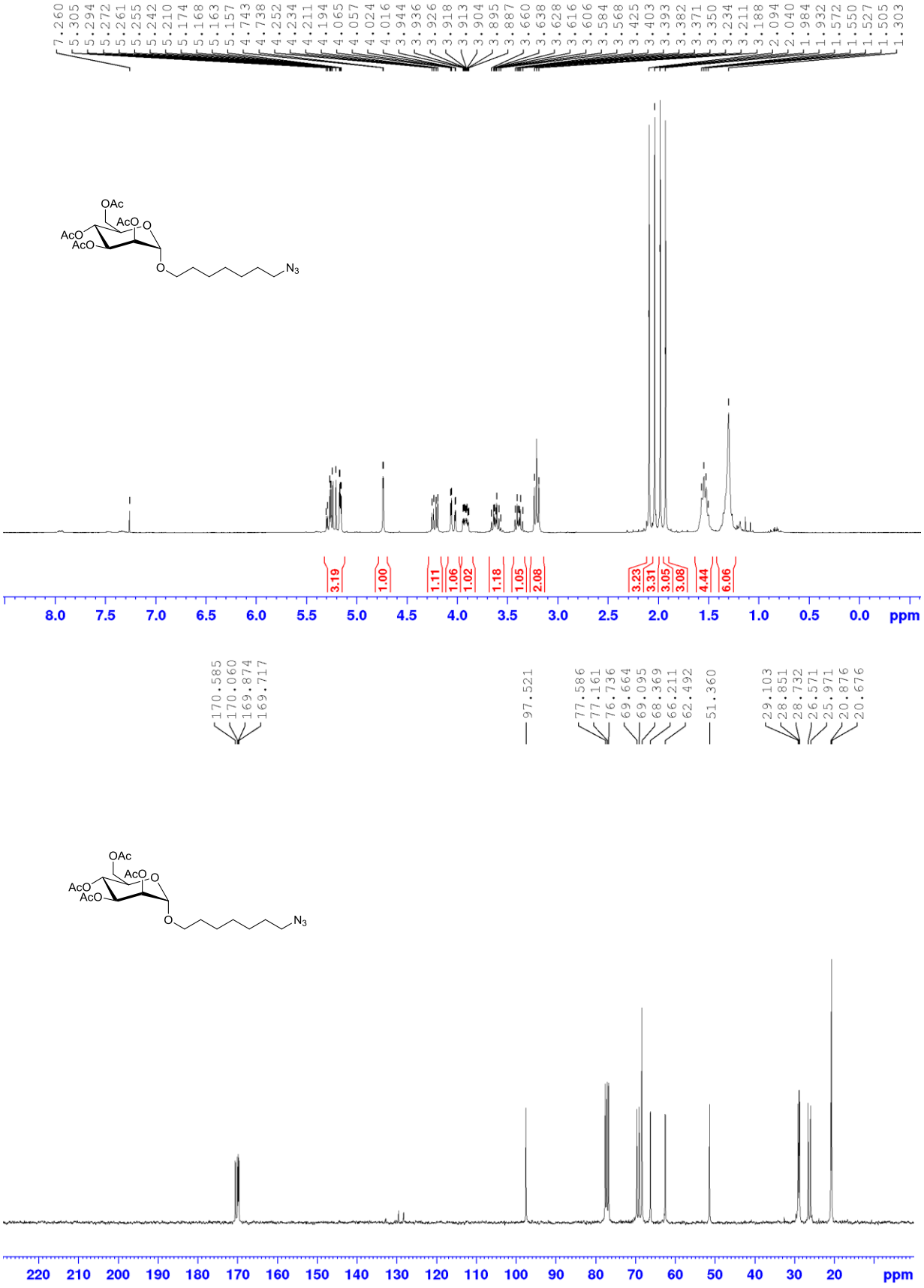

Figure A2. ^{1}H NMR and ^{13}C NMR of per-acetylated HMM ($CDCl_3$)

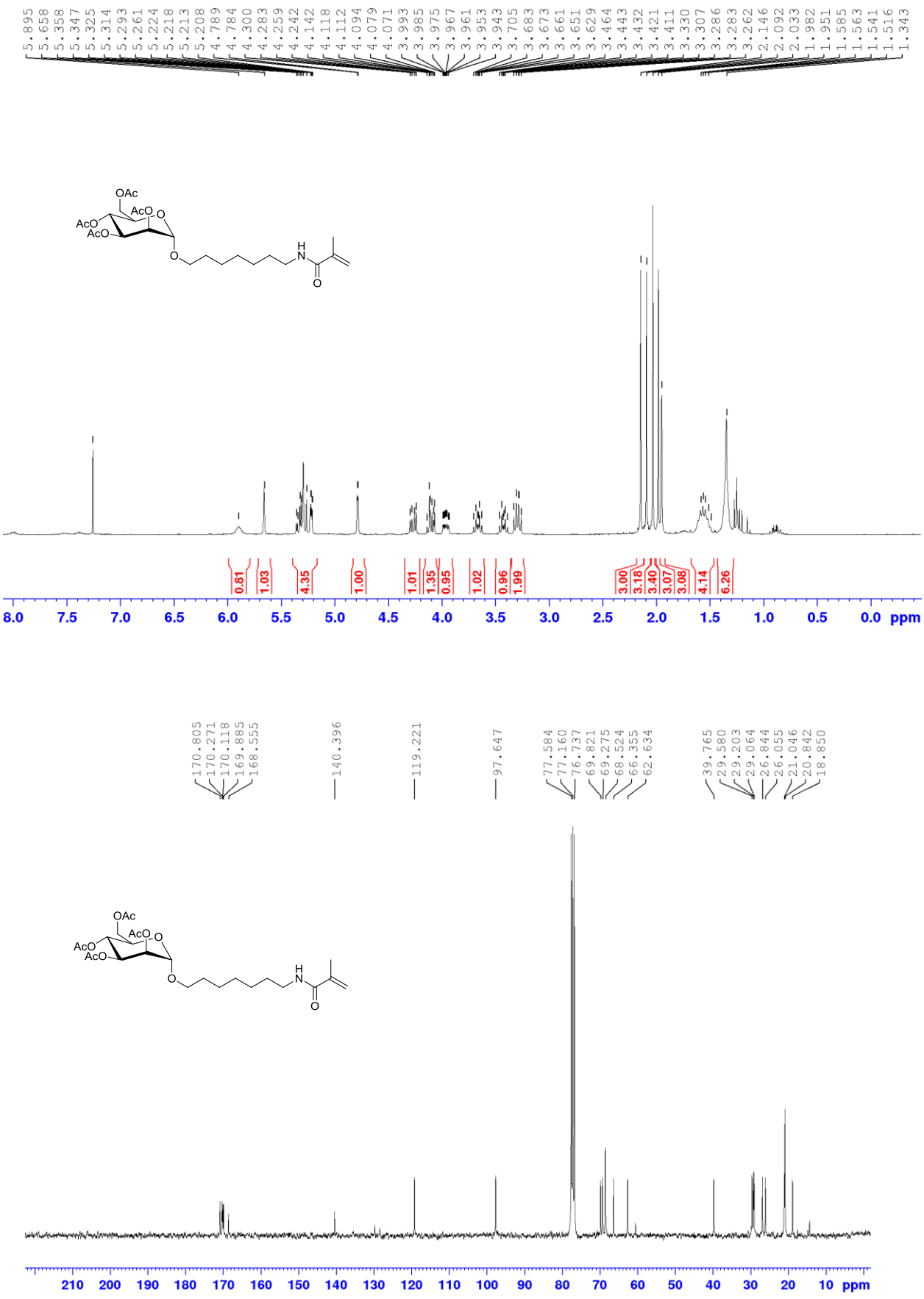

Figure A3. ^{1}H NMR and ^{13}C NMR of azido-functionalized mannoside (8, $CDCl_3$)

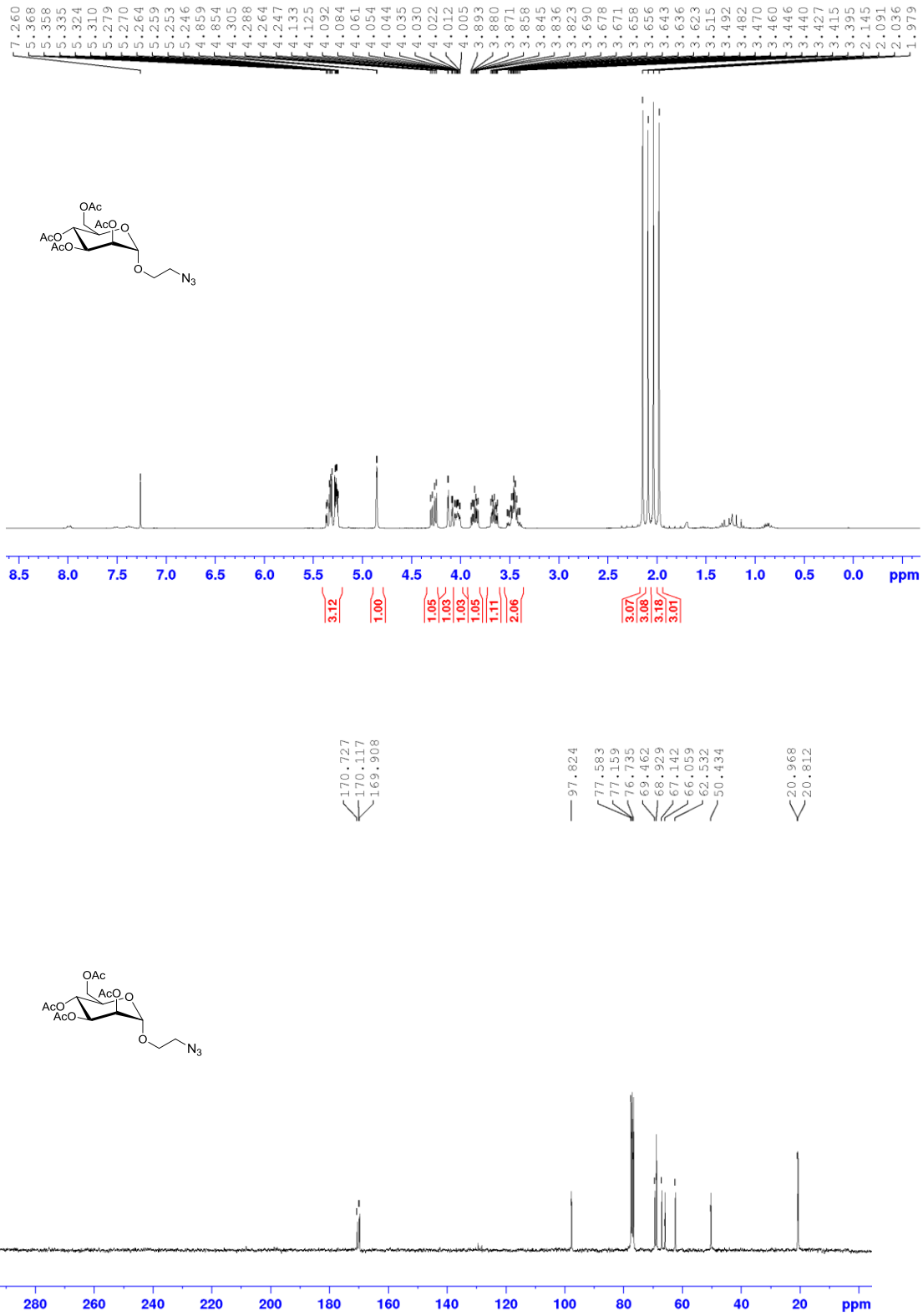

Figure A4. ^{1}H NMR and ^{13}C NMR of per-acetylated EMM ($CDCl_3$)

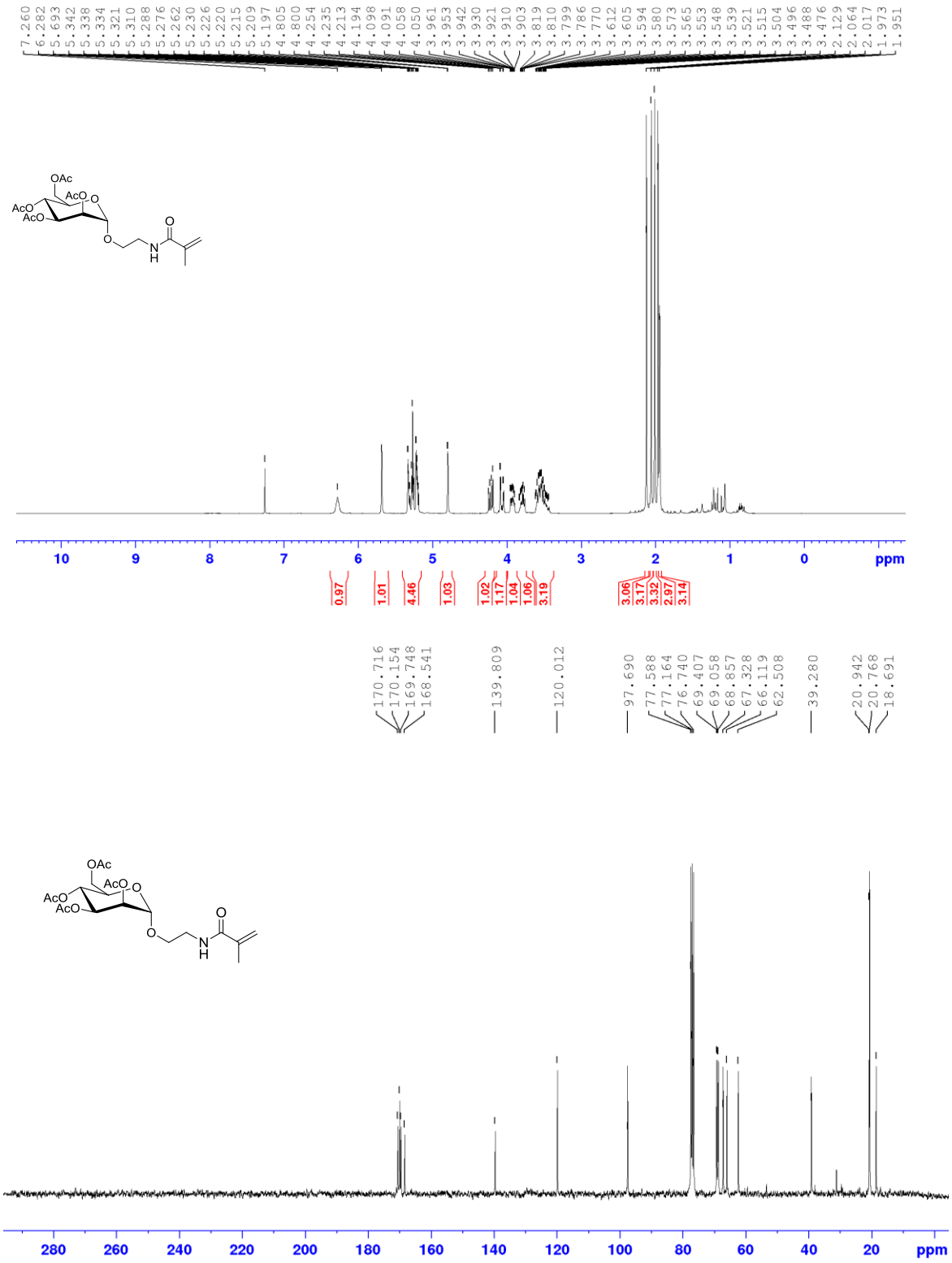

Figure A5. ^{1}H NMR and ^{13}C NMR of EMM (D_2O)

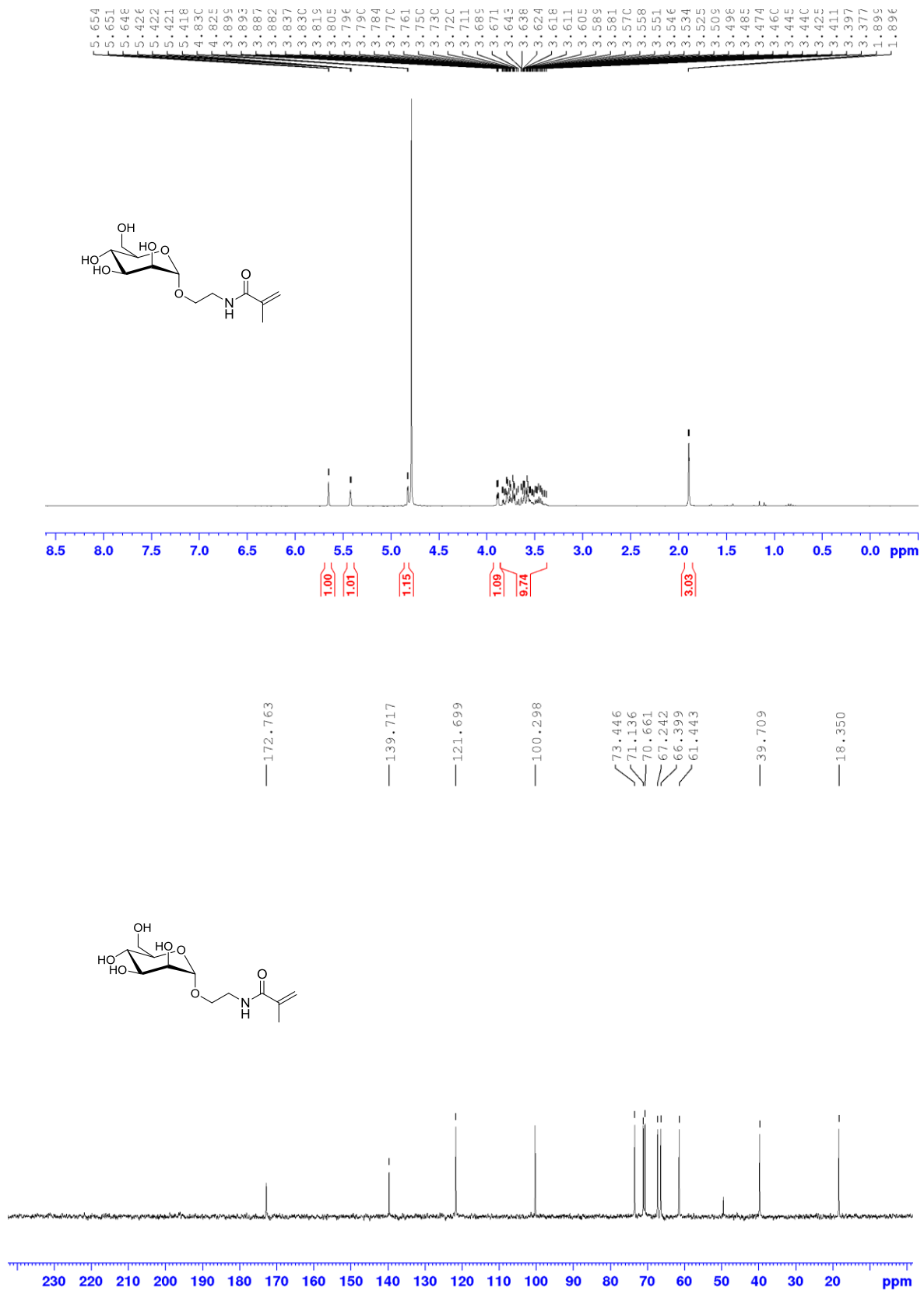

Figure A6. ^{1}H NMR and ^{13}C NMR of the NHS-functionalized CPADB (CDCl3)

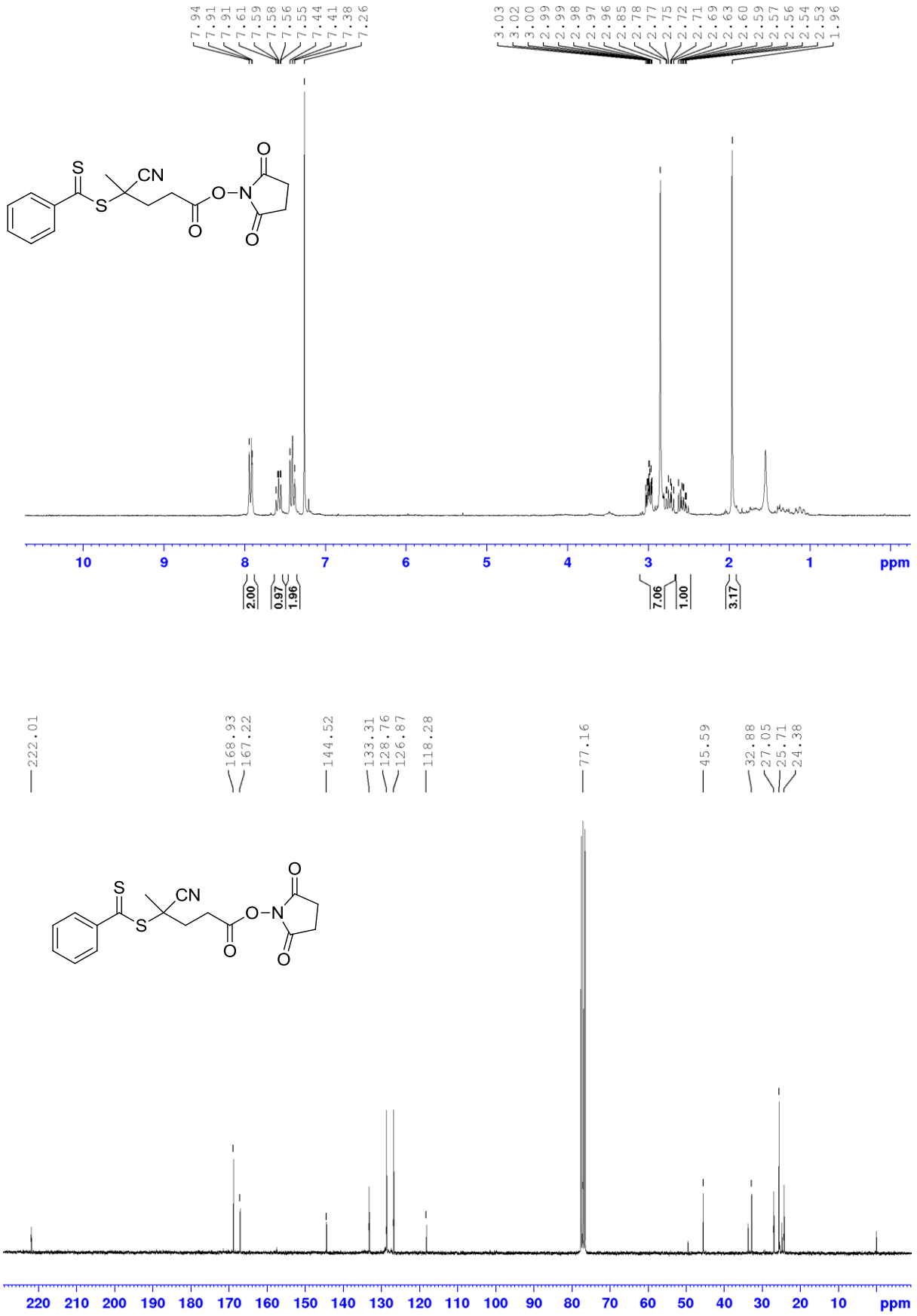

Figure A7. ^{1}H NMR of chain-end modification of DTB groups for glycopolymer L31 (D_2O): (A) Spectra of polymer before reaction; (B) Spectra of polymer after reaction.

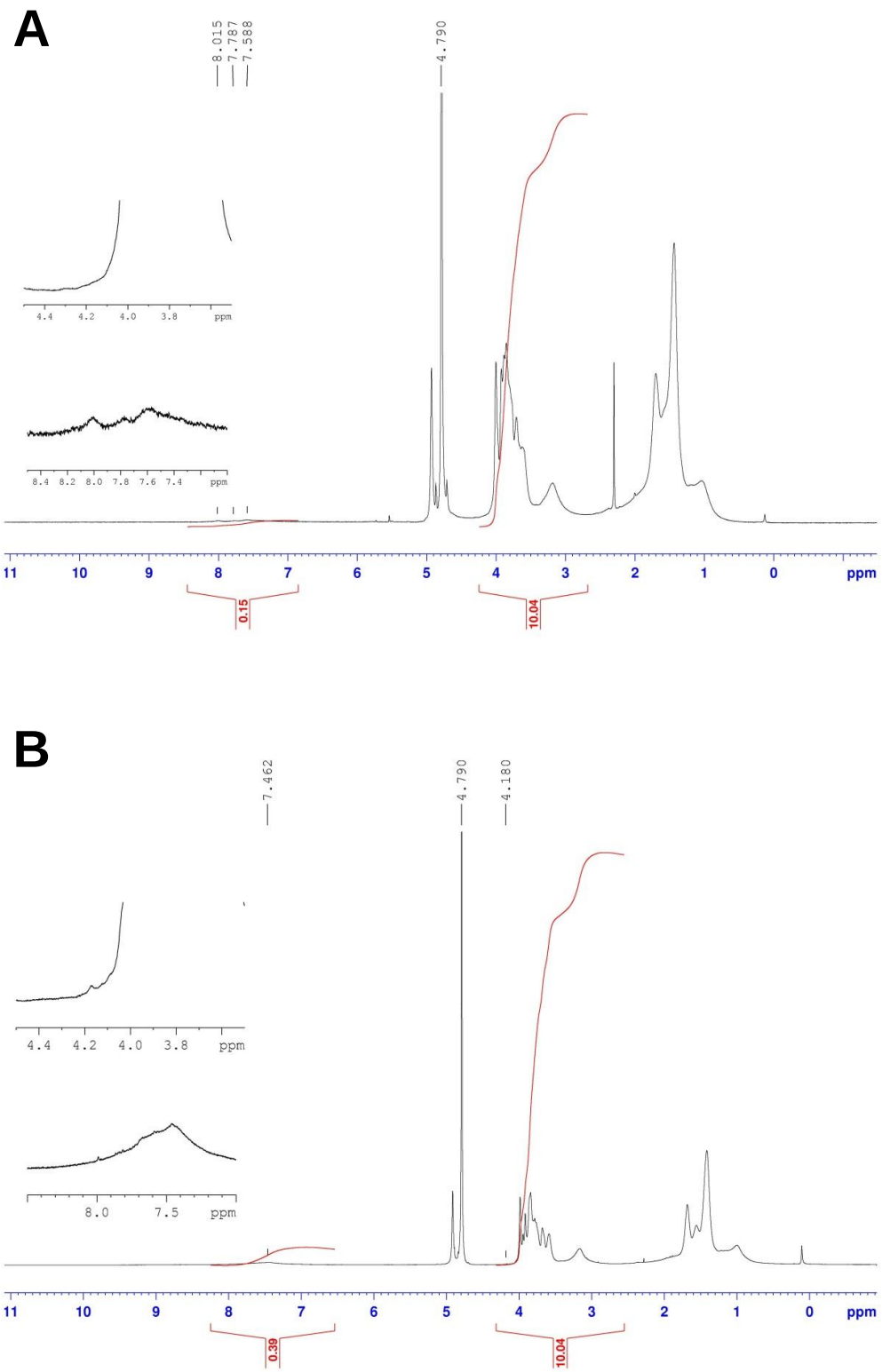

Annex 2. Pseudo first-order kinetic plots of homopolymerization (conditions were given in Chapter 2).

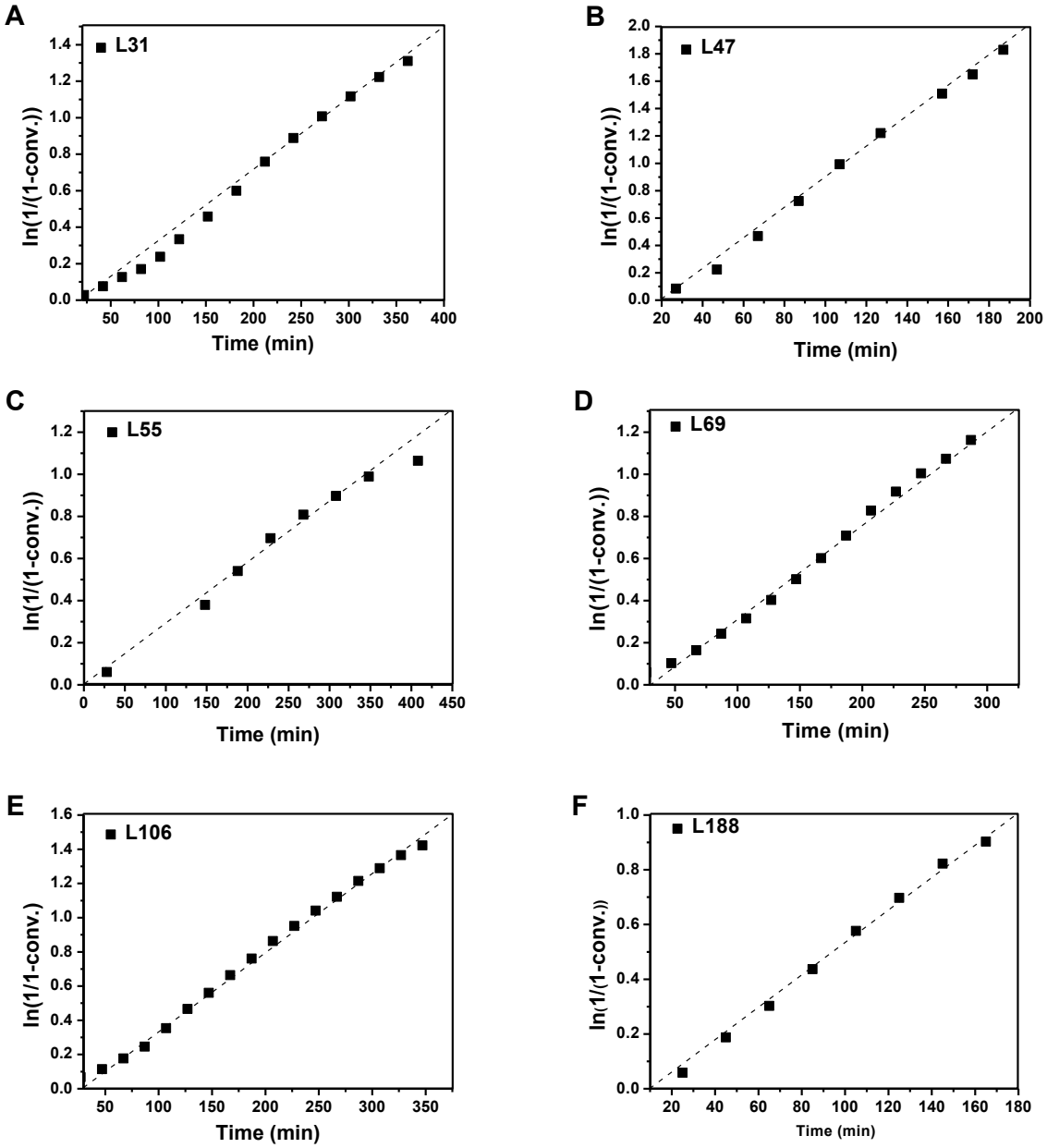

H

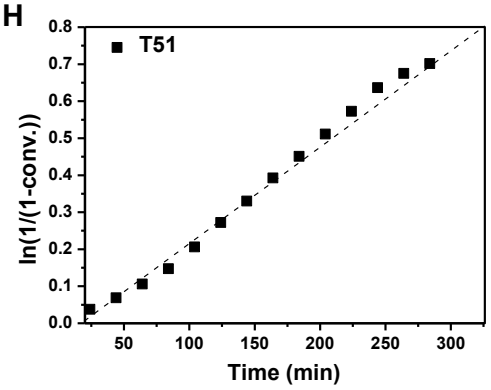

I

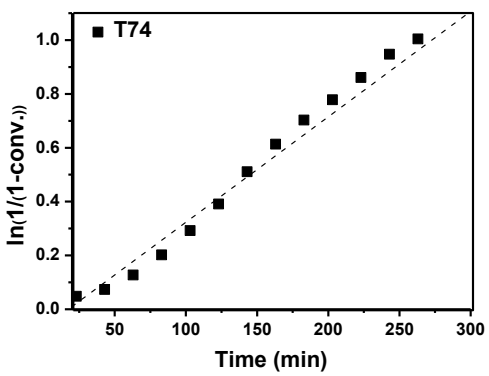

J

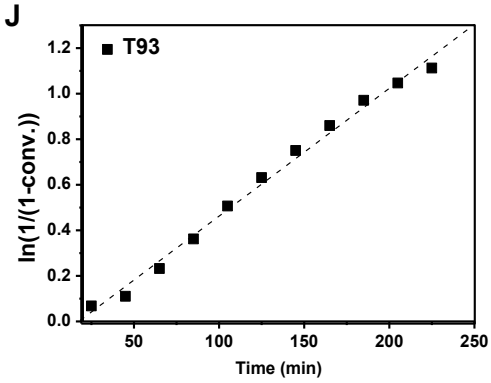

K

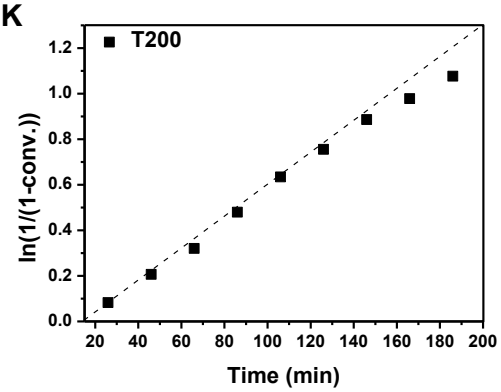

L

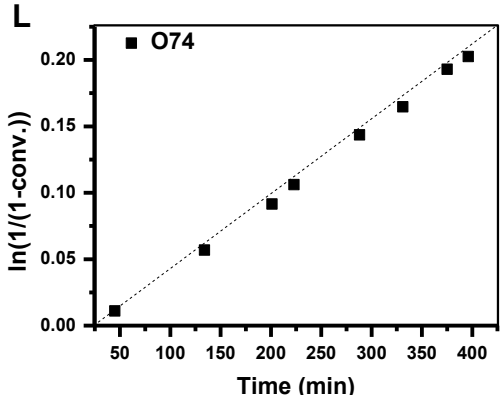

M

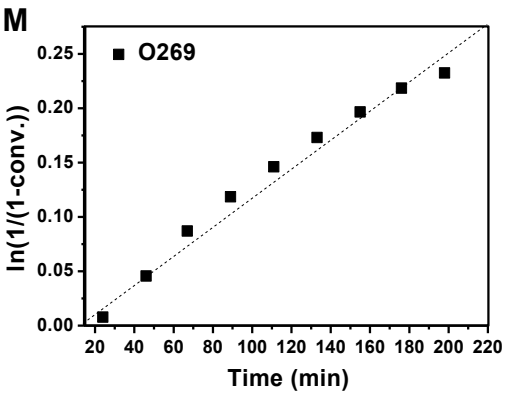

Annex 3. Pseudo first-order kinetic plots of synthesis of block copolymers (conditions given in Chapter 2).

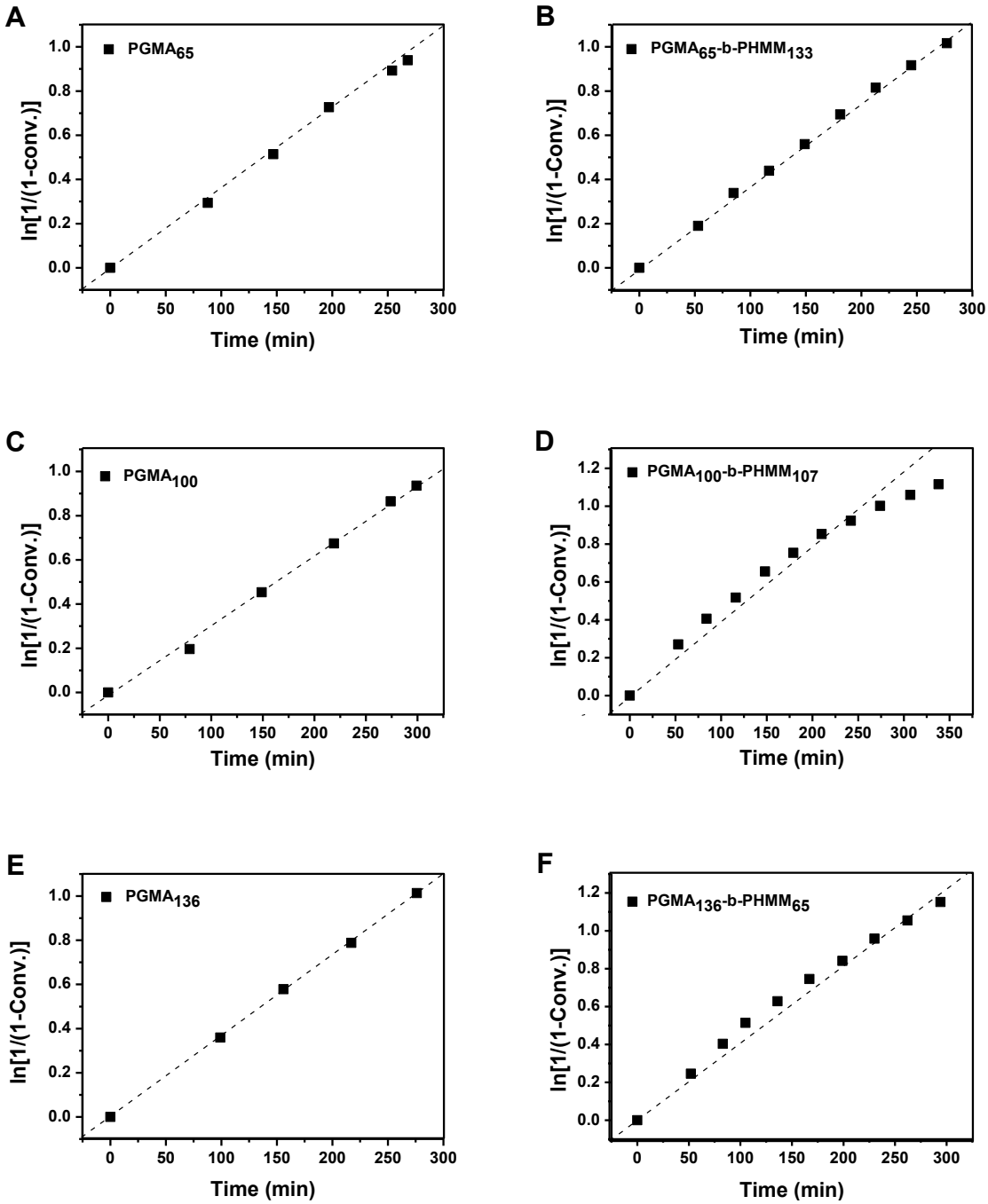

Annex 4. Pseudo first-order kinetic plots of synthesis of gradient and statistical copolymers

(condition given in Chapter 2).

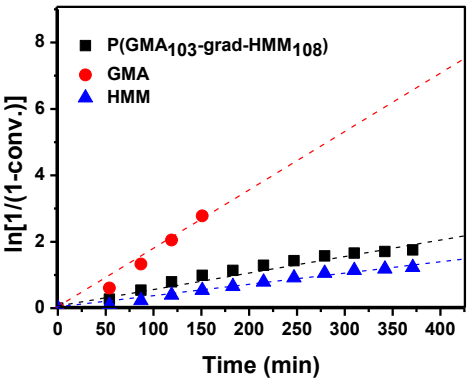

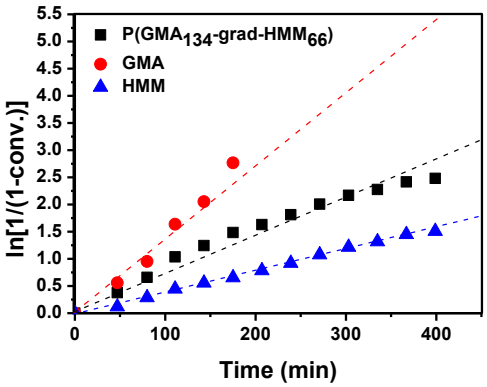

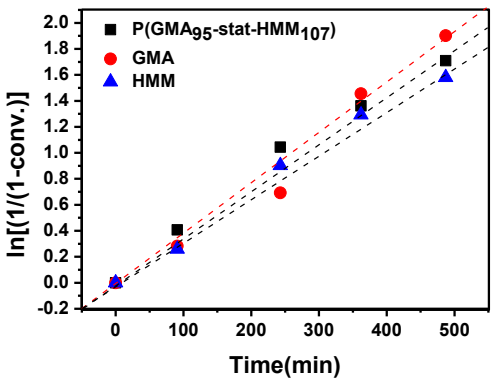

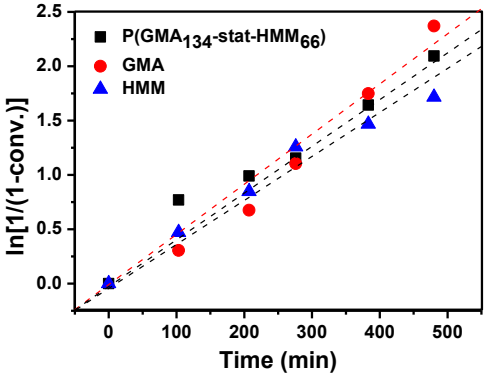

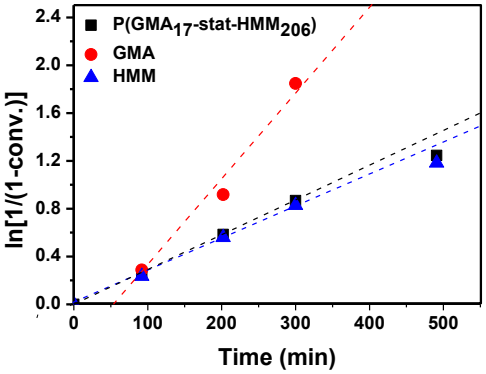

Annex 5. F_{HMM} versus conversion plots of gradient and statistical copolymers (condition given in Chapter 2)

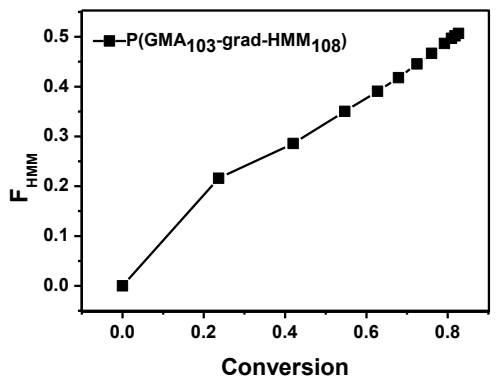

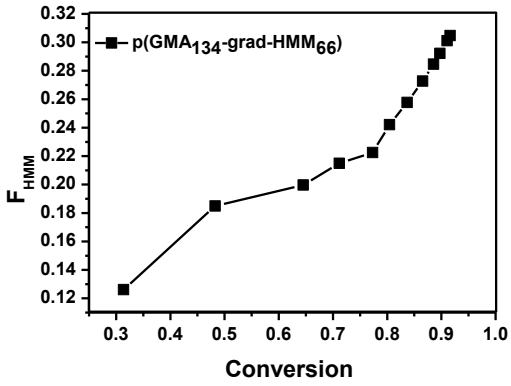

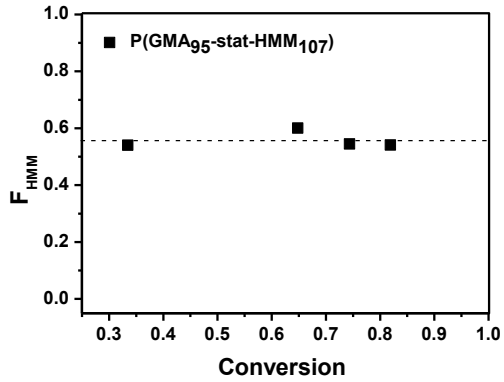

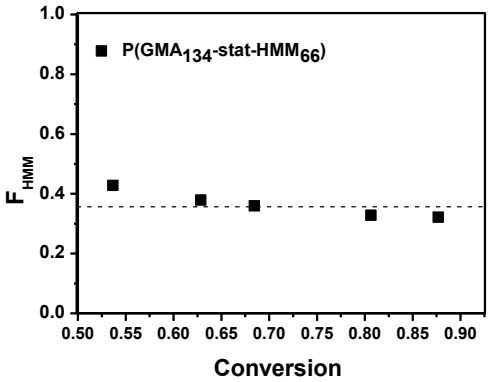

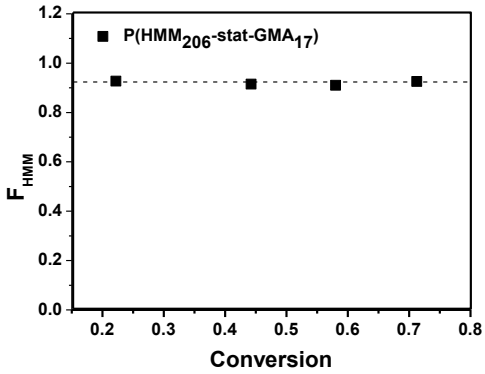

Annex 6. GPC traces of acetylated glyco-copolymers.

(THF as eluent, PS calibration)

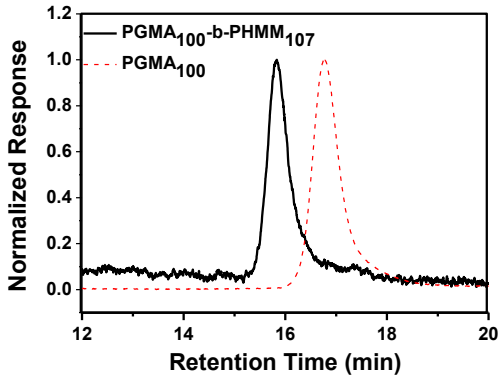

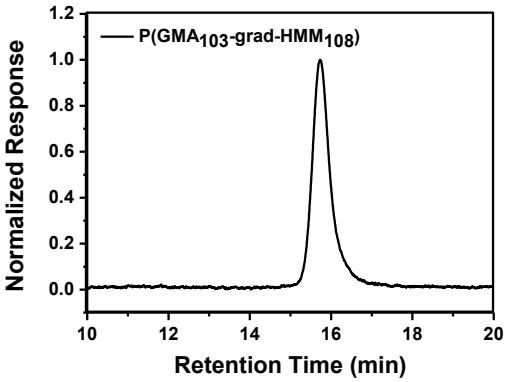

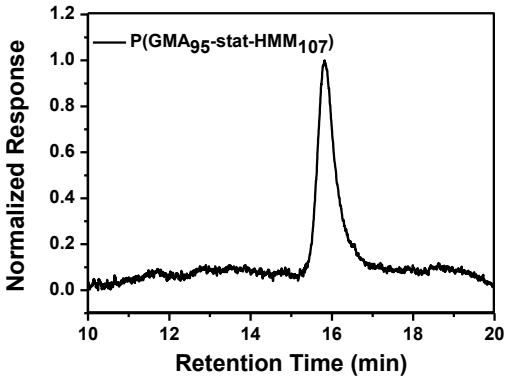

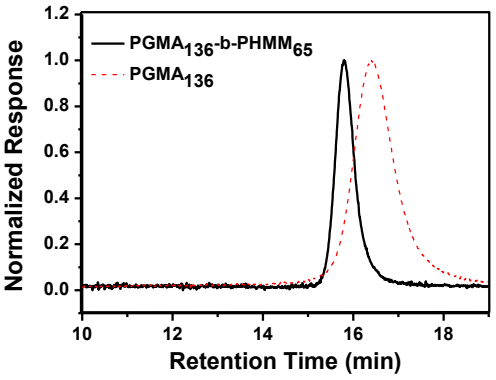

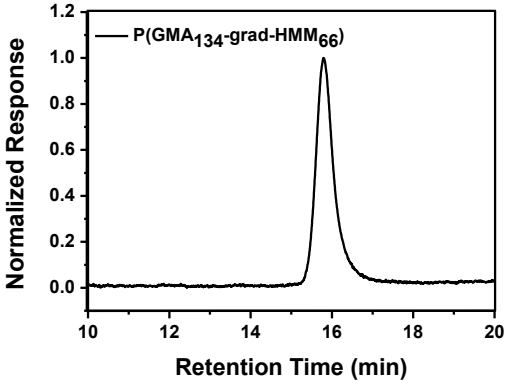

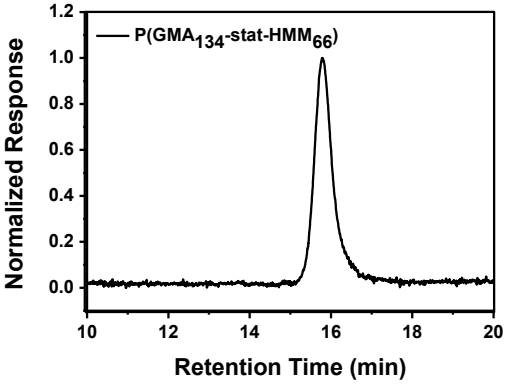

Annex 7. DLS of FimH-PHMM aqueous mixtures (HEPES buffer) obtained by sequential addition of glycopolymers.

L31

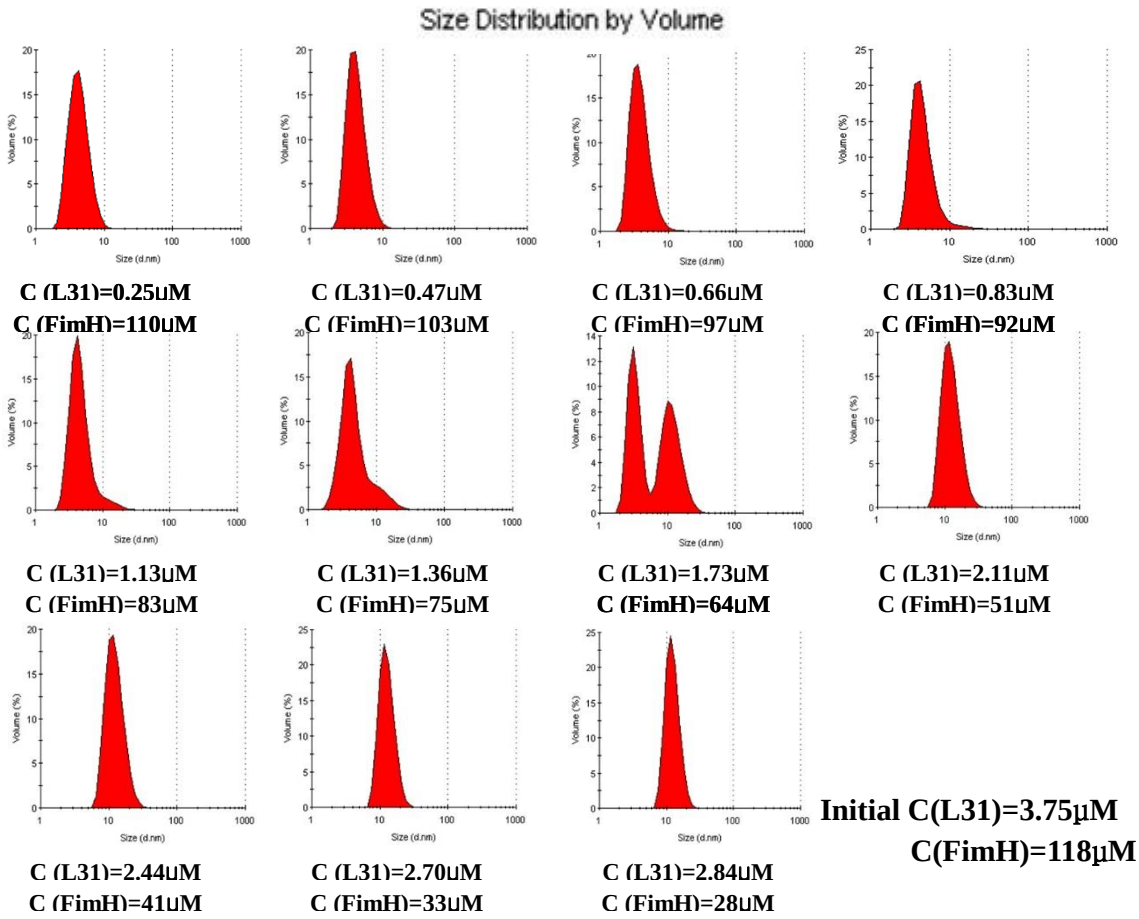

C (L31)=0.25µM
C (FimH)=110µM

C (L31)=0.47µM
C (FimH)=103µM

C (L31)=0.66µM
C (FimH)=97µM

C (L31)=0.83µM
C (FimH)=92µM

C (L31)=1.13µM
C (FimH)=83µM

C (L31)=1.36µM
C (FimH)=75µM

C (L31)=1.73µM
C (FimH)=64µM

C (L31)=2.11µM
C (FimH)=51µM

C (L31)=2.44µM
C (FimH)=41µM

C (L31)=2.70µM
C (FimH)=33µM

C (L31)=2.84µM
C (FimH)=28µM

Initial C(L31)=3.75µM
C(FimH)=118µM

L47 Initial C(L47)=2.44µM C(FimH)=83µM

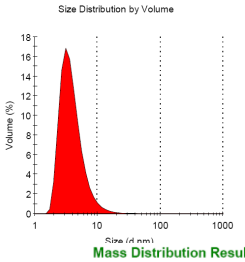

Mass Distribution Results

	%Ma...	Mean (n...	Mode (n...	StD (n...	%Pd	MW (kDa)*
Peak...	100.0	4.154	3.122	2.374	57.2	18.6
Peak ...	0.0	0.000	0.000	0.000	0	0.00
Peak ...	0.0	0.000	0.000	0.000	0	0.00

C (L47)=0.43µM
C (FimH)=68µM

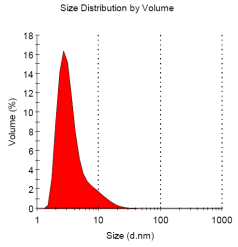

Mass Distribution Results

	%Ma...	Mean (n...	Mode (n...	StD (n...	%Pd	MW (kDa)*
Peak...	100.0	4.091	2.696	3.160	77.2	18.0
Peak ...	0.0	0.000	0.000	0.000	0	0.00
Peak ...	0.0	0.000	0.000	0.000	0	0.00

C (L47)=0.73µM
C (FimH)=58µM

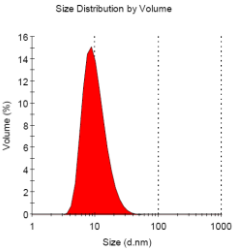

Mass Distribution Results

	%Ma...	Mean (n...	Mode (n...	StD (n...	%Pd	MW (kDa)*
Peak...	100.0	10.50	8.721	4.828	46.0	163
Peak ...	0.0	0.000	0.000	0.000	0	0.00
Peak ...	0.0	0.000	0.000	0.000	0	0.00

C (L47)=1.12µM
C (FimH)=45µM

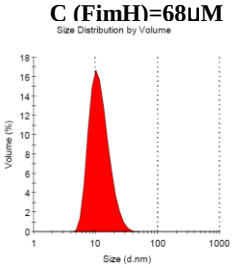

Mass Distribution Results

	%Ma...	Mean (n...	Mode (n...	StD (n...	%Pd	MW (kDa)*
Peak...	100.0	12.16	10.10	4.799	39.5	230
Peak ...	0.0	0.000	0.000	0.000	0	0.00
Peak ...	0.0	0.000	0.000	0.000	0	0.00

C (L47)=1.30µM
C (FimH)=39µM

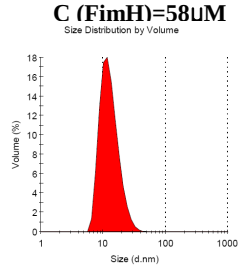

Mass Distribution Results

	%Ma...	Mean (n...	Mode (n...	StD (n...	%Pd	MW (kDa)*
Peak...	100.0	13.14	11.70	4.801	36.5	275
Peak ...	0.0	3855	3580	1115	28.9	1.63e8
Peak ...	0.0	0.000	0.000	0.000	0	0.00

C (L47)=1.54µM
C (FimH)=31µM

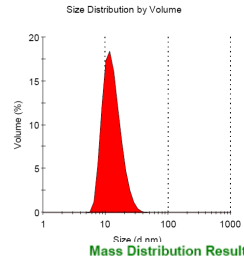

Mass Distribution Results

	%Ma...	Mean (n...	Mode (n...	StD (n...	%Pd	MW (kDa)*
Peak...	100.0	13.18	11.70	4.639	35.2	278
Peak ...	0.0	3870	3580	1142	29.5	1.65e8
Peak ...	0.0	0.000	0.000	0.000	0	0.00

C (L47)=1.85µM
C (FimH)=20µM

L55 Initial C(L55)=2.09µM C(FimH)=83µM

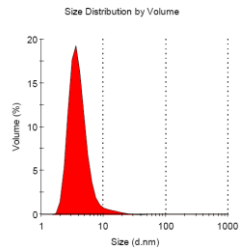

Mass Distribution Results

	%Ma...	Mean (n...	Mode (n...	StD (n...	%Pd	MW (kDa)*
Peak...	100.0	4.360	3.615	4.506	103.4	20.8
Peak ...	0.0	0.000	0.000	0.000	0	0.00
Peak ...	0.0	0.000	0.000	0.000	0	0.00

C (L55)=0.26µM
C (FimH)=72µM

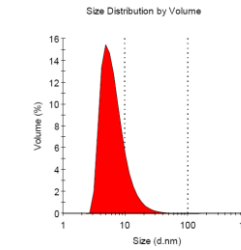

Mass Distribution Results

	%Ma...	Mean (n...	Mode (n...	StD (n...	%Pd	MW (kDa)*
Peak...	100.0	7.399	4.849	10.36	140.0	71.9
Peak ...	0.0	0.000	0.000	0.000	0	0.00
Peak ...	0.0	0.000	0.000	0.000	0	0.00

C (L55)=0.64µM
C (FimH)=64µM

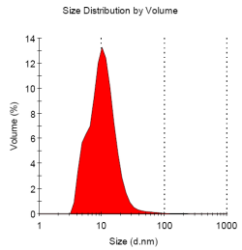

Mass Distribution Results

	%Ma...	Mean (n...	Mode (n...	StD (n...	%Pd	MW (kDa)*
Peak...	100.0	11.71	10.10	10.33	88.3	210
Peak ...	0.0	0.000	0.000	0.000	0	0.00
Peak ...	0.0	0.000	0.000	0.000	0	0.00

C (L55)=0.76µM
C (FimH)=53µM

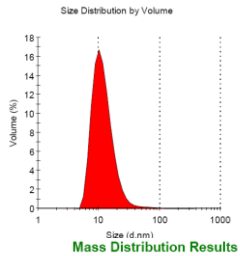

Mass Distribution Results

	%Ma...	Mean (n...	Mode (n...	StD (n...	%Pd	MW (kDa)*
Peak...	100.0	13.20	10.10	13.27	100.6	278
Peak ...	0.0	4171	4801	1067	25.6	1.97e8
Peak ...	0.0	0.000	0.000	0.000	0	0.00

C (L55)=1.05µM
C (FimH)=41µM

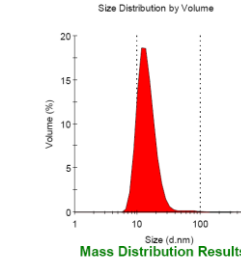

Mass Distribution Results

	%Ma...	Mean (n...	Mode (n...	StD (n...	%Pd	MW (kDa)*
Peak...	1.5	99.36	58.77	60.88	61.3	3.13e4
Peak ...	98.5	14.42	11.70	5.224	36.2	342
Peak ...	0.0	5184	5560	737.0	14.2	3.27e8

C (L55)=1.32µM
C (FimH)=31µM

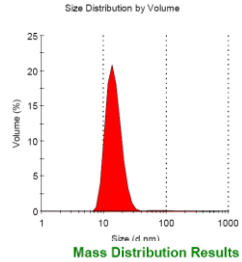

Mass Distribution Results

	%Ma...	Mean (n...	Mode (n...	StD (n...	%Pd	MW (kDa)*
Peak...	2.2	166.1	78.82	137.0	82.5	1.04e5
Peak ...	97.6	14.81	13.54	4.402	29.7	365
Peak ...	0.2	3959	4145	1116	28.2	1.74e8

C (L55)=1.58µM
C (FimH)=20µM

L69 Initial C(L69)=1.67µM C(FimH)=83µM

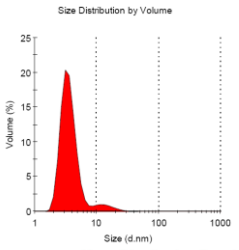

Mass Distribution Results

	%Ma...	Mean (n...	Mode (n...	StD (n...	%Pd	MW (kDa)*
Peak...	6.2	14.83	11.70	6.051	40.8	366
Peak ...	0.0	284.0	295.3	162.5	57.2	3.66e5
Peak ...	93.8	3.633	3.122	1.112	30.6	13.6

C (L69)=0.77µM
C (FimH)=46µM

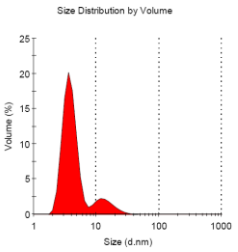

Mass Distribution Results

	%Ma...	Mean (n...	Mode (n...	StD (n...	%Pd	MW (kDa)*
Peak...	85.8	3.870	3.615	1.013	26.2	15.8
Peak ...	14.1	14.40	11.70	5.866	40.7	341
Peak ...	0.0	194.8	122.4	115.8	59.5	1.51e5

C (L69)=0.98µM
C (FimH)=34µM

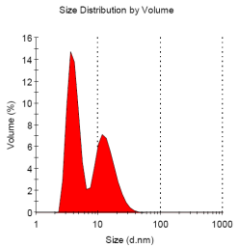

Mass Distribution Results

	%Ma...	Mean (n...	Mode (n...	StD (n...	%Pd	MW (kDa)*
Peak...	43.9	13.98	11.70	5.808	41.5	318
Peak ...	0.1	173.7	105.7	100.1	57.7	1.16e5
Peak ...	0.1	3511	3091	1148	32.7	1.31e8

C (L69)=1.07µM
C (FimH)=31µM

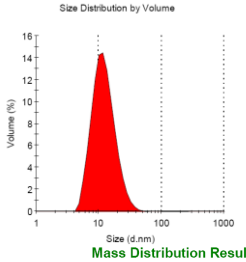

Mass Distribution Results

	%Ma...	Mean (n...	Mode (n...	StD (n...	%Pd	MW (kDa)*
Peak...	99.8	12.90	11.70	5.789	44.9	264
Peak ...	0.1	202.5	190.1	113.3	56.0	1.66e5
Peak ...	0.0	4284	4801	1061	24.8	2.09e8

C (L69)=1.18µM
C (FimH)=24µM

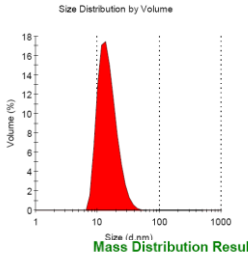

Mass Distribution Results

	%Ma...	Mean (n...	Mode (n...	StD (n...	%Pd	MW (kDa)*
Peak...	99.6	15.24	13.54	5.753	37.8	390
Peak ...	0.3	235.0	220.2	140.7	59.9	2.35e5
Peak ...	0.1	3781	3580	1127	29.8	1.56e8

C (L69)=1.32µM
C (FimH)=18µM

L106 Initial C(L106)=1.08µM C(FimH)=83µM

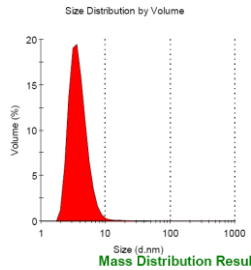

Mass Distribution Results

	%Ma...	Mean (n...	Mode (n...	StD (n...	%Pd	MW (kDa)*
Peak...	100.0	4.035	3.615	2.378	58.9	17.4
Peak ...	0.0	0.000	0.000	0.000	0	0.00
Peak ...	0.0	0.000	0.000	0.000	0	0.00

C (L106)=0.14µM
C (FimH)=73µM

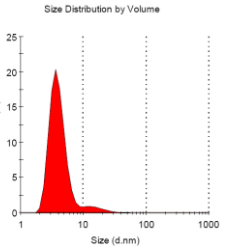

Mass Distribution Results

	%Ma...	Mean (n...	Mode (n...	StD (n...	%Pd	MW (kDa)*
Peak...	5.7	17.71	11.70	14.49	81.8	554
Peak ...	94.3	4.037	3.615	1.320	32.7	17.4
Peak ...	0.0	0.000	0.000	0.000	0	0.00

C (L106)=0.32µM
C (FimH)=58µM

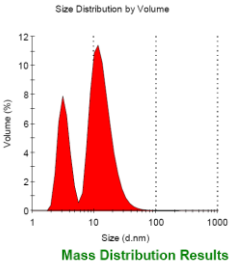

Mass Distribution Results

	%Ma...	Mean (n...	Mode (n...	StD (n...	%Pd	MW (kDa)*
Peak...	29.5	3.349	3.122	0.7415	22.1	11.2
Peak ...	70.5	14.51	11.70	10.38	71.5	347
Peak ...	0.0	0.000	0.000	0.000	0	0.00

C (L106)=0.42µM
C (FimH)=51µM

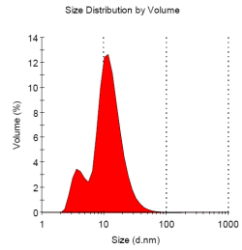

Mass Distribution Results

	%Ma...	Mean (n...	Mode (n...	StD (n...	%Pd	MW (kDa)*
Peak...	16.1	4.052	3.615	0.9298	22.9	17.6
Peak ...	83.9	14.15	11.70	10.46	73.9	327
Peak ...	0.0	0.000	0.000	0.000	0	0.00

C (L106)=0.54µM
C (FimH)=42µM

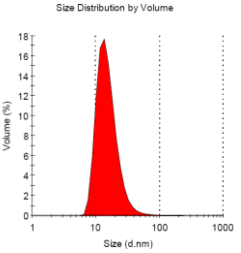

Mass Distribution Results

	%Ma...	Mean (n...	Mode (n...	StD (n...	%Pd	MW (kDa)*
Peak...	100.0	16.17	13.54	10.25	63.4	448
Peak ...	0.0	0.000	0.000	0.000	0	0.00
Peak ...	0.0	0.000	0.000	0.000	0	0.00

C (L106)=0.68µM
C (FimH)=31µM

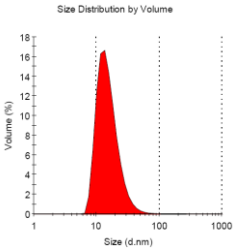

Mass Distribution Results

	%Ma...	Mean (n...	Mode (n...	StD (n...	%Pd	MW (kDa)*
Peak...	100.0	16.36	13.54	11.09	67.8	460
Peak ...	0.0	0.000	0.000	0.000	0	0.00
Peak ...	0.0	0.000	0.000	0.000	0	0.00

C (L106)=0.82µM
C (FimH)=20µM

Linear 188 **Initial C(L188)=0.61µM C(FimH)=83µM** **Hepes Buffer, 20℃**

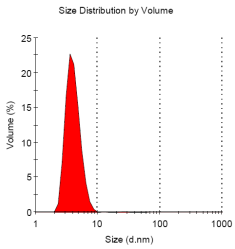

Mass Distribution Results

	%Ma...	Mean (n...	Mode (n...	StD (n...	%Pd	MW (kDa)*
Peak...	99.3	4.149	3.615	1.113	26.8	18.6
Peak ...	0.6	34.34	24.36	21.13	61.5	2610
Peak ...	0.0	487.9	458.7	253.9	52.0	1.30e6

C (L188)=0.09µM

C (FimH)=73µM

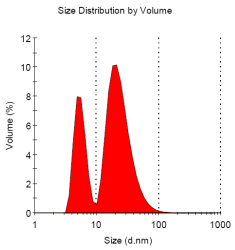

Mass Distribution Results

	%Ma...	Mean (n...	Mode (n...	StD (n...	%Pd	MW (kDa)*
Peak...	69.0	27.01	21.04	28.56	105.7	1490
Peak ...	31.0	5.593	4.849	1.298	23.2	37.3
Peak ...	0.1	4110	4145	1079	26.3	1.90e8

C (L188)=0.25µM

C (FimH)=48µM

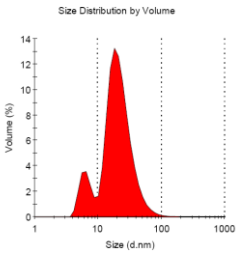

Mass Distribution Results

	%Ma...	Mean (n...	Mode (n...	StD (n...	%Pd	MW (kDa)*
Peak...	13.5	6.392	6.503	1.240	19.4	51.0
Peak ...	86.2	24.13	18.17	16.39	67.9	1140
Peak ...	0.3	574.8	342.0	279.2	48.6	1.90e6

C (L188)=0.39µM

C (FimH)=30µM

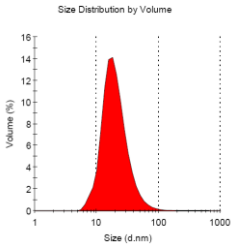

Mass Distribution Results

	%Ma...	Mean (n...	Mode (n...	StD (n...	%Pd	MW (kDa)*
Peak...	100.0	22.96	18.17	25.31	110.2	1020
Peak ...	0.0	0.000	0.000	0.000	0	0.00
Peak ...	0.0	0.000	0.000	0.000	0	0.00

C (L188)=0.43µM

C (FimH)=24µM

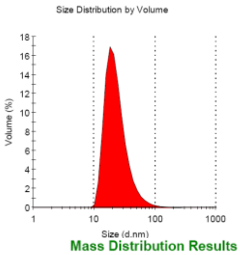

Mass Distribution Results

	%Ma...	Mean (n...	Mode (n...	StD (n...	%Pd	MW (kDa)*
Peak...	100.0	24.86	18.17	15.37	61.8	1230
Peak ...	0.0	0.000	0.000	0.000	0	0.00
Peak ...	0.0	0.000	0.000	0.000	0	0.00

C (L188)=0.50µM

C (FimH)=15µM

T51 **Initial C(T51)=2.25µM C(FimH)=83µM**

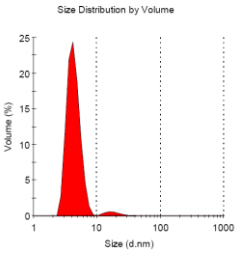

Mass Distribution Results

	%Ma...	Mean (n...	Mode (n...	StD (n...	%Pd	MW (kDa)*
Peak...	0.1	162.4	105.7	97.12	59.8	9.89e4
Peak ...	3.1	18.38	15.69	5.747	31.3	604
Peak ...	96.8	4.343	4.187	1.022	23.5	20.7

C (T51)=0.28µM

C (FimH)=73µM

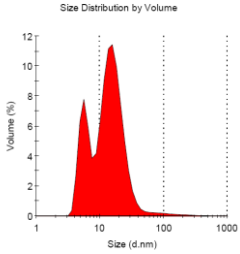

Mass Distribution Results

	%Ma...	Mean (n...	Mode (n...	StD (n...	%Pd	MW (kDa)*
Peak...	25.9	5.738	5.615	1.039	18.1	39.6
Peak ...	74.1	19.70	15.69	25.09	127.3	711
Peak ...	0.0	4304	4801	1024	23.8	2.12e8

C (T51)=0.68µM

C (FimH)=58µM

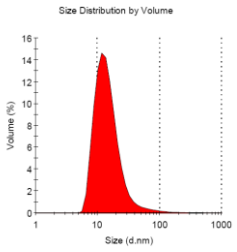

Mass Distribution Results

	%Ma...	Mean (n...	Mode (n...	StD (n...	%Pd	MW (kDa)*
Peak...	99.9	17.29	11.70	20.90	120.9	524
Peak ...	0.1	4816	4801	920.5	19.1	2.75e8
Peak ...	0.0	0.000	0.000	0.000	0	0.00

C (T51)=0.93µM

C (FimH)=48µM

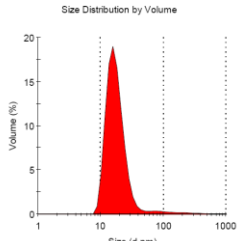

Mass Distribution Results

	%Ma...	Mean (n...	Mode (n...	StD (n...	%Pd	MW (kDa)*
Peak...	3.7	186.5	68.06	166.9	89.5	1.37e5
Peak ...	96.1	17.84	15.69	6.618	37.1	563
Peak ...	0.1	4259	4801	1053	24.7	2.06e8

C (T51)=1.70µM

C (FimH)=20µM

T74 **Initial C(T74)=1.55µM C(FimH)=83µM**

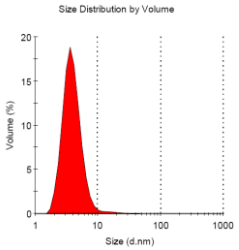

Mass Distribution Results

	%Ma...	Mean (n...	Mode (n...	StD (n...	%Pd	MW (kDa)*
Peak...	100.0	4.257	3.615	3.920	92.1	19.7
Peak ...	0.0	0.000	0.000	0.000	0	0.00
Peak ...	0.0	0.000	0.000	0.000	0	0.00

C (T74)=0.19µM

C (FimH)=73µM

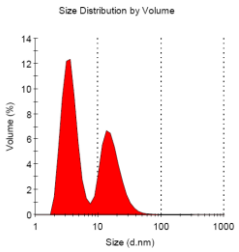

	%Ma...	Mean (n...	Mode (n...	StD (n...	%Pd	MW (kDa)*
Peak...	59.8	3.644	3.615	1.078	29.6	13.7
Peak ...	40.2	18.12	13.54	15.48	85.4	584
Peak ...	0.0	0.000	0.000	0.000	0	0.00

C (T74)=0.47µM

C (FimH)=58µM

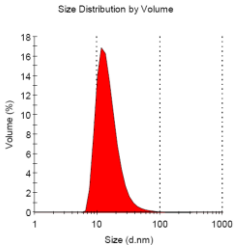

	%Ma...	Mean (n...	Mode (n...	StD (n...	%Pd	MW (kDa)*
Peak...	100.0	16.26	11.70	13.42	82.6	453
Peak ...	0.0	0.000	0.000	0.000	0	0.00
Peak ...	0.0	0.000	0.000	0.000	0	0.00

C (T74)=0.64µM

C (FimH)=48µM

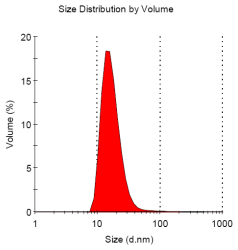

	%Ma...	Mean (n...	Mode (n...	StD (n...	%Pd	MW (kDa)*
Peak...	100.0	19.02	13.54	20.81	109.4	654
Peak ...	0.0	3805	3580	1123	29.5	1.59e8
Peak ...	0.0	0.000	0.000	0.000	0	0.00

C (T51)=1.25µM

C (FimH)=16µM

T93 **Initial C(T93)=1.24µM C(FimH)=83µM**

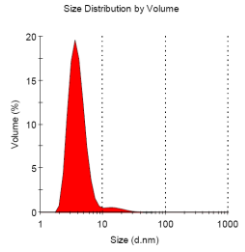

	%Ma...	Mean (n...	Mode (n...	StD (n...	%Pd	MW (kDa)*
Peak...	3.9	19.58	13.54	22.60	115.5	700
Peak ...	96.1	4.017	3.615	1.281	31.9	17.2
Peak ...	0.0	0.000	0.000	0.000	0	0.00

C (T93)=0.155µM

C (FimH)=73µM

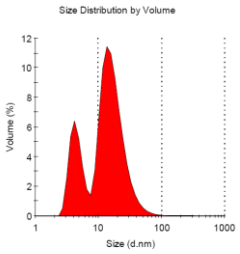

	%Ma...	Mean (n...	Mode (n...	StD (n...	%Pd	MW (kDa)*
Peak...	26.3	4.581	4.187	1.166	25.4	23.4
Peak ...	73.7	18.51	13.54	15.14	81.8	614
Peak ...	0.0	0.000	0.000	0.000	0	0.00

C (T93)=0.37µM

C (FimH)=58µM

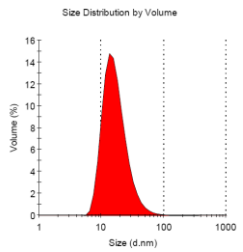

	%Ma...	Mean (n...	Mode (n...	StD (n...	%Pd	MW (kDa)*
Peak...	100.0	18.42	13.54	14.41	78.2	608
Peak ...	0.0	3604	3091	1147	31.8	1.40e8
Peak ...	0.0	0.000	0.000	0.000	0	0.00

C (T93)=0.52µM

C (FimH)=48µM

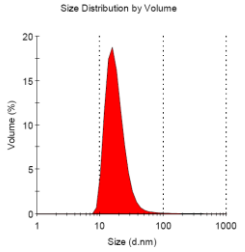

	%Ma...	Mean (n...	Mode (n...	StD (n...	%Pd	MW (kDa)*
Peak...	100.0	19.57	15.69	17.53	89.6	700
Peak ...	0.0	4015	4145	1120	27.9	1.80e8
Peak ...	0.0	0.000	0.000	0.000	0	0.00

C (T93)=0.84µM

C (FimH)=26µM

T200 **Initial C(T200)=0.58µM C(FimH)=83µM**

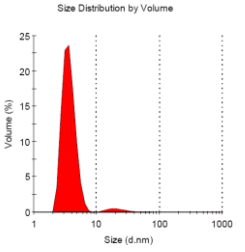

	%Ma...	Mean (n...	Mode (n...	StD (n...	%Pd	MW (kDa)*
Peak...	3.4	23.31	18.17	12.13	52.0	1050
Peak ...	0.0	1576	1990	965.9	61.3	2.02e7
Peak ...	96.5	3.683	3.615	0.8798	23.9	14.1

C (T200)=0.24µM

C (FimH)=48µM

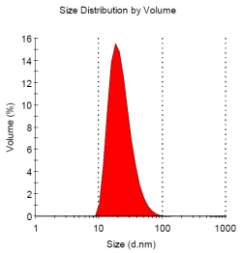

	%Ma...	Mean (n...	Mode (n...	StD (n...	%Pd	MW (kDa)*
Peak...	99.1	23.31	18.17	10.79	46.3	1050
Peak ...	0.9	1997	1990	1022	51.2	3.51e7
Peak ...	0.0	0.000	0.000	0.000	0	0.00

C (T200)=0.31µM

C (FimH)=38µM

O74 **Initial C(O74)=1.55μM C(FimH)=83μM** **Hepes Buffer, 20℃**

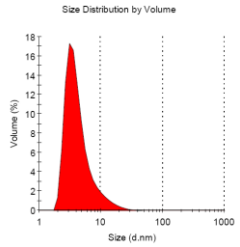

	%Ma...	Mean (n...	Mode (n...	StD (n...	%Pd	MW (kDa)*
Peak...	100.0	4.722	3.122	3.344	70.8	25.1
Peak ...	0.0	1467	1718	826.4	56.3	1.70e7
Peak ...	0.0	0.000	0.000	0.000	0	0.00

C (O74)=0.516μM

C (FimH)=55μM

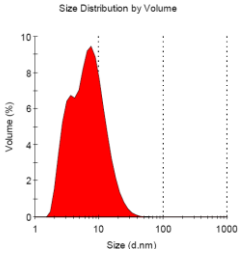

	%Ma...	Mean (n...	Mode (n...	StD (n...	%Pd	MW (kDa)*
Peak...	28.5	3.224	3.615	0.6907	21.4	10.3
Peak ...	71.4	9.142	7.531	4.977	54.4	118
Peak ...	0.1	1238	1281	640.4	51.8	1.14e7

C (O74)=0.775μM

C (FimH)=41μM

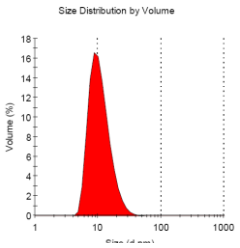

	%Ma...	Mean (n...	Mode (n...	StD (n...	%Pd	MW (kDa)*
Peak...	99.9	11.26	8.721	4.678	41.6	192
Peak ...	0.1	808.1	825.0	371.1	45.9	4.22e6
Peak ...	0.0	2535	1718	1082	42.7	6.13e7

C (O74)=0.91μM

C (FimH)=34μM

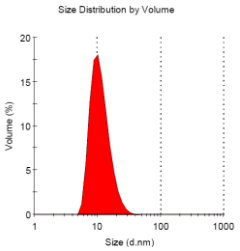

	%Ma...	Mean (n...	Mode (n...	StD (n...	%Pd	MW (kDa)*
Peak...	99.9	11.46	10.10	4.305	37.6	200
Peak ...	0.0	311.1	295.3	199.8	64.2	4.53e5
Peak ...	0.0	3398	3091	1152	33.9	1.22e8

C (O74)=1.15μM

C (FimH)=22μM

O269 **Initial C(O269)=0.43µM C(FimH)=83µM**

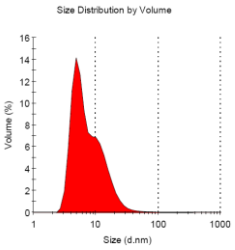

	%Ma...	Mean (n...	Mode (n...	StD (n...	%Pd	MW (kDa)*
Peak...	100.0	9.179	4.849	12.62	137.5	119
Peak ...	0.0	0.000	0.000	0.000	0	0.00
Peak ...	0.0	0.000	0.000	0.000	0	0.00

C (O269)=0.14µM

C (FimH)=55µM

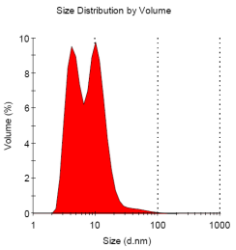

	%Ma...	Mean (n...	Mode (n...	StD (n...	%Pd	MW (kDa)*
Peak...	45.2	4.537	4.187	1.124	24.8	22.9
Peak ...	54.8	12.71	10.10	10.93	86.0	255
Peak ...	0.0	0.000	0.000	0.000	0	0.00

C (O269)=0.21µM

C (FimH)=41µM

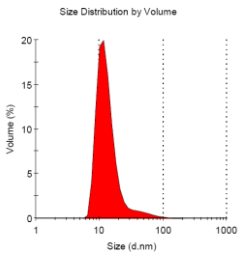

	%Ma...	Mean (n...	Mode (n...	StD (n...	%Pd	MW (kDa)*
Peak...	100.0	14.88	11.70	11.62	78.1	369
Peak ...	0.0	0.000	0.000	0.000	0	0.00
Peak ...	0.0	0.000	0.000	0.000	0	0.00

C (O269)=0.31µM

C (FimH)=22µM

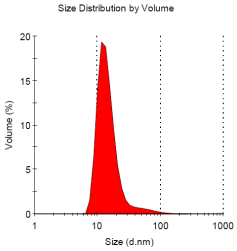

	%Ma...	Mean (n...	Mode (n...	StD (n...	%Pd	MW (kDa)*
Peak...	100.0	16.73	11.70	14.81	88.6	485
Peak ...	0.0	0.000	0.000	0.000	0	0.00
Peak ...	0.0	0.000	0.000	0.000	0	0.00

C (O269)=0.35µM

C (FimH)=14µM

FOLIO ADMINISTRATIF

THESE SOUTENUE DEVANT L'INSTITUT NATIONAL DES SCIENCES APPLIQUEES DE LYON

NOM : YAN DATE de SOUTENANCE : Le 13 Février 2015

Prénoms : Xibo

TITRE : Heptyl mannoside based polymers and nanocapsules: Towards potent anti-adhesive glycomaterials and nanocarriers

NATURE : Doctorat Numéro d'ordre : 2015-ISAL-0011

Ecole doctorale : Matériaux

Spécialité : Matériaux polymères

RESUME :
Ce travail de thèse est consacré à la préparation de glycopolymères porteurs de groupements pendants mannoside d'heptyle et à l'évaluation de la capacité de ces ligands multivalents à inhiber la fixation bactérienne sur les cellules humaines.
Nous avons synthétisé, par polymérisation radicalaire contrôlée, une série de glycopolymères linéaires ou en étoile présentant des masses molaires, des densités en mannoside et des microstructures modulables dans le but d'évaluer l'influence de ces paramètres sur les processus d'interactions avec diverses souches de bactéries E coli (AIEC LF82 et UTI 89). Nous avons tout d'abord mis en évidence par diffusion dynamique et statique de la lumière, la formation d'agrégats entre ces glycopolymères et FimH, la lectine à l'origine de la fixation de souches de bactéries E coli, traduisant des interactions fortes entre les motifs mannosides et les sites de reconnaissance au mannose de la lectine. Nous avons ensuite évalué l'aptitude de ces ligands multivalents à bloquer l'adhésion bactérienne d'AIEC LF82 (impliquée dans la maladie de Crohn) sur des cellules épithéliales intestinales T84. Il a été démontré en conditions in vitro que l'ajout de 10 nM ou 100 nM d'unités mannoside (respectivement en pré- ou post-incubation) réduit de moitié l'adhésion des bactéries sur les cellules épithéliales. L'effet anti-adhésif de ces glycopolymères a été confirmé par des tests ex vivo réalisés sur des intestins isolés de souris transgéniques CEABAC10.
Enfin, nous avons exploité la technique de nanoprécipitation pour l'élaboration de nanocapsules de glycopolymères à cœur huileux. Le procédé développé permet la synthèse de nanocapsules de dimensions contrôlées, porteuses de groupements fonctionnels (fluorophores, ligands) ou de particules métalliques et l'encapsulation de molécules actives à cœur en une seule étape.

MOTS-CLES : Glycopolymers, Nanocapsules, FimH antagonists, Nanoprecipitation

Laboratoire (s) de recherche :IMP@INSA

Directeur de thèse: BERNARD Julien, FLEURY Etienne

Président de jury : GANACHAUD François

Composition du jury :

BERNARD Julien	Chargé de Recherche CNRS (INSA de Lyon)	Directeur de thèse
BOUCKAERT Julie	Chargée de Recherche CNRS (Université de Lille 1)	Examinateur
FLEURY Etienne	Professor (INSA de Lyon)	Directeur de thèse
GANACHAUD François	Directeur de Recherche CNRS (INSA de Lyon)	Examinateur
MALKOCH Michael	Professor (KTH Royal Institute of Technology)	Rapporteur
NICOLAS Julien	Chargé de Recherche CNRS (Université Paris-Sud)	Rapporteur